

TESIS DOCTORAL

DIOXINAS Y FURANOS (PCDD/Fs) EN LA ELECTRO-
OXIDACIÓN DE FÁRMACOS UTILIZADOS EN LA PANDEMIA
DE COVID-19. ANÁLISIS EXPERIMENTAL Y TEÓRICO

PhD THESIS

DIOXINS AND FURANS (PCDD/Fs) IN THE ELECTRO-
OXIDATION OF DRUGS USED IN THE COVID-19 PANDEMIC.
EXPERIMENTAL AND THEORETICAL ANALYSIS

AUTORA

SOPHIE M. SCHRÖDER BARRAZA

DIRECTORAS

DRA. M^a FRESNEDO SAN ROMÁN SAN EMETERIO

PROF. DRA. INMACULADA ORTIZ URIBE

UNIVERSIDAD DE CANTABRIA

Escuela de **Doctorado** de la Universidad de Cantabria

Santander 2022



Universidad de Cantabria

Escuela Técnica Superior de Ingenieros Industriales y de Telecomunicación

Departamento de Ingenierías Química y Biomolecular

**DIOXINS AND FURANS (PCDD/Fs) IN THE ELECTRO-OXIDATION OF
DRUGS USED IN THE COVID-19 PANDEMIC. EXPERIMENTAL AND
THEORETICAL ANALYSIS**

**Dioxinas y Furanos (PCDD/Fs) en la electro-oxidación de fármacos utilizados
en la pandemia de COVID-19. Análisis experimental y teórico**

Memoria de tesis doctoral presentada para optar al título de
Doctor por la Universidad de Cantabria. Programa Oficial de Doctorado
en Ingeniería Química, de la Energía y de Procesos.

Sophie M. Schröder Barraza

Dirigida por:

Dr. M^a Fresnedo San Román San Emeterio

Prof. Dr. Inmaculada Ortiz Uribe

Santander, 2022

*Programa Oficial de Doctorado en Ingeniería Química, de la Energía y de Procesos
(BOE núm. 16, de 19 de enero de 2015. RUCT: 5601000)*

The research described in this PhD thesis was performed in the Sustainable Process Engineering group (SPE) and in the Advanced Separation Processes group (ASP) of the Department of Chemical and Biomolecular Engineering at the University of Cantabria.

This research was financially supported by the Spanish Ministry of Science, Innovation and Universities through the Projects CTM2014-58029-R (MINECO/FEDER,UE), “Identificación y cuantificación de las variables responsables de la potencial formación de PCDD/Fs en procesos de oxidación avanzada”; CTM2017-87740-R (AEI/FEDER, UE) “Aplicación de Tecnologías Ambientales a Matrices Líquidas Conteniendo Contaminantes Orgánicos Emergentes Precursores de la Formación de Derivados Clorados (PCDD/Fs)”.

The author of the thesis would also like to express her gratitude to the Spanish Ministry of Science, Innovation and Universities for the FPI research fellowship (PRE2018-083526). Thanks to this financial aid, a predoctoral short stay have been conducted. This research stay was developed in the Department of Chemistry and Biochemistry, “Faculdade de Ciências da Universidade do Porto” (Porto, Portugal) over the period January 28th-May 3rd 2022, under the supervision of Dr. Pedro Alexandrino Fernandes and Dr. Pedro Ferreira.

Due to all these, a warm thanks towards these institutions is extended.

“DIOXINS AND FURANS (PCDD/Fs) IN THE ELECTRO-OXIDATION OF DRUGS USED IN THE COVID-19 PANDEMIC. EXPERIMENTAL AND THEORETICAL ANALYSIS”

Sophie M. Schröder Barraza

Copyright © S.M. Schröder Barraza. Spain, 2022. All rights reserved.

AGRADECIMIENTOS

En primer lugar, quisiera expresar mi más sincero agradecimiento a mis directoras de tesis, la Dra. María Fresnedo San Román San Emeterio y la Prof. Dra. Inmaculada Ortiz Uribe, por darme la oportunidad de realizar mi tesis doctoral bajo su supervisión, pero sobre todo por la ayuda, las sugerencias constructivas, los consejos y el tiempo brindados a lo largo de estos últimos años. Gracias por la dedicación e implicación en cada etapa de la tesis, no ha sido un periodo fácil atravesando una pandemia. Quisiera agradecer también no solo el apoyo académico, si no la consideración y el apoyo personal recibido, muy necesario en ciertas ocasiones.

I would like to acknowledge Dr. Pedro A. Fernandes for giving me the opportunity to work at the Faculdade de Ciências, in the Department of Chemistry and Biochemistry (Universidade do Porto, Portugal), and to Prof. Maria João Ramos, headmaster of the department, for allowed me to perform there the predoctoral research stay. I would like to thank all the support received and your concern and involvement in making this work go ahead. Special thanks to the recent Dr. Pedro Ferreira, for your dedication and constant support, and of course for your patience in teaching and helping me. I also want to give a warm thanks to all the members of the research group, for all the given help, both in academic and personal things, Rui, João, Filipa, Carola, Pedro Paiva, Antoine and the other João. Foi um prazer partilhar convosco almoços, jantares, passeios, conversas, Cards Against Humanity e muitas cervejas!

Por otra parte, también quisiera agradecer al personal administrativo, técnico, y resto de profesorado del departamento de Ingenierías Química y Biomolecular de la Universidad de Cantabria por la asistencia recibida. Muchas gracias a Sonia, por su dedicación y tiempo en el análisis de las muestras, y por la paciencia con el HRGC-HRMS, que tanta guerra ha dado. También, gracias Gema por tener siempre una sonrisa en la cara para ayudarte en lo que necesites; Elena, siempre tan resolutiva y eficaz, y a Óscar, por la ayuda con el análisis de tantas muestras en el HPLC y GC-MS, cuántas palabras en tus silencios! A Carmen, por tu ayuda, charlas, positividad, cafés de Mac, comidas, siempre dispuesta, ¡es una suerte tenerte de amiga y compañera! Al resto de mis compañeros de 335-H, por escuchar mis quejas y pensamientos siempre (Elena sobre todo y más en estos últimos meses, siempre con un sticker para la ocasión, y un comentario para hacerme reír!). Al resto de compañeros de departamento, por tener siempre un par de palabras amables que alegran el día.

Lupuleros, todo empezó con AWs casuales y cafés en Fabio, y derivó en unos amigos increíbles: Marta y su felicidad y creatividad, Andrea y sus pensamientos, cariñosidades y torpezas, Aitor y su buhardilla/Rubicón (aaupa ahí!), Álvaro, profe de ELOX y la persona con mejor oído que conozco (2º aaupa ahí!), Juan, vecino de mesa, siempre sacando una sonrisa con sus chistes malísimos (has estado en un laberinto?) (3º aaupa ahí!), y Sara, entregada mamá de Ciri y Kira (y peces), siempre alegre y con ganas de hacer planes. A todos, gracias por tantos momentos: cerves, Ángel, zumba, Camino, paseos, Topera, Río, charlas, bailes, cumpleaños, festivales, cafés, cócteles.

A mi Clau, desde aquel 21.09.2009 (es mi cumple!), por ser una gran amiga y compañera, de clase, de comer SIEMPRE, de lab, de vida. Tantos momentos compartidos, gracias por hacer las cosas fáciles, animar, y quitar hierro a situaciones y problemas. Y también, por dar pie a mi incorporación al *Comando*, que decir chicas, que suerte tengo, sois geniales.

A Pau, encuentro casual hace muchos años, ¡y cuánto lo agradezco! Gracias por tus consejos, tu apoyo en tantos momentos, siempre ahí, aunque ahora sea en la distancia, por siempre hacerme sentir como en mi segunda casa (con padres postizos incluidos!), gracias. Mi Sarita, tan lejos en BCN, por escucharme siempre, por sufrir conmigo y alegrarte como si te pasase a ti. Tantos mini-afterworks entre semana que tanto me faltan ahora, eres maravillosa.

A Bé, nunca podré agradecerte lo suficiente tu paciencia, cariño y fuerza que me aportas. Desde el primer día, por saber esperar, tus constantes ánimos, por escogerme para caminar juntos durante todos estos años, por seguir construyendo un futuro contigo (4º aaúpa ahí!). Y por último y más importante, a mis padres, por ser el mayor apoyo que alguien podría tener, tan pendientes de mí siempre. Por escucharme siempre, mis alegrías y mis problemas, dándome los mejores consejos que la experiencia de la vida os ha dado, siempre tan acertados. A pesar de las dificultades y contratiempos que os han ido surgiendo, siempre habéis afrontado todo con mucha fuerza, ¡cuánto me queda por aprender de vosotros! Admiro mucho vuestra actitud ante la vida, sois extraordinarios.

Gracias.

-Sophie

TABLE OF CONTENTS

Summary/Resumen	XV
-----------------------	----

Chapter 1. Motivation

1.1. Emerging contaminants and water pollution.....	5
1.1.1. Pharmaceutical and personal care products group (PPCPs): drugs.....	9
1.1.2. Polychlorinated dibenzo-p-dioxins and furans: PCDD/Fs	12
<i>Homologues and congeners</i>	12
<i>Toxicity</i>	14
<i>Sources and generation</i>	15
1.2. Advanced Oxidation Processes (AOPs)	18
1.2.1. Electrochemical oxidation.....	20
1.3. Intermediate by-products formed during the application of AOPs	24
1.4. The role of computational chemistry in the development of PCDD/Fs formation mechanisms	26
1.5. Background, thesis scope and outline	29
1.6. References.....	33

Chapter 2. Materials and methods.....

2.1. Chemical reagents.....	53
2.2. Electrochemical experiments.....	55
2.2.1. EOX-Drugs & EOX-Intermediates	56
2.3. Analytical measurements of drugs and intermediates.	58
2.3.1. Liquid chromatography analysis	58
<i>High-Performance Liquid Chromatography (HPLC)</i>	58
2.3.2. Qualitative screening analysis of organics in electro-oxidated solutions	60
<i>Extraction and concentration</i>	60
<i>Gas chromatography analysis</i>	64
2.4. Analysis of PCDD/Fs	65

2.4.1. Standard method EPA 1613: Tetra- through Octa-Chlorinated Dioxins and Furans by Isotope Dilution HRGC/HRMS	65
<i>L-L extraction with DCM</i>	68
<i>Concentration I</i>	68
<i>H₂SO₄ treatment and filtration</i>	69
<i>Concentration II</i>	70
<i>Filtration</i>	70
<i>Purification</i>	71
<i>Concentration III</i>	71
2.4.2. HRGC-HRMS analysis	72
2.4.3. Quality control and quality assurance in the analysis of PCDD/Fs	73
2.5. Computational calculations.....	73
2.5.1. Working methodology in computational chemistry within the framework of PCDD/Fs formation mechanisms	75
2.6. References.....	79

Chapter 3. Electrochemical oxidation (EOX) of COVID-19 drugs..... 51

3.1. Limiting current density	87
3.2. Drugs electrochemical oxidation.....	89
3.2.1. EOX-Drugs experiments	89
3.2.2. EOX-Intermediates experiments.....	94
3.2.3. Radicals' formation: theoretical analysis on drugs degradation	98
<i>Influence of radical chlorine in drugs' degradation</i>	98
<i>Influence of radical sulphate in drugs' degradation</i>	100
3.3. Analysis of the degradation intermediates	103
3.3.1. Identification of DEX intermediates: kinetic study	105
3.3.2. Identification of AMX intermediates: kinetic study	109
3.3.3. Identification of PAR intermediates: kinetic study	113
3.3.4. Identification of STR intermediates: kinetic study.....	117
3.4. References.....	122

Chapter 4. PCDD/Fs during EOX of drugs: toxicity assessment 135

4.1. Analysis of the PCDD/Fs formed from drugs' EOX	137
4.1.1. Homologue profiles analysis	138
4.1.2. 2,3,7,8-congeners analysis.....	142
4.1.3. Toxicity assessment in terms of TEQ	146
4.2. New methodology for TEQ calculation: TCS photocatalysis as case study.	150
4.2.1. PCDD/Fs formation kinetics	151
4.2.2. Statistical analysis to obtain the alternative TEQ models.....	154
<i>Methodology applied to address the statistical analysis.....</i>	<i>155</i>
4.3. References.....	165

Chapter 5. Computational Chemistry in the theoretical PCDD/Fs formation mechanisms173

5.1. Computational chemistry background.....	175
5.1.1. Computational methodology.....	176
<i>Electron density.....</i>	<i>177</i>
<i>Computational calculation steps</i>	<i>179</i>
5.1.2. Mechanism proposal from drugs to the formation of PCDD/Fs.....	187
5.2. Description of the combined mechanism through DFT	190
5.2.1. Combined mechanism: 1 st step - breakage of the drugs	190
<i>Amoxicillin.....</i>	<i>190</i>
<i>Paracetamol.....</i>	<i>193</i>
<i>Sertraline.....</i>	<i>198</i>
5.2.2. Combined mechanism: 2 nd step - intermediate and final molecules formation	
201	
<i>Formation of 3,4-dichlorophenol from hydroquinone</i>	<i>201</i>
<i>PCDD/Fs formation from 3,4-dichlorophenol</i>	<i>205</i>
5.2.3. Energy profiles of the reaction mechanisms	210
<i>Drug molecules breakage</i>	<i>210</i>
<i>Intermediates and PCDD/Fs formation.....</i>	<i>214</i>
5.3. References.....	218

Chapter 6. Conclusions/Conclusiones 227

Annexes 247

Annex I – Nomenclature..... 249

 General nomenclature..... 249

 PCDD/Fs nomenclature..... 253

Annex II – Concentration of labelled EPA 1613 solutions 254

Annex III – Recoveries of labelled EPA 1613 solutions..... 257

Annex IV– GC-MS: by-products analysis. 261

Annex V – GC-MS chromatograms..... 272

Annex VI – Degradation mechanisms..... 273

Annex VII – Additional tables 277

Annex VIII – Additional AMX pathway 279

Annex IX – Scientific contributions..... 281

 IX.1. List of papers published in indexed journals 281

 IX.2. Book chapter 282

 IX.3. Congress contributions 282

 IX.4. Dissemination activities..... 284

 IX.5. Final degree project co-direction..... 284

SUMMARY

The current situation of water resources within the framework of the global pandemic COVID-19, along with water sustainable management, through recycling and safe reuse, are the main protagonists of this Doctoral Thesis, in line with Sustainable Development Goals (SDGs) and especially with the "goal number 6, Clean Water and Sanitation". Until now, the treatment to apply in the fight against the SARS-CoV-2 virus, has led to intensive consumption of the determined drugs, which finally end in the aquatic medium, giving rise to the called Emerging Contaminants (EC). Due to the persistent and dangerous nature of these compounds, the need arises to investigate what treatments and operating conditions are adequate to remove them. Within this context, various drugs have been used to fight against the virus SARS-CoV-2 and its symptoms, as they are dexamethasone (DEX), amoxicillin (AMX), paracetamol (PAR) and sertraline (STR), and, consequence, increasing their presence in the environment, as in like rivers or lakes. In this context, the advanced oxidation processes (AOPs), based on the formation of elevated concentrations of powerful oxidizing agents, with hydroxyl radicals ($\cdot\text{OH}$) among them, are presented as an attractive option facing the treatment wastewater containing ECs. Nevertheless, previous studies have demonstrated that under the application of some AOPs, and using certain operating conditions, may be possible that intermediate compounds or by-products can be generated because of incomplete mineralization of the initial organic compounds. These by-products can even more toxic than the initial compounds, so that, they can increase the toxicity of the final sample. In this way, polychlorinated dibenzo-p-dioxins and furans (PCDD/Fs), a family of unintentionally produced molecules, catalogued as persistent organic pollutants due to high persistency, bioaccumulation and environmental high toxicity, regulated internationally by the Stockholm Convention (2001), can be formed from precursor molecules (intermediates or by-products) generated after applying AOPs. In order to corroborate this hypothesis, this doctoral thesis has assessed the formation of PCDD/Fs and the final toxicity of the samples, after applying electrochemical oxidation to matrices containing the most used drugs in the fight against COVID-19, namely, dexamethasone (DEX), amoxicillin (AMX), paracetamol (PAR) and sertraline (STR).

Firstly, in Chapter 1, it is given an overview of the water situation worldwide is addressed, together with the increasing presence of COVID-19 drugs in the environment. In addition, the fundamentals of AOPs, and specifically, electrochemical oxidation (EOX), are detailed, focusing on the application to drugs-containing solutions and the associated by-products generation.

To follow, in Chapter 2 are presented the experimental set-up used to carry out the experimental part of the thesis, and the chemicals involved in all the stages, such as the degradation experiments, the intermediates analysis and the PCDD/Fs preparation and analytical by EPA 1613 method. Furthermore, the employed analytical techniques, such as chromatography liquid and gas are described. To end, the computational set up, with the procedure carried out to perform the simulations is detailed using the computational chemistry software GAUSSIAN 16.

Although the electrochemical oxidation of different drugs has widely been studied in the literature, studies about its application to COVID-19 related drugs are still scarce. In this sense, in Chapter 3 is reported the electrochemical oxidation of DEX, AMX, PAR and STR, employing two different electrolytic media, NaCl and Na₂SO₄+NaCl, with the following degradation order: STR > AMX > PAR > DEX. The obtained results show that degradation was faster with NaCl media in all cases, which was further corroborated by a theoretical analysis of the main radicals present in the solution and thus, involved in the reactions. The degradation of highly concentrated solutions was also carried out, in order to analyse the intermediate by-products formed during the degradation of the compounds. Several chlorophenols, well-known PCDD/Fs precursor compounds, were found in all the drugs' degradations with NaCl media. With Na₂SO₄+NaCl medium, in addition to chlorophenols, also some molecules, which can be precursors of PCDD/Fs precursors, such as hydroquinone or chlorohydroquinone were also found.

The assessment of PCDD/Fs formation is the main objective of this work, which is addressed in chapter 4. For this, both the analysis of the homologue groups together with the 2,3,7,8-PCDD/Fs congeners has been performed, for the two electrolytic media employed (NaCl and Na₂SO₄+NaCl). Elevated concentrations of the homologue groups were found, being the highest when using NaCl. Specifically, when treating amoxicillin with NaCl, the generated PCDD/Fs reached the highest values among all the analysed (2661.3 pg L⁻¹), followed by paracetamol (563.5 pg L⁻¹). In the congeners case, amoxicillin was also the compound which generated the elevated concentration, in particular, with NaCl (249.3 pg L⁻¹). Along with the congeners analysis, the toxicity in terms of toxic

equivalents (TEQ) was analysed, and surprisingly, dexamethasone reached the highest TEQ, due to the presence of congeners with elevated I-TEF, such as 1,2,3,7,8-PeCDD. Finally, a new methodology for TEQ calculation was developed in order to reduce the analytical effort. After a multivariable analysis to reduce the number of congener pairs and to evaluate the correlation between the congeners and TEQ, a new model was proposed which uses just two congeners to calculate the TEQ. After this, multiple linear regression was applied to obtain 5 models with highly correlated congeners, thus, reducing the number of congeners needed to calculate TEQ from 17 to 2. These models were applied to literature PCDD/Fs profile data, fitting properly to them. This part was developed with the software Statgraphics Centurion XVI.

Chapter 5 comprises the theoretical study of the PCDD/Fs formation pathways from the electro-oxidised COVID-19 related drugs, leaving aside dexamethasone due to its complexity. For this, density functional theory (DFT) with GAUSSIAN 16 was applied to evaluate, on the one hand, the degradation mechanisms of the drugs, and on the other hand, the formation mechanisms of PCDD/Fs from the formed precursors in the first part of the theoretical study. The degradation and formation pathways are described thoroughly accompanied with the energy profiles and the imaginary frequencies correspondent to each transition state achieved.

This thesis contains novel results regarding the degradation electrochemical oxidation of drugs related to COVID-19 pandemic, emphasizing the importance of not underestimating the related formation intermediate compounds during this treatment, nor the final produced compounds, the PCDD/Fs, and its associated toxicity. Besides, it contributes with new information about the theoretical formation pathways from precursor compounds to dioxins and furans from a computational chemistry point of view using software GAUSSIAN 16.

RESUMEN

La situación actual de los recursos hídricos en el marco de la pandemia mundial COVID-19, junto con la gestión sostenible del agua, a través del reciclaje y la reutilización segura, son los principales protagonistas de esta tesis doctoral, en línea con los Objetivos de Desarrollo Sostenible (ODS) y especialmente con el "objetivo número 6, Agua Limpia y Saneamiento". Hasta ahora, el tratamiento a aplicar en la lucha contra el virus SARS-CoV-2, ha llevado a un consumo intensivo de determinados fármacos, que finalmente acaban en el medio acuático, dando lugar a los llamados Contaminantes Emergentes (CE). Debido a la naturaleza persistente y peligrosa de estos compuestos, surge la necesidad de investigar qué tratamientos y condiciones operativas son adecuados para eliminarlos. En este contexto, se han utilizado diversos fármacos para combatir el virus SARS-CoV-2 y sus síntomas, como son la dexametasona (DEX), la amoxicilina (AMX), el paracetamol (PAR) y la sertralina (STR), y, en consecuencia, se ha incrementado su presencia en el medio ambiente, como en ríos o lagos. En este contexto, los procesos de oxidación avanzada (POAs), basados en la formación de elevadas concentraciones de potentes agentes oxidantes, con los radicales hidroxilo ($\cdot\text{OH}$) entre ellos, se presentan como una opción atractiva de cara al tratamiento de aguas residuales que contienen CEs. Sin embargo, estudios previos han demostrado que, bajo la aplicación de algunos POAs, y utilizando ciertas condiciones de operación, puede ser posible que se generen compuestos intermedios o subproductos debido a la mineralización incompleta de los compuestos orgánicos iniciales. Estos subproductos pueden ser incluso más tóxicos que los compuestos iniciales, por lo que, pueden aumentar la toxicidad de la muestra final. De este modo, las dibenzo-p-dioxinas y furanos policlorados (PCDD/Fs), una familia de moléculas producidas de forma no intencionada, catalogadas como contaminantes orgánicos persistentes por su alta persistencia, bioacumulación y alta toxicidad ambiental, reguladas internacionalmente por el Convenio de Estocolmo (2001), pueden formarse a partir de moléculas precursoras (intermedias o subproductos) generadas tras la aplicación de POAs. Para corroborar esta hipótesis, en esta tesis doctoral se ha evaluado la formación de PCDD/Fs y la toxicidad final de las muestras, tras aplicar la oxidación electroquímica a matrices que contienen los fármacos más utilizados en la lucha contra el COVID-19, a saber, dexametasona (DEX), amoxicilina (AMX), paracetamol (PAR) y sertralina (STR).

En primer lugar, en el Capítulo 1, se ofrece una visión general de la situación del agua en todo el mundo y se aborda la creciente presencia de fármacos COVID-19 en el medio ambiente. Además, se detallan los fundamentos de los POAs y, en concreto, de la oxidación electroquímica (OE), centrándose en la aplicación a soluciones que contienen fármacos y en la generación de subproductos asociados.

A continuación, en el Capítulo 2 se presenta el equipo experimental utilizado para llevar a cabo la parte experimental de la tesis, y los productos químicos que intervienen en todas las etapas, como los experimentos de degradación, el análisis de los intermedios y la preparación y el análisis de las PCDD/Fs por el método EPA 1613. Además, se describen las técnicas analíticas empleadas, como la cromatografía de líquidos y de gases. Para finalizar, se detalla el equipo computacional, con el procedimiento llevado a cabo para realizar las simulaciones utilizando el software de química computacional GAUSSIAN 16.

Aunque la oxidación electroquímica de diferentes fármacos ha sido ampliamente estudiada en la literatura, los estudios sobre su aplicación a fármacos relacionados con la COVID-19 son todavía escasos. En este sentido, en el Capítulo 3 se reporta la oxidación electroquímica de DEX, AMX, PAR y STR, empleando dos medios electrolíticos diferentes, NaCl y Na₂SO₄+NaCl, con el siguiente orden de degradación STR > AMX > PAR > DEX.. Los resultados obtenidos muestran que la degradación fue más rápida con el medio NaCl en todos los casos, lo que fue corroborado por un análisis teórico de los principales radicales presentes en la solución y, por tanto, implicados en las reacciones. También se llevó a cabo la degradación de soluciones altamente concentradas, con el fin de analizar los subproductos intermedios formados durante la degradación de los compuestos. En todas las degradaciones de los fármacos con medios de NaCl se encontraron varios clorofenoles, conocidos compuestos precursores de PCDD/Fs. Con el medio Na₂SO₄+NaCl, además de los clorofenoles, también se encontraron algunas moléculas que pueden ser precursoras de los PCDD/Fs, como la hidroquinona o la clorohidroquinona.

La evaluación de la formación de PCDD/Fs es el principal objetivo de este trabajo, la cual se aborda en el Capítulo 4. Para ello, se ha realizado el análisis de los grupos homólogos junto con los congéneres 2,3,7,8-PCDD/Fs, para los dos medios electrolíticos empleados (NaCl y Na₂SO₄+NaCl). Se encontraron concentraciones elevadas de los grupos homólogos, siendo las más altas cuando se utilizó NaCl como electrolito. En concreto, al tratar la amoxicilina con NaCl, los PCDD/Fs generados

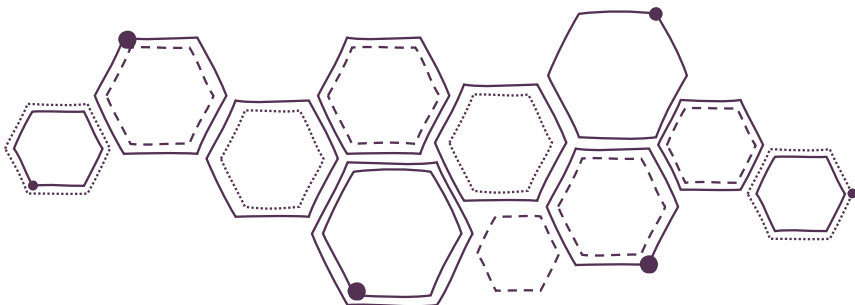
alcanzaron los valores más altos de entre todos los analizados (2661.3 pg L⁻¹), seguido del paracetamol (563.5 pg L⁻¹). En el caso de los congéneres, la amoxicilina también fue el compuesto que generó la concentración más elevada, en particular, con el NaCl (249.3 pg L⁻¹). Junto con el análisis de congéneres, se analizó la toxicidad en términos de equivalentes tóxicos (TEQ), y sorprendentemente, la dexametasona alcanzó el TEQ más alto, debido a la presencia de congéneres con I-TEF elevados, como el 1,2,3,7,8-PeCDD. Por último, se desarrolló una nueva metodología para el cálculo del TEQ con el fin de reducir el esfuerzo analítico. Tras un análisis multivariable para reducir el número de pares de congéneres y evaluar la correlación entre los congéneres y el TEQ, se propuso un nuevo modelo que utiliza sólo dos congéneres para calcular el TEQ. A continuación, se aplicó una regresión lineal múltiple para obtener 5 modelos con congéneres altamente correlacionados, reduciendo así el número de congéneres necesarios para calcular el TEQ de 17 a 2. Estos modelos se aplicaron a los datos de perfiles de PCDD/Fs de la literatura, ajustándose adecuadamente a ellos.

El Capítulo 5 comprende el estudio teórico de las vías de formación de PCDD/Fs a partir de los fármacos del COVID-19 electrooxidados, pero dejando de lado la dexametasona debido a su complejidad. Para ello, se aplicó la teoría funcional de la densidad (DFT) con GAUSSIAN 16 para evaluar, por un lado, los mecanismos de degradación de los fármacos, y por otro, los mecanismos de formación de PCDD/Fs a partir de los precursores formados en la primera parte del estudio teórico. Las vías de degradación y formación se describen minuciosamente acompañadas de los perfiles energéticos y las frecuencias imaginarias correspondientes a cada estado de transición alcanzado. Esta parte se ha desarrollado con el software Statgraphics Centurion XVI.

Esta tesis contiene resultados novedosos sobre la degradación aplicando oxidación electroquímica de fármacos relacionados con la pandemia de COVID-19, destacando la importancia de no subestimar la formación de compuestos intermedios relacionados durante este tratamiento, ni los compuestos finales producidos, los PCDD/Fs, y su toxicidad asociada. Además, se aporta nueva información sobre las vías teóricas de formación de compuestos precursores a dioxinas y furanos desde el punto de vista de la química computacional utilizando el software GAUSSIAN 16.



MOTIVATION



Abstract

The current situation of water resources within the framework of the global pandemic COVID-19, along with water sustainable management, through recycling and safe reuse, are the main protagonists of this PhD Thesis, in line with Sustainable Development Goals (SDGs) and especially with the "goal number 6, Clean Water and Sanitation". Until now, the treatment to apply in the fight against the SARS-CoV-2 virus, has led to an intensive consumption of determined drugs, which are finally ending in the aquatic medium, as Emerging Contaminants (EC). Given the persistent and dangerous nature of these compounds, the need arises to investigate what treatments and operating conditions are adequate to remove them.

In this way, Chapter 1 presents a brief classification of the pharmaceutical and personal care products group (PPCPs), deepening into the pharmaceuticals (drugs). In this context, the advanced oxidation processes (AOPs) are presented as an attractive option facing the treatment of wastewater containing drugs, standing out electrochemical oxidation (EOX) because of its innumerable advantages. Nevertheless, previous studies have demonstrated that under the application of some AOPs, and using certain operating conditions, may be possible that intermediate compounds can be generated, possibly more toxic than the initial ones, like polychlorinated dibenzo-p-dioxins and furans (PCDD/Fs). Their toxicity and generation sources have thoroughly addressed in this chapter, which ends with the background, scope, outline and objectives proposed to give an answer to the hypothesis planned in this doctoral thesis.

1.1. Emerging contaminants and water pollution

Clean and abundant water is a vital requisite for all forms of life; growing contamination is a critical environmental and social concern. In this context, the world population has exponentially increased during the last decades, being currently (beginning of the 2020s) 7.9 billion people. The United Nations forecasted that by 2030 the population will reach 8.5 billion people, and 9.7 billion by 2050 (United Nations, 2022). These numbers, together with the consequent urbanization and industrial activity, are leading to an increase in waste production and water demand, especially by industry and energy sectors; the latter is expected to grow to 24% by 2050 (UNESCO, 2020). Water usage has increased by a factor of 6 in the last 100 years and is constantly growing at a rate of 1% every year, causing, among other issues, water scarcity in some regions of the planet. This problem has been aggravated due to climate change, which has provoked a rise in temperatures, together with long dry spells, causing problems with food security and environmental sustainability. Currently, 25% of the world's population (2 billion people living in 17 different countries) face extremely high levels of water stress, where mainly agriculture and industries withdraw more than 80% of the available water on average every year (Hofste et al., 2019).

As stated in The United Nations World Water Development Report 2021, the vast majority of wastewater volume (approximately 80%) is discharged directly into the ecosystems without any previous treatment, causing harmful effects on several aspects (human health, environment, quality of freshwater resources...) (UNESCO, 2021). Therefore, the sustainable management of water resources to provide fresh water, constitutes a very important challenge for the 21st century scientific community.

In this context, the 2030 Agenda and Sustainable Development Goals (SDGs) of the United Nations, in the sustainable goal number 6, Clean Water and Sanitation, where the water issue is addressed, establishes the need to ensure the availability and sustainable management of water, by reducing the pollution, minimizing the release of hazardous chemicals and materials, and increasing the water recycling and safe reuse in a global way. Specifically, Target 6.3 aims to diminish pollution, and improve the removal, management, and treatment of wastewater (United Nations, 2021). Within this perspective, wastewater appears as a valuable non-conventional resource, that can be used to cover water necessities, changing the common thinking of "treatment and disposal" to "reuse, recycle and resource recovery" (UNESCO, 2017).

Additionally, in the last decades, the world's freshwater resources are being polluted due to the presence of new pollutants, the so-called "Emerging Contaminants" (ECs). ECs are more and more present in waters, becoming an important issue to deal with in both developed and developing countries (UNESCO, 2020). They are defined as chemical compounds that are present at trace concentrations (from $\mu\text{g L}^{-1}$ to ng L^{-1}), which currently are not regulated or monitored, due to their effects are not totally known, but may be under examination facing future regulations (Dulio et al., 2018; Hube and Wu, 2021). Since they have been found in several matrices (food sources, soil or aquatic mediums), in consequence, they can move into the environment through different sources such as industrial and household wastewater, hospital effluents or water discharge, among others, producing adverse effects in the human beings and in the ecosystems (diabetes, cardiovascular problems, fertility and reproductive issues, degradation of aquatic ecosystems...) (Schröder et al., 2022). Besides, these pollutants possess some negative characteristics, such as persistence or bioaccumulation. In accordance with the NORMAN database (Norman Network, 2022), more than 700 ECs are listed so far in the European aquatic environment, classified into 20 groups associated with their origin: industrial additives, surfactants, steroid hormones and other endocrine-disrupting compounds (EDCs), flame retardants, pharmaceutical compounds, and disinfection by-products, etc., but the list is in constant growth (Dulio et al., 2018). Among them, the group of Pharmaceutical and Personal Care Products (PPCPs) is one of the major and most repeatedly detected groups in the environment (Varsha et al., 2022; Vasilachi et al., 2021). Table 1.1 presents a brief classification of ECs, along with the most representative compounds of each group.

The problem associated with ECs emissions is getting worse over the years, and this has led to taking action for its mitigation. The EU Water Framework Directive, which is the main legal instrument for water protection in Europe gathered, through the Norman Network 1036 compounds to be observed (Norman Network, 2022; Vargas-Berrones et al., 2020). In contrast, in the United States, the Safe Drinking Water Act (SDWA) only comprises 94 compounds (SDWA, 2022). Moreover, the United States Environmental Protection Agency (US EPA) through National Primary Drinking Water Regulations (NPDWR) possess 81 compounds in its 5th Contaminant Candidate List (CCL) on October 28th, 2022 (US EPA, 2022), which are lists of drinking water contaminants that are known or anticipated to occur in public water systems and are not currently subject to US EPA drinking water regulations. Contaminants listed on the CCL may require future regulation under the SDWA.

Table 1.1. Main categories of ECs (Varsha et al., 2022; Vasilachi et al., 2021).

ECs Group	Representative compounds
Pesticides	2,4-D, fenoprop, tebuthiuron, pentachlorophenol, diuron
Pharmaceutical and Personal Care Products (PPCPs)	<ul style="list-style-type: none"> • <i>β-blockers</i>: atenolol, metoprolol, propranolol, timolol, sotalol • <i>Analgesics, anti-inflammatory drugs</i>: Ibuprofen, diclofenac, fenoprofen, codein, paracetamol • <i>Antibiotics</i>: amoxicillin, clarithromycin, erythromycin • <i>Psychiatric drugs</i>: diazepam, carbamazepine, sertraline • <i>Disinfectants</i>: triclosan, triclocarban • <i>Lipid regulators</i>: fenofibric acid, gemfibrozil, bezafibrate • <i>X-ray contrasting agents</i>: Iopromide, iopamidol, diatrizoate • <i>Steroids and hormones</i>: dexamethasone, estradiol, estrone, estriol, diethylstilbestrol (DES)
Flame retardants	<ul style="list-style-type: none"> • Polybrominated diphenyl ethers (PBDEs): polybrominated biphenyls (PBBs), polybrominated dibenzo-p-dioxins and furans (PBDD/Fs) • Tetrabromo bisphenol A, C10-C13 chloroalkanes, tris (2-chloroethyl) phosphate, Hexabromocyclododecanes (HBCDs)
Surfactants	Alkylphenol ethoxylates, 4-nonylphenol, 4-octylphenol
Food additives	Acesulfame
Perfluorinated compounds	Perfluoro octane sulfonates (PFOs), perfluorooctanoic acid (PFOA)
Gasoline additives	Dialkyl ethers, methyl-t-butyl ether (MTBE)
Biocides	Parabens, neonicotinoids
UV filters	Benzophenone-3, homosalate, octocrylene, 4-MBC, B3P
Particles	Microplastics
Anthropogenic markers	Bromoform, nicotine, benzotriazole methyl-1H

The European Union together with the US EPA emphasized and collected 126 ECs in a Priority Pollutant list (PPs) attributable to their high threat towards the aquatic biota and human health (EU, 2013; US EPA, 2014). Afterwards, Watch Lists were established to improve the available information on identifying the substances of greatest concern. In 2015, the European Union added 10 ECs as potential priority candidates to the Watch List in the Decision 2015/495/EU (EU, 2015). Then, in 2018, five of these substances were retired and three new ones were added to the Watch List in the Decision 2018/840, being

a total number of 8 (EU, 2018). In 2020 it was set another Watch List in the Decision 2020/1161 (EU, 2020), but it was repealed in 2022 in the Decision 2022/1307 (EU, 2022a), therefore remaining on force the Watch List of 2018. In addition, on October 26th 2022, the Commission implemented a proposal to review the list of priority substances in surface water, where 24 substances are proposed for addition (EU, 2022b).

Among the PPs, the Persistent Organic Pollutants (POPs) are classified as chemicals (intentionally or unintentionally produced) that also cause adverse effects to humans and ecosystems, being gradually accumulated and thus, transported far from their origins through the air, water, or migratory species, entering finally in the food chain. This group comprises pesticides (like DDT), industrial chemicals (polychlorinated biphenyls, PCBs) or unintentionally formed by-products from industrial processes (dioxins and furans, PCDD/Fs) (EU, 2009). Finally, the Stockholm Convention on Persistent Organic Pollutants in 2001 established 12 key POPs, the “Dirty Dozen”, where the nations agreed to diminish and/or eliminate the manufacture, use and discharge of those 12 POPs. Currently, the last version of the Stockholm Convention established 30 POPs on the list (Stockholm Convention, 2019). In Figure 1.1 is detailed the current legislation in a schematic form, in order to a better comprehension.

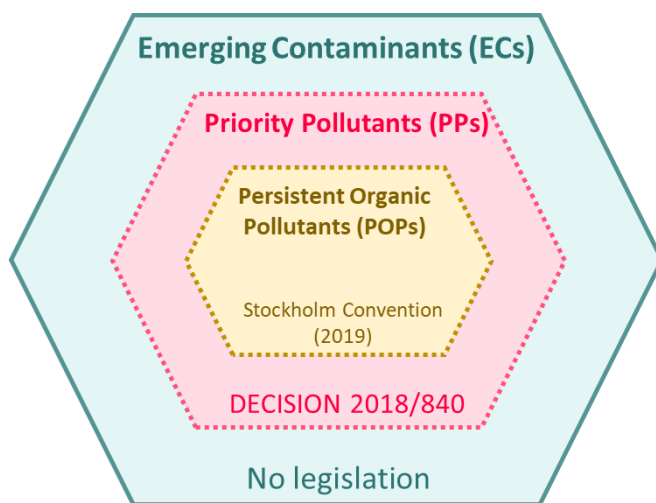


Figure 1.1. Scheme of emerging, priority and persistent pollutants and their respective current regulations.

1.1.1. Pharmaceutical and personal care products group (PPCPs): drugs

The group of Pharmaceutical and Personal Care Products includes products employed both for human health and cosmetic care or veterinary and agricultural uses (Ávila and García, 2015). PPCPs comprise diverse chemicals, including all types of pharmaceutical compounds (both prescription and over-the-counter medications) and non-medicinal use chemicals, like fragrances, disinfectants, or UV-filters. They are not classified as POPs, although some of them may have similar characteristics, like their persistence, owing to their continued release into the environment; the world production of PPCPs has increased in various folds, causing a severe exposure of these metabolites in the world's population, via different aquatic systems, among others systems (Silori et al., 2022).

Inside PPCPs, pharmaceutical compounds or mostly known as drugs, have received special attention in the last decades, they are considered as ECs because they are still unregulated or are under a regulation process due to their recent recognition as potentially dangerous to ecosystems. Drugs can be present in their initial form, as metabolites or as degradation by-products, and their occurrence in the environment is caused mainly by the use of pharmaceutical products and therapeutic drugs, pharmaceutical industry wastes and hospital wastewaters (Rivera-Utrilla et al., 2013). The most detected groups are analgesics and anti-inflammatory drugs, antibiotics, antiepileptics, psychiatric drugs and β -blockers. Table 1.2 presents a brief classification, together with some examples of the most common drugs present in wastewaters.

Table 1.2. Drugs in residual effluents (Deblonde et al., 2011; Silori et al., 2022).

Pharmaceutical compounds	Representative compounds
Analgesics, anti-inflammatory drugs	Ibuprofen, diclofenac, fenoprofen, codein, paracetamol, tramadol
Antibiotics	Amoxicillin, clarithromycin, erythromycin, doxycycline
Antiepileptics	Carbamazapine, gabapentin, phenytoin, lamotrigine
Lipid regulators	Fenofibric acid, gemfibrozil, bezafibrate
Psychiatric drugs	Diazepam, carbamazepine, sertraline, citalopram
β -blockers	Atenolol, metoprolol, propranolol, timolol, sotalol

The presence in the environment of most compounds listed in Table 1.2 is in steady increase, especially during the last two years owing to the COVID-19 pandemic, which has produced a huge impact on all aspects of our lives, demonstrating the importance of clean water, sanitation, and hygiene, crucial to stop the virus propagation (WHO and UNICEF, 2020). Specifically, various pharmaceuticals have been used to fight against the virus SARS-CoV-2 and its symptoms; antiviral/antiprotozoals drugs, anti-inflammatory action drugs (glucocorticoids or antibiotics), and painkillers to combat main symptoms, as well as some psychiatric drugs to treat people's mental health, which has also been affected causing anxiety or depression episodes. Figure 1.2 shows the principal pharmaceuticals (with their corresponding molecular structures) employed in the fight against the COVID-19 pandemic.

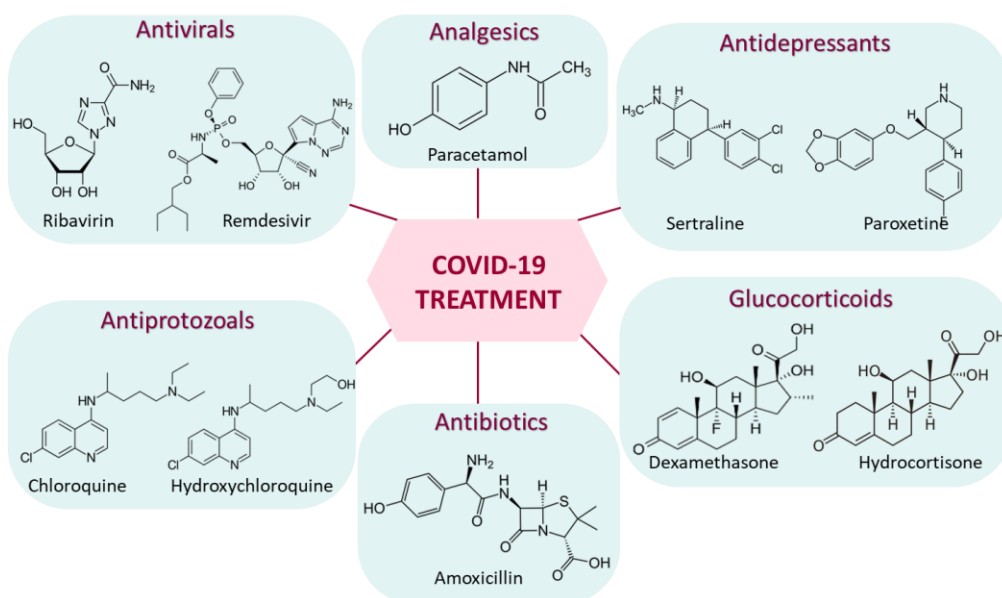


Figure 1.2. Main pharmaceutical compounds employed to fight COVID-19 (Diaz-Camal et al., 2022; Morales-Paredes et al., 2022; Musee et al., 2021).

Among the anti-inflammatory drugs, two of the mostly employed are dexamethasone (DEX) and amoxicillin (AMX). Dexamethasone is a glucocorticoid drug with anti-inflammatory and immunosuppressive activity (Morales-Paredes et al., 2022; Musee et al., 2021; WHO, 2021). According to the World Health Organization (WHO), when employing dexamethasone, the mortality was reduced by about one-third for patients with ventilators, and to one-fifth for patients needing just oxygen (WHO, 2021). Dexamethasone has been detected in several water matrices around the world such as

in tap water and river water, in concentrations between 0.36-12 ng L⁻¹ (Shen et al., 2020; Wee et al., 2022, 2020, 2019), or in wastewater, with elevated concentrations, up to 236 ng L⁻¹ (Musee et al., 2021). It is expected an increase in the next few years due to its application to treat the virus symptoms, specifically, it has predicted that concentrations as high as 55.6 ng L⁻¹ can be identified in the United States, where this drug has not been previously detected (Morales-Paredes et al., 2022). Amoxicillin is one of the most frequent antibiotic options, with anti-inflammatory properties. It has been dispensed as antimicrobial medication to a high percentage of hospitalized people, especially those who were suspected of a bacterial infection or pneumonia during the COVID-19 pandemic (Adebisi et al., 2021; Mohamad et al., 2022; Ruiz-Garbajosa and Cantón, 2021). Values between 0.38-5.2 µg L⁻¹ have been detected in the influent of wastewater treatment plants (WWTPs) and concentrations up to 2.91 µg L⁻¹ were detected in treated waters (Li et al., 2022; Sengar and Vijayanandan, 2022). The European Union has included amoxicillin in the Watch List 2018.

In the case of painkillers or analgesics, such as paracetamol (PAR), they have been very useful to palliate COVID-19 virus provoked symptoms, such as strong headaches, fever, or other kind of aches like throat pain. On March 17th, 2020, the WHO recommended the use of paracetamol for its effectiveness; and as a consequence, its employment grew by +111% (Enners et al., 2021). It has been reported that both amoxicillin and paracetamol suffered a huge increase during the full lockdown of the population in 2020 in New Haven (USA), with data taken from 19 March 2020 to 30 June 2020 (Nason et al., 2021). It was detected in elevated concentration (37.9 µg L⁻¹) in the influent of WWTPs from April-December 2020 in New Haven, USA; and in lesser concentrations in groundwater (0.147 µg L⁻¹) and in river water (0.343-0.432 µg L⁻¹) in different parts of the world, like Italy, Pakistan or South Africa (Cappelli et al., 2022; Khan et al., 2022; Madikizela et al., 2022).

Analysing the antidepressants, sertraline (STR), which belongs to serotonin reuptake inhibitors (SSRIs), was the most prescribed drug in 2019 in the United Kingdom. More than £113 million were reached in additional sales in 2020 in comparison with 2019, however unexpectedly, the sales units just grew 10.4%. This was principally due to a price increase, provoked by a shortage in the manufacture of the active pharmaceutical ingredient (API), which affected the production of sertraline; a rise in the demand and the low availability of the drug led to this situation (Diaz-Camal et al., 2022; FDA, 2020; Rabeea et al., 2021). In the United States, it was registered a scarcity during the pandemic period (May 2020-September 2021) due to its high demand (US FDA, 2020). It

was also confirmed its increase in New Haven (USA) during the lockdown period of the population (Nason et al., 2021). The concentrations detected in the environment achieved values up to 218 ng L⁻¹ in river water and coastal waters (Arnnok et al., 2017; Castillo-Zacarias et al., 2021; Dehm et al., 2021) and up to 0.06 µg L⁻¹ in treated wastewater (Sengar and Vijayanandan, 2022). Before COVID-19 (2015-2019), the concentrations detected in the influent and effluent of a WWTP varied from 0.77 to 114 ng L⁻¹, experimenting an increase after this period (2020-2021), reaching values from 25 to 417 ng L⁻¹ (Diaz-Camal et al., 2022).

1.1.2. Polychlorinated dibenzo-p-dioxins and furans: PCDD/Fs

Polychlorinated dibenzo-p-dioxins (PCDDs) and polychlorinated dibenzofurans (PCDFs), most known as dioxins and furans, comprise a family of unintentionally produced molecules, classified inside of the POPs group (section 1.1). The contamination problem associated with PCDD/Fs has been addressed since the 80s, with several countries involved in the fight to mitigate the PCDD/Fs emission (Fiedler, 2007), starting with the creation of release inventories (Harrad and Jones, 1992; Sheffield, 1985; Thomas and Spiro, 1995). Later on, in 2001, the Stockholm Convention on Persistent Organic Pollutants was established and came into force in 2004, with the aim of “protecting human health and the environment from persistent pollutants” by decreasing their discharge to the ecosystems (Fiedler, 2007). For involuntarily generated POPs like PCDD/Fs, it is necessary to take measures to mitigate their release from human sources with a final goal of the total elimination. In this way, the European Union approved the Regulation 850/2004/EC for the prohibition and minimization of PCDD/Fs release in a general way. More recently, several water policies included PCDD/Fs in their guidelines, the latest one, the 2013/39/EU (2013) which incorporated PCDD/Fs as priority substances, renewing the Regulations 2000/60/EC and 2008/105/EC (European Union, 2013). The maximum permissible levels by the EU in the Regulation 1881/2006 is between 1.5-12 pg g⁻¹ fat for different types of food, like milk or dairy products, meat or fish (European Union, 2006).

Homologues and congeners

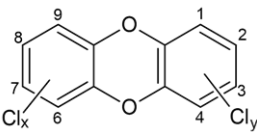
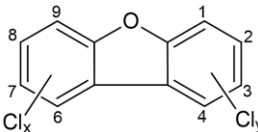
PCDD/Fs have pretty analogous structures (shown in Table 1.3), being a set of almost planar tricyclic aromatic molecules with practically the same physical and chemical properties, these are, low vapor pressure, high thermal stability, high solubility in organic or fat mediums (including human fatty tissues) and predisposition to bind to

the organic matter in soil and sediments (Fiedler, 2003). Because of their physicochemical properties and their biological stability they persist in the environment during huge periods of time, traveling through long distances, and being extensively disseminated throughout the ecosystems: air, soil, water, and sediments (Lee et al., 2022; Vallejo et al., 2015a; Weber et al., 2008).

Despite they are low water-soluble molecules, PCDD/Fs have been widely identified in several aquatic ecosystems, like rivers or lakes, due to several water discharges proceeding from agricultural and industrial sources, that may contain dioxins and furans precursors or even PCDD/Fs (Schröder et al., 2021). Due to their environmental presence, lipophilic nature, and persistent character, together with their intrinsic toxicity PCDD/Fs represent an issue of serious concern for living beings, because they can penetrate food (usually, in fatty foods such as fish/shellfish, meat or dairy products, vegetables, among others) (Fischer et al., 2011; Schröder et al., 2022). PCDD/Fs can cause diseases in human beings, for instance, immune disorders, reproductive and development difficulties, or even cancer, when long-term exposure takes place. In conformity with animal and human epidemiology data, tetrachlorodibenzo-p-dioxin (TCDD) was considered by the International Agency for Research on Cancer (IARC) as a “known human carcinogen” (World Health Organization, 2016).

A total number of 210 congeners of PCDD/Fs have been identified and classified into 75 PCDDs and 135 PCDFs. These congeners are classified depending on the number of chlorine atoms they can have attached; this is from no chlorine atoms up to eight. Congeners with an identical number of chlorine atoms are classified into groups named homologues; and in this way, PCDDs and PCDFs can be divided into various homologue groups. Table 1.3 details the different names and number of congeners of each homologue group (Kulkarni, 2019).

Table 1.3. PCDDs and PCDFs homologue classification.

PCDDs			PCDFs	
				
No. of Cl	Homologue group name	No. of congeners	Homologue group name	No. of congeners
1	Monochlorodibenzo-p-dioxin	2	Monochlorodibenzofuran	4
2	Dichlorodibenzo-p-dioxin	10	Dichlorodibenzofuran	16
3	Trichlorodibenzo-p-dioxin	14	Trichlorodibenzofuran	28
4	Tetrachlorodibenzo-p-dioxin	22	Tetrachlorodibenzofuran	38
5	Pentachlorodibenzo-p-dioxin	14	Pentachlorodibenzofuran	28
6	Hexachlorodibenzo-p-dioxin	10	Hexachlorodibenzofuran	16
7	Heptachlorodibenzo-p-dioxin	2	Heptachlorodibenzofuran	4
8	Octachlorodibenzo-p-dioxin	1	Octachlorodibenzofuran	1
TOTAL		75	TOTAL	135

Toxicity

The toxicity of the PCDD/Fs is determined by i) the position of the chlorine atoms in the molecule and, ii) the number of chlorine atoms present. Specifically, positions 2, 3, 7 and 8 deserve particular interest, because of their very toxic effects; and among all the possible combinations, 2,3,7,8-TCDD is the most toxic form of dioxin, is considered one of the most toxic unintentionally human-made compounds (Hites, 2011). Usually, dioxins and furans are present in a solution as a mixture of several isomers. To facilitate the toxicity assessment of the PCDD/Fs containing solutions, a series of toxic equivalency factors (TEFs) and toxic equivalents (TEQs) have been established. The total toxicity of a sample is related to the most toxic congener, 2,3,7,8-TCDD, being expressed as 2,3,7,8-TCDD TEQ concentration. Two different TEF scales exist: the International toxic equivalency factor (I-TEF), determined by a scientific research committee, the NATO Committee on the Challenge of Modern Society (NATO/CCMS), and a recent one, established due to a re-examination of the I-TEFs, the World Health Organization Toxic Equivalency Factors (WHO-TEFs), which incorporates PCBs (Van den Berg et al., 2006).

All these TEFs are summarized in Table 1.4. The concentration of PCDD/Fs is transformed into one value of TEQ of the isomer 2,3,7,8-TCDD; the final value is obtained by summing each congener concentration times its correspondent TEF; thus, giving a global view of the potential toxicity of the sample as shown in Eq. 1.1. where i and j correspond to the respective number of PCDD of PCDF congeners:

$$\text{TEQ} = \sum_i(\text{PCDD}_i \cdot \text{TEF}_i) + \sum_j(\text{PCDF}_j \cdot \text{TEF}_j) \quad (1.1)$$

In the United States, the US EPA through the SDWA determined first, a level of zero pg L^{-1} of 2,3,7,8-TCDD, but, considering the capability and costs to remove this compound, they updated the concentration to a more realistic value, with a maximum level of 30 pg L^{-1} (US EPA, 2013).

Table 1.4. Toxic equivalency factors for the 17 2,3,7,8-PCDD/Fs congeners of the PCDD/Fs.

PCDDs			PCDFs		
Congener	I-TEF	WHO-TEF 2005	Congener	I-TEF	WHO-TEF 2005
2,3,7,8-TCDD	1.0	1	2,3,7,8-TCDF	0.1	0.1
1,2,3,7,8-PeCDD	0.5	1	1,2,3,7,8-PeCDF	0.05	0.03
1,2,3,4,7,8-HxCDD	0.1	0.1	2,3,4,7,8-PeCDF	0.5	0.3
1,2,3,6,7,8-HxCDD	0.1	0.1	1,2,3,4,7,8-HxCDF	0.1	0.1
1,2,3,7,8,9-HxCDD	0.1	0.1	1,2,3,6,7,8-HxCDF	0.1	0.1
1,2,3,4,6,7,8-HpCDD	0.01	0.01	1,2,3,7,8,9-HxCDF	0.1	0.1
OCDD	0.001	0.0003	2,3,4,6,7,8-HxCDF	0.1	0.1
			1,2,3,4,6,7,8-HpCDF	0.01	0.01
			1,2,3,4,7,8,9-HpCDF	0.01	0.01
			OCDF	0.001	0.0003

Sources and generation

There are many different sources of PCDD/Fs generation, and in most cases, they are unintentionally formed as trace pollutants in many processes related to combustion. On the one hand, they are found in naturally occurring processes, such as the inadequate or incomplete combustion of forest fires, volcanic eruptions activity, or even in a

biological manner from chlorinated precursors (Kulkarni, 2019). On the other hand, they can be produced by human sources, which are considered the predominant ones, such as industrial activities. Nevertheless, the largest source of PCDD/Fs release to the environment in gas phase comes from the incineration of several wastes, for instance, municipal or hospital wastes, together with hazardous waste and sewage sludge incinerators, burning residues (mainly organic matter) with an elevated content of chlorine and metals (Bo et al., 2022; Kawamoto and Weber, 2021; Kulkarni, 2019). Likewise, wood burning or cement kilns, among other combustion processes are important PCDD/Fs release sources (Karstensen, 2008; Klima et al., 2020; Lavric et al., 2004; Richards and Agranovski, 2017). Due to the air transport, PCDD/Fs can be disseminated and transported to additional matrices called reservoirs, which embrace landfills and contaminated soils (Bo et al., 2022; Fiedler, 2003; Kawamoto and Weber, 2021; Klima et al., 2020; Kulkarni et al., 2008; Weber et al., 2008). Moreover, several biological and photochemical processes can be included. The action of microorganisms over chlorinated phenolic compounds results in the formation of dioxins under certain environmental conditions (OCDD and HpCDD can be formed by photolysis of pentachlorophenol) (Baker and Hites, 2000; Kulkarni, 2019; Kulkarni et al., 2008).

PCDD/Fs can be also released in aqueous phase, even though they are low water-soluble molecules. For example, the paper industry (pulp and paper mills) including pulp bleaching, gives rise to dioxins and furans formation due to the chlorination of natural phenolic compounds in the aqueous phase, present in wood pulp (Kawamoto and Weber, 2021; Wang et al., 2014; Xiao et al., 2017). Another common PCDD/Fs release source to aqueous systems is the metal industry, which involves several high-temperature processes to produce, for instance, iron or steel, principally in washing stages (Yang et al., 2020; Zou et al., 2012).

Finally, the manufacture of different chemical products, specifically chlorinated phenolic compounds, PCBs or phenoxy herbicides (well-known precursor compounds) can generate PCDD/Fs (Kulkarni et al., 2008; Sidhu and Edwards, 2002). Currently, the production of some of these chemical compounds is prohibited in several countries. For instance, the fabrication in Spain of γ -hexachlorocyclohexane, better known as lindane; however, the consequences of its production process are currently evident. During the 1980s, the residues from the manufacturing process of this compound were disposed of in illegal landfills, leading to the release of PCDD/Fs in the aquatic environment, in soils,

etc, yet present today (Gómez-Lavín et al., 2018). Figure 1.3 summarises the main sources of dioxins and furans formation.

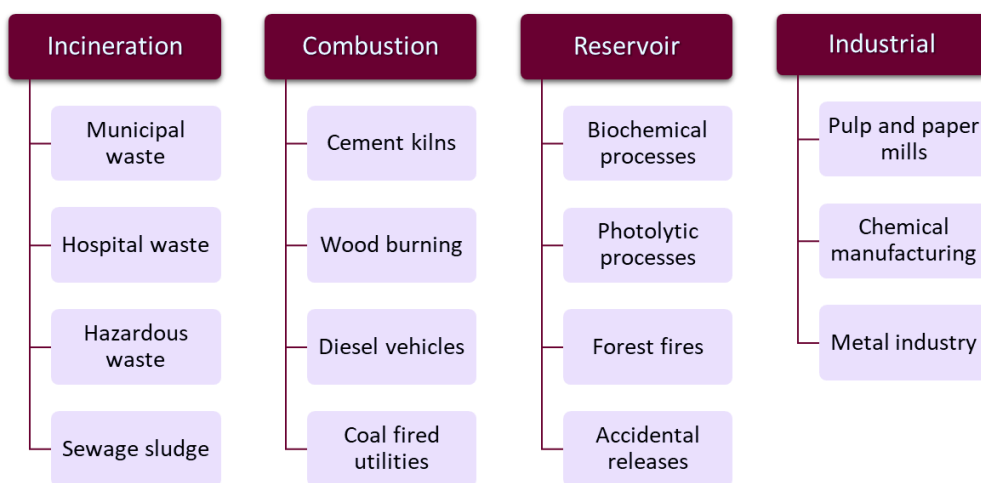


Figure 1.3. Main sources of PCDD/Fs formation.

Three main routes of PCDD/Fs formation are widely described in the literature (Zhang and Buekens, 2016) and resumed in Figure 1.4:

- i) the formation via the “*novo synthesis*”: this is the catalytic formation at low-medium temperatures (200-600 °C) through the degradation of carbon compounds in the presence of a chlorine source.
- ii) high temperature (>500 °C) pyrogenic processes, especially in the anoxic clouds which subsist to the flaming combustion. Dioxins and furans are formed through fast thermal reactions from a diversity of reactive gases.
- iii) formation through precursor compounds, such as chlorophenols (CPs) or chlorobenzenes (CBz) through the condensation of two molecules; or polychlorinated diphenyl ethers (PCDEs) and polychlorinated biphenyls (PCBs), during the application of oxidative/reductive remediation technologies (Addink and Olie, 1995; Vallejo et al., 2015a).

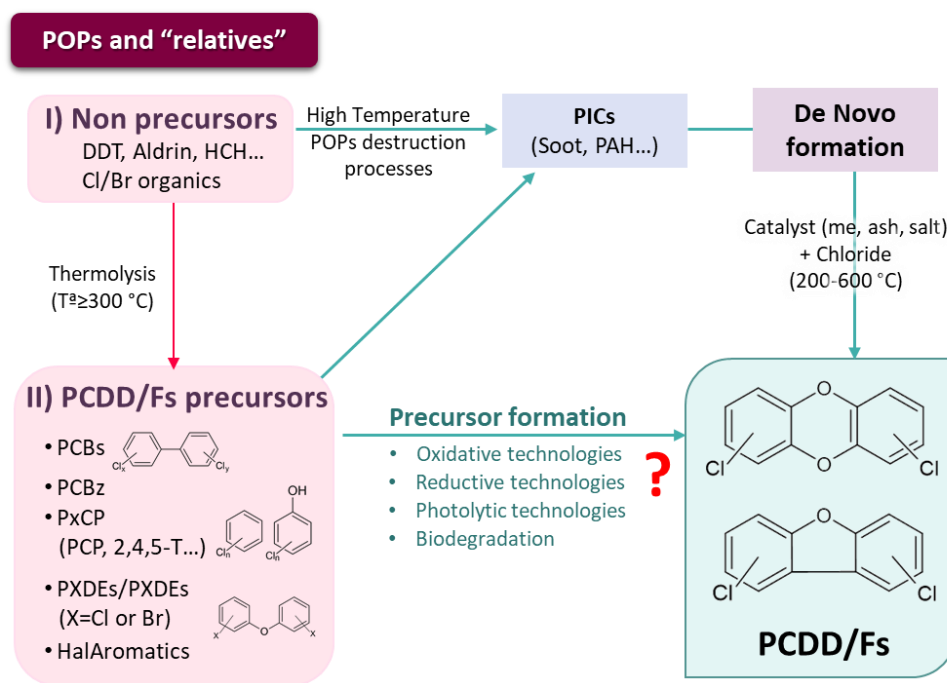


Figure 1.4. Potential PCDD/Fs formation pathways from POPs destruction. Adapted from Weber, (2007).

1.2. Advanced Oxidation Processes (AOPs)

As it has described in section 1.1.1, the presence of ECs in the environment is in constant increase. This is mainly attributable to the intensification of their use, the lack of effectiveness of wastewater treatment plants conventional treatments to eliminate them, and the absence of legislation, therefore releasing their ECs-containing effluents. The remediation of polluted environments and the conservation and protection of the healthiest ones has turned into a real necessity to avoid human health and ecosystem risks (Golovko et al., 2021; Sörengård et al., 2019; Zhou et al., 2019). This, in conjunction with the implementation of legislative policies of the governments, that contemplate regulation limits of ECs discharge, have led to the necessity of development of new technologies, able to destroy these types of pollutants from wastewaters. In this context, Advanced Oxidation Processes (AOPs) appear as promising technologies successfully applied in the last years, treating waters containing emerging organic pollutants such as PPCPs, perfluoroalkyl substances (PFAS), pesticides, or flame retardants, among other different compounds (Barisci and Suri, 2021; Kaplan et al., 2020; Marta Vallejo et al., 2013). Nowadays, the greatest challenge is to reach an equilibrium between the

operational costs (high consumption rates, chemical input) and the environmental implications caused by the application of these AOPs as by-products generation, carbon footprint, etc (Miklos et al., 2018).

AOPs can be defined as water oxidation technologies based on the formation of elevated concentrations of powerful oxidizing agents, such as hydroxyl radicals ($\cdot\text{OH}$) at sufficient concentration to successfully eliminate contaminants from water (Oturán and Aaron, 2014). $\cdot\text{OH}$ possess a high oxidation potential, between 1.55 V vs. NHE (basic medium) and 2.8 V vs. NHE (acidic medium), being highly reactive due to the unpaired electrons, and non-selective oxidizers (Wang and Xu, 2012). Among other advantages, $\cdot\text{OH}$ can be easily generated, they are harmless, and the rate of the reaction can be controlled. AOPs are all technologies where chain-reaction sequences take place, and usually involve radical cycle propagation once is formed (Wang and Xu, 2012).

AOPs can be classified depending on the method of $\cdot\text{OH}$ generation (Figure 1.5): i) electrochemical processes, which comprise anodic oxidation, electro-fenton, photo-electrocatalysis, photo-electrofenton, sono-electrofenton; ii) photolytic and photocatalytic processes, such as UV or UV/catalyst; iii) Fenton processes, like the conventional Fenton, or Fenton-combined processes, sono-Fenton or photo-fenton; iv) ozone based processes, which include ozonation, or heterogeneous and homogeneous catalytic ozonation, and finally v) other AOPs, like sonolysis, wet oxidation or supercritical oxidation.

The principal advantages of AOPs can be summed up as follows: non-selective oxidation, rapid degradation rates, easy implementation, no generation of solid residuals, lesser footprint or no need for regeneration to maintain the efficiency of the process (Linden and Mohseni, 2014; Priyadarshini et al., 2022). Nevertheless, even though AOPs possess the capacity to mineralise a large number of organic compounds, they can produce several unwanted by-products during the oxidation process. These by-products can be even more toxic than the parent compounds, so the final toxicity of the sample can be higher than the original. The formation of by-products can interfere with the treatment efficiency, increasing the capital costs and probably causing the need of applying another subsequent treatment to eliminate these by-products (Linden and Mohseni, 2014). In the case that the final by-products are biodegradable, their removal through a combination of different AOPs is advised, resulting in new greener technologies, however, this area is still in development (Sievers, 2011).

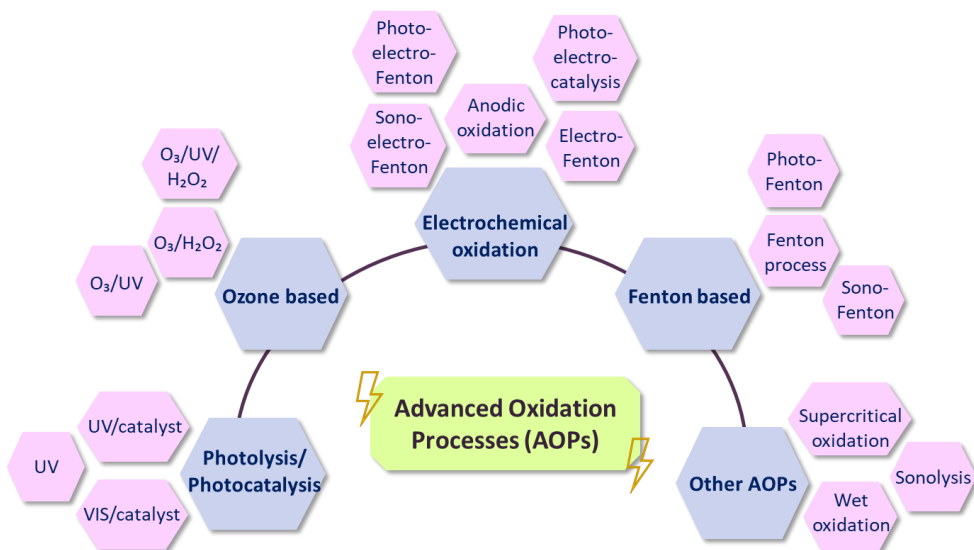


Figure 1.5. Main classification of the AOPs.

Among all AOPs, electrochemical oxidation (EOX) is a widely applied technology to remediate water contamination problem, just like it is reflected in the high number of works published during the last two decades (Sirés et al., 2014; Solá-Gutiérrez et al., 2018, 2019; Marta Vallejo et al., 2013). This technology is one of the cleanest as it relies in the role of electrons and the formation of radical species, so that; it does not require additional chemicals (for example, H_2O_2). EOX also presents high efficiency, is simple to automate, easy to handle (modular design), flexible (able to treat a long range of pollutant concentrations), and able to work in a safe environment, due to the atmospheric pressure and moderate temperature conditions needed (Duan and Sedlak, 2021; Muff, 2014; Sirés et al., 2014). Due to the advantages of this technology, as well as its high operational capacity in the removal of organic pollutants, electrochemical oxidation has been selected as the reference technology to carry out the study proposed in this doctoral thesis; potential PCDD/Fs formation during the electrochemical oxidation of aqueous samples containing pharmaceutical compounds used in the COVID-19 pandemic.

1.2.1. Electrochemical oxidation

Electrochemical oxidation, or anodic oxidation, is considered one of the greenest technologies, and easy to operate. It is based on redox chemistry produced when applying a potential difference (energy), high enough to establish an electron flux between the anode and the cathode of the electrochemical cell, thus, oxidizing the

chemical compounds (in the anode) through electron losing, and reducing other species formed (in the cathode), by electron gaining (Schröder et al., 2022).

Two different mechanisms can occur when electrochemical oxidation is applied to organic matter (Figure 1.6):

- i) Direct oxidation. The oxidation of the species take place after the adsorption on the anode surface, due to the direct exchange of electrons between the organic matter and the anode. First, the organic matter diffuses through the anode surface, and then it is oxidized.
- ii) Indirect oxidation. The species can exchange electrons producing electroactive species, generated on the anode surface, which oxidize the organic matter. One of the main reactions that take place is the $\cdot\text{OH}$ formation from water. Depending on the medium, other typical species that can be formed are sulphate and chlorine radicals, produced when chloride and sulphate species are present in the solution. These other radicals also contribute to the oxidation process helping to the $\cdot\text{OH}$ radicals in the pollutants' degradation (Panizza and Cerisola, 2009).

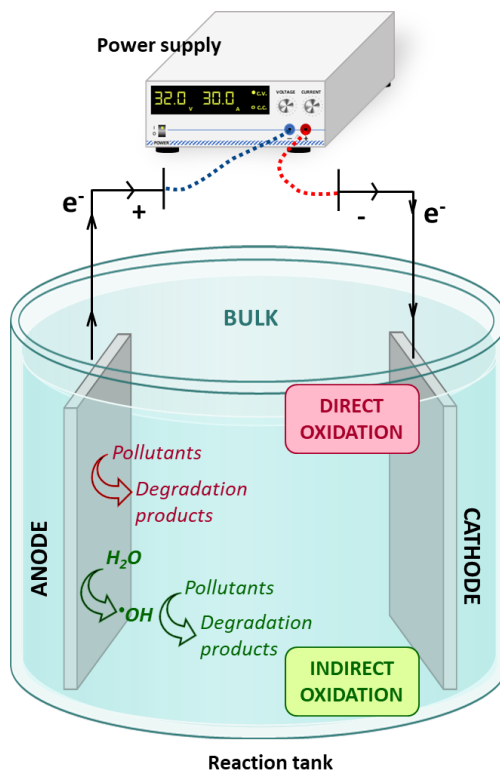


Figure 1.6. Electro-oxidation mechanisms: direct and indirect oxidation.

Among other operating parameters in electrochemical oxidation, the electrode material is one of the key variables, due to the strong influence on the selectivity and effectiveness of the electrochemical processes. The anode must have the following characteristics: high physicochemical stability, enough electrical conductivity, low cost, and high durability. Generally, the most employed materials are graphite-based (BDD, activated carbon fibre (ACF), glassy carbon or graphite), mixed metal oxides (MMO) of Ti, Ru, Ir, Sn, Ta and/or Sb. Moreover, another type of anodes are those known as DSA-type electrodes (Dimensionally Stable Anodes). DSA consists of a Ti substrate coated with a layer of metal oxide or MMO (Martínez-Huitle et al., 2015). The most common materials for cathode are carbon-based ones (carbon felt, reticulated vitreous carbon or graphite) or stainless steel (Muff, 2014; Sirés et al., 2014).

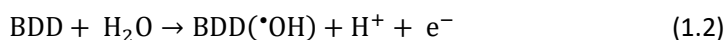
The interaction, between $\cdot\text{OH}$ radicals and the anode surfaces, has great importance for the activity of electrodes, which can be classified into “active anodes” or “non-active anodes”. Active anodes are composed of materials that possess oxidation states, so they can interact in a stronger way with the adsorbed $\cdot\text{OH}$ (chemisorption), producing metal oxides with high oxidation states. Conversely, non-active anodes form physisorbed active oxygen ($\cdot\text{OH}$) due to a weak interaction between the anode and the $\cdot\text{OH}$ radicals, helping in the complete mineralization of the organic compounds (Muff, 2014). For these types of electrodes, $\cdot\text{OH}$ cannot react with the components of their surface. For a while, they can oxidize also other species such as anions contained in bulk solution, which explains the formation of radical species and the rise in effectiveness in the production of oxidants (Sirés et al., 2014). Examples of non-active anodes are antimony-doped tin oxide (ATO), lead oxide (PbO_2), or boron-doped diamond (BDD), which have a high oxygen evolution potential. These non-active anodes can also be combined with other metals, e.g., BDD in Nb substrate, Nb/BDD. In Table 1.5 is depicted the classification of various anode materials according to their oxidation potential in acid medium. The anodes marked as $\text{DSA}^{\text{®}}\text{-Cl}_2$ and $\text{DSA}^{\text{®}}\text{-O}_2$ are usually employed in the chlor-alkali industry and the water electrolysis, respectively.

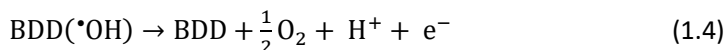
Table 1.5. Oxidation potential of several anode materials in acid media. Adapted from Martínez-Huitle et al. (2015) and Muff (2014).

Anode composition	Oxidation potential (V)	Overpotential of O ₂ evolution (V)	Adsorption enthalpy of M-•OH
RuO ₂ -TiO ₂ (DSA [®] -Cl ₂)	1.4-1.7	0.18	Chemisorption of •OH
IrO ₂ -Ta ₂ O ₅ (DSA [®] -O ₂)	1.5-1.8	0.25	
Ti/Pt	1.7-1.9	0.30	⋈
Ti/PbO ₂	1.8-2.0	0.50	⋈
Ti/SnO ₂ - Sb ₂ O ₅	1.9-2.2	0.70	
p-Si/BDD	2.2-2.6	1.3	Physisorption of •OH

Lately, BDD has attracted a lot of interest because it has been found as the most effective anode material to degrade recalcitrant compounds during electrochemical oxidation. BDD anode possesses the loosest interaction with the large amounts of generated •OH radicals, being the electrode with the highest oxidation power and thus, having a great reactivity to organics oxidation. It has been proven its effectiveness towards pharmaceuticals, pesticides, surfactants or phenols, among other ECs (Martínez-Huitle et al., 2015). This material possesses such good properties, as great chemical and electrochemical stability, low adsorption capacities (thus, preventing fouling), extended lifetime, very low capacitance and the largest potential window measured in aqueous electrolytes (Donoso et al., 2021; Luong et al., 2009). Moreover, BDD anodes have an important feature, a very high overpotential for both oxygen and hydrogen evolution (Luong et al., 2009). On the contrary, BDD anodes also have some drawbacks, such as their susceptibility to deactivation by anodic corrosion, or their high cost, due to the elevated content in diamond and boron (10^{18} – 10^{21} atom cm³) (Luong et al., 2009; Martínez-Huitle et al., 2015).

•OH radicals are formed in the region of water discharge. The EOX of water molecules takes place via a sequence of one-electron reactions, giving rise to •OH generation, via Eq. 1.2, using BDD anode. After this, •OH takes part in the transformation of organic compounds (R) to CO₂ and water (Eq. 1.3). Further, the reaction between R and •OH (Eq. 1.3) competes with the •OH radicals discharge in the anode to produce oxygen (Eq. 1.4) (Muff, 2014).





Due to BDD belonging to the non-active anodes -the weak adsorption of $\cdot\text{OH}$ on the anode surface, complete mineralization of the pollutants can be reached (Eq. 1.3).

1.3. Intermediate by-products formed during the application of AOPs

Even though AOPs have been successfully applied to the elimination of many emerging contaminants in aqueous media, occasionally, because of incomplete mineralization of the parent organic compounds, other chemicals can be generated in an unintentional manner, and sometimes, they are even more toxic than the initial compounds. The application of AOPs to pharmaceutical compounds' containing aqueous matrices has been extensively studied in the last decades, paying special attention to the experimental conditions, and to a lesser extent, to the formation of undesired by-products. Between some of these by-products, benzenes or phenols can be found, with their chlorinated products, formed when oxidation takes place in a chloride medium. It is well known that these groups of substances can take the role of precursors of the toxic compounds PCDD/Fs (Fernández-Castro et al., 2016; Solá-Gutiérrez et al., 2019, 2018; Vallejo et al., 2015a, 2014).

In previous works carried out in this research line, it was corroborated the presence and formation of PCDD/Fs when treating aqueous matrices with chlorophenols in solution, by means of AOPs; Vallejo et al. (2015b) summarized the main compounds which act as PCDD/Fs precursors, when applying photolytic and photocatalytic treatments, Fenton or electrochemical oxidation, such as chlorophenols, chloronitrobenzene and triclosan (5-chloro-2-(2,4-dichlorophenoxy) phenol). Moreover, they were corroborated that, applying electrochemical oxidation and Fenton treatment to 2-chlorophenol (2-CP) containing solutions, higher PCDD/Fs amounts were generated in comparison with the initial samples, reaching values up to 390 ng L⁻¹ of total PCDD/Fs concentration (Fernández-Castro et al., 2016; Marta Vallejo et al., 2013; Vallejo et al., 2014, 2015a). Later on, electrochemical oxidation, as well as photolytic and photocatalytic remediation treatments were employed to treat solutions containing triclosan (Schröder et al., 2021, 2020; Solá-Gutiérrez et al., 2019, 2018), finding various PCDD/Fs precursors, such as (2,4-dichlorophenol or catechol, which gave rise to high

concentrations of dioxins and furans. All these previously studied molecules contain chlorine atoms in their structure, if besides they are present in a chlorine medium, PCDD/Fs formation is even more favoured.

Entering the pharmaceutical compounds use to fight against the virus SARS-CoV-2 and its symptoms, starting with dexamethasone, there are not many studies about its degradation, and therefore, their degradation by-products have also not been investigated in depth. Its degradation has usually been carried out by different types of photolytic/photocatalytic treatments, which achieved pretty good results in terms of degradation (Calza et al., 2001; Cantalupi et al., 2020; da Silva et al., 2016, 2015; Ghenaatgar et al., 2019; Guo et al., 2017; Markic et al., 2018; Pazoki et al., 2016; Pretali et al., 2021; Rasolevandi et al., 2019). Other authors applied different AOPs, for instance, electrochemical oxidation, employing EOX with a BDD anode (Grilla et al. 2021), or applying bio-electrochemical treatment (Guo et al., 2021). In all cases, poorly addressed degradation pathways were identified, along with the corresponding by-products. Quaresma et al., (2021), study the ozonation process, in addition to the chlorination process. In some cases, degradation mechanisms have been proposed. During the degradation process, one of the most detected dexamethasone by-products is prednisolone, together with different variations of the initial DEX, or the hydroxylation of the DEX molecule (Grilla et al., 2021; Guo et al., 2017; Quaresma et al., 2021; Rasolevandi et al., 2019).

The electrochemical oxidation of amoxicillin and paracetamol has been further studied, with increasing interest in the last few years. Among the most common by-products formed in different electrochemical treatments, hydroquinone and benzoquinone or the chlorinated molecular structure of the parent compound are worth mentioning, which can lead to chlorophenol derivatives through the cleavage of the main molecule (Ganiyu et al., 2019, 2016; Le et al., 2017; Liu et al., 2019a; Olvera-Vargas et al., 2018; Waterston et al., 2006; Zhang et al., 2018). Some authors also observed various hydroxylated by-products, commonly different hydroxylation of the parent compound, both in the amoxicillin and the paracetamol when applying EOX or EOX-combined treatments (Frontistis et al., 2017; Ganiyu et al., 2019; Kaur et al., 2019a, 2019b; Pan et al., 2020; Pan and Sun, 2021; Tan et al., 2020). In particular, Kaur et al., 2019a and 2019b, found chlorinated derivatives during the EOX treatment of amoxicillin, using Ti/RuO₂ anodes, with NaCl as electrolyte. Zhang et al. (2018) found 2-chlorohydroquinone during the electrocatalytic degradation of paracetamol; meanwhile, Liu et al. (2019) observed, also during paracetamol degradation, the chlorination of the phenolic ring, employing

Na₂SO₄ and NaCl in conjunction with the electrolyte medium and using graphite electrodes.

Currently, there is a lack of sertraline degradation studies. Commonly, various photo-remediation treatments have been applied and studied, but their by-products generation has not been sufficiently analysed. Sertraline is the only studied molecule in this doctoral thesis that possess chlorine atoms in its structure, making it a potential PCDD/Fs precursor. Thereby, Jiménez-Holgado et al. (2021) during the degradation by photo-transformation of sertraline found 3,4-dichlorophenol. Various hydroxylated by-products of the parent compound, mono-, di-, or tri-hydroxylated sertraline, were also detected after the application of photo-transformation technologies (Bojanowska-Czajka et al., 2022; Calza et al., 2021; Jakimska et al., 2014; Jiménez-Holgado et al., 2021) or during biotransformation of sertraline (Gornik et al., 2020).

In this way, it is a matter of great interest to have adequate knowledge of the formation of these by-products during the application of oxidation processes, which will allow assessing properly a successful degradation of ECs, minimizing the final toxicity of the samples. As far as the author's knowledge, the formation of PCDD/Fs from the degradation of dexamethasone, amoxicillin, paracetamol, and sertraline, pharmaceuticals used in the fight against covid COVID-19, has not been reported in the literature, so this study has an important novel character, whose results will be key for the treatment of wastewater containing, at least, four of the main drugs used in the first global pandemic of the last 100 years.

1.4. The role of computational chemistry in the development of PCDD/Fs formation mechanisms

Computational chemistry is a branch of chemistry that employ mathematical methods to study and resolve chemical problems through the application of techniques and computational simulations of molecular systems automated for its execution on a computer (Young, 2001a). It uses theories, concepts, and models of theoretical chemistry, based on physical treatments of matter from classical physics, quantum and mechanics statistical, incorporated into scientific software, specially designed to calculate the structure and/or static and dynamic properties of molecules and molecular aggregates in the gaseous state and in solution and of solid bodies. In the late 70s, computational chemistry appears as a molecule design tool, impulsed by pharmaceutical companies. Nowadays, it is more appreciated as a prediction tool, helping to a better

understanding and facilitating the chemical development of many processes. Due to the fast advance in computer science, along with the development of more refined commercial programs, the implementation of computational methods and more precise basis sets (a set of functions combined to create molecular orbitals) had led to an improvement of the modelling possibilities. The applications of computational chemistry can be diverse, from simulation and prediction the structure and compound properties, to more precise calculations, being very useful in various fields, like organic, inorganic, and analytical chemistry or biochemistry. Thanks to computational chemistry, researchers can deepen into the determination of different parameters, such as molecular geometry, the energy of the molecule and the transition states, calculation of different spectra (IR, UV and NMR) or the interactions between a substrate with an enzyme, among other possibilities (Lewars, 2011). The employment of computational chemistry has led to get faster results, and also, the elimination of an important part of the experimental work, and with this, a laboratory costs reduction, appearing as an eco-friendly tool. Furthermore and added to the previous facts, there are some atomic parameters that are experimentally impossible to obtain, making indispensable the help of this growing science (Cuevas and Cortés, 2003; Young, 2001a).

Inside computational chemistry, quantum chemistry (QC) studies the characteristics and the behaviour of atomic and subatomic particles and implies the determination of an electronic structure, by solving the Schrödinger equation (Lam et al., 2020). QC describes the molecule with direct treatment of the electronic structure; however, to achieve good results for applications of practical interest different approximations are necessary, classified as follows, (Lam et al., 2020; Lewars, 2011):

- i. *ab initio* approach (or wave function theory; WFT), based on the Schrödinger equation (Eq. 1.5) (Kantz and Schreiber, 2004), and hence, on how the electrons are moving in each molecular orbital, evaluates the energy and the electronic distribution in the molecule. These types of calculations are quite slow.

$$\nabla^2\Psi + \frac{8\pi^2m}{\hbar^2}(E - V)\Psi = 0 \quad (1.5)$$

where ∇^2 is the Laplacian operator (Eq. 1.6), Ψ the probability wave function, defined over space and time (Eq. 1.7), m the mass of the particle, \hbar the Plank's constant, E the total energy and V the potential energy influencing the particle.

$$\nabla^2 = \frac{\partial^2}{\partial x^2} + \frac{\partial^2}{\partial y^2} + \frac{\partial^2}{\partial z^2} \quad (1.6)$$

$$\text{Prob}(V) = \int_V \Psi^2 \cdot dx \cdot dy \cdot dz \quad (1.7)$$

- ii. density functional theory method (DFT). It is a relatively new method (1980's), based on the Schrödinger equation as well. Here, the electron distribution is determined without defining the wave function, so the energy is calculated based on the charge or the total electron density (measurable value by X-ray diffraction or electron diffraction). Is by far the most extensively applied theoretical method. In DFT, the functional is the electron density, which is function of the space and time. The "functional" is a function that takes functions as its argument; that is, a function whose domain is a set of functions (Graves, 1948).
- iii. semiempirical approach, is based on the Hartree-Fock formalism, having a Hamiltonian and a wave function. In this context, certain parts of information (commonly some costly calculations, such as two-electron integrals) are approximated or omitted by parametrization with experimental data, or more precisely *ab initio* data. The results are not as rigorous as *ab initio* and DFT calculations (Young, 2001b).

Commonly, semiempirical methods are employed for bigger molecules, meanwhile, *ab initio* and DFT are suggested for the research of small-scale molecules. These last two methods are normally employed for quantum chemical calculations, achieving great reliability in obtained values (Lewars, 2011). Deepening into DFT, despite that it is a simple function that just depends on "x, y, z", it contains all the information of the system. Thus, it is possible to calculate the total number of electrons by the integration of the electronic density into the whole space. The local maximum corresponds to the position of the atomic nucleus, and it is possible to calculate the nucleus charge, so the electronic density would be enough to calculate the energy of the system (Jensen, 2007).

The calculations employing DFT require less computational time than other advanced *ab initio* methods (which commonly use bigger basis sets), reaching the same accuracy, even though DFT uses larger basis sets. So, it is possible to apply both theories to acquire information about bond energies, ideal-gas thermochemistry, adsorption, solvation, reaction kinetics, properties of materials and analytical information. The most used family of computational methods is DFT with the functional B3LYP as the dominating DFT approach (Becke, three-parameter, Lee-Yang-Parr exchange-correlation functional), and the functional Minnesota M06 in the second place (Lam et al., 2020).

These two functionals are normally *less demanding* and suitable enough for structural optimizations.

Owing to the elevated toxicity of dioxins and furans, it is of great interest to know the principal formation pathways involved in the transformation from oxidation intermediates, such as precursor or not precursor compounds in chloride presence, to PCDD/Fs, with the aim of avoiding their formation after applying oxidation processes. This knowledge will let to select the operating variables of the oxidation process more adequately in order to avoid the PCDD/Fs formation. Accordingly, several authors proposed and studied the most hypothetical formation pathways, considering the energetic barriers, from precursor molecules such as chlorophenols, catechol, phenols or chlorobenzenes, among others (Xu et al., 2010; Yang et al., 2017; Zhang et al., 2010, 2014). But typically, the published works focus on gas phase reactions (both homogeneous and heterogeneous), being the studies referring to aqueous phase still scarce.

1.5. Background, thesis scope and outline

This PhD thesis has been carried out in the framework of the investigation line “Potential formation of PCDD/Fs during the treatment aqueous matrices by AOPs”, followed in the last years within the Sustainable Process Engineering group (SPE) and the Advanced Separation Processes group (ASP), of the Department of Chemical and Biomolecular Engineering of the University of Cantabria. This research line focuses on the evaluation of the potential formation of PCDD/Fs in different aqueous matrices after applying remediation technologies, like AOPs. In particular, the aqueous matrices to treat are characterised by containing direct precursors or not precursors -such as organic compounds in chloride medium- of dioxins and furans. Therefore, they may be able to produce the potential formation of the PCDD/Fs, and as consequence, an increase in the final toxicity of the sample. So, the proper evaluation of the matrix, the technology to be applied and the operating conditions to apply, are key to the implementation of AOPs as wastewater treatment technologies.

The start of this investigation line came from the hand of the PhD thesis of Vallejo (2014). Vallejo et al. (2015a, 2014, 2013) focused on the PCDD/Fs formation during the electrochemical and Fenton oxidation of the direct precursor 2-chlorophenol (2-CP) containing solutions, corroborating their formation, and its variation in quantity when modifying the operating conditions. Furthermore, as a case study, the application of

electrochemical and Fenton oxidation to landfill leachates, which contains also a lot of precursor compounds, and the assessment of PCDD/Fs together with the toxicity analysis, has been carried out (Vallejo et al., 2013). Continuing with this precursor, the PhD thesis of Fernández-Castro (2017) studied the dioxins and furans formation and its variation in terms of quantity during Fenton oxidation of 2-CP solutions, analysing the influence of the operating variables such as concentration H_2O_2 , Fe^{2+} and temperature. The quantification of the non-chlorinated and low chlorinated CDD/Fs was carried out for the first time in AOPs application. This thesis went one step further, studying the role of reactive oxygen species (ROS) in AOPs (Fernández-Castro et al., 2015). The work of Fernández-Castro (2017) is the first study of this investigation line, where the computational chemistry was employed, developing a mechanistic study of the PCDD/Fs formation was performed from 2-CP molecule (Fernández-Castro et al., 2016). Based on the results obtained so far, Solá-Gutiérrez (2019) used a more complex direct precursor, widely used as a disinfectant and the electrochemical oxidation and photolytic technologies, equally corroborated the formation of dioxins and furans, to a greater or lesser extent, depending on the operating conditions of these processes. In addition, the obtained results showed that it is not possible to determine dioxins and furans with a low degree of chlorination using the EPA 1613 method, given their potential formation in the high-performance gas chromatograph, due to the high temperatures of the injector and low molecular weights of these compounds (San-Román et al., 2020; Solá-Gutiérrez et al., 2020, 2019, 2018).

Gathering all the experimental results, and the advance in knowledge that has been obtained in this line of research, with the aim of validating the hypothesis regarding the formation of PCDD/Fs in aqueous media containing organic compounds -in chloride presence-, this doctoral thesis has delved into the behaviour of emerging pollutants, generated as a consequence of high consumption of drugs or disinfectants, etc, not precursors of dioxins and furans.

Until now, the treatment applied in the fight against the SARS-CoV-2 virus, has led to an intensive consumption of the determined drugs, which are finally ending in the aquatic medium, as Emerging Contaminants (EC). So, in this PhD thesis, it is proposed to study the formation of dioxins and furans, from compounds which are not precursors. With the aim to make a step forward in the knowledge, for this investigation, aqueous matrices containing traces of drugs employed in the fight against COVID-19, dexamethasone, amoxicillin, paracetamol and sertraline, have been selected. Together with the efficiency of the treatment of the primary compound, on the one hand, the

potential formation of by-products or intermediates and PCDD/Fs has been studied, followed by the analysis of the formation and degradation mechanisms. This development has been carried out both in experimentally and theoretically manner, using computational chemistry. In this sense, this doctoral thesis is constituted by five chapters that have allowed to reach the proposed objectives, confirming the starting hypothesis, and whose content is shown below.

Chapter 1 gives an overview of water situation worldwide, within the framework of the global pandemic COVID-19. Moreover, it is presented a brief classification of the pharmaceutical and personal care products group (PPCPs), deepening into the pharmaceuticals (drugs), with a special focus on those related with COVID-19. In this context, the advanced oxidation processes (AOPs) are presented, highlighting the Electrochemical oxidation (EOX). Then, the polychlorinated dibenzo-p-dioxins and furans (PCDD/Fs) are addressed, along with their toxicity issue and generation sources. To end, the background, scope, outline and objectives of this PhD thesis are described.

Chapter 2 details all the chemical reagents employed to perform the experiments, as well as the laboratory equipment, both for the experiments and the measurement of the samples. Moreover, the analytical methods and techniques, used to analyse the different types of samples -drugs degradation experiments, intermediates experiments- are detailed. EPA 1613 method, employed for the PCDD/FS analysis is deeply described. Finally, the working methodology employed in Computational Chemistry to obtain the theoretical reaction mechanisms about the PCDD/Fs formation, is explained.

Chapter 3 reports the results of electrochemical oxidation experiments using BDD anodes, performed to remediate solutions with the COVID-19 related pharmaceutical compounds. It is detailed the influence of two electrolyte mediums, NaCl and, Na₂SO₄ combined with NaCl. Furthermore, the identification of the intermediate compounds formed during electro-oxidation of these four drugs, along with the kinetic analysis of their formation/degradation has been carried out. In addition, a theoretical analysis of the radical's formation chloride and sulphate in order to understand the behaviour of the degradation kinetics of each drug has been carried out.

Chapter 4 develops the analysis of the PCDD/Fs generated during the EOX-Drugs experiments, both for homologues and congeners, depending on the electrolyte medium used, deepening into their distribution and in the lesser or greater degree of chlorination. With this, the toxicity assessment in terms of TEQ has been performed for the degradation of each drug. Finally, an alternative methodology for TEQ calculation

has been proposed from the specific case study about the photocatalytic oxidation of triclosan (TCS), starting with a multivariable analysis and after the application of multiple linear regression, five new models were obtained.

Chapter 5 describes in a theoretically manner using computational chemistry, and specifically, the density functional theory (DFT), the possible PCDD/Fs formation pathways from the breakage of the drugs amoxicillin (AMX), paracetamol (PAR) and sertraline (STR), and of the by-products generated, after applying electrochemical oxidation (EOX). For this, a combined mechanism consisting of two steps has been proposed. 1st step is the breakage of the drugs, and the 2nd step is intermediate and final molecules formation. Finally, the energy profile of each mechanism has been calculated, which helped to describe the mechanisms.

Chapter 6 summarizes the main conclusions obtained in this doctoral thesis, and also some possible challenges for future work are set out.

This PhD thesis has been developed within the Project CTM2017-87740-R (AEI/FEDER, UE) “Aplicación de Tecnologías Ambientales a Matrices Líquidas Conteniendo Contaminantes Orgánicos Emergentes Precursores de la Formación de Derivados Clorados (PCDD/Fs)”, and the associated FPI research fellowship (PRE2018-083526), provided by the Spanish Ministry of Science, Innovation and Universities.

Thanks to this financial aid, a predoctoral short stay have been conducted. This research stay was developed in the Department of Chemistry and Biochemistry, “Faculdade de Ciências da Universidade do Porto” (Porto, Portugal) over the period January 28th-May 3rd 2022, under the supervision of Dr. Pedro Alexandrino Fernandes and Dr. Pedro Ferreira.

1.6. References

- Addink, R., Olie, K., 1995. Mechanisms of Formation and Destruction of Polychlorinated Dibenzop-dioxins and Dibenzofurans in Heterogeneous Systems. *Environ. Sci. Technol.* 29, 1425–1435. <https://doi.org/10.1021/es00006a002>
- Adebisi, Y.A., Jimoh, N.D., Ogunkola, I.O., Uwizeyimana, T., Olayemi, A.H., Ukor, N.A., Lucero-Prisno, D.E., 2021. The use of antibiotics in COVID-19 management: a rapid review of national treatment guidelines in 10 African countries. *Trop. Med. Health* 49. <https://doi.org/10.1186/s41182-021-00344-w>
- Arnnok, P., Singh, R.R., Burakham, R., Pérez-Fuentetaja, A., Aga, D.S., 2017. Selective Uptake and Bioaccumulation of Antidepressants in Fish from Effluent-Impacted Niagara River. *Environ. Sci. Technol.* 51, 10652–10662. <https://doi.org/10.1021/acs.est.7b02912>
- Ávila, C., García, J., 2015. Pharmaceuticals and Personal Care Products (PPCPs) in the Environment and Their Removal from Wastewater through Constructed Wetlands. *Compr. Anal. Chem.* 67, 195–244. <https://doi.org/10.1016/B978-0-444-63299-9.00006-5>
- Baker, J.I., Hites, R.A., 2000. Is combustion the major source of polychlorinated dibenzop-dioxins and dibenzofurans to the environment? A mass balance investigation. *Environ. Sci. Technol.* 34, 2879–2886. <https://doi.org/10.1021/es9912325>
- Barisci, S., Suri, R., 2021. Removal of polyfluorinated telomer alcohol by Advanced Oxidation Processes (AOPs) in different water matrices and evaluation of degradation mechanisms. *J. Water Process Eng.* 39, 101745. <https://doi.org/10.1016/j.jwpe.2020.101745>
- Bo, X., Guo, J., Wan, R., Jia, Y., Yang, Z., Lu, Y., Wei, M., 2022. Characteristics, correlations and health risks of PCDD/Fs and heavy metals in surface soil near municipal solid waste incineration plants in Southwest China. *Environ. Pollut.* 298, 118816. <https://doi.org/10.1016/j.envpol.2022.118816>
- Bojanowska-Czajka, A., Pyszynska, M., Majkowska-pilip, A., 2022. Degradation of Selected Antidepressants Sertraline and Citalopram in Ultrapure Water and Surface Water Using Gamma Radiation.
- Calza, P., Jiménez-Holgado, C., Coha, M., Chrimatopoulos, C., Dal Bello, F., Medana, C., Sakkas, V., 2021. Study of the photoinduced transformations of sertraline in aqueous media. *Sci. Total Environ.* 756, 143805. <https://doi.org/10.1016/j.scitotenv.2020.143805>
- Calza, P., Pelizzetti, E., Brussino, M., Baiocchi, C., 2001. Ion trap tandem mass spectrometry study of dexamethasone transformation products on light activated TiO₂ surface. *J. Am. Soc. Mass Spectrom.* 12, 1286–1295. [https://doi.org/10.1016/S1044-0305\(01\)00319-1](https://doi.org/10.1016/S1044-0305(01)00319-1)

- Cantalupi, A., Maraschi, F., Pretali, L., Albini, A., Nicolis, S., Ferri, E.N., Profumo, A., Speltini, A., Sturini, M., 2020. Glucocorticoids in freshwaters: Degradation by solar light and environmental toxicity of the photoproducts. *Int. J. Environ. Res. Public Health* 17, 1–15. <https://doi.org/10.3390/ijerph17238717>
- Cappelli, F., Longoni, O., Rigato, J., Rusconi, M., Sala, A., Fochi, I., Palumbo, M.T., Polesello, S., Roscioli, C., Salerno, F., Stefani, F., Bettinetti, R., Valsecchi, S., 2022. Suspect screening of wastewaters to trace anti-COVID-19 drugs: Potential adverse effects on aquatic environment. *Sci. Total Environ.* 824, 153756. <https://doi.org/10.1016/j.scitotenv.2022.153756>
- Castillo-Zacarías, C., Barocio, M.E., Hidalgo-Vázquez, E., Sosa-Hernández, J.E., Parra-Arroyo, L., López-Pacheco, I.Y., Barceló, D., Iqbal, H.N.M., Parra-Saldívar, R., 2021. Antidepressant drugs as emerging contaminants: Occurrence in urban and non-urban waters and analytical methods for their detection. *Sci. Total Environ.* 757. <https://doi.org/10.1016/j.scitotenv.2020.143722>
- Cuevas, G., Cortés, F., 2003. *Introducción a la química computacional*, 1st ed. Fondo de Cultura Económica.
- da Silva, W.L., Lansarin, M.A., dos Santos, J.H.Z., Da Rocha, Z.N., Pepe, I.M., 2016. Electrochemical and Catalytic Studies of a Supported Photocatalyst Produced from Petrochemical Residue in the Photocatalytic Degradation of Dexamethasone and Guaifenesin Drugs. *Water. Air. Soil Pollut.* 227. <https://doi.org/10.1007/s11270-016-2932-x>
- da Silva, W.L., Lansarin, M.A., Livotto, P.R., dos Santos, J.H.Z., 2015. Photocatalytic degradation of drugs by supported titania-based catalysts produced from petrochemical plant residue. *Powder Technol.* 279, 166–172. <https://doi.org/10.1016/j.powtec.2015.03.045>
- Deblonde, T., Cossu-Leguille, C., Hartemann, P., 2011. Emerging pollutants in wastewater: A review of the literature. *Int. J. Hyg. Environ. Health* 214, 442–448. <https://doi.org/10.1016/j.ijheh.2011.08.002>
- Dehm, J., Singh, S., Ferreira, M., Piovano, S., Fick, J., 2021. Screening of pharmaceuticals in coastal waters of the southern coast of Viti Levu in Fiji, South Pacific. *Chemosphere* 276, 130161. <https://doi.org/10.1016/j.chemosphere.2021.130161>
- Díaz-Camal, N., Cardoso-Vera, J.D., Islas-Flores, H., Gómez-Oliván, L.M., Mejía-García, A., 2022. Consumption and occurrence of antidepressants (SSRIs) in pre- and post-COVID-19 pandemic, their environmental impact and innovative removal methods: A review. *Sci. Total Environ.* 829. <https://doi.org/10.1016/j.scitotenv.2022.154656>
- Donoso, G., Dominguez, J.R., González, T., Correia, S., Cuerda-Correa, E.M., 2021. Electrochemical and sonochemical advanced oxidation processes applied to tartrazine removal. Influence of operational conditions and aqueous matrix. *Environ. Res.* 202. <https://doi.org/10.1016/j.envres.2021.111517>

-
- Duan, Y., Sedlak, D.L., 2021. An electrochemical advanced oxidation process for the treatment of urban stormwater. *Water Res.* X 13, 100127. <https://doi.org/10.1016/j.wroa.2021.100127>
- Dulio, V., van Bavel, B., Brorström-Lundén, E., Harmsen, J., Hollender, J., Schlabach, M., Slobodnik, J., Thomas, K., Koschorreck, J., 2018. Emerging pollutants in the EU: 10 years of NORMAN in support of environmental policies and regulations. *Environ. Sci. Eur.* 30. <https://doi.org/10.1186/s12302-018-0135-3>
- Enners, S., Gradl, G., Kieble, M., Böhm, M., Laufs, U., Schulz, M., 2021. Utilization of drugs with reports on potential efficacy or harm on COVID-19 before, during, and after the first pandemic wave. *Pharmacoepidemiol. Drug Saf.* 30, 1493–1503. <https://doi.org/10.1002/pds.5324>
- EU, 2022a. COMMISSION IMPLEMENTING DECISION (EU) 2022/1307 of 22 July 2022 117–121.
- EU, 2022b. Proposal for a Directive amending the Water Framework Directive, the Groundwater Directive and the Environmental Quality Standards Directive 0344.
- EU, 2020. Commission Implementing Decision (EU) 2020/1161-4 August 2020-establishing a watch list of substances for Union-wide monitoring in the field of water policy pursuant to Directive 2008/105/EC of the European Parliament and of the Council. *Off. J. Eur. Union* 257, 32–35.
- EU, 2018. COMMISSION IMPLEMENTING DECISION (EU) 2018/840 of 5 June 2018. *Off. J. Eur. Union* 2018, 5–8.
- EU, 2015. COMMISSION IMPLEMENTING DECISION (EU) 2015/495 of 20 March 2015 establishing a watch list of substances for Union-wide monitoring in the field of water policy pursuant to Directive 2008/105/EC of the European Parliament and of the Council. *Off. J. Eur. Union* L78/40, 20–30.
- EU, 2013. Directive 2013/39/EU of the European Parliament and of the Council of 12 August 2013 amending Directives 2000/60/EC and 2008/105/EC as regards priority substances in the field of water policy.
- EU, 2009. Persistent Organic Pollutants (POPs) [WWW Document]. URL https://ec.europa.eu/environment/chemicals/international_conventions/index_en.htm (accessed 8.18.22).
- European Union, 2013. Directive 2013/11/EU of the European Parliament and of the Council, Fundamental Texts On European Private Law. *Official Journal of the European Union*, European Union. <https://doi.org/10.5040/9781782258674.0032>
- European Union, 2006. COMMISSION REGULATION (EC) No 1881/2006 of 19 December 2006 setting maximum levels for certain contaminants in foodstuffs.
- FDA, 2020. Drugmakers Report Zoloft Shortage Amid COVID-19 [WWW Document]. URL <https://www.fdanews.com/articles/197425-drugmakers-report-zoloft-shortage-amid-covid-19> (accessed 10.31.22).

- Fernández-Castro, P., 2017. Progress in the reactivity of Advanced Oxidation media. Application to the Fenton treatment of 2-chlorophenol solutions. University of Cantabria.
- Fernández-Castro, P., San Román, M.F., Ortiz, I., 2016. Theoretical and experimental formation of low chlorinated dibenzo-p-dioxins and dibenzofurans in the Fenton oxidation of chlorophenol solutions. *Chemosphere* 161, 136–144. <https://doi.org/10.1016/j.chemosphere.2016.07.011>
- Fernández-Castro, P., Vallejo, M., San Román, M.F., Ortiz, I., 2015. Insight on the fundamentals of advanced oxidation processes: Role and review of the determination methods of reactive oxygen species. *J. Chem. Technol. Biotechnol.* 90, 796–820. <https://doi.org/10.1002/jctb.4634>
- Fiedler, H., 2007. National PCDD/PCDF release inventories under the Stockholm Convention on Persistent Organic Pollutants. *Chemosphere* 67. <https://doi.org/10.1016/j.chemosphere.2006.05.093>
- Fiedler, H., 2003. Dioxins and Furans (PCDD/PCDF), in: *Persistent Organic Pollutants*. Springer-Verlag, Berlin/Heidelberg, pp. 123–201. https://doi.org/10.1007/10751132_6
- Fischer, W.J., Schilter, B., Tritscher, A.M., Stadler, R.H., 2011. Contaminants of Milk and Dairy Products: Environmental Contaminants, in: *Encyclopedia of Dairy Sciences: Second Edition*. Academic Press, pp. 898–905. <https://doi.org/10.1016/B978-0-12-374407-4.00105-9>
- Frontistis, Z., Antonopoulou, M., Venieri, D., Konstantinou, I., Mantzavinos, D., 2017. Boron-doped diamond oxidation of amoxicillin pharmaceutical formulation: Statistical evaluation of operating parameters, reaction pathways and antibacterial activity. *J. Environ. Manage.* 195, 100–109. <https://doi.org/10.1016/j.jenvman.2016.04.035>
- Ganiyu, S.O., Oturan, N., Raffy, S., Cretin, M., Causserand, C., Oturan, M.A., 2019. Efficiency of plasma elaborated sub-stoichiometric titanium oxide (Ti₄O₇) ceramic electrode for advanced electrochemical degradation of paracetamol in different electrolyte media. *Sep. Purif. Technol.* 208, 142–152. <https://doi.org/10.1016/j.seppur.2018.03.076>
- Ganiyu, S.O., Oturan, N., Raffy, S., Cretin, M., Esmilaire, R., van Hullebusch, E., Esposito, G., Oturan, M.A., 2016. Sub-stoichiometric titanium oxide (Ti₄O₇) as a suitable ceramic anode for electrooxidation of organic pollutants: A case study of kinetics, mineralization and toxicity assessment of amoxicillin. *Water Res.* 106, 171–182. <https://doi.org/10.1016/j.watres.2016.09.056>
- Ghenaatgar, A., M.A.Tehrani, R., Khadir, A., 2019. Photocatalytic degradation and mineralization of dexamethasone using WO₃ and ZrO₂ nanoparticles: Optimization of operational parameters and kinetic studies. *J. Water Process Eng.* 32, 100969. <https://doi.org/10.1016/j.jwpe.2019.100969>

- Golovko, O., Örn, S., Söregård, M., Frieberg, K., Nassazzi, W., Lai, F.Y., Ahrens, L., 2021. Occurrence and removal of chemicals of emerging concern in wastewater treatment plants and their impact on receiving water systems. *Sci. Total Environ.* 754, 142122. <https://doi.org/10.1016/j.scitotenv.2020.142122>
- Gómez-Lavín, S., San Román, M.F., Ortiz, I., Fernández, J., de Miguel, P., Urtiaga, A., 2018. Dioxins and furans legacy of lindane manufacture in Sabiñánigo (Spain). The Bailín landfill site case study. *Sci. Total Environ.* 624, 955–962. <https://doi.org/10.1016/j.scitotenv.2017.12.162>
- Gornik, T., Kovacic, A., Heath, E., Hollender, J., Kosjek, T., 2020. Biotransformation study of antidepressant sertraline and its removal during biological wastewater treatment. *Water Res.* 181, 115864. <https://doi.org/10.1016/j.watres.2020.115864>
- Graves, L.M., 1948. What is a Functional? *Am. Math. Mon.* 55, 467–472. <https://doi.org/10.1080/00029890.1948.11999285>
- Grilla, E., Taheri, M.E., Miserli, K., Venieri, D., Konstantinou, I., Mantzavinos, D., 2021. Degradation of dexamethasone in water using BDD anodic oxidation and persulfate: reaction kinetics and pathways. *J. Chem. Technol. Biotechnol.* 96, 2451–2460. <https://doi.org/10.1002/jctb.6833>
- Guo, Y., Rene, E.R., Han, B., Ma, W., 2021. Enhanced fluoroglucocorticoid removal from groundwater in a bio-electrochemical system with polyaniline-loaded activated carbon three-dimensional electrodes: Performance and mechanisms. *J. Hazard. Mater.* 416, 126197. <https://doi.org/10.1016/j.jhazmat.2021.126197>
- Guo, Z., Guo, A., Guo, Q., Rui, M., Zhao, Y., Zhang, H., Zhu, S., 2017. Decomposition of dexamethasone by gamma irradiation: Kinetics, degradation mechanisms and impact on algae growth. *Chem. Eng. J.* 307, 722–728. <https://doi.org/10.1016/j.cej.2016.08.138>
- Harrad, S.J., Jones, K.C., 1992. A source inventory and budget for chlorinated dioxins and furans in the United Kingdom environment. *Sci. Total Environ.* 126, 89–107. [https://doi.org/10.1016/0048-9697\(92\)90486-C](https://doi.org/10.1016/0048-9697(92)90486-C)
- Hites, R.A., 2011. Dioxins: An overview and history. *Environ. Sci. Technol.* 45, 16–20. <https://doi.org/10.1021/es1013664>
- Hofste, R.W., Reig, P., Schleifer, L., 2019. 17 Countries, Home to One-Quarter of the World's Population, Face Extremely High Water Stress. *World Resour. Inst.* 1–6.
- Hube, S., Wu, B., 2021. Mitigation of emerging pollutants and pathogens in decentralized wastewater treatment processes: A review. *Sci. Total Environ.* 779, 146545. <https://doi.org/10.1016/j.scitotenv.2021.146545>
- Jakimska, A., Śliwka Kaszyńska, M., Nagórski, P., Kot Wasik, A., Namieśnik, J., 2014. Environmental Fate of Two Psychiatric Drugs, Diazepam and Sertraline: Phototransformation and Investigation of their Photoproducts in Natural Waters. *J. Chromatogr. Sep. Tech.* 05. <https://doi.org/10.4172/2157-7064.1000253>

- Jensen, F., 2007. Introduction to Computational Chemistry, Theoretical Chemistry Accounts.
- Jiménez-Holgado, C., Sakkas, V., Richard, C., 2021. Phototransformation of three psychoactive drugs in presence of sedimental water extractable organic matter. *Molecules* 26, 1–17. <https://doi.org/10.3390/molecules26092466>
- Kantz, H., Schreiber, T., 2004. 2. Part I - Basic topics. Fundamental Principles, in: *Computational Chemistry: A Practical Guide for Applying Techniques to Real-World Problems*. pp. 5–18.
- Kaplan, A., Mamane, H., Lester, Y., Avisar, D., 2020. Trace organic compound removal from wastewater reverse-osmosis concentrate by advanced oxidation processes with UV/O₃/H₂O₂. *Materials (Basel)*. 13, 1–13. <https://doi.org/10.3390/ma13122785>
- Karstensen, K.H., 2008. Formation, release and control of dioxins in cement kilns. *Chemosphere* 70, 543–560. <https://doi.org/10.1016/j.chemosphere.2007.06.081>
- Kaur, R., Kushwaha, J.P., Singh, N., 2019a. Amoxicillin electro-catalytic oxidation using Ti/RuO₂ anode: Mechanism, oxidation products and degradation pathway. *Electrochim. Acta* 296, 856–866. <https://doi.org/10.1016/j.electacta.2018.11.114>
- Kaur, R., Kushwaha, J.P., Singh, N., 2019b. Electro-oxidation of amoxicillin trihydrate in continuous reactor by Ti/RuO₂ anode. *Sci. Total Environ.* 677, 84–97. <https://doi.org/10.1016/j.scitotenv.2019.04.339>
- Kawamoto, K., Weber, R., 2021. Dioxin sources to the aquatic environment: Re-assessing dioxins in industrial processes and possible emissions to the aquatic. *Emerg. Contam.* 7, 52–62. <https://doi.org/10.1016/j.emcon.2021.01.002>
- Khan, H.K., Rehman, M.Y.A., Junaid, M., Lv, M., Yue, L., Haq, I. ul, Xu, N., Malik, R.N., 2022. Occurrence, source apportionment and potential risks of selected PPCPs in groundwater used as a source of drinking water from key urban-rural settings of Pakistan. *Sci. Total Environ.* 807, 151010. <https://doi.org/10.1016/j.scitotenv.2021.151010>
- Klima, V., Chadyšien, R., Ivanec-Goranina, R., Jasaitis, D., Vasiliauskiene, V., 2020. Assessment of Air Pollution with Polychlorinated. *Atmosphere (Basel)*. 11, 759–773. <https://doi.org/10.3390/atmos11070759>
- Kulkarni, P.S., 2019. Dioxins. *Encycl. Environ. Heal.* 2, 125–134. <https://doi.org/10.1016/B978-0-12-409548-9.11832-9>
- Kulkarni, P.S., Crespo, J.G., Afonso, C.A.M., 2008. Dioxins sources and current remediation technologies - A review. *Environ. Int.* 34, 139–153. <https://doi.org/10.1016/j.envint.2007.07.009>

- Lam, Y.H., Abramov, Y., Ananthula, R.S., Elward, J.M., Hilden, L.R., Nilsson Lill, S.O., Norrby, P.O., Ramirez, A., Sherer, E.C., Mustakis, J., Tanoury, G.J., 2020. Applications of Quantum Chemistry in Pharmaceutical Process Development: Current State and Opportunities. *Org. Process Res. Dev.* 24, 1496–1507. <https://doi.org/10.1021/acs.oprd.0c00222>
- Lavric, E.D., Konnov, A.A., De Ruyck, J., 2004. Dioxin levels in wood combustion - A review. *Biomass and Bioenergy* 26, 115–145. [https://doi.org/10.1016/S0961-9534\(03\)00104-1](https://doi.org/10.1016/S0961-9534(03)00104-1)
- Le, T.X.H., Nguyen, T. Van, Amadou Yacouba, Z., Zoungrana, L., Avril, F., Nguyen, D.L., Petit, E., Mendret, J., Bonniol, V., Bechelany, M., Lacour, S., Lesage, G., Cretin, M., 2017. Correlation between degradation pathway and toxicity of acetaminophen and its by-products by using the electro-Fenton process in aqueous media. *Chemosphere* 172, 1–9. <https://doi.org/10.1016/j.chemosphere.2016.12.060>
- Lee, M., Liang, G., Holland, S.I., O’Farrell, C., Osborne, K., Manefield, M.J., 2022. Dehalobium species implicated in 2,3,7,8-tetrachlorodibenzo-p-dioxin dechlorination in the contaminated sediments of Sydney Harbour Estuary. *Mar. Pollut. Bull.* 179, 113690. <https://doi.org/10.1016/j.marpolbul.2022.113690>
- Lewars, E.G., 2011. Computational chemistry: Introduction to the theory and applications of molecular and quantum mechanics, *Computational Chemistry: Introduction to the Theory and Applications of Molecular and Quantum Mechanics*. <https://doi.org/10.1007/978-90-481-3862-3>
- Li, P., Wang, Y., Huang, B., Guan, S., Luan, T., Lin, G., Yuan, K., 2022. Antibiotics in wastewater of Guangdong, China: distribution patterns, and their environmental risk due to incomplete removal. *Sci. Total Environ.* 849, 157889. <https://doi.org/10.1016/j.scitotenv.2022.157889>
- Linden, K.G., Mohseni, M., 2014. Advanced Oxidation Processes: Applications in Drinking Water Treatment, *Comprehensive Water Quality and Purification*. Elsevier Ltd. <https://doi.org/10.1016/B978-0-12-382182-9.00031-1>
- Liu, Y.J., Hu, C.Y., Lo, S.L., 2019a. Direct and indirect electrochemical oxidation of amine-containing pharmaceuticals using graphite electrodes. *J. Hazard. Mater.* 366, 592–605. <https://doi.org/10.1016/j.jhazmat.2018.12.037>
- Liu, Y.J., Hu, C.Y., Lo, S.L., 2019b. Direct and indirect electrochemical oxidation of amine-containing pharmaceuticals using graphite electrodes. *J. Hazard. Mater.* 366, 592–605. <https://doi.org/10.1016/j.jhazmat.2018.12.037>
- Luong, J.H.T., Male, K.B., Glennon, J.D., 2009. Boron-doped diamond electrode: Synthesis, characterization, functionalization and analytical applications. *Analyst* 134, 1965–1979. <https://doi.org/10.1039/b910206j>

- Madikizela, L.M., Nuapia, Y.B., Chimuka, L., Ncube, S., Etale, A., 2022. Target and Suspect Screening of Pharmaceuticals and their Transformation Products in the Klip River, South Africa, using Ultra-High-Performance Liquid Chromatography–Mass Spectrometry. *Environ. Toxicol. Chem.* 41, 437–447. <https://doi.org/10.1002/etc.5265>
- Markic, M., Cvetnic, M., Ukcic, S., Kusic, H., Bolanca, T., Bozic, A.L., 2018. Influence of process parameters on the effectiveness of photooxidative treatment of pharmaceuticals. *J. Environ. Sci. Heal. - Part A Toxic/Hazardous Subst. Environ. Eng.* 53, 338–351. <https://doi.org/10.1080/10934529.2017.1401394>
- Martínez-Huitle, C.A., Rodrigo, M.A., Sirés, I., Scialdone, O., 2015. Single and Coupled Electrochemical Processes and Reactors for the Abatement of Organic Water Pollutants: A Critical Review. *Chem. Rev.* 115, 13362–13407. <https://doi.org/10.1021/acs.chemrev.5b00361>
- Miklos, D.B., Remy, C., Jekel, M., Linden, K.G., Drewes, J.E., Hübner, U., 2018. Evaluation of advanced oxidation processes for water and wastewater treatment – A critical review. *Water Res.* 139, 118–131. <https://doi.org/10.1016/j.watres.2018.03.042>
- Mohamad, I.N., Wong, C.K.W., Chew, C.C., Leong, E.L., Lee, B.H., Moh, C.K., Chenasammy, K., Lim, S.C.L., Ker, H.B., 2022. The landscape of antibiotic usage among COVID-19 patients in the early phase of pandemic: a Malaysian national perspective. *J. Pharm. Policy Pract.* 15, 1–11. <https://doi.org/10.1186/s40545-022-00404-4>
- Morales-Paredes, C.A., Rodríguez-Díaz, J.M., Boluda-Botella, N., 2022. Pharmaceutical compounds used in the COVID-19 pandemic: A review of their presence in water and treatment techniques for their elimination. *Sci. Total Environ.* 814. <https://doi.org/10.1016/j.scitotenv.2021.152691>
- Muff, J., 2014. Electrochemical Oxidation - A Versatile Technique for Aqueous Organic Contaminant Degradation, *Chemistry of Advanced Environmental Purification Processes of Water: Fundamentals and Applications.* <https://doi.org/10.1016/B978-0-444-53178-0.00003-1>
- Musee, N., Kebaabetswe, L.P., Tichapondwa, S., Tubatsi, G., Mahaye, N., Leareng, S.K., Nomngongo, P.N., 2021. Occurrence, fate, effects, and risks of dexamethasone: Ecological implications post-covid-19. *Int. J. Environ. Res. Public Health* 18. <https://doi.org/10.3390/ijerph182111291>
- Nason, S.L., Lin, E., Eitzer, B., Koelmel, J., Peccia, J., 2021. Changes in Sewage Sludge Chemical Signatures During a COVID-19 Community Lockdown, Part 1: Traffic, Drugs, Mental Health, and Disinfectants. *Environ. Toxicol. Chem.* <https://doi.org/10.1002/etc.5217>
- Norman Network, 2022. Network of reference laboratories, research centres and related organisations for monitoring of emerging environmental substances [WWW Document]. URL <https://www.norman-network.net/>.

- Olvera-Vargas, H., Rouch, J.C., Coetsier, C., Cretin, M., Causserand, C., 2018. Dynamic cross-flow electro-Fenton process coupled to anodic oxidation for wastewater treatment: Application to the degradation of acetaminophen. *Sep. Purif. Technol.* 203, 143–151. <https://doi.org/10.1016/j.seppur.2018.03.063>
- Oturan, M.A., Aaron, J.J., 2014. Advanced oxidation processes in water/wastewater treatment: Principles and applications. A review. *Crit. Rev. Environ. Sci. Technol.* 44, 2577–2641. <https://doi.org/10.1080/10643389.2013.829765>
- Pan, G., Sun, X., Sun, Z., 2020. Fabrication of multi-walled carbon nanotubes and carbon black co-modified graphite felt cathode for amoxicillin removal by electrochemical advanced oxidation processes under mild pH condition. *Environ. Sci. Pollut. Res.* 27, 8231–8247. <https://doi.org/10.1007/s11356-019-07358-2>
- Pan, G., Sun, Z., 2021. Cu-doped g-C₃N₄ catalyst with stable CuO and Cu⁺ for enhanced amoxicillin degradation by heterogeneous electro-Fenton process at neutral pH. *Chemosphere* 283, 131257. <https://doi.org/10.1016/j.chemosphere.2021.131257>
- Panizza, M., Cerisola, G., 2009. Direct and mediated anodic oxidation of organic pollutants. *Chem. Rev.* 109, 6541–6569. <https://doi.org/10.1021/cr9001319>
- Pazoki, M., Parsa, M., Farhadpour, R., 2016. Removal of the hormones dexamethasone (DXM) by Ag doped on TiO₂ photocatalysis. *J. Environ. Chem. Eng.* 4, 4426–4434. <https://doi.org/10.1016/j.jece.2016.09.034>
- Pretali, L., Albini, A., Cantalupi, A., Maraschi, F., Nicolis, S., Sturini, M., 2021. TiO₂-photocatalyzed water depollution, a strong, yet selective depollution method: New evidence from the solar light induced degradation of glucocorticoids in freshwaters. *Appl. Sci.* 11. <https://doi.org/10.3390/app11062486>
- Priyadarshini, M., Das, I., Ghangrekar, M.M., Blaney, L., 2022. Advanced oxidation processes: Performance, advantages, and scale-up of emerging technologies. *J. Environ. Manage.* 316, 115295. <https://doi.org/10.1016/j.jenvman.2022.115295>
- Quaresma, A. V., Rubio, K.T.S., Taylor, J.G., Sousa, B.A., Silva, S.Q., Werle, A.A., Afonso, R.J.C.F., 2021. Removal of dexamethasone by oxidative processes: Structural characterization of degradation products and estimation of the toxicity. *J. Environ. Chem. Eng.* 9, 106884. <https://doi.org/10.1016/j.jece.2021.106884>
- Rabeea, S.A., Merchant, H.A., Khan, M.U., Kow, C.S., Hasan, S.S., 2021. Surging trends in prescriptions and costs of antidepressants in England amid COVID-19. *J. Pharm. Sci.* 29, 217–221. <https://doi.org/https://doi.org/10.1007/s40199-021-00390-z>
- Rasolevandi, T., Naseri, S., Azarpira, H., Mahvi, A.H., 2019. Photo-degradation of dexamethasone phosphate using UV/Iodide process: Kinetics, intermediates, and transformation pathways. *J. Mol. Liq.* 295, 111703. <https://doi.org/10.1016/j.molliq.2019.111703>
- Richards, G., Agranovski, I.E., 2017. Dioxin-like pcb emissions from cement kilns during the use of alternative fuels. *J. Hazard. Mater.* 323, 698–709. <https://doi.org/10.1016/j.jhazmat.2016.10.040>

- Rivera-Utrilla, J., Sánchez-Polo, M., Ferro-García, M.Á., Prados-Joya, G., Ocampo-Pérez, R., 2013. Pharmaceuticals as emerging contaminants and their removal from water. A review. *Chemosphere* 93, 1268–1287. <https://doi.org/10.1016/j.chemosphere.2013.07.059>
- Ruiz-Garbajosa, P., Cantón, R., 2021. Covid-19: Impact on prescribing and antimicrobial resistance. *Rev. Esp. Quimioter.* 34, 63–68. <https://doi.org/10.37201/req/s01.19.2021>
- San-Román, M.F., Solá-Gutiérrez, C., Schröder, S., Laso, J., Margallo, M., Vázquez-Rowe, I., Ortiz, I., Irabien, A., Aldaco, R., 2020. Potential formation of PCDD/Fs in triclosan wastewater treatment: An overall toxicity assessment under a life cycle approach. *Sci. Total Environ.* 707, 135981. <https://doi.org/10.1016/j.scitotenv.2019.135981>
- Schröder, S., Ortiz, I., San-Román, M.-F., 2022. Emerging Pollutants That Can Be Transformed into PCDD/Fs, in: Núñez-Delgado, A., Arias-Estévez, M. (Eds.), *The Handbook of Environmental Chemistry*. Springer Berlin Heidelberg, Berlin, Heidelberg, pp. 1–26. https://doi.org/10.1007/698_2022_851
- Schröder, S., San-Román, M.F., Ortiz, I., 2021. Dioxins and furans toxicity during the photocatalytic remediation of emerging pollutants. Triclosan as case study. *Sci. Total Environ.* 770, 144853. <https://doi.org/10.1016/j.scitotenv.2020.144853>
- Schröder, S., San-Román, M.F., Ortiz, I., 2020. Photocatalytic transformation of triclosan. Reaction products and kinetics. *Catalysts* 10, 1–15. <https://doi.org/10.3390/catal10121468>
- SDWA, 2022. Regulating Contaminants Under the Safe Drinking Water Act (SDWA). Updated January 5, 2022. Congr. Res. Serv.
- Sengar, A., Vijayanandan, A., 2022. Human health and ecological risk assessment of 98 pharmaceuticals and personal care products (PPCPs) detected in Indian surface and wastewaters. *Sci. Total Environ.* 807, 150677. <https://doi.org/10.1016/j.scitotenv.2021.150677>
- Sheffield, A., 1985. Sources and releases of PCDD's and PCDF's to the Canadian environment. *Chemosphere* 14, 811–814. [https://doi.org/10.1016/0045-6535\(85\)90193-6](https://doi.org/10.1016/0045-6535(85)90193-6)
- Shen, X., Chang, H., Sun, Y., Wan, Y., 2020. Determination and occurrence of natural and synthetic glucocorticoids in surface waters. *Environ. Int.* 134, 105278. <https://doi.org/10.1016/j.envint.2019.105278>
- Sidhu, S., Edwards, P., 2002. Role of phenoxy radicals in PCDD/F formation. *Int. J. Chem. Kinet.* 34, 531–541. <https://doi.org/10.1002/kin.10083>
- Sievers, M., 2011. Treatise on Water Science, in: *Treatise on Water Science*. pp. 377–408.

- Silori, R., Shrivastava, V., Singh, A., Sharma, P., Aouad, M., Mahlkecht, J., Kumar, M., 2022. Global groundwater vulnerability for Pharmaceutical and Personal care products (PPCPs): The scenario of second decade of 21st century. *J. Environ. Manage.* 320, 115703. <https://doi.org/10.1016/j.jenvman.2022.115703>
- Sirés, I., Brillas, E., Oturan, M.A., Rodrigo, M.A., Panizza, M., 2014. Electrochemical advanced oxidation processes: Today and tomorrow. A review. *Environ. Sci. Pollut. Res.* 21, 8336–8367. <https://doi.org/10.1007/s11356-014-2783-1>
- Solá-Gutiérrez, C., 2019. Traceability of PCDD/Fs formation in the advanced oxidation of TCS. University of Cantabria.
- Solá-Gutiérrez, C., San Román, M.F., Ortiz, I., 2018. Fate and hazard of the electrochemical oxidation of triclosan. Evaluation of polychlorodibenzo-p-dioxins and polychlorodibenzofurans (PCDD/Fs) formation. *Sci. Total Environ.* 626, 126–133. <https://doi.org/10.1016/j.scitotenv.2018.01.082>
- Solá-Gutiérrez, C., Schröder, S., San-Román, M.F., Ortiz, I., 2020. Critical review on the mechanistic photolytic and photocatalytic degradation of triclosan. *J. Environ. Manage.* <https://doi.org/10.1016/j.jenvman.2020.110101>
- Solá-Gutiérrez, C., Schröder, S., San Román, M.F., Ortiz, I., 2019. PCDD/Fs traceability during triclosan electrochemical oxidation. *J. Hazard. Mater.* 369, 584–592. <https://doi.org/10.1016/j.jhazmat.2019.02.066>
- Söregård, M., Campos-Pereira, H., Ullberg, M., Lai, F.Y., Golovko, O., Ahrens, L., 2019. Mass loads, source apportionment, and risk estimation of organic micropollutants from hospital and municipal wastewater in recipient catchments. *Chemosphere* 234, 931–941. <https://doi.org/10.1016/j.chemosphere.2019.06.041>
- Stockholm Convention, 2019. Stockholm Convention on persistent organic pollutants (POPs) - Texts and Annexes - United Nations Environment programme (UNEP), United Nations Environment programme (UNEP). Châtelaine, Switzerland.
- Tan, T.Y., Zeng, Z.T., Zeng, G.M., Gong, J.L., Xiao, R., Zhang, P., Song, B., Tang, W.W., Ren, X.Y., 2020. Electrochemically enhanced simultaneous degradation of sulfamethoxazole, ciprofloxacin and amoxicillin from aqueous solution by multi-walled carbon nanotube filter. *Sep. Purif. Technol.* 235, 116167. <https://doi.org/10.1016/j.seppur.2019.116167>
- Thomas, V.M., Spiro, T.G., 1995. An Estimation of Dioxin Emissions in the United States. *Toxicol. Environ. Chem.* 50, 1–37.
- UNESCO, 2021. The United Nations World Water Development Report 2021: Valuing water, Water Politics. <https://doi.org/10.4324/9780429453571-2>
- UNESCO, 2020. The United Nations World Water Development Report 2020: Water and climate change.

MOTIVATION

- UNESCO, 2017. The United Nations World Water Development Report 2017. Wastewater: The untapped resource, The United Nations World Water Development Report. Wastewater: The Untapped Resource.
- United Nations, 2022. World Population Prospects, World Population Prospects 2022. <https://doi.org/10.18356/cd7acf62-en>
- United Nations, 2021. The Sustainable Development Goals Report 2021. United Nations Publ. issued by Dep. Econ. Soc. Aff. 1–64.
- US EPA, 2022. Contaminant Candidate List 5 - CCL 5 [WWW Document]. URL <https://www.epa.gov/ccl/contaminant-candidate-list-5-ccl-5> (accessed 11.11.22).
- US EPA, 2014. EPA's priority pollutant list. <https://www.epa.gov/sites/production/files/2015-09/documents/priority-pollutant-list-epa.pdf>, 249.
- US EPA, 2013. National Primary Drinking Water Regulations. *Drink. Water Contam.* 141–142.
- US FDA, 2020. US FDA Drug Shortages [WWW Document]. *Fda.* URL <https://www.accessdata.fda.gov/scripts/drugshortages/default.cfm> (accessed 9.21.22).
- Vallejo, M., 2014. Assessment of polychlorinated dibenzo-p-dioxins and dibenzofurans, PCDD/Fs, in the application of advanced oxidation processes. University of Cantabria.
- Vallejo, M., Fernández-Castro, P., San Román, M.F., Ortiz, I., 2015a. Assessment of PCDD/Fs formation in the Fenton oxidation of 2-chlorophenol: influence of the iron dose applied. *Chemosphere* 137, 135–141. <https://doi.org/10.1016/j.chemosphere.2015.06.056>
- Vallejo, Marta., San Román, M.F., Irabien, A., Ortiz, I., 2013. Comparative study of the destruction of polychlorinated dibenzo-p-dioxins and dibenzofurans during Fenton and electrochemical oxidation of landfill leachates. *Chemosphere* 90, 132–138. <https://doi.org/10.1016/j.chemosphere.2012.08.018>
- Vallejo, Marta, San Román, M.F., Ortiz, I., 2013. Quantitative assessment of the formation of polychlorinated derivatives, PCDD/Fs, in the electrochemical oxidation of 2-chlorophenol as function of the electrolyte type. *Environ. Sci. Technol.* 47, 12400–12408. <https://doi.org/10.1021/es403246g>
- Vallejo, M., San Román, M.F., Ortiz, I., Irabien, A., 2015b. Overview of the PCDD/Fs degradation potential and formation risk in the application of advanced oxidation processes (AOPs) to wastewater treatment. *Chemosphere* 118, 44–56. <https://doi.org/10.1016/j.chemosphere.2014.05.077>

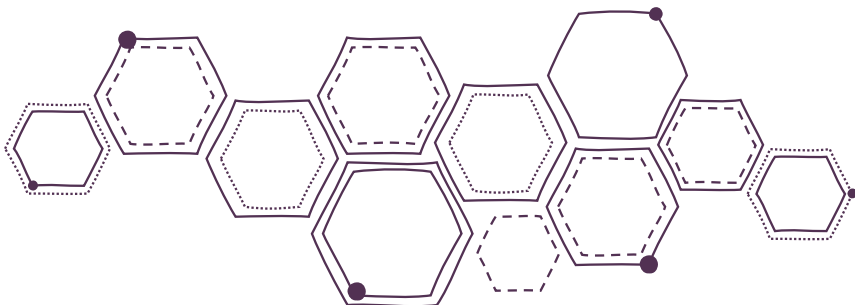
- Vallejo, M., San Román, M.F., Ortiz, I., Irabien, A., 2014. The critical role of the operating conditions on the fenton oxidation of 2-chlorophenol: Assessment of PCDD/Fs formation. *J. Hazard. Mater.* 279, 579–585. <https://doi.org/10.1016/j.jhazmat.2014.07.020>
- Van den Berg, M., Birnbaum, L.S., Denison, M., De Vito, M., Farland, W., Feeley, M., Fiedler, H., Hakansson, H., Hanberg, A., Haws, L., Rose, M., Safe, S., Schrenk, D., Tohyama, C., Tritscher, A., Tuomisto, J., Tysklind, M., Walker, N., Peterson, R.E., 2006. The 2005 World Health Organization reevaluation of human and mammalian toxic equivalency factors for dioxins and dioxin-like compounds. *Toxicol. Sci.* 93, 223–241. <https://doi.org/10.1093/toxsci/kfl055>
- Vargas-Berrones, K., Bernal-Jácome, L., Díaz de León-Martínez, L., Flores-Ramírez, R., 2020. Emerging pollutants (EPs) in Latin América: A critical review of under-studied EPs, case of study -Nonylphenol-. *Sci. Total Environ.* 726, 138493. <https://doi.org/10.1016/j.scitotenv.2020.138493>
- Varsha, M., Senthil Kumar, P., Senthil Rath, B., 2022. A review on recent trends in the removal of emerging contaminants from aquatic environment using low-cost adsorbents. *Chemosphere* 287, 132270. <https://doi.org/10.1016/j.chemosphere.2021.132270>
- Vasilachi, I.C., Asimnicesei, D.M., Fertu, D.I., Gavrilescu, M., 2021. Occurrence and fate of emerging pollutants in water environment and options for their removal. *Water (Switzerland)* 13, 1–34. <https://doi.org/10.3390/w13020181>
- Wang, J.L., Xu, L.J., 2012. Advanced oxidation processes for wastewater treatment: Formation of hydroxyl radical and application. *Crit. Rev. Environ. Sci. Technol.* 42, 251–325. <https://doi.org/10.1080/10643389.2010.507698>
- Wang, X., Zhang, H., Ni, Y., Du, Q., Zhang, X., Chen, J., 2014. Kinetics of PCDD/Fs formation from non-wood pulp bleaching with chlorine. *Environ. Sci. Technol.* 48, 4361–4367. <https://doi.org/10.1021/es404347h>
- Waterston, K., Wang, J.W., Bejan, D., Bunce, N.J., 2006. Electrochemical waste water treatment: Electrooxidation of acetaminophen. *J. Appl. Electrochem.* 36, 227–232. <https://doi.org/10.1007/s10800-005-9049-z>
- Weber, R., 2007. Relevance of PCDD/PCDF formation for the evaluation of POPs destruction technologies - Review on current status and assessment gaps. *Chemosphere* 67, 109–117. <https://doi.org/10.1016/j.chemosphere.2006.05.094>
- Weber, R., Gaus, C., Tysklind, M., Johnston, P., Forter, M., Hollert, H., Heinisch, E., Holoubek, I., Lloyd-Smith, M., Masunaga, S., Moccarelli, P., Santillo, D., Seike, N., Symons, R., Torres, J.P.M., Verta, M., Varbelow, G., Vijgen, J., Watson, A., Costner, P., Woelz, J., Wycisk, P., Zennegg, M., 2008. Dioxin- and POP-contaminated sites - Contemporary and future relevance and challenges: Overview on background, aims and scope of the series. *Environ. Sci. Pollut. Res.* 15, 363–393. <https://doi.org/10.1007/s11356-008-0024-1>

- Wee, S.Y., Aris, A.Z., Yusoff, F.M., Praveena, S.M., 2019. Occurrence and risk assessment of multiclass endocrine disrupting compounds in an urban tropical river and a proposed risk management and monitoring framework. *Sci. Total Environ.* 671, 431–442. <https://doi.org/10.1016/j.scitotenv.2019.03.243>
- Wee, S.Y., Haron, D.E.M., Aris, A.Z., Yusoff, F.M., Praveena, S.M., 2020. Active pharmaceutical ingredients in Malaysian drinking water: consumption, exposure, and human health risk. *Environ. Geochem. Health* 42, 3247–3261. <https://doi.org/10.1007/s10653-020-00565-8>
- Wee, S.Y., Ismail, N.A.H., Haron, D.E.M., Yusoff, F.M., Praveena, S.M., Aris, A.Z., 2022. Pharmaceuticals, hormones, plasticizers, and pesticides in drinking water. *J. Hazard. Mater.* 424, 127327. <https://doi.org/10.1016/j.jhazmat.2021.127327>
- WHO, 2021. Coronavirus disease (COVID-19): Dexamethasone [WWW Document]. URL <https://www.who.int/emergencies/diseases/novel-coronavirus-2019/question-and-answers-hub/q-a-detail/coronavirus-disease-covid-19-dexamethasone> (accessed 9.19.22).
- WHO, UNICEF, 2020. Water, sanitation, hygiene and waste management for the COVID-19 virus. *World Heal. Organ.* 1–9.
- World Health Organization, 2016. Dioxins and their effects on human health [WWW Document]. URL <https://www.who.int/news-room/fact-sheets/detail/dioxins-and-their-effects-on-human-health> (accessed 6.21.21).
- Xiao, Q., Song, X., Li, W., Zhang, Y., Wang, H., 2017. A primary estimation of PCDD/Fs release reduction from non-wood pulp and paper industry in China based on the investigation of pulp bleaching with chlorine converting to chlorine dioxide. *Chemosphere* 185, 329–335. <https://doi.org/10.1016/j.chemosphere.2017.06.119>
- Xu, F., Wang, H., Zhang, Q., Zhang, R., Qu, X., Wang, W., 2010. Kinetic properties for the complete series reactions of chlorophenols with OH radicals - Relevance for dioxin formation. *Environ. Sci. Technol.* 44, 1399–1404. <https://doi.org/10.1021/es9031776>
- Yang, L., Liu, G., Zheng, M., Zhao, Y., Jin, R., Wu, X., Xu, Y., 2017. Molecular Mechanism of Dioxin Formation from Chlorophenol based on Electron Paramagnetic Resonance Spectroscopy. *Environ. Sci. Technol.* 51, 4999–5007. <https://doi.org/10.1021/acs.est.7b00828>
- Yang, Q., Yang, L., Shen, J., Yang, Y., Wang, M., Liu, X., Shen, X., Li, C., Xu, J., Li, F., Li, D., Liu, G., Zheng, M., 2020. Polychlorinated dibenzo-p-dioxins and dibenzofurans (PCDD/Fs) emissions from electric arc furnaces for steelmaking. *Emerg. Contam.* 6, 330–336. <https://doi.org/10.1016/j.emcon.2020.08.005>
- Young, D., 2001a. 1. Introduction, in: *Computational Chemistry: A Practical Guide for Applying Techniques to Real-World Problems.* pp. 1–4. <https://doi.org/https://doi.org/10.1002/0471220655.ch1>

- Young, D., 2001b. 4. Semiempirical Methods, in: *Computational Chemistry: A Practical Guide for Applying Techniques to Real-World Problems*. pp. 32–41. https://doi.org/10.1007/978-1-4615-4189-9_9
- Zhang, M., Buekens, A., 2016. De novo synthesis of dioxins: a review. *Int. J. Environ. Pollut.* 60, 63. <https://doi.org/10.1504/ijep.2016.10002958>
- Zhang, Q., Huang, W., Hong, J. ming, Chen, B.Y., 2018. Deciphering acetaminophen electrical catalytic degradation using single-form S doped graphene/Pt/TiO₂. *Chem. Eng. J.* 343, 662–675. <https://doi.org/10.1016/j.cej.2018.02.089>
- Zhang, Q., Yu, W., Zhang, R., Zhou, Q., Gao, R., Wang, W., 2010. Quantum chemical and kinetic study on dioxin formation from the 2,4,6-TCP and 2,4-DCP precursors. *Environ. Sci. Technol.* 44, 3395–3403. <https://doi.org/10.1021/es1004285>
- Zhang, Y., Zhang, D., Gao, J., Zhan, J., Liu, C., 2014. New understanding of the formation of PCDD/Fs from chlorophenol precursors: A mechanistic and kinetic study. *J. Phys. Chem. A* 118, 449–456. <https://doi.org/10.1021/jp410077g>
- Zhou, Y., Meng, J., Zhang, M., Chen, S., He, B., Zhao, H., Li, Q., Zhang, S., Wang, T., 2019. Which type of pollutants need to be controlled with priority in wastewater treatment plants: Traditional or emerging pollutants? *Environ. Int.* 131. <https://doi.org/10.1016/j.envint.2019.104982>
- Zou, C., Han, J., Fu, H., 2012. Emissions of PCDD/Fs from Steel and Secondary Nonferrous Productions. *Procedia Environ. Sci.* 16, 279–288. <https://doi.org/10.1016/j.proenv.2012.10.039>

2

MATERIALS AND METHODS



Abstract

This chapter presents the chemical reagents, experimental equipment, analytical methods and analytical equipment, that have been employed to perform the proposed experiments in this PhD thesis. Furthermore, the methodology to carry out each type of experiment is explained. The different chemical reagents used for the degradation of the drugs, called as EOX-Drugs, and to carry out the electrochemical oxidation experiments, named as EOX-Intermediates, which the aim of identifying by-products, are detailed. Finally, the chemical reagents used for the preparation and analysis of the intermediates and PCDD/Fs samples are described. Next, the analytical methods applied to analyse the degradation of the drugs, the intermediates formed and naturally, the dioxins and furans, are detailed, as well as the techniques of liquid chromatography (HPLC) and gas chromatography (GC-MS and HRGC/HRMS) employed for such analysis. Then, the preparation of the different samples to be analysed is detailed, emphasising the PCDD/Fs sample preparation analysis following EPA 1613 method. It has been described deeply given the high analytical complexity to carry it out, due to the numerous stages of which it consists, among other aspects to take into account. In addition, quality control and quality assurance in the analysis of PCDD/Fs are detailed. Finally, the working methodology employed in Computational Chemistry is described to obtain the theoretical reaction mechanisms about the PCDD/Fs formation.

2.1. Chemical reagents

This section describes the main characteristics of the chemicals used in the electrochemical experiments. Moreover, the standards used for the analytical measurements are also included. The reagents used for the experiments are listed in Table 2.1 and the specific chemicals used for PCDD/Fs analysis by EPA 1613 method are detailed in Table 2.2.

Table 2.1. Summary of the chemicals employed for EOX experiments.

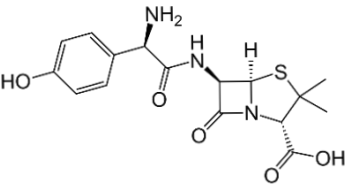
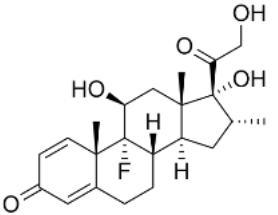
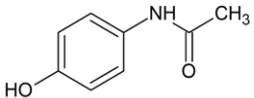
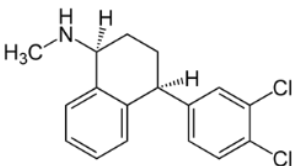
Name	Chemical formula	Purity	Supplier
2,4-dichlorophenol	C ₆ H ₄ Cl ₂ O	99%	Sigma-Aldrich
2,8-dichlorodibenzo-p-dioxin	C ₁₂ H ₆ Cl ₂ O ₂	>98%	Wellington Laboratories
Acetic acid	C ₂ H ₄ O ₂	100%	Merck
Acetonitrile	C ₂ H ₃ N	LiChrosolv® 99.9%	Merck
Amoxicillin trihydrate	C ₁₆ H ₂₅ N ₃ O ₈ S · 3H ₂ O	≥95%	Sigma-Aldrich
Dexamethasone	C ₂₂ H ₂₉ FO ₅	≥98%	Sigma-Aldrich
Formic acid	CH ₂ O ₂	98%	Panreac
Methanol	CH ₄ O	99.9% HPLC	Riedel-de Haën
Nitric acid	HNO ₃	65%	Scharlau
Paracetamol	C ₈ H ₉ NO ₂	≥99%	Sigma-Aldrich
Sertraline hydrochloride	C ₁₇ H ₁ Cl ₂ N · HCl	>98%	TCI
Sodium chloride	NaCl	99.5%	Panreac
Sodium sulphate	Na ₂ SO ₄	99%	Merck
Sulphuric acid	H ₂ SO ₄	98%	Merck-Millipore
Phosphate buffer salts	Na ₂ HPO ₄	98%	Panreac
	KH ₂ PO ₄	99%	Panreac

Table 2.2. Reagents used for PCDD/Fs analysis for the application of EPA 1613 method.

Reagent	Supplier
Acetone (Suprasolv®)	Merck-Millipore
Dichloromethane (UniSolv®)	Merck-Millipore
Ethyl acetate (99.9%)	Sigma Aldrich
n-Hexane (UniSolv®)	Merck-Millipore
Toluene (UniSolv®)	Merck-Millipore
EPA 1613 CLS-CS4: calibration standard solutions	Wellington Laboratories
EPA 1613 ISS: internal standard spiking solution	Wellington Laboratories
EPA 1613 LCS: labelled compound stock solution	Wellington Laboratories

Finally, Table 2.3 highlighted the main properties of the four pharmaceutical compounds, dexamethasone, amoxicillin, paracetamol and sertraline, studied in this doctoral thesis.

Table 2.3. Main properties of the drugs used in this study.

Name and formula	Molecular weight	Water solubility (mg L ⁻¹)	Structure
Amoxicillin trihydrate C ₁₆ H ₂₅ N ₃ O ₈ S · 3H ₂ O	419.5	4150	
Dexamethasone C ₂₂ H ₂₉ FO ₅	392.5	89	
Paracetamol C ₈ H ₉ NO ₂	151.1	14000	
Sertraline hydrochloride C ₁₇ H ₁₄ Cl ₂ N · HCl	342.7	3800	

2.2. Electrochemical experiments

A schematic diagram of the experimental set-up employed in the electrochemical experiments is shown in Figure 2.1, where the numbers indicate the different parts of the plant. It is a medium/high power laboratory-scale electrochemical plant provided with LED technology, manufactured by APRIA Systems S.L. (Spain). It consists of a feed tank where the solution is placed before the beginning of the experiments, then, the solution is pumped into the electrochemical cell or the photocatalytic reactor (depending on how the different available valves are disposed, according to the experiment to be performed) using a magnetic pump, all connected with Teflon tubing. The electrochemical cell is an ELOXlabB-S210, with two rectangular electrodes placed in parallel: an anode of Nb/BDD (niobium/boron-doped-diamond) and a cathode made of stainless steel (AISI 316), with a total anodic area of 210 cm² and an electrode gap of 2 mm. The power supply has an electric current range of 0-30 A, and the output voltage range is 1-32 V. In the case of the photocatalytic reactor, it is a 0.25 L jacketed annular Pyrex reaction vessel with UVA-LEDs positioned within the inner tube of the reactor; LEDs can operate in UV-A ($\lambda=365-370$ nm) and visible light ($\lambda=400-700$ nm). The electric power of the LEDs ranges from 0-53 W in the UV-A spectra / 0-49 W in the VIS spectra. Furthermore, the system includes a magnetic stirring plate that operates at 1000 rpm to maintain the homogeneity of the solution, and a refrigeration bath to keep the temperature constant (Schröder et al., 2020). For a better comprehension, in Figure 2.2 it can be observed a picture of the experimental set-up.

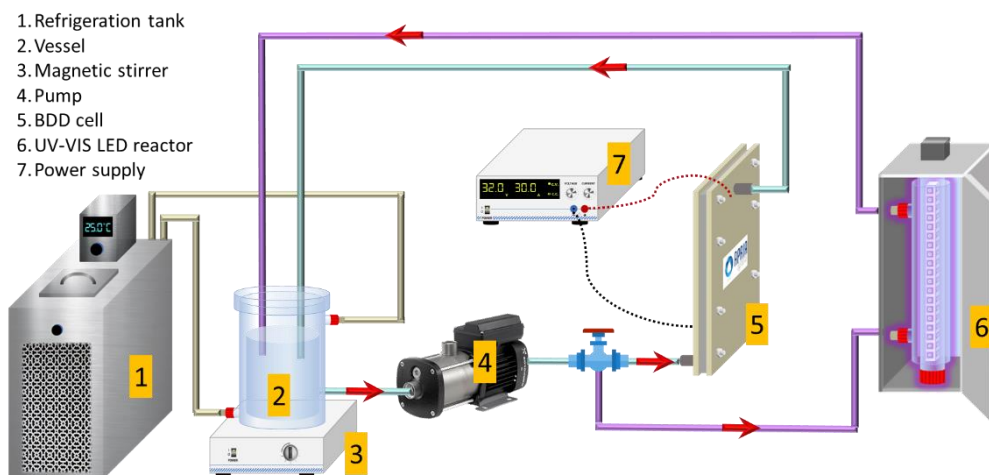


Figure 2.1. Schematic diagram of the electrochemical and photocatalytic oxidation experimental set-up.



Figure 2.2. Experimental set-up used in the electrochemical oxidation experiments (APRIA Systems., S.L.).

The electrochemical oxidation experiments were conducted in batch mode at a constant temperature of 25 °C, and were run at galvanostatic mode, which means, at a constant current density (J). The experiments carried out have been classified into two different types depending on their purpose: i) degradation experiments (EOX-Drugs) and, ii) experiments designed for the analysis of the intermediate compounds in a qualitatively manner (EOX-Intermediates).

2.2.1. EOX-Drugs & EOX-Intermediates

Depending on the type of the experiment, the employed initial concentration of the pharmaceutical compounds, dexamethasone (DEX), amoxicillin (AMX), paracetamol (PAR) and sertraline (STR), was different. Despite the fact that in real wastewaters the concentration of these drugs is in the order of $\mu\text{g L}^{-1}$ - ng L^{-1} , in this thesis, the initial concentration used for EOX-Drugs was 10 mg L^{-1} . This level of concentration was selected in order of avoiding detection problems in HPLC and with this, follow properly the drug degradation. Moreover, in a real-life context, an EOX treatment could be thought after the application of further treatments to concentrate the wastewaters, such as ultrafiltration (UF) or reverse osmosis (RO), where the drugs concentrations are expected to reach the order of mg L^{-1} . For EOX-Intermediates experiments, the initial concentration used was established according to the solubility limit (Table 2.3); 80 mg L^{-1} .

¹ for DEX (0.2 mM) and 3000 mg L⁻¹ for AMX, PAR and STR (7.1, 19.8 and 8.7 mM, respectively). which allow the detection of the by-products formed. The solubility of PAR is 14000 mg L⁻¹, but 3000 mg L⁻¹ was selected to work in the same conditions. Furthermore, according to these initial concentrations, the current density applied was 4.8 A m⁻² for all the EOX-Drugs experiments, and for the EOX-Intermediates experiments, 48 A m⁻² were applied for DEX, 1000 A m⁻² for AMX and PAR, and 900 A m⁻² for STR (limit current density: 25.7 A m⁻² for DEX; 960 A m⁻² for AMX; 963.6 A m⁻² for PAR and 851 A m⁻² for STR, respectively). Two different electrolytic mediums were employed, NaCl (56 mM) and a mixture of Na₂SO₄ with NaCl (21 mM + 2.8 mM). The concentration of 2.8 mM of NaCl was selected to be added to the 21 mM of Na₂SO₄, in order to simulate the equivalent amount of the common chlorine (Cl⁻) content in wastewater treatment plants effluents, around 100 mg L⁻¹ (measured for this doctoral thesis). The concentration of the selected electrolytic mediums was chosen in order to achieve a conductivity value of 7.5 mS cm⁻¹, according to the aforementioned studies developed in this line of investigation (Solá-Gutiérrez, 2019; Vallejo, 2014).

The methodology to carry out the experiments was the same, both for EOX-Drugs and for EOX-Intermediates. First, the correct amount of the correspondent drug was weighted and dissolved with ultrapure water in a volumetric flask (volume = 2 L), by stirring with the help of a magnetic stirrer until it is completely dissolved. In the DEX and STR experiments, it was necessary to keep stirring the solutions overnight prior to the experiment to ensure the total dissolution. After this, the correspondent electrolyte was added to the solution and placed in the feed tank, the pump was turned on and also, the refrigeration system was set to 25 °C. To guarantee the homogeneity of the solution, it was recirculated through the system for 5 minutes, before switching on the power supply, where it was selected the specific electric current in each case. The pH and the temperature were monitored through the entire experiment, and the flow rate was kept constant at 300 L h⁻¹ for all experiments, being the pH not modified in any case, with values between 5.5-6.8. Samples were taken from the feed tank at regular time intervals, and analysed according to methods described below, to determine the concentration of the primary compound, the intermediates formed, or the PCDD/Fs. All the experiments have been performed in duplicate, and the standard deviation was calculated for each pair of experiments. The experimental conditions employed in the different electrochemical experiments are detailed in Table 2.4 and Table 2.5. The experiments were stopped when the pollutant was completely degraded.

Table 2.4. Experimental conditions applied in EOX-Drugs experiments.

Electrochemical experiments (EOX-Drugs)	
Pharmaceuticals (mg L ⁻¹)	10
J (A m ⁻²)	4.8
Volume (L)	2
Temperature (°C)	25
Flow rate (L min ⁻¹)	300
Electrolyte (mM)	NaCl: 56.3
	Na ₂ SO ₄ + NaCl: 21.1 + 2.8

Table 2.5. Experimental conditions applied in the EOX-Intermediates experiments.

Electrochemical experiments (EOX-Intermediates)				
	Dexamethasone	Amoxicillin	Paracetamol	Sertraline
Concentration (mg L ⁻¹)	80		3000	
J _{applied} (A m ⁻²)	48	1000	1000	900
Volume (L)		2		
Temperature (°C)		25		
Flow rate (L min ⁻¹)		300		
Electrolyte (mM)		NaCl: 56.3		
		Na ₂ SO ₄ + NaCl: 21.1 + 2.8		

2.3. Analytical measurements of drugs and intermediates

2.3.1. Liquid chromatography analysis

High-Performance Liquid Chromatography (HPLC)

This analytical technique was employed to follow-up the DEX, AMX, PAR and STR drugs during the oxidation process, both in EOX-Drugs and EOX-Intermediates. In EOX-Drugs experiments, the samples were analysed without any previous dilution, as well as the DEX samples of the EOX-Intermediates. On the contrary, the samples of EOX-Intermediates of AMX, PAR and STR, were diluted 100 times (1:100).

Isocratic elution methods

Oxidized pharmaceuticals' containing samples have been quantitatively analysed using an Agilent Series 1100 High-Performance Liquid Chromatograph (HPLC) coupled to a Diode Array Detector (DAD) 1260 (Figure 2.3). The separation occurred with a Zorbax Extend-C18 column ($L = 150$ mm; $\varnothing_i = 3$ mm; $5 \mu\text{m}$). In all cases, the temperature column was kept at 30°C , and the injection volume was $50 \mu\text{L}$.

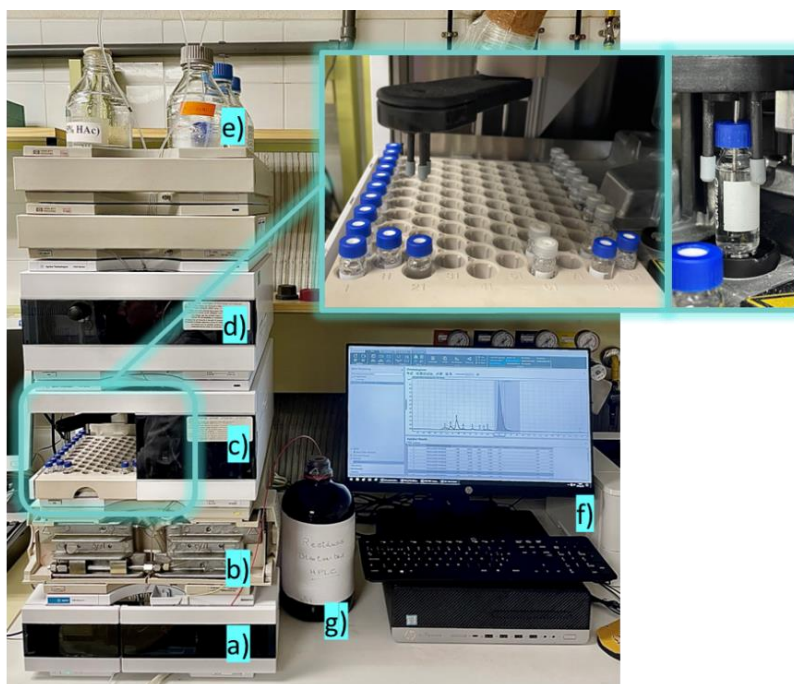


Figure 2.3. High-Performance Liquid Chromatograph (Agilent Series 1100) employed for analysis of the DEX, AMX, PAR and STR, with the different modules: a) UV-VIS module, b) column, c) auto-sampler, d) pump module, e) solvents, f) computer and g) waste solvent recipient.

Table 2.6 details the isocratic elution methods, with the concentrations and mobile phases employed for the analysis of the pharmaceutical compounds. The isocratic methods used for HPLC measures of DEX, AMX and PAR were taken from the bibliography (Bian et al., 2019; Guo et al., 2017; Tan et al., 2020; Youssef et al., 2019). For the STR measures, it was more complicated to establish a proper method to detect the compound. The selected method was based on that reported by Ferrarini et al. (2010) was partially adapted, changing the methanol used as mobile phase (proposed by the authors) by acetonitrile (ACN), and reducing the concentrations of the phosphate buffer to 0.02 M (instead of 0.1 M).

Table 2.6. Conditions applied for the analysis of the DEX, AMX, PAR and STR in HPLC.

	Dexamethasone	Amoxicillin	Paracetamol	Sertraline
Mobile phases	Acetonitrile:Ultrapure water			Acetonitrile: Phosphate buffer 0.02 M (pH=4.5)
Proportion	40:60	5:95	25:75	50:50
Flow rate (mL min ⁻¹)	0.5	0.5	0.7	0.6
Wavelength	240	228	248	205
Retention time	3.1	1.9	1.2	2

2.3.2. Qualitative screening analysis of organics in electro-oxidated solutions

This method was employed to follow the evolution of the intermediate compounds generated during the electrochemical oxidation experiments (EOX-Intermediates).

Extraction and concentration

For the qualitative determination of the oxidation by-products, two different methods were followed, with different initial sample volume, depending on the initial drug concentration employed. The objective is to concentrate the samples in order to detect in a proper way the intermediates formed, otherwise, due to their such low concentrations, they would be very hard or impossible to detect. For the dexamethasone analysis, 80 mg L⁻¹ were used as initial concentration (the limit of its solubility in water), avoiding the use of organic solvents for its dissolution. 100 mL of the initial sample were added to a separatory funnel and extracted four times with 20 mL of dichloromethane each time (Figure 2.4a). The organic extract (Figure 2.4b) was concentrated in two steps, first employing a rotatory evaporator of up to 1 mL (Figure 2.4c), and secondly, using a N₂ stream (Figure 2.4d).

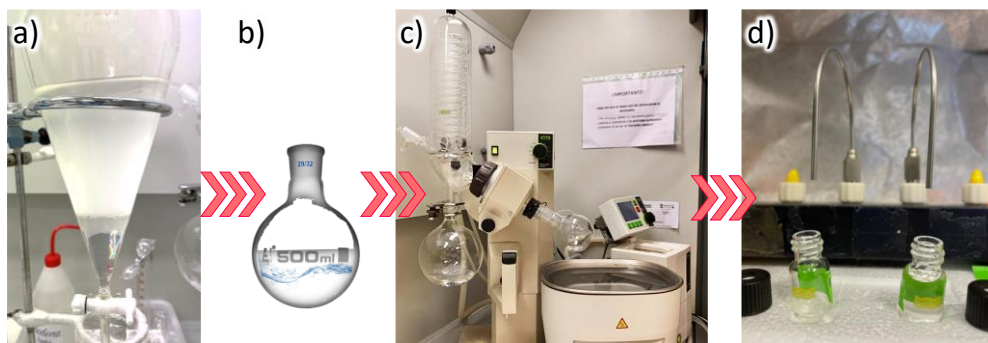


Figure 2.4. Concentration steps for the DEX samples.

For the rest of the drugs (amoxicillin, paracetamol, and sertraline) the procedure was different, due to their high solubility in water (above 3000 mg L^{-1}). For all of them, an initial concentration of 3000 mg L^{-1} was used (see Table 2.5). 30 mL of the initial solution were needed, which that extracted twice with 20 mL of dichloromethane in separatory funnels (Figure 2.5a). Subsequently, they were concentrated up to 1 mL approximately with a N_2 stream utilizing a TurboVap evaporator with a temperature bath of $30 \text{ }^\circ\text{C}$ (Figure 2.5b). Finally, they were transferred to amber vials (Figure 2.5c) and evaporated up to 1 mL of with a N_2 stream. Finally, the concentrated extract was analysed using a GC-MS Shimadzu QP2010 equipped with an auto-sampler (Figure 2.6).

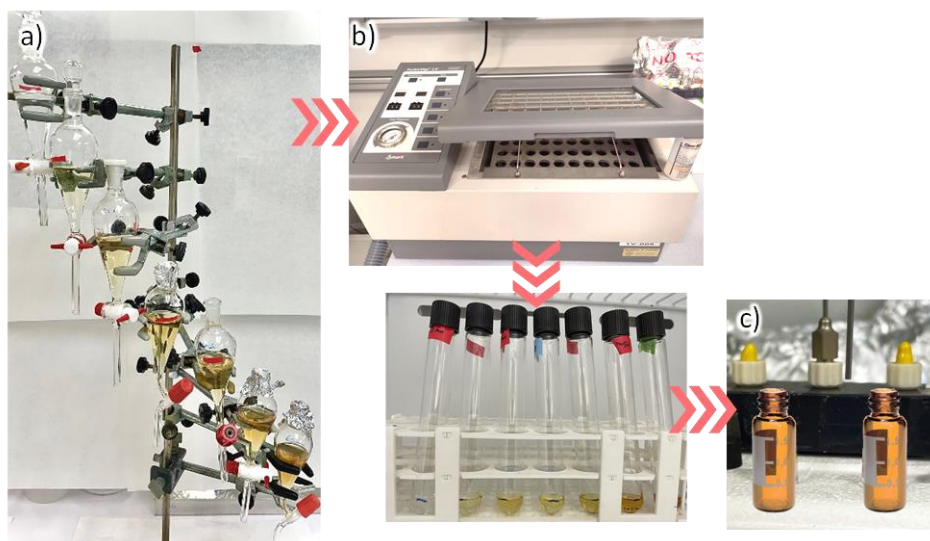


Figure 2.5. Concentration steps for the AMX, PAR and STR samples.

Gas chromatography analysis

Qualitative analysis of the by-products formed during the electrochemical oxidation experiments was performed by gas chromatography-mass spectrometry (GC-MS). The employed GC-MS was a Shimadzu QP2010 Ultra equipped with an auto-sampler (Figure 2.6). The separation occurred in an HP-5MS column (30 m x 0.25 mm x 0.1 mm). The mass spectrometer was operated in the electron impact ionization mode (70 eV). The analytical method employed was different for the various chemical compounds studied. Table 2.7 summarises the main parameters of each analytical method used for the detection of by-products generated during the drugs EOX process. The initial method applied was employed by Vallejo (2014), partially modified depending on the pharmaceutical compound to analyse.



Figure 2.6. GC-MS Shimadzu QP2010 equipped with an auto-injector AOC-20i employed in the intermediate compounds analysis.

The correspondent identification of the intermediates detected, formed during the electrochemical oxidation treatment was carried out by the comparison of their mass spectra with those from the NIST08 spectra database. A match percentage was obtained by comparing the mass spectrum and the characteristic ions of a peak with that of a known compound from the library. The compound was deemed identified and reported if the match percentage was higher than 70%. The peak area was taken as a reference for the concentration of the compound, the bigger area, the higher concentration of the compounds. The different concentration changes of these intermediates were determined by comparing the evolution of their characteristic peak areas at different oxidation times.

Table 2.7. GC-MS methods for the analysis of the intermediates found during EOX of DEX, AMX, PAR and STR.

	Dexamethasone	Amoxicillin	Paracetamol	Sertraline
Column	HP5-MS (L= 30 m; ϕ_i = 0.25 mm)			
Film thickness	0.1 mm			
T^a GC-MS oven	100 °C hold 2 min, rate 20 °C min ⁻¹ to 280 °C, hold 10 min, rate 20 °C min ⁻¹ to 300 °C, hold 3 min	100 °C hold 2 min, rate 20 °C min ⁻¹ to 320 °C, hold 3 min	100 °C hold 2 min, rate 20 °C min ⁻¹ to 280 °C, hold 3 min, rate 10 °C min ⁻¹ to 300 °C, hold 3 min.	100 °C hold 2 min, rate 20 °C min ⁻¹ to 300 °C, hold 5 min
GC				
Carrier gas	He			
Column flow	0.80 mL min ⁻¹			
Pressure	54.8 kPa			
Volume sample	1 μ L			
Injection mode	Splitless			
Split ratio	10			
Injector T^a	285 °C			
Start time/ End time	2 min/25 min	3 min/15 min	3 min/18 min	3 min/16 min
Transfer line T^a	290 °C			
MS				
Ion source T^a	230 °C			
Full scan mode	Range from m/z 45 to 400	Range from m/z 45 to 450	Range from m/z 45 to 250	Range from m/z 45 to 350

2.4. Analysis of PCDD/Fs

2.4.1. Standard method EPA 1613: Tetra- through Octa-Chlorinated Dioxins and Furans by Isotope Dilution HRGC/HRMS

PCDD/Fs were analysed after the application of the preparation Standard Method U.S. EPA 1613 by isotope dilution and high-resolution gas chromatography coupled to high-resolution mass spectrometry (HRGC-HRMS) (US EPA, 1994). It consists of several consecutive and very precisely steps, condensed in Figure 2.7, such as liquid-liquid extraction and several concentration and purification steps, with the purpose of

condition the samples prior to their analysis in HRGC-HRMS (Fernández-Castro et al., 2016; Vallejo et al., 2013, 2014). Usually, the required time to perform all these concentrations and purification stages takes approximately five days for each sample (one data). In addition, due to the employment of high purity solvents, added to the high number of stages, the economic cost is considerable, estimated at around 400-500 euros/sample, therefore, it is worth noting the value of the obtained results.

In order to guarantee the analysis of the PCDD/Fs, two standard solutions have been employed: 1613 LCS, a solution/mixture of fifteen $^{13}\text{C}_{12}$ -labelled chlorinated dibenzo-p-dioxins (2,3,7,8- $^{13}\text{C}_{12}$ -PCDDs) and dibenzofurans (2,3,7,8- $^{13}\text{C}_{12}$ -PCDFs) utilized to calculate the recoveries of the labelled compounds obtained through the various stages followed to prepare the sample before the analysis; and ISS, an internal standard, which is added to the sample previous to the chromatographic analysis, to calculate the concentrations of the labelled compounds (1,2,3,4-TCDD $^{13}\text{C}_{12}$ y 1,2,3,7,8,9-HxCDD $^{13}\text{C}_{12}$) and the OCDF. EPA 1613 CLS-CS4 has been utilized as calibration standard solution. For further consultation, in Annex II are gathered the concentrations of the 1613 ICS, ISS and CLS-CL4 standards employed. The EPA 1613 method stages are detailed hereunder. PCDD/Fs are present in the order of pg L^{-1} , so all the following stages must be executed with extreme caution to maintain the quality of the samples obtained through all the process.

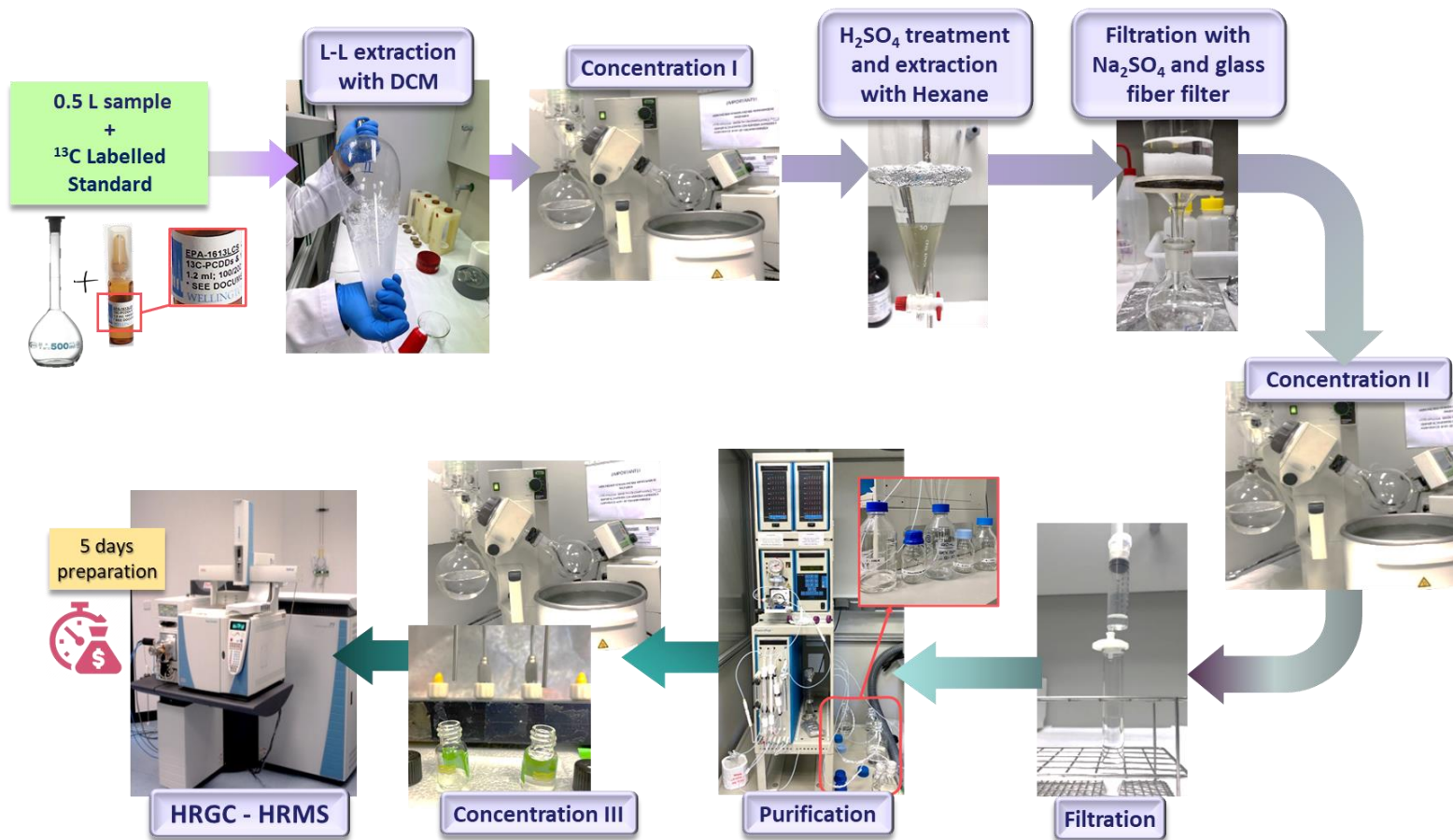


Figure 2.7. Scheme of the different consecutive steps for the analytical determination of PCDD/Fs (US EPA, 1994).

L-L extraction with DCM

500 mL of the sample were incorporated into a 2 L separatory funnel and spiked with 10 μL of a fifteen mass ^{13}C -labeled PCDD/Fs solution, from TCDD/Fs to OCDD/Fs (EPA 1613 LCS), previously dissolved in 0.5 mL of acetone Suprasolv[®]. The vial with the labelled PCDD/Fs was washed three times with dichloromethane, and added to the aqueous sample, placed in the separatory funnel. Then, 60 mL of dichloromethane (DCM) UniSolv[®] were added to the separatory funnel and thereafter, the mixture was shaken vigorously for 3 minutes, with the aim of extracting the PCDD/Fs from the aqueous phase to the organic phase. Later on, the PCDD/Fs contained in the organic phase were transferred to a round-bottom flask. This extraction process is repeated three times, transferring each time the organic phase to the round-bottom flask, having at last 180 mL of organic phase (Figure 2.8).

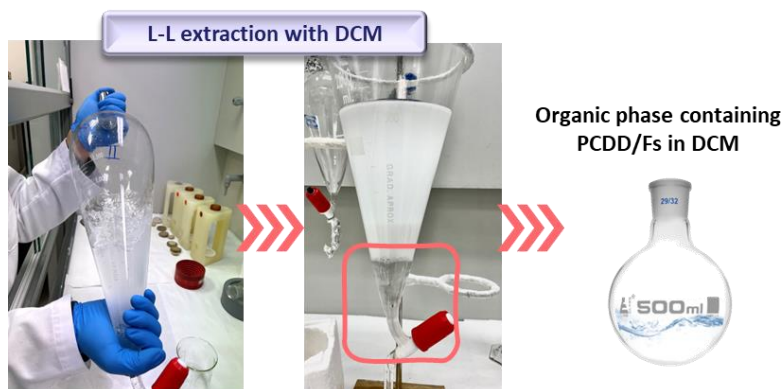


Figure 2.8. Extraction of PCDD/Fs from the aqueous phase to the organic phase (US EPA, 1994).

Concentration I

The organic extract is placed in a rotatory evaporator Büchi R-210 and evaporates almost to dryness at 35 °C, decreasing the pressure from 750 to 600 mbar. At this point, the extract is rinsed with DCM and once more, concentrated nearly to dryness, in triplicate (Figure 2.9).

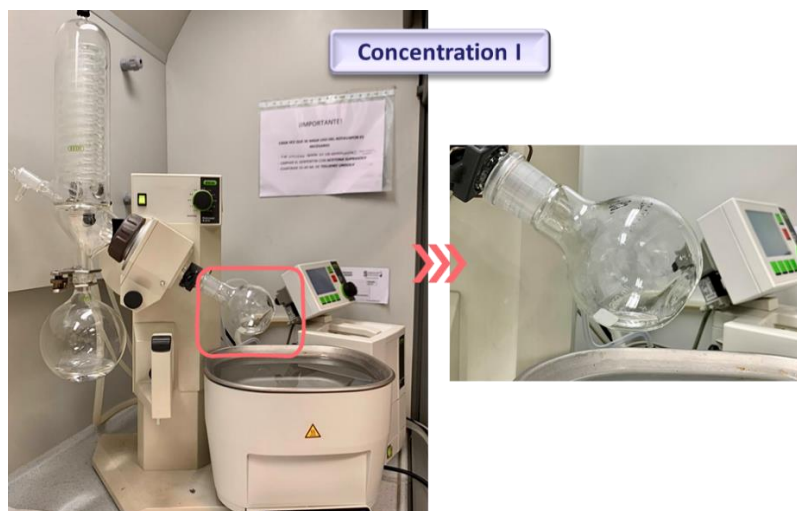


Figure 2.9. Concentration step in a rotatory evaporator Büchi R-210 (US EPA, 1994).

H₂SO₄ treatment and filtration

Here, with the aim of eliminating the organic matter, the extract coming from the previous step, was treated with H₂SO₄ and with n-hexane. Firstly, the evaporated extract was passed to another separatory funnel of 250 mL, where 75 mL of n-hexane UniSolv[®] and after, 50 mL of H₂SO₄ were added; the mixture was shaken for 3 minutes. This process was repeated two times. The organic phase in n-hexane; was filtered through a glass fibre filter and Na₂SO₄ placed on a Buchner glass funnel (Figure 2.10).

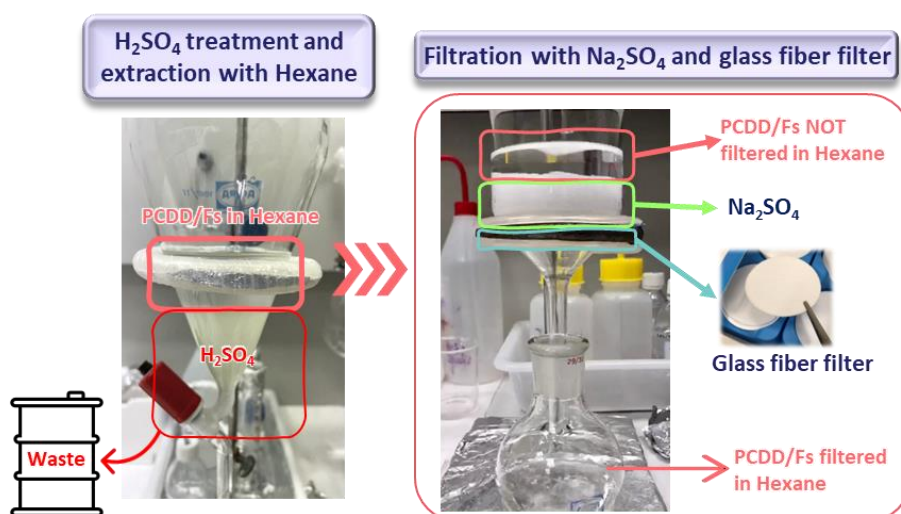


Figure 2.10. H₂SO₄ and filtration and drying with Na₂SO₄ treatment (US EPA, 1994).

Concentration II

The organic phase in n-hexane, was placed again for concentration in the rotatory evaporator, until dryness, at 35 °C and decreasing the pressure from 600 to 300 mbar. When just one drop is in the flask, the extract was rinsed with n-hexane and evaporated again nearly to dryness; this procedure was performed in triplicate (Figure 2.11).

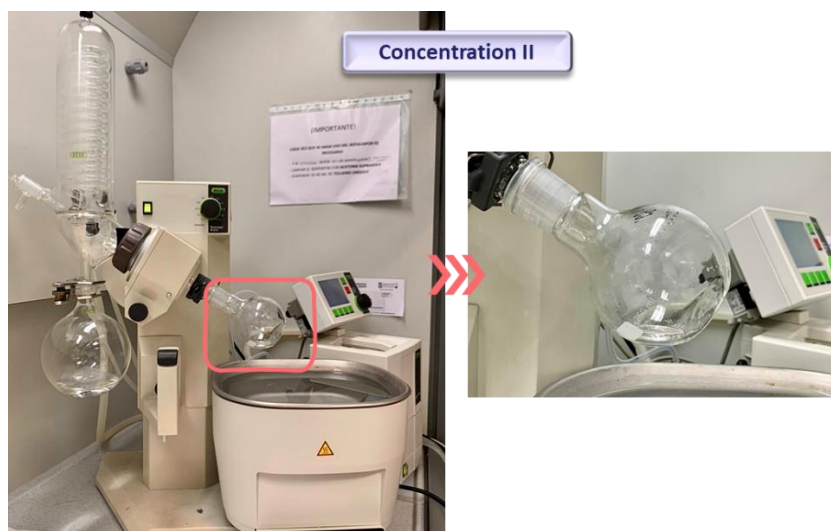


Figure 2.11. Concentration step in a rotatory evaporator Büchi R-210 (US EPA, 1994).

Filtration

The organic extract from the previous stage was filtered with a filter syringe with 0.45 μm PTFE filter, in a test tube, until a volume of 14 mL of n-hexane (Figure 2.12).

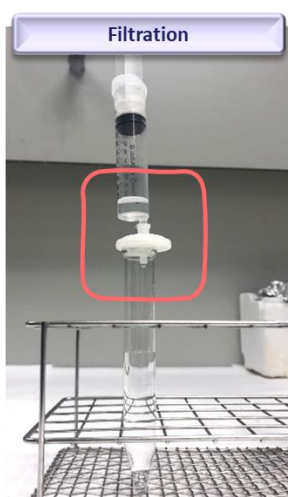


Figure 2.12. PCDD/Fs syringe filtration step (US EPA, 1994).

Purification

The filtered extract was purified by solid-liquid adsorption chromatography performed in an automated system, Power-Prep™ (Fluid Management Systems Inc., Waltham). This clean-up system is a high-speed sample processing workstation, based on the use in a sequential manner of multilayer silica, basic alumina and PX-21 carbon adsorbents. The filtered extract was pumped from the containing vial through the different columns employing several solvents, and mixtures solvents: n-hexane, n-hexane/dichloromethane (90/10 v/v), n-hexane/dichloromethane (50/50 v/v), toluene/ethyl acetate (50/50 v/v) and toluene. The resultant purified extract contains the PCDD/Fs in 75 mL of toluene, eluted from the carbon column. In Figure 2.13 this extraction system is shown.



Figure 2.13. Automated clean-up system (Power-Prep™, Fluid Management Systems Inc., Waltham).

Concentration III

In this last concentration step, toluene was evaporated in the rotatory evaporator, close to dryness at 35 °C and decreasing the pressure from 150 to 85 mbar; the round-bottom flask was rinsed three times with DCM, each time with approximately a volume of 2 mL (Figure 2.14a). Finally, this last drop was transferred into a vial to be concentrated to dryness using a gentle N₂ stream, in a minivap unit (Figure 2.14b).

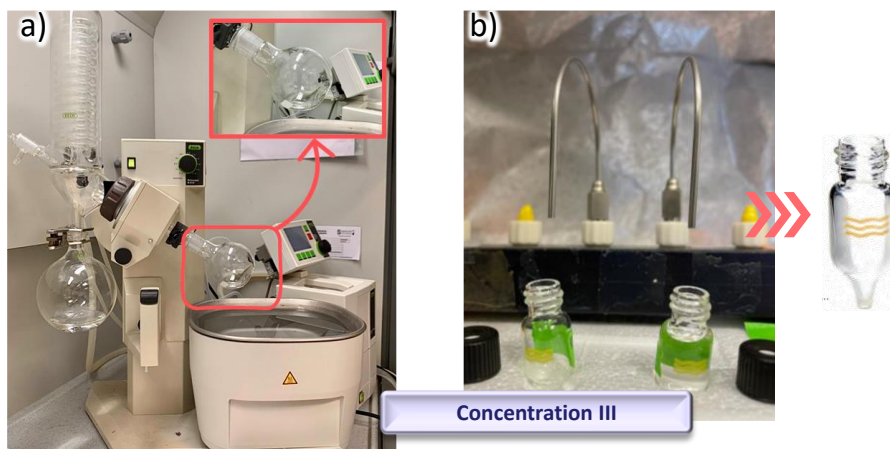


Figure 2.14. a) Concentration step in a rotatory evaporator Büchi R-210, and b) concentration step with an N₂ stream (US EPA, 1994).

2.4.2. HRGC-HRMS analysis

Purified samples were analysed in the Chromatographic Service (SERCROM) of the University of Cantabria. Prior to the chromatographic analysis, internal syringe standards (EPA 1613 ISS) were added to the sample.

The analysis was conducted by HRGC-HRMS, using a TRACE GC UltraTM gas chromatograph equipped with a split/splitless injector (Thermo Electron S.p.A.) and a DB-5 fused silica capillary column (J&W Scientific) (Figure 2.15). The column was started with a temperature of 120 °C, was kept constant for 2 min, and finally, gradually increased in 3 steps to 210 °C, 230 °C and 310 °C at 15, 1 and 3 °C min⁻¹, respectively, for the analysis from tetra- to octa-CDD/Fs. The column was linked, through a heated transfer line kept at 270 °C, to a DFS high-resolution magnetic sector mass spectrometer with a BE geometry (Figure 2.15). The source employed a positive electron ionization (EI+) mode with ionization energy of 45 eV, and the temperature was set at 270 °C. The mass spectrometer was operated in SIM mode at 10000 resolution power (10% valley definition). Detection limits were calculated as the concentration values that gave instrumental responses within a signal-to-noise ratio of 3.



Figure 2.15. HRGC-HRMS (Thermo Fisher Scientific), SERCROM, University of Cantabria.

The isotopic dilution method was applied to conduct the quantitative determination of the PCDD/Fs. Relative response factors (RRFs), acquired from the calibration curve by the analysis of 1613CSL and 1613CS-1–CS-4 standard solution mixtures for tetra- to octa-PCDD/Fs were used to determine the dioxins and furans concentration in the samples. The recoveries of the labelled standards were calculated by the use of a combination of two labelled PCDD/Fs (contained within the ISS).

2.4.3. Quality control and quality assurance in the analysis of PCDD/Fs

It is of the utmost importance to guarantee the accuracy of the method, as well as the recoveries and the absence of contamination during the analysis. It was proven, on the one hand, that the recoveries of the samples were within the ranges established by the US EPA method, detailed individually in Annex II, and on the other hand, blanks assays were performed, covering the whole sample preparation process, with ultrapure water spiked with LCS standard (also detailed in Annex II). This blanks' analysis showed that PCDD/Fs were present in negligible concentrations, showing the near absence of contamination, and in addition, these blanks were subtracted from the detected PCDD/Fs concentrations for each realised experiment, in order to ensure the reliability of the results obtained.

2.5. Computational calculations

In this doctoral thesis, density functional theory (DFT) has been selected as method, to obtain the computational calculations related to the characteristics and the behaviour of atomic and subatomic particles, which implies the determination of an

electronic structure, by solving the Schrödinger's equation (Lam et al., 2020). To this, the software Gaussian 16 has been employed. Gaussian 16 is a computational software able to solve the molecular Schrödinger's equation, based on the theory of molecular orbitals (TOM) (Foresman and Frisch, 2015). From some initial parameters, as the method family (*ab initio* methods, DFT or semiempirical), level of theory (B3LYP, HF, APFD...), basis functions (6-31G(d), 6-311+G(d)...), initial coordinates of the molecule (in Cartesian coordinates, indicating x, y and x position of the atoms, or in internal ones, matrix-z, indicating the distances, angles and dihedrals) and the charge and multiplicity, the molecular wave function can be calculated, obtaining different atomic and molecular properties (Cuevas and Cortés, 2003; Foresman and Frisch, 2015; Jensen, 2007; Lewars, 2016).

The level of theory, also known as theoretical method, are different approximations to the Schrödinger equation, each one with its own accuracy, computational cost and resource requirements; is composed by the functional and the basis set. The functional is combination of functions, in DFT, is the electron density as a function of the (x,y,z) positions of the atoms, and the basis set are a collection of other mathematical functions used to build the quantum mechanical wavefunction for a molecular system (Foresman and Frisch, 2015). In this thesis, the level of theory applied for the geometry and energy optimizations, the calculation of the transition states and the intrinsic reaction coordinate calculations (IRC) was uB3LYP/6-31G(d,p), with "uB3LYP" as the functional and "6-31G(d,p)" as the basis set.

Additional calculations, such as single point energy (SPE) calculations were carried out with a much larger basis set, 6-311++G(2df,2pd); to obtain a more realistic description of the atomic orbitals. Moreover, in this latter case, the term "Empirical dispersion" (GD3BJ) has been added, to help in the description of the medium- long-range dispersion (Van der Waals type of interactions). In all cases, the solvent effect (water) was considered. As a consequence of the higher time consumed, quantum calculations were carried out in the QTREX supercomputer, which belongs to the computer cluster of LAQV, REQUIMTE (Associated Laboratory for Green Chemistry of the Network of Chemistry and Technology), of the Chemistry and Biochemistry Department of the Faculdade de Ciências (Universidade do Porto, Portugal). The current configuration of the computational system has a total of 1568 CPU cores and little more than 83k GPU cores, spread across a platform with an ultrafast infinite band network and 10 Gbit/s links between master and slave nodes (LAVQ REQUIMTE, 2022). Figure 2.16

represents an example of the computational set-up employed for the development of the theoretical part of the doctoral thesis.

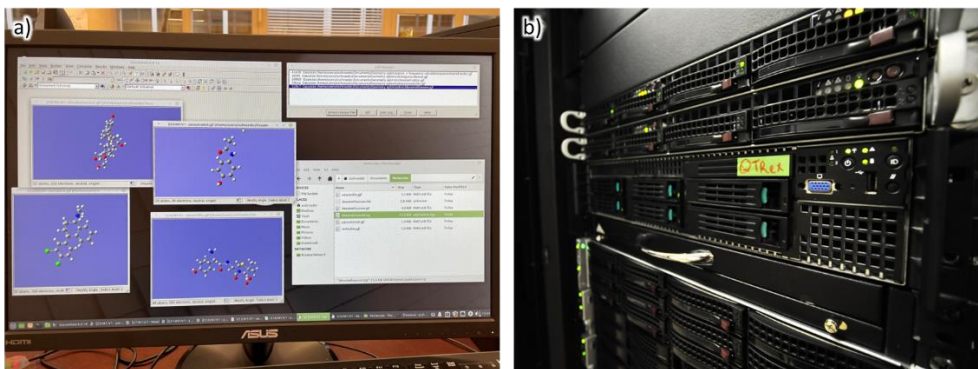


Figure 2.16. a) Example of the visualisation of the program and b) Supercomputer QTREX of the LAQV, REQUIMTE.

2.5.1. Working methodology in computational chemistry within the framework of PCDD/Fs formation mechanisms

The principal steps to carry out the simulations using Gaussian software are described below:

- *1st Step.* First, it is necessary to draw the molecule of interest in the software Gaussview, included in the Gaussian package, which is the graphical interface of Gaussian. It helps, on the one hand, to build the molecule/molecules that are going to be used and with this, to create the input file with the atomic coordinates of each atom of the system, and on the other hand, in the interpretation of the output file (results) of software Gaussian (e.g., to plot properties, animate vibrations, visualize computed spectra, etc.) (Figure 2.17).
- *2nd Step.* Then, the input file program is prepared. The screen of an input file is a *black screen* (known as command window or terminal), which consists of certain “blocks”, detailed in Figure 2.18. In this case the Linux operating system, with its correspondent terminal has been used. The different sections of the input file are colour-boxed and described in this figure:
 - ✓ *Number of processors to be used (red colour).* Here it can be defined the desired number of processors to be used for the calculation.
 - ✓ *Checkpoint file (green colour).* Name of the file that saves the intermediate calculations as a backup.

- ✓ *The “code line” (light blue colour)*. Here it is introduced the necessary code depending on the type of calculation to be performed, for instance, optimisation, frequency calculations, IRC.... Those different types of calculations. With the correspondent code lines are widely explained in Chapter 5.
- ✓ *Job title (purple colour)*. Name of the type of calculation.
- ✓ *Charge and spin multiplicity (deep blue colour)*. Here it is indicated the charge and multiplicity of the system, and it can be modified depending on the desired calculation.
- ✓ *Internal coordinates (yellow colour)*. Space positions (x, y, z) of all the atoms of the system.
- ✓ *Atom connectivity (pink colour)*. Information of the atoms bonding within the molecule.
- ✓ *Additional information (orange colour)*. Many calculations require additional input, so this section contains this type of additional modifications, such freeze a specific bond, or other calculations, as the code to perform a scan.
- *3rd Step*. Once it is prepared, it is launched in the supercomputer (Figure 2.16b).
- *4th Step*. To visualise the results, the output file is opened in Gaussview. In Figure 2.17, it can be seen the different types of results to consult (Chapter 5) in the drop-down menu.

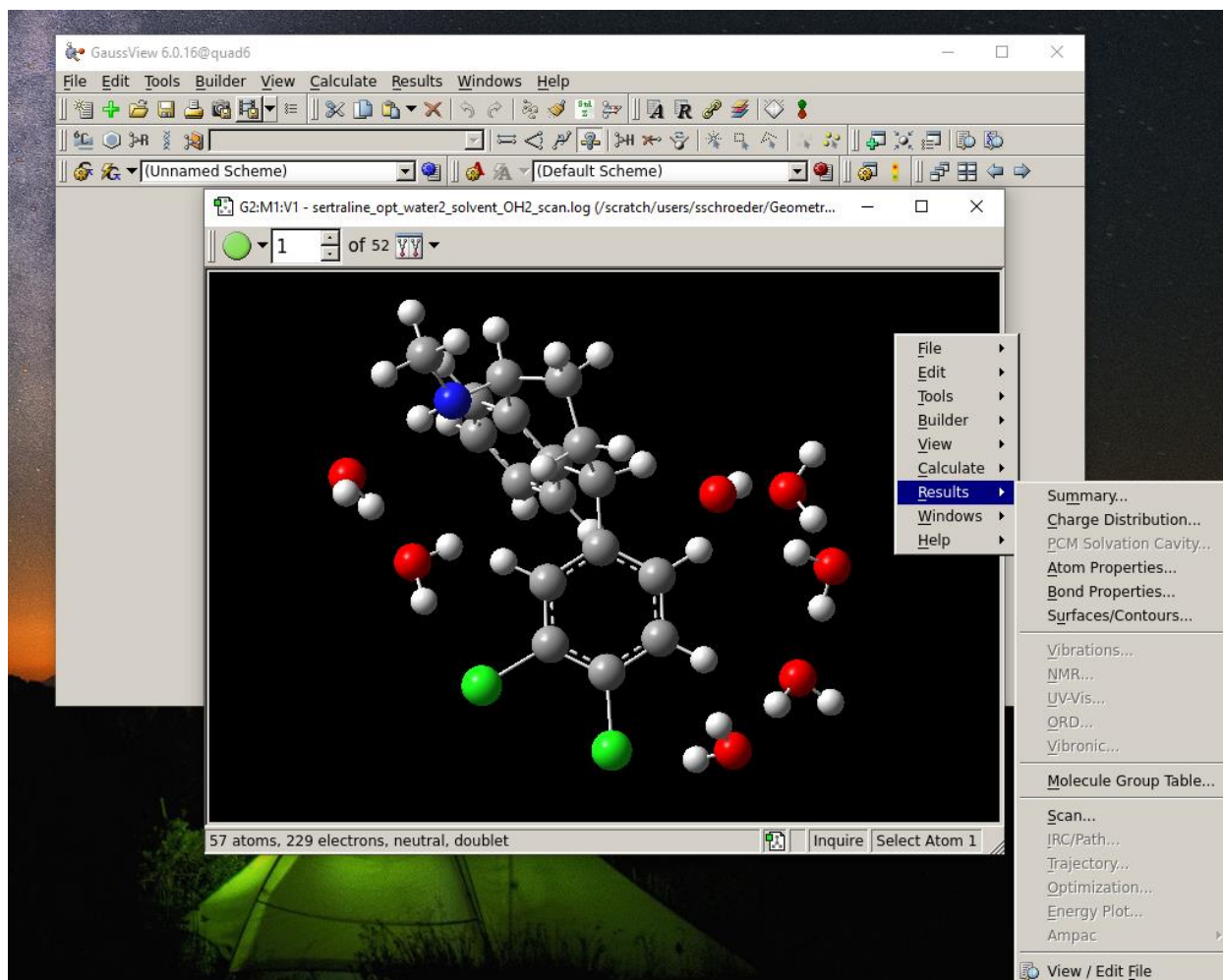


Figure 2.17. Gaussview visualisation program, with the different types of results to consult in the drop-down menu.

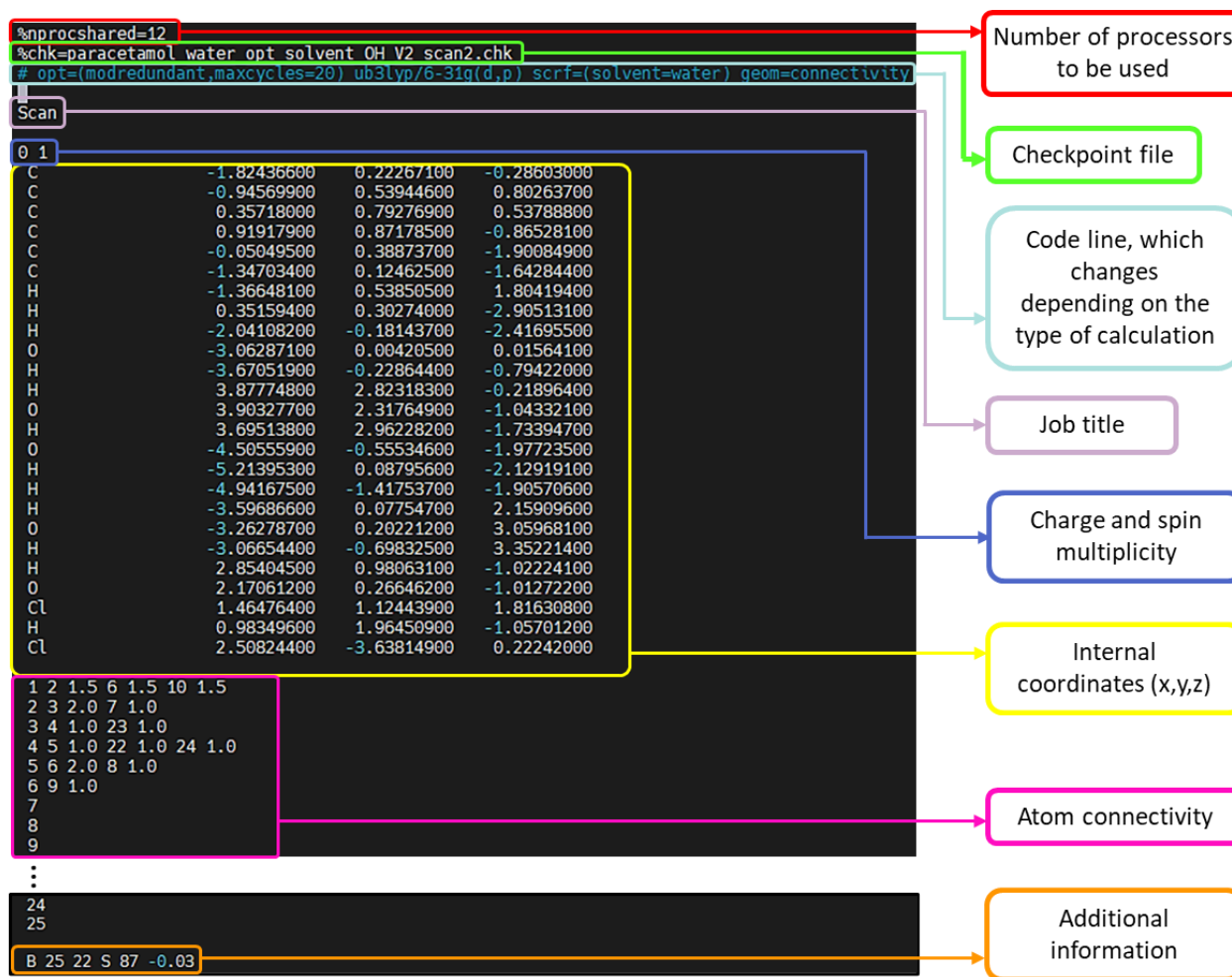


Figure 2.18. Structure of a Gaussian input file with the different blocks of the program depicted in colours.

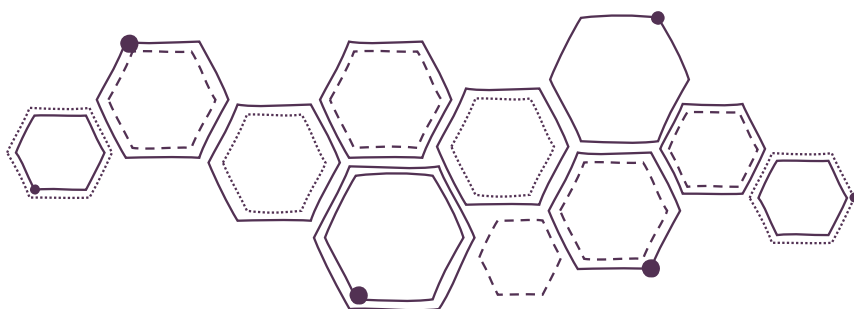
2.6. References

- Bian, X., Xia, Y., Zhan, T., Wang, L., Zhou, W., Dai, Q., Chen, J., 2019. Electrochemical removal of amoxicillin using a Cu doped PbO₂ electrode: Electrode characterization, operational parameters optimization and degradation mechanism. *Chemosphere* 233, 762–770. <https://doi.org/10.1016/j.chemosphere.2019.05.226>
- Cuevas, G., Cortés, F., 2003. *Introducción a la química computacional*, 1st ed. Fondo de Cultura Económica.
- Fernández-Castro, P., San Román, M.F., Ortiz, I., 2016. Theoretical and experimental formation of low chlorinated dibenzo-p-dioxins and dibenzofurans in the Fenton oxidation of chlorophenol solutions. *Chemosphere* 161, 136–144. <https://doi.org/10.1016/j.chemosphere.2016.07.011>
- Ferrarini, A., Huidobro, A.L., Pellati, F., Barbas, C., 2010. Development and validation of a HPLC method for the determination of sertraline and three non-chiral related impurities. *J. Pharm. Biomed. Anal.* 53, 122–129. <https://doi.org/10.1016/j.jpba.2010.01.036>
- Foresman, J.B., Frisch, Æ., 2015. *Exploring Chemistry with Electronic Structure Methods*, 3rd ed. Wallingford, CT.
- Guo, Z., Guo, A., Guo, Q., Rui, M., Zhao, Y., Zhang, H., Zhu, S., 2017. Decomposition of dexamethasone by gamma irradiation: Kinetics, degradation mechanisms and impact on algae growth. *Chem. Eng. J.* 307, 722–728. <https://doi.org/10.1016/j.cej.2016.08.138>
- Jensen, F., 2007. *Introduction to Computational Chemistry, Theoretical Chemistry Accounts*.
- Lam, Y.H., Abramov, Y., Ananthula, R.S., Elward, J.M., Hilden, L.R., Nilsson Lill, S.O., Norrby, P.O., Ramirez, A., Sherer, E.C., Mustakis, J., Tanoury, G.J., 2020. Applications of Quantum Chemistry in Pharmaceutical Process Development: Current State and Opportunities. *Org. Process Res. Dev.* 24, 1496–1507. <https://doi.org/10.1021/acs.oprd.0c00222>
- LAVQ REQUIMTE, 2022. Computer cluster - Specifications [WWW Document]. URL https://laqv.requimte.pt/research/technical-resources/182-computer_cluster (accessed 11.2.22).
- Lewars, E.G., 2016. *Computational chemistry: Introduction to the theory and applications of molecular and quantum mechanics: Third Edition 2016, Computational Chemistry: Introduction to the Theory and Applications of Molecular and Quantum Mechanics: Third Edition 2016*. <https://doi.org/10.1007/978-3-319-30916-3>

- Schröder, S., San-Román, M.F., Ortiz, I., 2020. Photocatalytic transformation of triclosan. Reaction products and kinetics. *Catalysts* 10, 1–15. <https://doi.org/10.3390/catal10121468>
- Solá-Gutiérrez, C., 2019. Traceability of PCDD/Fs formation in the advanced oxidation of TCS. University of Cantabria.
- Tan, T.Y., Zeng, Z.T., Zeng, G.M., Gong, J.L., Xiao, R., Zhang, P., Song, B., Tang, W.W., Ren, X.Y., 2020. Electrochemically enhanced simultaneous degradation of sulfamethoxazole, ciprofloxacin and amoxicillin from aqueous solution by multi-walled carbon nanotube filter. *Sep. Purif. Technol.* 235, 116167. <https://doi.org/10.1016/j.seppur.2019.116167>
- US EPA, 1994. Method 1613B Tetra- through Octa-Chlorinated Dioxins and Furans by Isotope Dilution HRGC/HRMS. *Environ. Prot.*
- Vallejo, M., 2014. Assessment of polychlorinated dibenzo-p-dioxins and dibenzofurans, PCDD/Fs, in the application of advanced oxidation processes. University of Cantabria.
- Vallejo, M., San Román, M.F., Ortiz, I., 2013. Quantitative assessment of the formation of polychlorinated derivatives, PCDD/Fs, in the electrochemical oxidation of 2-chlorophenol as function of the electrolyte type. *Environ. Sci. Technol.* 47, 12400–12408. <https://doi.org/10.1021/es403246g>
- Vallejo, M., San Román, M.F., Ortiz, I., Irabien, A., 2014. The critical role of the operating conditions on the fenton oxidation of 2-chlorophenol: Assessment of PCDD/Fs formation. *J. Hazard. Mater.* 279, 579–585. <https://doi.org/10.1016/j.jhazmat.2014.07.020>
- Youssef, S.H., Mohamed, D., Hegazy, M.A.M., Badawey, A., 2019. Analytical methods for the determination of paracetamol, pseudoephedrine and brompheniramine in Comtrex tablets. *BMC Chem.* 13, 1–15. <https://doi.org/10.1186/s13065-019-0595-6>

3

ELECTROCHEMICAL OXIDATION (EOX) OF COVID-19 DRUGS



Abstract

In this chapter, the degradation results of the main drugs used intensively in the fight against the SARS-CoV-2 virus and its consequences, are described. As case study, the drugs dexamethasone (DEX), amoxicillin (AMX), paracetamol (PAR), and sertraline (STR) and electrochemical oxidation (EOX) with a boron-doped diamond (BDD) anode, as removal treatment were selected. In this PhD thesis, two different electrolyte media have been employed, sodium chloride (NaCl) and sodium sulphate (Na₂SO₄) in combination with sodium chloride. These two salts are frequently found, especially in wastewaters, and consequently, they are widely applied in EOX processes.

So, the obtained results include, on the one hand, the study of the degradation of these four drugs (EOX-Drugs), and on the other hand, the identification, through GC-MS, of the intermediates formed during the EOX treatment (EOX-Intermediates), employing both electrolytes. Additionally, the kinetics of the drugs oxidation and the formed by-products to verify the degradation efficiency and toxicity of the samples, have been studied. For EOX-Drugs experiments, an initial concentration of 10 mg L⁻¹ of each compound has been employed and for EOX-Intermediates, between 80 and 3000 mg L⁻¹ have been used, with the aim of identifying properly those by-products, which are present at very low concentrations. Finally, a theoretical analysis of the radical's formation chloride and sulphate in order to understand the behaviour of the degradation kinetics of each drug has been carried out.

3.1. Limiting current density

As long as the concentration of the reactant at the electrode surface is greater than zero, an increase in the applied potential in the cell corresponds to an increase in the reaction rate and a decrease in the concentration of the reactant. Therefore, an increase in current intensity is produced, since this parameter indicates the number of electrons that are transferred between the two electrodes. Under these conditions, the process is under electric current control (100% of efficiency). As the reactant concentration approaches zero, an increase in potential does not correspond to an increase in reaction rate, and therefore the current intensity does not change with the applied potential. In this case, the process is then under the control of mass transport. This evolution of constant intensity with potential is maintained until another electrochemical process occurs, such as the decomposition of the electrolyte or the anodic evolution of oxygen from the water. On this regimen, secondary reactions start to appear, resulting in a decrease in current effectiveness (Cañizares et al., 2006, 2004).

Previous to the experimental development, the limiting current density (J_{lim}) has been determined (current density $J=I/A$, being I the intensity and A the effective electrode area). The current density that determines the limit between two different operating regimes: when the current density (J) is lower than J_{lim} , the process is under electric current control ($J < J_{lim}$), and when J is higher than J_{lim} , the process is under mass-transport control ($J > J_{lim}$). In this context, a theoretical method was proposed by Panizza and Cerisola (2009) for a mass-transport control process. In the limit conditions, so the concentration of the reactant at the electrode surface is equal to zero and $J=J_{lim}$, the speed of the electrochemical process and that of mass transfer are equal, obtaining the expression:

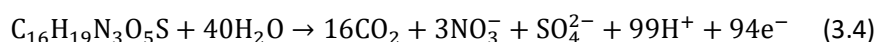
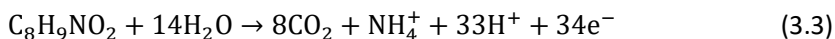
$$J_{lim} = n \cdot F \cdot k_m \cdot C_{org} \quad (3.1)$$

where J_{lim} is the limiting current density ($A \cdot m^{-2}$) necessary to carry out the organics' oxidation, n is the number of electrons participating in the electrochemical oxidation of the selected compound, F is the Faraday constant (96485 C mol^{-1}), k_m is the mass transport coefficient ($m \cdot s^{-1}$) and C_{org} is the concentration of the selected organic compound in the solution ($mol \cdot m^{-3}$). Where Eq. 3.1 can be expressed as a function of limiting current (I_{lim}) and area (A):

$$k_m = I_{lim} / (n \cdot F \cdot A \cdot C_{org}) \quad (3.2)$$

where k_m is the mass transport coefficient ($m\ s^{-1}$), n the number of exchanged electrons, F is the Faraday constant ($96485\ C\ mol^{-1}$), A is the electrochemical cell area (m^2) and C_{org} is the concentration of the compound that is oxidized.

The number of exchanged electrons in the reaction depends on the compound involved. Eqs. 3.2 and 3.3 detail the number of exchanged electrons for the paracetamol ($34\ e^-$) and amoxicillin ($94\ e^-$), respectively (Brillas et al., 2005; Ganiyu et al., 2019; Orimolade et al., 2020; Oturan et al., 2017; Quand-Même et al., 2015; Sopaj et al., 2015).

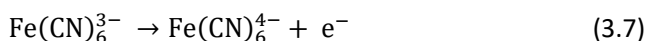
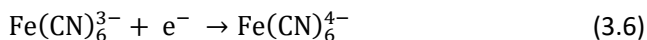


For dexamethasone and sertraline, J_{lim} was calculated differently, because of the non-availability of the mineralisation equations in the literature. Here, J_{lim} was calculated with the same previous equation (Eq. 3.1), but as a function of COD, through Eq. 3.4:

$$J_{lim} = 4 \cdot F \cdot k_m \cdot COD \quad (3.5)$$

being 4 is the number of exchanged electrons, F is the Faraday constant ($96485\ C\ mol^{-1}$), k_m is the mass transport coefficient ($m\ s^{-1}$) and COD is the chemical oxygen demand ($mol\ O_2\ m^{-3}$).

For the electrochemical cell used during the experimental stage, k_m was experimentally determined through the ferrocyanide/ferrocyanide redox system, after applying a series of potentials to the EOX cell. Representing the current intensity measured against the applied potential, the limit intensity corresponds to the horizontal zone of the I-V curve (Solá-Gutiérrez, 2019).



Employing the limiting current density experimentally obtained, 1.5 A, and Eq. 3.1, k_m achieved the value $1.48 \cdot 10^{-5}\ m\ s^{-1}$. k_m value and an initial concentration of $10\ mg\ L^{-1}$ of each pharmaceutical compound, applied to the Eq. 3.1, yielded the following J_{lim} values: $3.2\ A\ m^{-2}$ for dexamethasone, amoxicillin, and paracetamol, and $2.8\ A\ m^{-2}$ for sertraline; therefore, to guarantee a mass-transport controlled process, a J_{lim} value of $4.8\ A\ m^{-2}$ was applied in all cases (corresponding to 0.1 A). For the EOX-Intermediates experiments, the J_{lim} for dexamethasone was $25.7\ A\ m^{-2}$, but the J applied was $48\ A\ m^{-2}$

(corresponding with 1 A). For amoxicillin and paracetamol, J_{lim} was 960 A m^{-2} and the J applied was 1000 A m^{-2} (21 A). Finally, for the sertraline case, J_{lim} was 851 A m^{-2} and the J applied was 900 A m^{-2} (19 A). In all cases, the applied current density (A) was calculated for a total anodic area of for a total anodic area of 210 cm^2 . Table 3.1 summarizes the values of calculated J_{lim} , applied J , and the corresponding electric current (calculated as the applied J times the total anodic area (m^2)), for all the experiments. The applied electric current is the one set in the power supply for the experiments.

Table 3.1. Electric parameters for EOX-Drugs and EOX-Intermediates experiments.

	Concentration (mg L^{-1})	Calculated J_{lim} (A m^{-2})	Applied J (A m^{-2})	Applied electric current (A)
Dexamethasone	10	3.2	4.8	0.1
	80	25.7	48	1
Amoxicillin	10	3.2	4.8	0.1
	3000	960	1000	21
Paracetamol	0	3.2	4.8	0.1
	3000	963	1000	21
Sertraline	10	2.8	4.8	0.1
	3000	851	900	19

3.2. Drugs electrochemical oxidation

3.2.1. EOX-Drugs experiments

The evaluation of the degradation of the solutions containing dexamethasone (DEX), amoxicillin (AMX), paracetamol (PAR), and sertraline (STR), by the application of electro-oxidation treatment using a BDD anode, was carried out starting with 10 mg L^{-1} of concentration and working in galvanostatic mode. With the correspondent amounts of electrolyte, a conductivity value of 7.5 mS cm^{-1} was achieved. The preparation of the solutions and the methodology employed to perform the experiments are detailed in Chapter 2, section 2.2.1. Moreover, the experiments were performed in duplicate, with the standard deviation calculated for each pair of experiments to represent the experimental error.

Figure 3.1 depicts the degradation curves of the four drugs used to treat SARS-CoV-2 and its consequences, employing NaCl (Figure 3.1a) and $\text{Na}_2\text{SO}_4 + \text{NaCl}$ (Figure 3.1b) as electrolytes, plotted against the specific electrical charge (Q). Q is calculated as the

electric current (A) times the time (h) and divided by the total treated volume (L). As can be seen, the concentration of each compound is expressed in mM, to have the possibility of making a proper comparison between the degraded pharmaceuticals.

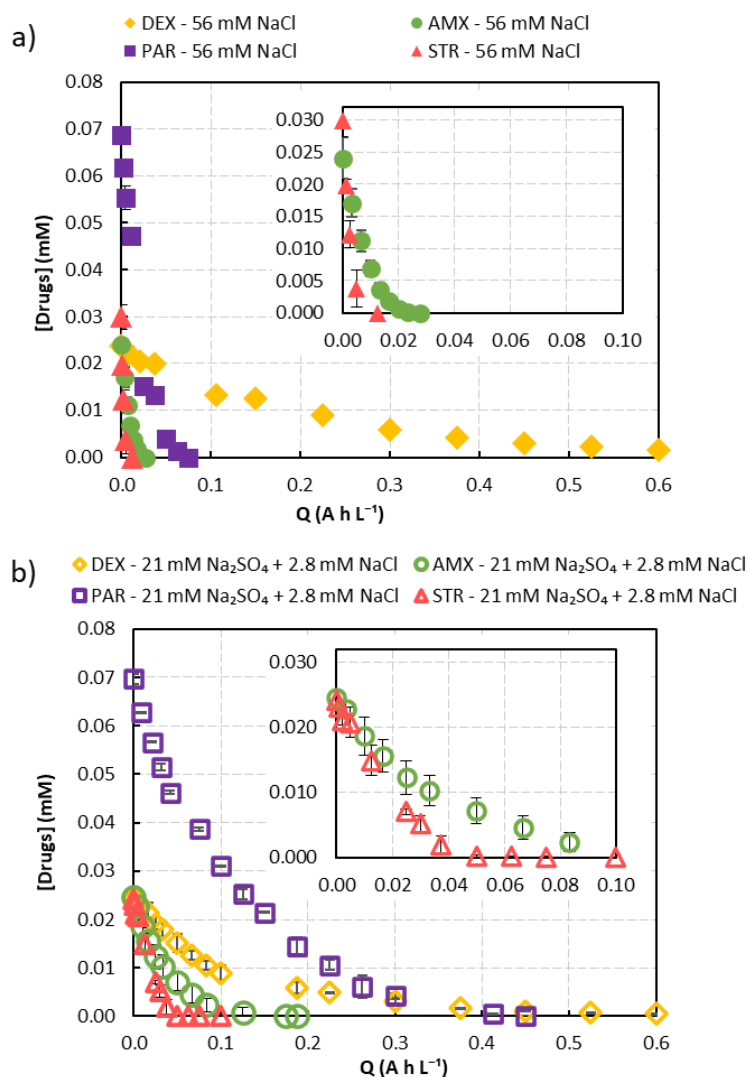


Figure 3.1. Electrochemical degradation of DEX, AMX, PAR and STR versus the specific charge, employing the electrolytes a) NaCl and b) $Na_2SO_4 + NaCl$.

In the first place, it can be seen how the degradation kinetics of all the compounds, for both electrolytes, show the same trend, with a greater or lesser slope (Figure 3.1a and Figure 3.1b). In NaCl medium, for the degradation of AMX, PAR and STR, the specific electrical charge, Q , was below $0.1 A h L^{-1}$ (Figure 3.1a). In the case of DEX, the final Q value was almost the same both for NaCl and Na_2SO_4+NaCl electrolyte mediums,

approximately 0.6 A h L^{-1} (Figure 3.1a and Figure 3.1b). As it is described in Chapter 2, the molecular structure of each drug possesses high importance. Its robustness, or on the contrary having weak bonds on the structure, can affect deeply in the degradation process. PAR, AMX and STR are more or less large molecules, but they have several weak bonds where the molecule can break easily, which produces their fast degradation, at different times depending on the electrolyte used (Figure 3.1a and 3.1b). Conversely, the molecule of DEX has a very strong structure, is a very robust and stable molecule, which makes difficult its breakage, being its degradation more difficult, independently of the electrolyte used (Figure 3.1a and 3.1b).

To reach 50% of degradation, 1, 4, 7 and 50 minutes were necessary, for STR, AMX, PAR and DEX when using 56 mM of NaCl (Figure 3.1a). In the case of the other electrolyte, Na_2SO_4 (21 mM) + NaCl (2.8 mM), 5, 15, 35, and 50 minutes were needed for degradation of STR, AMX, PAR and DEX respectively (Figure 3.1b). In conclusion, when the combined electrolyte was employed, the degradation of the compounds was slower, except in the case of DEX, whose deviation can be attributed to the experimental error (Figure 3.1a and 3.1b). In this way, the literature widely studies the role of chlorine and sulphate species and radicals. Authors as Carvalho et al. (2007) and Moreira et al. (2017), analysed the behaviour of the chloride and sulphate species and radicals during an EOX process, concluding that NaCl medium was more effective than Na_2SO_4 medium, among other things, due to the higher amount of oxidising species present in the bulk and their oxidant capacity. This analysis, from a theoretical point of view, is carried out in greater depth in section 3.2.3.

Finally, with the aim to analyse the rate of degradation of each drug, the kinetic equation was determined by adjusting the experimental data of Figure 3.1 (a and b) to a pseudo-first-order kinetic equation. The pseudo-first-order constants obtained varied between $0.011\text{-}0.999 \text{ min}^{-1}$. Figure 3.2 represents these kinetic adjustments for DEX (Figure 3.2a), AMX (Figure 3.2b), PAR (Figure 3.2c) and STR (Figure 3.2d). Table 3.2 summarizes the values of the pseudo-first-order kinetic constants and their corresponding determination coefficient, R^2 .

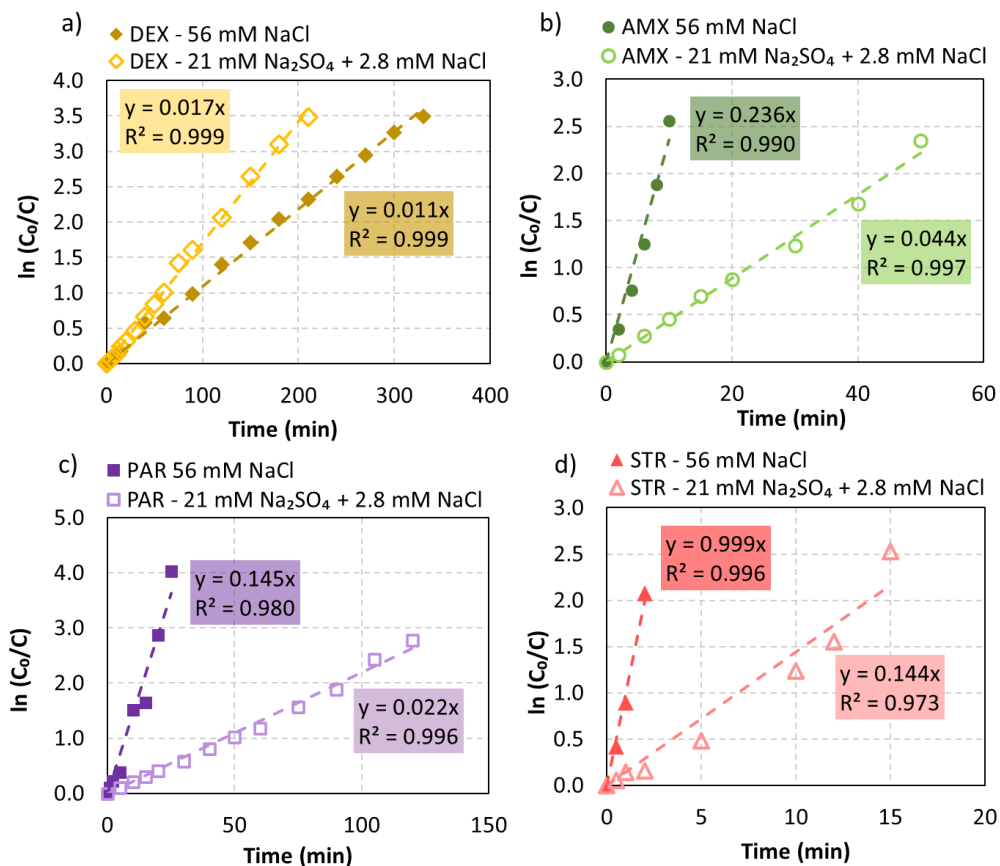


Figure 3.2. Pseudo-first order kinetic fittings of the four COVID-19 drugs: a) DEX, b) AMX, c) PAR and d) STR (EOX-Drugs experiments), with $[\text{Drugs}]_0 = 10 \text{ mg L}^{-1}$.

Table 3.2. Pseudo-first-order rate constants for the COVID-19 drugs: DEX, AMX, PAR and STR (EOX-Drugs experiments) and determination coefficient (R^2).

Compound	mM	Electrolyte			
		NaCl		$\text{Na}_2\text{SO}_4 + \text{NaCl}$	
		k (min^{-1})	R^2	k (min^{-1})	R^2
DEX	0.025	0.011	0.999	0.017	0.998
AMX	0.024	0.236	0.990	0.044	0.996
PAR	0.066	0.145	0.980	0.022	0.996
STR	0.029	0.999	0.995	0.144	0.973

The literature contains scarce information on the kinetic degradation of the drugs DEX, AMX, PAR and STR, and still less about the electrochemical oxidation. Not long ago, Grilla et al. (2021) obtained good results in terms of the degradation of DEX, achieving a 90% elimination working with an initial concentration of 0.5 mg L^{-1} (0.001 mM). They employed an electrochemical cell with a BDD anode, a $J=0.2 \text{ A m}^{-2}$ and sulphate medium (0.1 M of Na_2SO_4). With these conditions, they obtained a pseudo-first-order constant of 0.043 min^{-1} . Then, they treated 2.0 mg L^{-1} of DEX (0.005 mM) with a $J=0.05 \text{ A m}^{-2}$ in the same electrolyte medium (0.1 M of Na_2SO_4), obtaining a pseudo-first-order constant of 0.010 min^{-1} . These values of kinetic constants are in the same order of magnitude that the obtained in this study ($k=0.017 \text{ min}^{-1}$) (Table 3.2), when 10 mg L^{-1} of DEX (0.025 mM) were treated with $J=4.8 \text{ A m}^{-2}$ and the combined electrolyte medium, 21 mM of Na_2SO_4 + 2.8 mM of NaCl . Arsand et al. (2013) applied a combined electrochemical treatment, electrocoagulation, to a $100 \text{ } \mu\text{g L}^{-1}$ of DEX ($0.25 \text{ } \mu\text{M}$), reaching 38% of DEX elimination in 45 minutes, with $J=164 \text{ A m}^{-2}$ and NaCl as electrolyte (2 g L^{-1} , 56 mM), but they did not provide values of the kinetic constant, so it is not possible to perform an appropriate comparison with the parameter obtained in this study (Table 3.2).

In the case of the amoxicillin degradation, in the literature are reflected works in which a complete degradation was achieved, employing a concentration of 36.5 mg L^{-1} (0.1 mM), different current densities ($J=0.41\text{-}20.83 \text{ mA cm}^{-2}$), a BDD anode and a Na_2SO_4 electrolyte medium (50 mM). They obtained different values of pseudo-first-order constant in a wide range, $k=0.020\text{-}6.5 \text{ min}^{-1}$ (Ganiyu et al., 2016; Oturan et al., 2017; Sopaj et al., 2015). Other studies were focused on treating higher concentrations, in the range $47.5\text{-}100 \text{ mg L}^{-1}$ ($0.13\text{-}0.27 \text{ mM}$), and accordingly, applied higher current densities ($15\text{-}44.4 \text{ mA cm}^{-2}$) in Na_2SO_4 medium ($21.1\text{-}50 \text{ mM}$), obtaining kinetic pseudo-first-order constant values in the range $0.06\text{-}0.60 \text{ min}^{-1}$ (Panizza and Cerisola, 2009; Silva et al., 2019). In this doctoral thesis, 10 mg L^{-1} (0.024 mM) of amoxicillin were treated, using milder operation conditions, this is applying a current density of 4.8 A m^{-2} (0.48 mA cm^{-2}). As a result, a pseudo-first-order constant of 0.044 min^{-1} was obtained for the combined electrolyte medium, $\text{Na}_2\text{SO}_4\text{+NaCl}$ ($21 \text{ mM} + 2.8 \text{ mM}$, respectively) (Table 3.2). This kinetic constant is within the range of the values reported in the literature previously described ($0.020\text{-}0.06 \text{ min}^{-1}$), for comparable experimental conditions.

In the treatment of paracetamol solutions, usually higher concentrations are studied in the literature, between $28.7\text{-}1000 \text{ mg L}^{-1}$ ($0.19\text{-}6.62 \text{ mM}$), employing a BDD anode, and Na_2SO_4 as electrolyte. Among the reviewed works, some authors evaluate the degradation of PAR in terms of mineralisation of the compound. Working with 190

mg L⁻¹ of PAR (1.2 mM), Peralta-Hernández et al. (2016) obtained a series of kinetic constants with values between 0.004-0.006 min⁻¹ for J values of 100-300 mA cm⁻², achieving mineralisation values between 50%-75% respectively. On the other side, Waterston et al. (2006) achieved 73% and 82% of TOC reduction when treating with 144 mg L⁻¹ (0.75 mM) of paracetamol and 25 mM of Na₂SO₄, but using much less energy, 54.4 mA cm⁻², finding a pseudo-first-order constant of k=0.022 min⁻¹. Lastly, Ganiyu et al. (2019) achieved ≈90% of TOC reduction when treating 30.2 mg L⁻¹ (0.2 mM) of PAR, at a J=5 mA cm⁻² employing 50 mM of Na₂SO₄ as electrolyte, but no the kinetic constant values were given. In this study, utilizing a lower concentration, 10 mg L⁻¹ of paracetamol (0.066 mM), a J= 0.48 mA cm⁻², and in Na₂SO₄ (21 mM) + NaCl (2.8 mM) as electrolyte, a pseudo-first-order constant of 0.022 min⁻¹ was obtained (Table 3.2). Assuming that TOC belongs to PAR, the pseudo-first-order constant achieved by Waterston et al. (2006), k=0.022 min⁻¹, is the same as the value here reported.

Regarding the remediation of sertraline, several works use AOPs to treat sertraline-containing solutions, however, just only two of them apply electrochemical oxidation. Radjenovic et al. (2011) selected a reverse osmosis concentrate (ROC) from Brisbane, Australia, which contained several spiked pharmaceuticals and pesticides, with an initial STR concentration of 17 µg L⁻¹ (0.05 µM), reaching at least a 70% of elimination, even for lower current densities (1-10 A m⁻²), but they did not provide the values of the kinetic constants. Recently, Rachidi et al. (2021) applied a combined electrochemical treatment, electrofenton, reaching a degradation yields of 100%, working with 34.2 mg L⁻¹ (0.1 mM), a J=80 mA cm², Na₂SO₄ as electrolyte (50 mM) and 0.1 mM of Fe²⁺. The obtained pseudo-first-order constant was 0.90 min⁻¹, a similar value to the one achieved in this study, 0.999 min⁻¹ (Table 3.2).

3.2.2. EOX-Intermediates experiments

Next, the degradation of highly concentrated solutions (EOX-Intermediates experiments) was carried out, with the aim of being able to analyse subsequently the different reaction by-products formed during the electrochemical oxidation of the solutions containing, 80 mg L⁻¹ for DEX (0.2 mM) and 3000 mg L⁻¹ for AMX, PAR and STR (7.1, 19.8 and 8.7 mM, respectively) (Chapter 2). The oxidation of each drug for both electrolytes is depicted separately in Figure 3.3.

As expected, and in the same way as the behaviour observed in the EOX-Drugs degradation experiments, for AMX, PAR and STR, the degradation is faster when using a NaCl medium, being the specific electrical charge (Q) below 10 A h L⁻¹ for all the

compounds. Dexamethasone was eliminated in the same way, employing both NaCl and $\text{Na}_2\text{SO}_4 + \text{NaCl}$. For DEX, the specific electrical charge is lower than for the other compounds, between $3\text{--}6 \text{ A h L}^{-1}$, due to the initial concentration used, 80 mg L^{-1} versus 3000 mg L^{-1} . In these experiments, to achieve a 50% of degradation, around 8, 12, 20, and 50 minutes were needed, for STR, AMX, PAR and DEX, respectively, when employing 56 mM of NaCl. The degradation order (increasing degradation time) follows the same tendency as in the low concentration experiments (EOX-Drugs, Figure 3.1): $\text{STR} > \text{AMX} > \text{PAR} > \text{DEX}$.

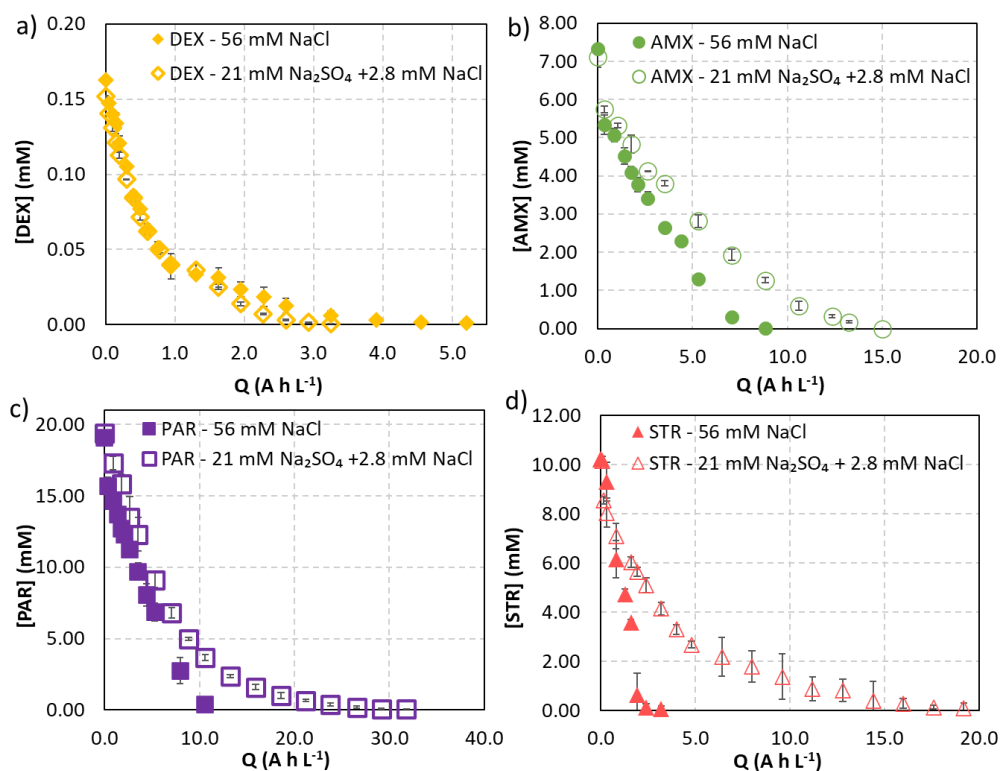


Figure 3.3. Degradation of the of the COVID-19 drugs with the specific charge: a) DEX, b) AMX, c) PAR and d) STR; with $[\text{DEX}]_0 = 80 \text{ mg L}^{-1}$ and $[\text{AMX}, \text{PAR}, \text{STR}]_0 = 3000 \text{ mg L}^{-1}$.

In the case of the electrolyte medium $21 \text{ mM Na}_2\text{SO}_4 + 2.8 \text{ mM NaCl}$, the experiments were slower than with NaCl. 20, 30, and 50 minutes were needed to reach 50% of degradation for AMX, PAR and STR, respectively. In addition, for these working conditions, the degradation order follows the same trend than for the rest of the experiments and conditions, $\text{STR} > \text{AMX} > \text{PAR} > \text{DEX}$.

It is worth noting the case of the DEX. DEX required the same degradation time that was employed in the experiments EOX-Drugs (10 mg L^{-1}), around 50 minutes for achieving 50% of degradation regarding the total amount, regardless of the type of electrolyte. Once again, it can be seen how the complexity and robustness of DEX make its degradation independent of concentration and electrolytic medium. In general terms, DEX requires a critical mass of radicals and oxidizing species for its degradation, which suggests a strong dependence on hydroxyl radicals, highly oxidizing, and generated under all operating conditions and to the same extent. In this way, a deeper analysis, from a theoretical point of view on radical and species oxidants, is carried out in section 3.2.3.

Finally, as for the previous case, the kinetics of the drugs' degradation were determined by fitting the data to a pseudo-first order kinetic equation. The pseudo-first-order kinetic constants obtained varied between $0.011\text{-}0.101 \text{ min}^{-1}$. Figure 3.4 represents the kinetic fittings obtained for each drug, DEX (Figure 3.4a), AMX (Figure 3.4b), PAR (Figure 3.4c) and STR (Figure 3.4d). In Table 3.3 are gathered all the kinetic constants, those from EOX-Drugs experiments and EOX-Intermediate experiments. For DEX degradation, the pseudo-first-order constants are practically the same for all conditions and experiments, finding them in the range of 0.011 to 0.017 min^{-1} . As expected, AMX and STR have faster degradation when the initial concentration is lower (EOX-Drugs, both electrolytes). The same situation occurs with PAR, except for $\text{Na}_2\text{SO}_4\text{+NaCl}$ medium, whose pseudo-first-order constants are similar for high and low concentrations, between 0.022 to 0.026 min^{-1} . Finally, for the STR case again, it was faster with NaCl (0.144 min^{-1}) than for $\text{Na}_2\text{SO}_4\text{+NaCl}$ medium (0.04 min^{-1}). The range value of the pseudo-first-order constants for all the operating conditions is found between 0.011 to 0.999 min^{-1} .

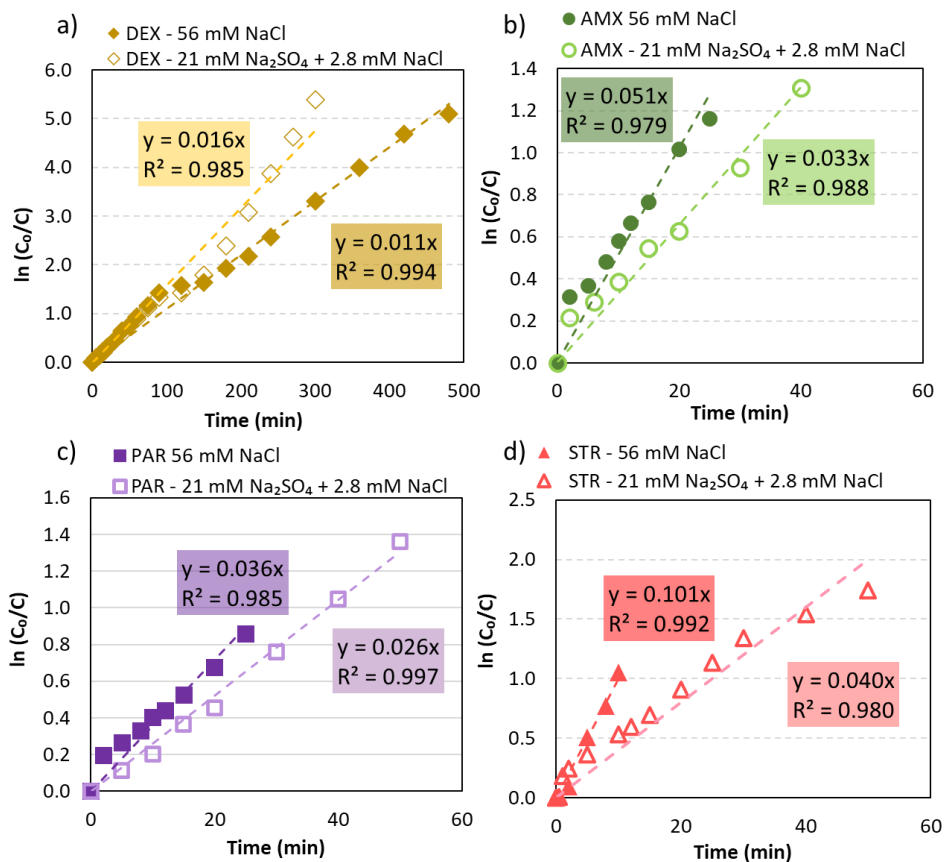


Figure 3.4. Pseudo-first order kinetic fittings of the four COVID-19 drugs: a) DEX, b) AMX, c) PAR and d) STR, with $[\text{DEX}]_0 = 80 \text{ mg L}^{-1}$, and $[\text{AMX,PAR,STR}]_0 = 3000 \text{ mg L}^{-1}$.

Table 3.3. Pseudo-first-order rate constants for the COVID-19 drugs: DEX, AMX; PAR and STR (both for EOX-Drugs and EOX-Intermediates experiments).

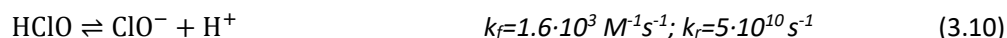
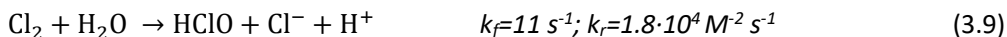
Drug	Exp.	mM	Electrolyte			
			NaCl		Na_2SO_4 + NaCl	
			k (min^{-1})	R^2	k (min^{-1})	R^2
DEX	EOX-Drugs	0.025	0.011	0.999	0.017	0.998
	EOX-Intermediates	0.200	0.011	0.994	0.016	0.985
AMX	EOX-Drugs	0.024	0.236	0.990	0.044	0.996
	EOX-Intermediates	7.150	0.051	0.980	0.033	0.988
PAR	EOX-Drugs	0.066	0.145	0.980	0.022	0.996
	EOX-Intermediates	19.800	0.036	0.986	0.026	0.997
STR	EOX-Drugs	0.029	0.999	0.995	0.144	0.973
	EOX-Intermediates	8.800	0.101	0.992	0.040	0.980

3.2.3. Radicals' formation: theoretical analysis on drugs' degradation

In an electrochemical oxidation process, several species may coexist in the bulk solution, and among them, the reactive species formed from the different compounds added to the medium, which act as electrolytes. Next, it is described from a theoretical point of view, the potential formation of radicals in a medium NaCl or Na₂SO₄, and how they can have contributed to the oxidative degradation of the drugs studied.

Influence of radical chlorine in drugs' degradation

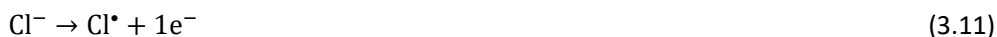
When employing sodium chloride, reactive species of chlorine are generated independently of the electrode materials. Depending on the solution pH, the main species that can be formed are Cl₂, HClO, and/or ClO⁻, at pH <3.0, 3.0–8.0 and >8.0 (Eqs. 3.8-3.10) (Ganiyu et al., 2021; Ghernaout et al., 2020; Grebel et al., 2010; Pastoriza Otero, 2011):



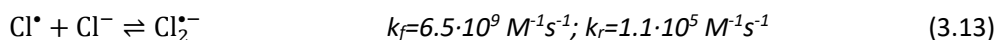
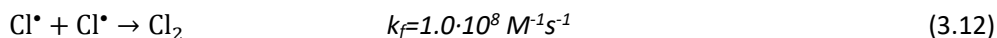
where k_f is the kinetic constant of the forward reaction and k_r is the kinetic constant of the reverse reaction.

Brocenschi et al., (2016) studied the influence of Cl⁻ ions, adding 0.36 mM to 1.85 μmol L⁻¹ estrone containing solution (compound with a similar structure to dexamethasone), reaching a 100% degradation (10 minutes, J=10 mA cm⁻²), independently of the pH (pH 3.0, 7.0 and 10.0). They attribute the degradation both to the •OH radicals and the different chlorine species formed (Cl₂, HClO and ClO⁻). Barazesh et al. (2016) also observed a considerable increase in the removal rates of some trace contaminants, as anticonvulsants, herbicides or antibiotics, when adding 10 mM of chloride and working at pH=8.0, in contrast with the observed rates when using borate-buffered electrolyte (i.e., a rise of 4–20 times). Compounds with strong electron-donating fractions, such as anilines (sulfamethoxazole) or phenolic groups (paracetamol) among others, were eliminated faster owing to reactions with electro-generated HOCl.

With the BDD anode, and employing concentrations from 0.1 to 2.5 g L⁻¹ of NaCl, it has been noted that the direct oxidation of chloride ions produces stable oxidants such as Cl[•] (Brito et al., 2015; Lin et al., 2020; Sirés et al., 2014):

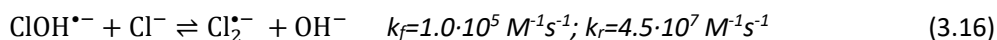
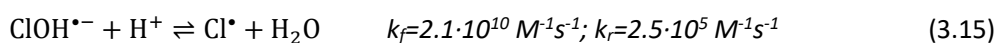
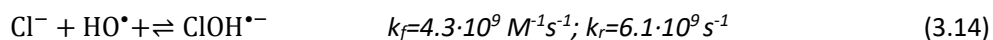


At pH values between 5.0 to 6.0, Cl^\bullet radical can react in different manners, forming with itself Cl_2 (Eq. 3.12), with chloride ion, forming dichloride radical anion ($\text{Cl}_2^{\bullet-}$) (Eq. 3.13), and as radical scavengers. These mechanisms can restrict its role in the course of contaminants degradation during electrochemical oxidation:



When Cl^\bullet is present in the solutions, it can be reactive towards the majority of organic contaminants at near diffusion-controlled rates (10^8 – $10^{10} \text{ M}^{-1} \text{ s}^{-1}$). $\text{Cl}_2^{\bullet-}$ radical can react with organic compounds in an analogous manner to Cl^\bullet , but normally at a slower rate (2-4 orders of magnitude) (Radjenovic and Sedlak, 2015). Supposing that all the reactions are under diffusion control, the Cl^\bullet formation relies on the Cl^- concentration with respect to the concentration of the organic compounds (S): at low ratio ($[\text{Cl}^-]/[\text{S}] < 1$), the predominant reaction is Cl^\bullet with substrates, however, at high ratio ($[\text{Cl}^-]/[\text{S}] > 1$), and $\text{Cl}_2^{\bullet-}$ formation will preferentially happen. This behaviour was studied by Park et al. (2009) determining that the relatively high Cl^- concentration (50 mM), compared to the substrate concentration, ≈ 1.0 mM of chlorophenols and organic acids, induced the formation of $\text{Cl}_2^{\bullet-}$ from Cl^\bullet .

On the other hand, $\text{ClOH}^{\bullet-}$ radical can also be produced, through the oxidation of chloride by the electrochemically produced hydroxyl radicals ($^\bullet\text{OH}$) (Eq. 3.14), to recombine with other species present in the medium, Eq. 3.15 and 3.16:



Finally, other chlorine oxo-species can be formed, like, ClO_2^- , ClO_3^- and ClO_4^- . Sánchez-Carretero et al., (2011) determined that these species are formed when the specific electrical charge (Q) is higher than 15 A h L^{-1} (current density of 300 A m^{-2}), performing EOX experiments with 0.1 M of NaCl at different pH values and current densities, using a BDD anode. In order to understand the role of species and radicals generated in chloride medium during the EOX process and their influence on the degradation of the drugs studied, Figure 3.5 shows the principal reactions of radicals'

formation and other reactive species from chloride mediums and the degradation with the time of AMX and STR using NaCl as electrolyte (EOX-Drugs experiments).

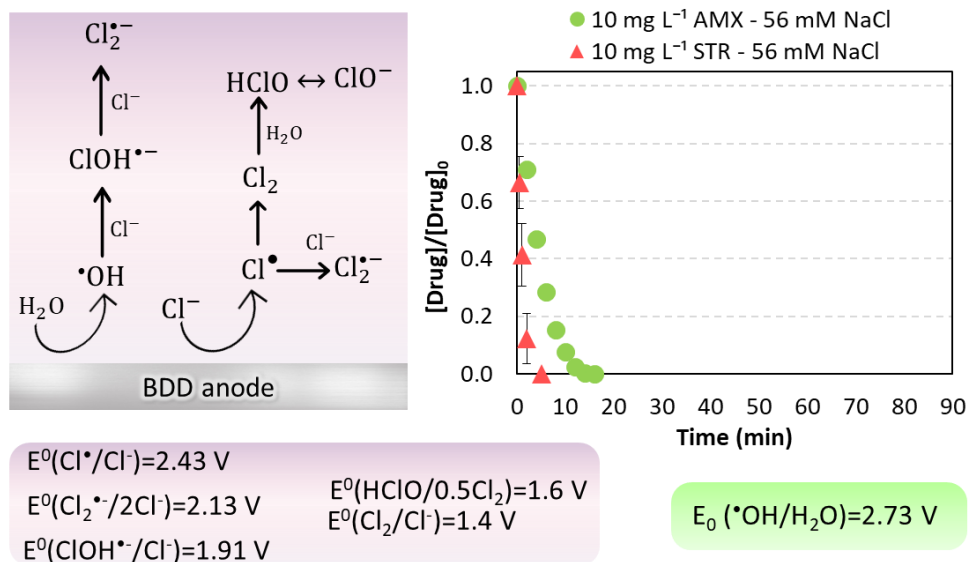


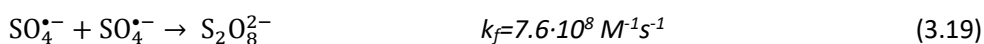
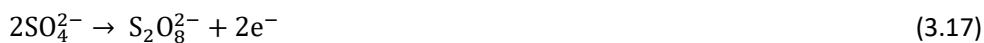
Figure 3.5. Dimensionless representation of AMX and STR degradation, together with the main radicals and species involved and their associated oxidation potentials.

In Figure 3.5 are detailed the oxidizing power of chloride radicals and species (Armstrong et al., 2015; Cañizares et al., 2006; Hamad et al., 2018; Kandavelu et al., 2016; Micó et al., 2013; Murugananthan et al., 2011; Radjenovic and Petrovic, 2017; Scialdone et al., 2009; Sharma, 2011); scarcely, 5 and 10 minutes are needed to degrade at 100% STR and AMX, respectively. As reflected in the literature, taking into account the formation rate of the oxidising species and radicals (Eqs. 3.8-3.16), the redox potential (Figure 3.9) and the degradation rate of the organic compounds by $\cdot\text{OH}$ radicals (10^9 - $10^{11} \text{ M}^{-1} \text{ s}^{-1}$) (Barazesh et al., 2016), the main species and radicals which participate in the degradation of AMX, and STR (by extension DEX and PAR) could be $\cdot\text{OH}$ (2.73 V), $\text{Cl}\cdot$ (2.43 V), $\text{Cl}_2\cdot^-$ (2.13 V), $\text{ClO}\cdot^-$ (1.91 V), HClO (1.6 V) and Cl_2 (1.4 V).

Influence of radical sulphate in drugs' degradation

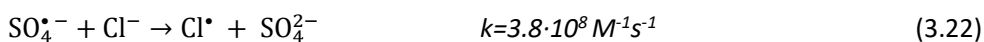
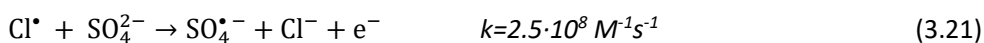
In sulphate medium, reactive species such as $\text{S}_2\text{O}_8^{2-}$ or $\text{SO}_4^{\cdot-}$ can be formed, at certain current densities. Persulphate radicals ($\text{S}_2\text{O}_8^{\cdot-}$) can be produced through three different pathways: i) oxidation of SO_4^{2-} at the anode (Eq. 3.17), ii) reaction of SO_4^{2-} with the electrogenerated $\cdot\text{OH}$ (Eq. 3.18) and, iii) by recombination of the $\text{SO}_4^{\cdot-}$ formed (Eq. 3.19) (Chen et al., 2018; Farhat et al., 2015; Lan et al., 2017; Serrano, 2018; Wojnárovits

and Takács, 2019). Likewise, sulphate radicals ($\text{SO}_4^{\bullet-}$) can be generated through the oxidation of SO_4^{2-} at the anode, just by one-electron transfer reaction (Saha et al., 2022) (Eq. 3.20):



From a thermodynamic point of view, $\text{SO}_4^{\bullet-}$ are more powerful oxidants than $\text{S}_2\text{O}_8^{2-}$, so $\text{SO}_4^{\bullet-}$ can attack in a selective manner, and quickly react with the organic contaminants, whilst $\text{S}_2\text{O}_8^{2-}$ react more slowly (Wojnárovits and Takács, 2019). Even though the oxidation reaction kinetics of organic contaminants with $\text{SO}_4^{\bullet-}$ are not well reported, reaction rates are usually assumed to be comparable to that of oxidation by OH^\bullet .

When sulphates and chloride make up an electrolytic medium, the removal efficiency can be affected. These species can act as radical scavengers or producers, or support the generation of secondary oxidants, with less oxidising power (Eqs. 3.21-3.22) (Anipsitakis et al., 2006; Calzadilla et al., 2021; Fang et al., 2012; Huie et al., 1991; Lan et al., 2017; Lei et al., 2019; Liang et al., 2006; Saha et al., 2022; Serrano, 2018; Wojnárovits and Takács, 2021):



In order to understand the role of species and radicals generated in sulphate and chloride medium during the EOX process and their influence on the degradation of the drugs studied, hereunder, the main causes are described from a theoretical point of view. For a better knowledge, in Figure 3.10 the main reactions of sulphate radicals' formation are summarised and also, other reactive species generated in combined electrolytic medium, such as mediums of sulphate combined with chloride. Furthermore, the degradation over time of AMX and STR using NaCl + Na₂SO₄ as electrolyte (EOX-Drugs experiments) is depicted as an example, in dimensionless manner.

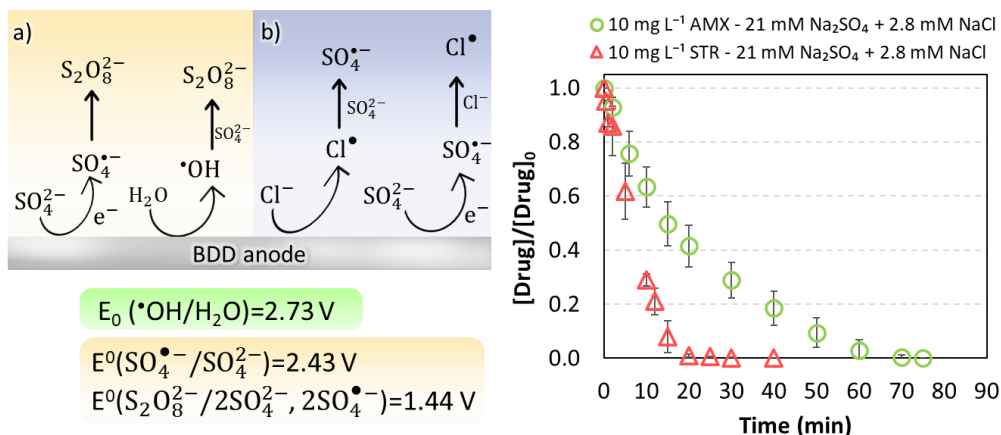


Figure 3.6. Principal mechanisms of radicals' formation from a) a sulphate source and b) chlorine in conjunction with sulphate sources. Partially adapted from Saha et al. (2022).

Dimensionless representation of AMX and STR degradation by EOX process.

As can be seen in Figure 3.6, in Na₂SO₄ (21 mM) + NaCl (2.8 mM) medium, the STR took 20 minutes to degrade compared to the 5 minutes in medium NaCl (Figure 3.5). In the same way, the AMX degraded in 70 minutes, compared to 10 minutes in medium NaCl. This behaviour can be explained on the basis of the radical and oxidant species existing:

- Sulphate radicals ($\text{SO}_4^{\bullet-}$) possess higher half-life (30-40 μs) than $\cdot\text{OH}$ (<1 μs) (Oh et al., 2016; Xia et al., 2020), however, their standard electrode potential (2.43 V) is lower than the standard electrode potential of $\cdot\text{OH}$ (2.73 V) (Fernández-Castro et al., 2015).
- For the sulphate radical, the second-order rate constants with the organic compounds, frequently are one/two orders of magnitude lesser ($\approx 10^5$ - $10^9 \text{ M}^{-1} \text{ s}^{-1}$) than for $\cdot\text{OH}$ radicals (10^6 - $10^{11} \text{ M}^{-1} \text{ s}^{-1}$), independently of the type of substrate present in water (Chapter 1).
- Although there are more radical species chloride with higher or equal redox potential than radical sulphate (Figure 3.6), they are in lower amount (21 mM Na₂SO₄ versus 2.8 mM NaCl).

In this way, the main species and radicals that participate in the degradation of AMX, and STR (and by extension DEX and PAR) in Na₂SO₄+NaCl medium, are mainly $\cdot\text{OH}$ radical (2.73 V), followed by $\text{SO}_4^{\bullet-}$ radical (2.43 V) and the specie $\text{S}_2\text{O}_8^{2-}$ (1.44 V) (Armstrong et al., 2015; Farhat et al., 2015; Liang et al., 2006; Niu et al., 2020; Stanbury, 1989; Wojnárovits and Takács, 2019) and finally, given its low concentration, the rest of

the radicals and chloride species, Cl^\bullet (2.43 V), $\text{Cl}_2^{\bullet-}$ (2.13 V), $\text{ClOH}^{\bullet-}$ (1.91 V), HClO (1.6 V) and Cl_2 (1.4 V), which justifies the need for a longer oxidation time compared to the experiments carried out in NaCl medium (Figure 3.5).

3.3. Analysis of the degradation intermediates

As studied in Chapter 1, and in line with the premise of this doctoral thesis, it is well-known for studies carried out previously in the research groups (SPE and ASP) (Fernández-Castro et al., 2016; Schröder et al., 2021; Solá-Gutiérrez et al., 2019; Vallejo et al., 2013), that even though the degradation of the primary compounds may be complete, intermediates (by-products) can be generated during the oxidation process, which could lead to an increase in the final toxicity in the degraded sample. Among these by-products, this doctoral thesis has focused mainly on the identification of PCDD/Fs precursors that are representative of the final toxicity of the sample, such as chlorinated molecules like triclosan, some chlorophenols, such as 2,4-dichlorophenol and 2-chlorophenol or precursor compounds of these PCDD/Fs precursors, like hydroquinone or chlorohydroquinones which can be transformed in chlorophenols in chloride presence (Fernández-Castro et al., 2016; Schröder et al., 2021; Solá-Gutiérrez et al., 2019, 2018; Vallejo et al., 2014, 2013). In this direction, the selection of the AOP to be applied, as well as the operating variables (electrolyte used), can be determinants for the treatment of wastewater with this type of composition (Schröder et al., 2020; Solá-Gutiérrez et al., 2019). So, it has been reported in the literature that the pharmaceuticals under study in this doctoral thesis generate by-products during their degradation, such as hydroquinone and benzoquinones, or different chlorophenols (Siciliano et al., 2021). In order to identify these types of intermediates, a qualitative analysis during the electro-oxidation experiments using both electrolytes, has been carried out. For this purpose, very high concentrations of each pharmaceutical compound were employed, 80 mg L⁻¹ for DEX and 3000 mg L⁻¹ for AMX, PAR and STR, in order to be able to identify and analyse properly the potentially generated compounds. For this, kinetics experiments that let to know the formation mechanism of these by-products of the reaction were carried out. The analysis procedure has been described in Chapter 2, section 2.3.2.

The formation of by-products from the electrochemical oxidation of pharmaceuticals is justified starting from the $\bullet\text{OH}$ radicals formed in the BDD anode, and the different chlorine and sulphate radicals produced from the electrolytes:

- a) $\bullet\text{OH}$, a non-selective oxidant, is likely to react over to the C=C bond of the benzene ring, provoking the breakage of the molecules (Farhat et al., 2015; Saha et al., 2022).

The principal reaction in presence of Cl^- is the electrophilic addition of $\cdot\text{OH}$ on the aromatic ring leading to the production of chlorophenol (Hamad et al., 2018).

- b) In the case of chlorine radicals, such Cl^\bullet and $\text{Cl}_2^{\bullet-}$ (Eqs. 3.11 and 3.13), mainly, they follow three pathways of reaction: i) single electron transfer (SET), ii) H-abstraction, iii) addition pathways (chlorine addition) by the formation of Cl^\bullet -adducts (Lei et al., 2019; Park et al., 2009). Lei et al. (2019) observed that when Cl^\bullet reacted with various trace organic contaminants such as different β -lactams, macrolides or antipyretics analgesics, various chlorinated by-products are formed. Although they confirmed that H-abstraction dominated the reactions of Cl^\bullet for paracetamol and amoxicillin forming phenoxy radical. They observed Cl^\bullet -adducts in the reactions of Cl^\bullet with amoxicillin as well (Lei et al., 2019). So, chlorine addition can be predictable as the other most probable pathway, leading to the formation of chlorinated by-products (Lei et al., 2021). $\text{Cl}_2^{\bullet-}$, similar to Cl^\bullet , reacts via the already mentioned reaction pathways: direct electron transfer, H-abstraction and electrophilic addition (Park et al., 2009). Moreover, it has been proven that Cl^\bullet is very reactive towards many trace organic contaminants, and $\text{Cl}_2^{\bullet-}$ is more selective (Lei et al., 2019). For example, organic trace contaminants with electron-rich parts showed high reactivity towards $\text{Cl}_2^{\bullet-}$; so this radical can play an important role in the degradation of the studied pharmaceutical compounds (Lei et al., 2019).
- c) The radical $\text{SO}_4^{\bullet-}$, during the degradation of organic compounds, acts according to three main pathways of reaction, which are more or less the same than those for chlorine radicals: i) electron transfer to aromatic organic contaminants, ii) H-abstraction from carbon atoms of the organics contaminants with saturated bonds, and iii) additive reactions (electrophilic/radical additions) which take place when the unsaturated bonds are broken (Dong et al., 2021; Oh et al., 2016). Frequently, $\text{SO}_4^{\bullet-}$, tends to react primarily via electron transfer mechanisms, it is electrophilic, so that easily reacts with electron-donating groups such as amino, hydroxyl, alkoxy groups, π electrons present on aromatic molecules and other organic compounds that contain unsaturated bonds, being predisposed to attack the conjugation bond in the molecules (Lee et al., 2020; Oh et al., 2016; Saha et al., 2022; Xia et al., 2020).

Hereafter, the main by-products identified during the EOX-Intermediates experiments for each drug are described in the following sections. Moreover, the possible breakdown pathways of each drug are also listed, according to the existing literature. For each drug, a table with a selection of the detected compounds is presented, for both electrolytic media. This selection was carried out considering the

compounds formed in a higher amount, i.e., visible and defined peaks, with the highest area (see Chapter 2, section 2.3.1). On the other hand, the type of compound is also important, because this study is centered on the precursor compounds formation, or compounds that can be precursor of the precursors when they are in presence of a chloride source; so, the selection also considers this point. The rest of the detected compounds that do not satisfy this criterion, are not detailed in section 3.3, they are shown in Annex IV.

3.3.1. Identification of DEX intermediates: kinetic study

During experiments EOX-Intermediates of DEX, scarce PCDD/Fs precursor compounds have been detected. The main identified by-products next to retention time (RT) are detailed in Table 3.4 (NaCl medium and Na₂SO₄+NaCl medium), with full names and the acronyms of each one for a better comprehension, and the rest of the detected compounds are detailed in Annex IV. It may be the case that some of the compounds expected to be found, are in concentrations under the detection limit of the gas chromatograph employed (Chapter 2). At least, the well-known PCDD/Fs precursor, 2,4-dichlorophenol, has been identified in chloride medium (Schröder et al., 2020; Solá-Gutiérrez et al., 2019) (Chapter 1). The rest of the detected compounds, for NaCl experiments, were NAP, PTN, PTCP and BCM; and for Na₂SO₄+NaCl experiments MDOD, MDEO, DHT, MTT and PRED (Table 3.4). It is worth highlighting some compounds such as 1-dehydrotestosterone (DHT), methandrostenolone (MTT) or beclomethasone (BCM), as well as DEX fragments, as 9-(S)-methyl-delta-5(10)-octalin-1,6-dione (MDOD) or naphthalene (NAP) since they are DEX-alike compounds.

Table 3.4. Main intermediate compounds identified during the DEX degradation (EOX-Intermediates. Electrolyte: NaCl and Na₂SO₄+NaCl).

NaCl		Na ₂ SO ₄ +NaCl	
RT (min) Compound	Molecule	RT (min) Compound	Molecule
4.92 Naphthalene (NAP)		8.65 9-(S)-methyl-delta-5(10)-octalin-1,6-dione (MDOD)	
6.74 2,4-dichlorophenol (2,4-DCP)		14.67 3-methoxy-16,16-dimethyl-1,3,5(10)-estratrien-17-one (MDEO)	
8.13 1-propyl-1,2,3,4-tetrahydro Naphthalene (PTN)		19.38 1-dehydro- testosterone (DHT)	
11.62 2-phenyl-2',5,5'- trichlorophenol (PTCP)		19.95 Methandro- stenolone (MTT)	
18.83 Beclomethasone (BCM)		23.45 Prednisolone (PRED)	

The main degradation pathways for dexamethasone has been studied mainly in photo-assisted technologies, and just one recent work (Grilla et al., 2021) analyses the by-products of an electro-remediation process (using a BDD anode). In the literature, the next pathways for the breakage of the DEX molecule in the different by-products found in EOX-Intermediates experiments are proposed:

The first step in the DEX degradation occurs via oxidative attack facilitated by $\cdot\text{OH}$ at different reactive spots (Quaresma et al., 2021). Then, the degradation pathway can follow different starting points:

- i) Hydroxylation of the DEX molecule (depicted in Table 3.4 in blue colour) (Calza et al., 2001; Cantalupi et al., 2020; Guo et al., 2017; Pazoki et al., 2016; Pretali et al., 2021; Sulaiman et al., 2014). In this PhD thesis, none hydroxylated-DEX molecules have been detected with a matching highest than 70%, but there are signs (several steroid form molecules with lower matching percentage) of its presence.
- ii) Loss of the fluorine atom (depicted in Table 3.4 in yellow colour) (Guo et al., 2017; Pretali et al., 2021; Rasolevandi et al., 2019; Sulaiman et al., 2014) as occurs in all molecules of Table 3.4.
- iii) Transformation and/or loss of $-\text{CO}-\text{CH}_2\text{OH}$ group (depicted in Table 3.4 in green colour) (Babu et al., 2009; Calza et al., 2001; Cantalupi et al., 2020; Guo et al., 2017; Pazoki et al., 2016; Pretali et al., 2021; Quaresma et al., 2021; Sulaiman et al., 2014). In the case of compounds with similar structure to the DEX, the compounds MDOD, DHT and MTT have lost or modified this group (Table 3.4).
- iv) Finally, these starting pathways usually lead to a ring opening (depicted in Table 3.4 in red colour) (Babu et al., 2009; Guo et al., 2021, 2017; Pazoki et al., 2016; Pretali et al., 2021; Rasolevandi et al., 2019). The molecules NAP, 2,4-DCP, PTN and MDOD and PTCP (Table 3.4) come from the cleavage of some bonds of the molecule, leading to a ring opening, losing its steroid form, thus, generating DEX-fragments.

For further consultation, these pathways are summarised in Figure VI.1 of Annex VI.

In order to analyse the behaviour of the by-products generated during the degradation of the original compound (DEX), the kinetics of each of the intermediates shown in Table 3.4 have been represented in Figure 3.7 (NaCl medium) and 3.8 (medium $\text{Na}_2\text{SO}_4+\text{NaCl}$).

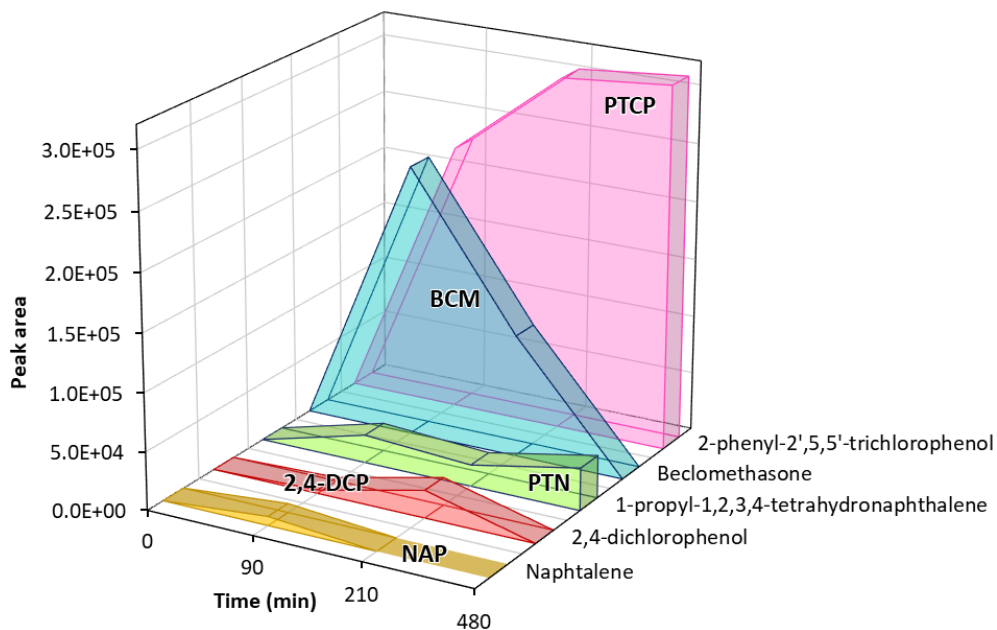


Figure 3.7. Kinetics of the by-products identified during DEX degradation (Electrolyte: NaCl).

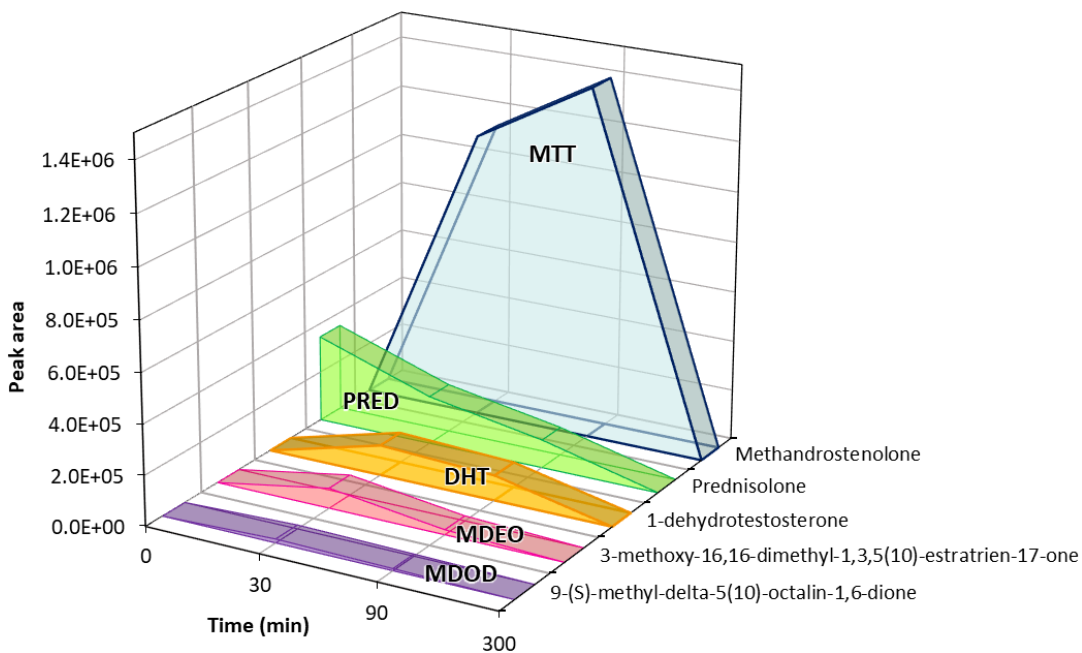


Figure 3.8. Kinetics of the by-products identified during DEX degradation (Electrolyte: Na₂SO₄+NaCl).

When using NaCl as electrolyte (Figure 3.7), all the intermediate compounds have the same tendency, they grow till a maximum, and then they decrease until practically zero values, with the exception of PTCP and PTN, which still have certain concentration at final time. PTCP is the highest compound formed, which reached its maximum at final time, 480 min, with a peak area of $3.1 \cdot 10^5$. Beclomethasone (BCM) (similar molecule to dexamethasone but with a chlorine atom on it) reaches a maximum at 90 min with a peak area $\approx 10^5$. The rest of the graphed compounds are formed in lower concentrations compared to those mentioned above, one order of magnitude less. The PCDD/Fs precursor, 2,4-dichlorophenol, reached a maximum concentration at 210 min, with a peak area in the order of 10^4 . Finally, NAP reached its maximum at 90 min (peak area of $7.8 \cdot 10^3$). For the other electrolytic medium, $\text{Na}_2\text{SO}_4 + \text{NaCl}$ (Figure 3.8), almost all the compounds follow the same trend than for NaCl medium, grow until a maximum and decreasing until zero values. The one with the greatest concentration corresponded to methandrostenolone (MTT), reached its maximum point at 90 minutes (peak area $\approx 10^6$), subsequently decreasing until practically its disappearance at the end of the experiment. It can be appreciated that prednisolone (PRED) is detected at initial time; it could be an impurity of dexamethasone, due to the similarity of the molecule shape (steroid shape). The rest of the compounds, DHT, MDEO and MDOD, are formed in lesser amounts, in the order of 10^4 - 10^5 (peak area), with maximum points at 30 minutes. It is noticeable that possible fragments of the dexamethasone degradation, PTN, MDOD and NAP, as well as some dexamethasone alike compounds (MDOD, MDEO and DHT), are the compounds formed in lower amounts, which allows to understand the difficulty of carrying out the degradation of the parent compound (section 3.2.1).

3.3.2. Identification of AMX intermediates: kinetic study

Experiments EOX-Intermediates of AMX allowed to identify a good number of precursors compounds of PCDD/Fs (see Table 3.5) such as 2,4-DCP, 4-CP, and 2,4,5-TCP, precursors compounds of the precursors of PCDD/Fs as Cl-BQ, HQ, Cl-HQ and 2,5-DCHQ, and compounds that correspond to a fragment of the AMX molecule, that can suffer some transformation like chlorine addition, as DMD, 3,4-DBA, 4-NC and PTCP. According to the established criteria for the identification of compounds (Chapter 2, section 2.3.2), Table 3.5 shows the main by-products detected during the electrochemical oxidation of AMX, using both NaCl and $\text{NaCl} + \text{Na}_2\text{SO}_4$ as electrolytes. As can be seen, practically almost all the detected compounds correspond to simple benzene molecules. The structure of AMX allows the rupture of the bonds and formation of this type of by-products relatively easily, which is consistent with its rapid degradation, as described in section 3.2.1.

Table 3.5. Main intermediate compounds identified during the AMX degradation (EOX-Intermediates. Electrolyte: NaCl and Na₂SO₄+NaCl).

NaCl		Na ₂ SO ₄ +NaCl	
<p style="text-align: center;">AMX</p>			
RT (min) Compound	Molecule	RT (min) Compound	Molecule
4.15 Chloro-p-benzoquinone (Cl-BQ)		4.85 Dimethadione (DMD)	
4.88 2,4-dichloro phenol (2,4-DCP)		5.63 Hydroquinone (HQ)	
4.98 4-chlorophenol (4-CP)		6.12 Chlorohydroquinone (Cl-HQ)	
5.57 Hydroquinone (HQ)		6.93 3,4-dichloro benzenamine (3,4-DBA)	
6.12 Chlorohydroquinone (Cl-HQ)		7.46 4-nitrocatechol (4-NC)	
6.35 2,4,5-trichloro phenol (2,4,5-TCP)		11.58 2-phenyl-2',5,5'- trichlorophenol (PTCP)	
7.73 2,5-dichloro- hydroquinone (2,5-DCHQ)			

The formation of the by-products found in EOX-Intermediates experiments, and depicted in Table 3.5, is described hereunder through the different AMX rupture pathways gathered from the literature:

- i) Break on the peptide bond (marked in red colour, Table 3.5) to produce two different fragments 2-amino(4-hydroxyphenyl) acetic acid and a bicyclic lactam product (Frontistis et al., 2017; Ganiyu et al., 2016). In this thesis, just one molecule has been detected produced from the breakage of the peptide bond, acetaminophen (see Annex IV), although it is not the same molecule than those detected in the literature.
- ii) Break of other bonds of the molecule (marked in blue colour, Table 3.5) (Frontistis et al., 2017) forming different fragments, like 4-NC or DMD (Table 3.5).
- iii) After the principal breakage of AMX molecule described in i), on the one hand, the opening of the β -lactam ring can occur generating fragments as DMD. On the other hand, some hydroxylation, dehydrogenation and/or chlorination reactions can occur on the phenolic ring, forming Cl-BQ, 2,4-DCP, 4-CP, HQ, Cl-HQ, 2,5-DCHQ and 2,4,5-TCP (depicted in green colour, Table 3.5) (Ferreira et al., 2020; Frontistis et al., 2017; Ganiyu et al., 2016; Tan et al., 2020). These products give rise to the formation of carboxylic acids, which has been reported in the literature (Ferreira et al., 2020; Ganiyu et al., 2016).
- iv) On the other hand, it has been corroborated the hydroxylation of the phenolic ring of the amoxicillin molecule (marked in orange colour, Table 3.5), given rise to some hydroxylated-amoxicillin by-products (Ferreira et al., 2020; Frontistis et al., 2017; Pan et al., 2020; Pan and Sun, 2021). Here, it has been detected fragments of hydroxylated AMX molecule, like HQ, and 4-NC (Table 3.5).
- v) The chlorination of the phenolic ring has been also detected (marked in purple colour, Table 3.5) (Ferreira et al., 2020). Siciliano et al. (2021) eliminate amoxicillin through a chlorination process, finding various chlorinated organic compounds among their by-products, like chlorophenols. Here, fragments of the chlorinated phenolic ring have been found, already described in pathway iii), because they can be formed both in one and the other pathway, like 2,4-DCP, 4-CP, Cl-HQ, 2,4,5-TCP and 3,4-DBA (Table 3.5). Other ones can be found in Annex IV, which were present in lesser concentrations, or do not satisfy the matching 70% criteria.

For further consultation, these pathways are summarised in Figure VI.2 of Annex VI.

To study the behaviour of the main by-products generated during the degradation of the AMX (EOX-Intermediates), the kinetics of each of the intermediates shown in Table 3.5 have been represented in Figure 3.9 (NaCl medium) and 3.10 ($\text{Na}_2\text{SO}_4 + \text{NaCl}$ medium).

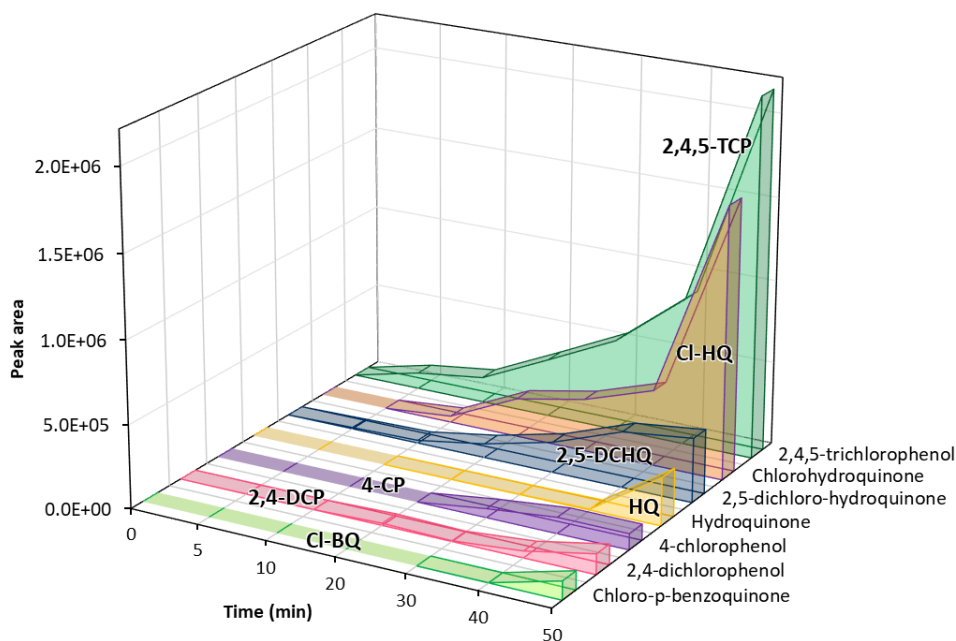


Figure 3.9. Kinetics of the by-products identified during AMX degradation (Electrolyte: NaCl).

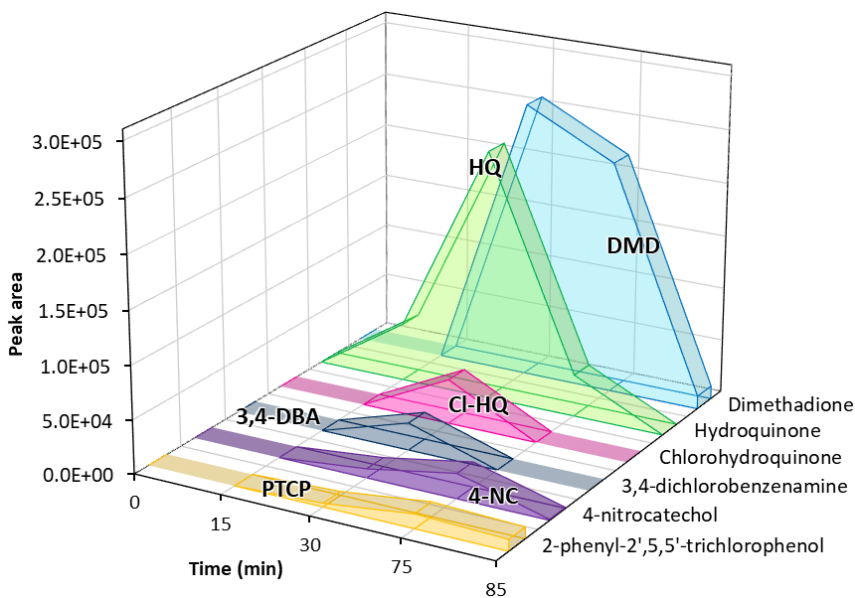


Figure 3.10. Kinetics of the by-products identified during AMX degradation (Electrolyte: Na₂SO₄+NaCl).

As can be observed in Figure 3.9, for the NaCl experiments, all the compounds follow the same tendency, constantly increasing with time until reaching the highest values at the end of the experiment. The by-product which is produced in the major

concentration (higher peak area) was 2,4,5-dichlorophenol, with a peak area value of $2.1 \cdot 10^6$, reaching its maximum at the final experimental time (50 min), when no amoxicillin left in the solution. Then, Cl-HQ appears as the second by-product formed attending at its concentration ($1.6 \cdot 10^6$ at 50 min), and following the concentration order, 2,5-DCHQ and HQ, reaching a peak area value of $3.8 \cdot 10^5$ and $2.8 \cdot 10^5$, respectively, finally, 4-chlorophenol, 2,4-dichlorophenol and chloro-p-benzoquinone are present in the same order of magnitude, $\approx 10^5$. For EOX-Intermediates using the combined electrolyte medium, $\text{Na}_2\text{SO}_4 + \text{NaCl}$, which are detailed in Figure 3.10, the evolution of the by-products follows a different tendency in NaCl case, all increase with time until a maximum, an ending in negligible concentrations. DMD is the compound formed in greatest amount, followed by HQ, with values in the order of $2\text{-}2.5 \cdot 10^5$. Then Cl-HQ and 3,4-DBA have the highest point at 30 min (values among $2.3\text{-}2.6 \cdot 10^5$). On the other hand, 4-nitrocatechol achieved a maximum at 75 min (peak area of $2.3 \cdot 10^4$), followed by 2-phenyl-2',5,5'-trichloro-phenol. At the final time of the experiment, almost all the compounds were totally degraded, with the exception of PTCP and DMD.

3.3.3. Identification of PAR intermediates: kinetic study

According to the criteria established for the identification of compounds by gas chromatography (Chapter 2, section 2.3.2), in Table 3.6 are detailed the principal by-products detected during the EOX of PAR, employing both NaCl and $\text{NaCl} + \text{Na}_2\text{SO}_4$ as electrolytes. For the PAR EOX-Intermediates experiments, as in the AMX case, some precursors compounds of PCDD/Fs (see Table 3.6) have been detected, for instance, such as 3,4-DCP, and 2,4,5-TCP, precursors compounds of the precursors of PCDD/Fs like BQ, Cl-BQ, 2,5-DCBQ, HQ, Cl-HQ, and 2,5-DCHQ, and compounds that correspond to a fragment of the PAR molecule, than can experiment some transformation like chlorine addition, as 1,3-BDO, 3,4-DBA and 4-NC. Surprisingly, a dioxin is detected in quite high concentration, 1-chlorodibenzo-p-dioxin (1-MCDD), whose formation can be attributed to the injector temperature of the gas chromatograph. In addition, PAR-alike molecules were detected, NHPA (chlorinated PAR) and 4-NP.

For generated intermediates during PAR electrochemical oxidation, the same as in AMX case, approximately all the detected by-products are kind-of benzene molecules, because the PAR shape, permits the breakage of some bonds, generating directly these kind of compounds in an easy way, which is corroborated with its fast elimination (section 3.2.1).

Table 3.6. Main intermediate compounds identified during the PAR degradation (EOX-Intermediates. Electrolyte: NaCl and Na₂SO₄+NaCl).

NaCl		Na ₂ SO ₄ +NaCl	
RT (min) Compound	Molecule	RT (min) Compound	Molecule
3.10 p-benzoquinone (BQ)		5.59 Hydroquinone (HQ)	
4.14 2-chloro-p- benzoquinone (Cl-BQ)		6.13 Chloro-hydroquinone (Cl-HQ)	
5.36 2,5-dichloro-p- benzoquinone (2,5-DCBQ)		6.71 3,4-dichloro Phenol (3,4-DCP)	
5.57 Hydroquinone (HQ)		6.94 3,4-dichloro benzenamine (3,4-DBA)	
6.12 Chlorohydroquinone (Cl-HQ)		7.1 1,3-benzenediol (1,3-BDO)	
6.35 2,4,5-trichlorophenol (2,4,5-TCP)		7.44 4-nitrocatechol (4-NC)	
7.11 4-nitrophenol (4-NP)		10.77 1-chlorodibenzo-p- dioxin (1-MCDD)	
7.73 2,5-dichloro- hydroquinone (2,5-DCHQ)			
8.80 N-(3-Chloro-4- hydroxyphenyl) acetamide (NHPA)			

The main degradation pathways of the paracetamol molecule, according to the available literature, are four:

- i) First, the $\cdot\text{OH}$ radicals favour the attack at the para- position with respect to the $\cdot\text{OH}$ functional group of the phenolic ring (see Table 3.6, marked in orange colour), and through a n-dealkylation at amine group, hydroquinone (HQ) is generated, and experiments a further transformation to p-benzoquinone (BQ) (Table 3.6) (De Luna et al., 2012; Ganiyu et al., 2019; Le et al., 2017; Liu et al., 2019; Olvera-Vargas et al., 2018; Periyasamy and Muthuchamy, 2018; Zhang et al., 2018).
- ii) $\cdot\text{OH}$ radicals can attack the peptide bond (pointed in blue colour, Table 3.6) with the formation of 4-nitrophenol (4-NP) (Ganiyu et al., 2019; Periyasamy and Muthuchamy, 2018; Sun et al., 2018).
- iii) Different hydroxylated paracetamol molecules can be formed, when $\cdot\text{OH}$ radicals attack to other positions of the phenolic ring (marked with green colour, Table 3.6), like 4-NC and 1,3-BDO, which are fragments of an hydroxylated PAR molecule (Ganiyu et al., 2019; Olvera-Vargas et al., 2018). Olvera-Vargas et al. (2018) stated that in pathway ii) the hydroxylation in the ortho- meta- position competes with hydroxylation in para- position (pathway i)).
- iv) Apart from these three main pathways, sometimes when the oxidation takes place in presence of chlorine (Cl^-) (pointed with purple colour, Table 3.6), different chlorinated by-products can be formed, such as NHPA (chlorinated paracetamol), Cl-HQ, 2,4,5-TCP, 3,4-DCP and 3,4-DBA (Liu et al., 2019; Zhang et al., 2018). So, the production of chlorinated intermediates also corroborated the positive effect of the chloride reactive species in the increasing rate of the paracetamol degradation (Zhang et al., 2018). Other chlorinated by-products as Cl-BQ, 2,5-DCBQ and 2,5-DCHQ can also be formed from the previously mentioned chlorinated by-products thought chlorination reactions in chlorine presence.

Finally, the mechanism ends with the carboxylic acids formation (De Luna et al., 2012; Ganiyu et al., 2019; Ghanbari et al., 2021; Le et al., 2017; Olvera-Vargas et al., 2018; Periyasamy and Muthuchamy, 2018; Sun et al., 2018; Zhang et al., 2018). For further consultation, these pathways are summarised in Figure VI.3 of Annex VI.

To study the behaviour of the main by-products generated during the degradation of the PAR (EOX-Intermediates), the kinetics of all the intermediates shown in Table 3.6 have been represented in Figure 3.11 (NaCl medium) and 3.12 ($\text{Na}_2\text{SO}_4+\text{NaCl}$ medium).

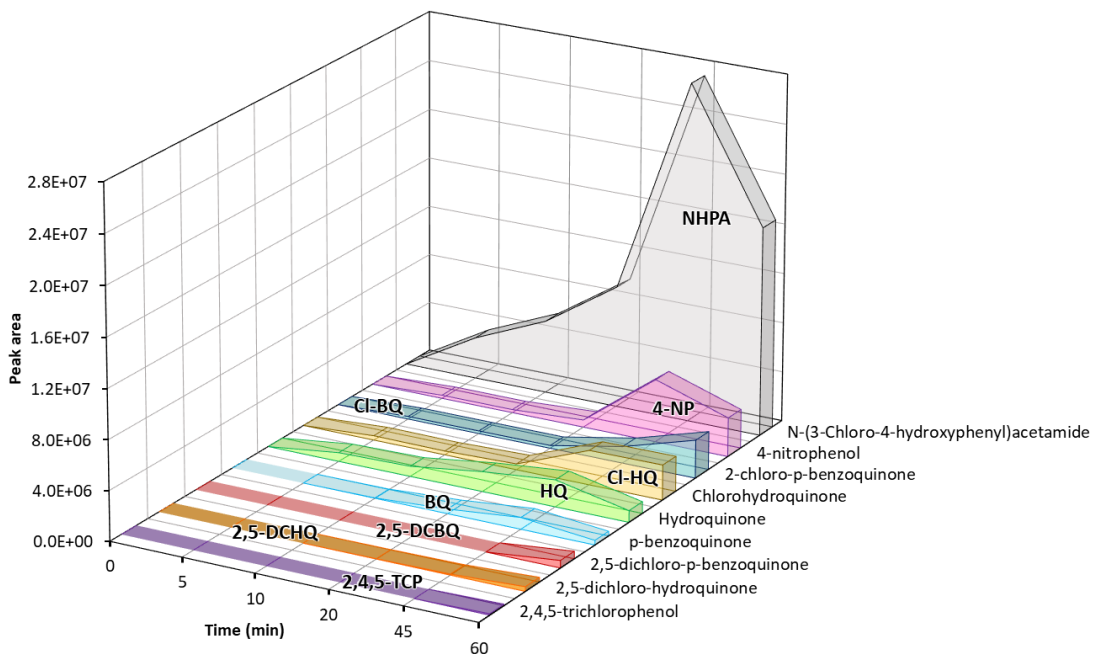


Figure 3.11. Kinetics of the by-products identified during PAR degradation (Electrolyte: NaCl).

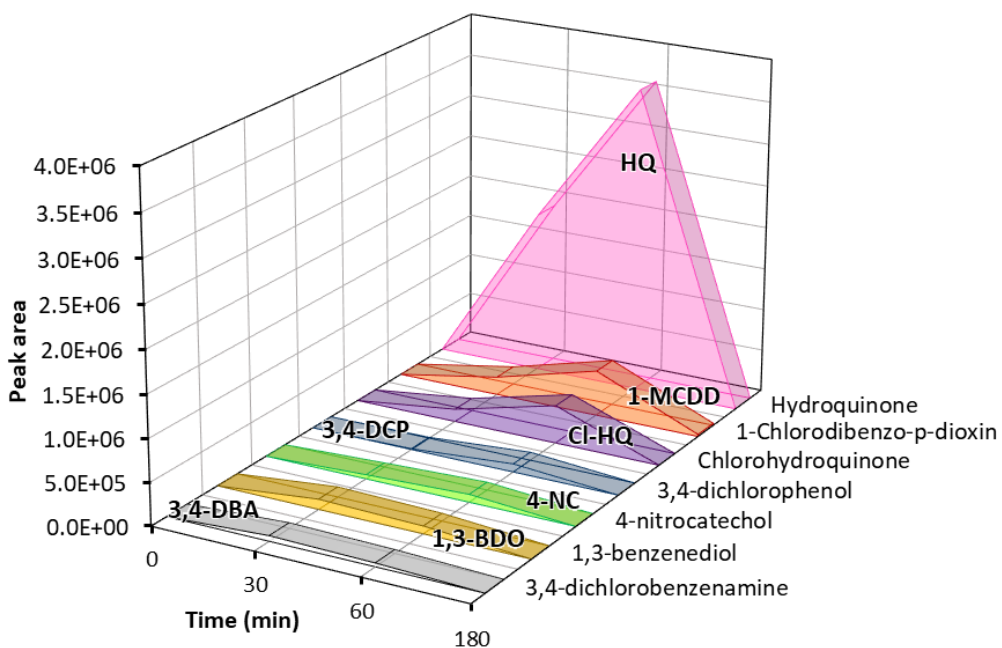


Figure 3.12. Kinetics of the by-products identified during PAR degradation (Electrolyte: Na₂SO₄+NaCl).

Related to the kinetic analysis, for the NaCl case (Figure 3.11), it can be seen that some compounds follow the same tendency, growing constantly up to reach a maximum at 45 min, and the decreasing to low concentration values, NHPA, 4-NP, Cl-BQ, HQ and BQ; and other ones which reached their maximum at final experimental time, Cl-HQ, 2,5-DCBQ, 2,5-DCHQ and 2,4,5-TCP (60 min). The compound formed in a greatest amount was NHPA, this is a chlorinated paracetamol molecule, with a maximum value of $2.73 \cdot 10^7$ at 45 min of experiment. Then, attending to the concentration order, 4-NP reached its highest point also at 45 min ($2.73 \cdot 10^6$). The next six by-products, all of the hydro- and benzoquinone family, chloro-p-benzoquinone (Cl-BQ), chlorohydroquinone (Cl-HQ), hydroquinone (HQ), p-benzoquinone (BQ), 2,5-p-benzoquinone (2,5-pBQ) and 2,5-dichlorohydroquinone (2,5-DCHQ), possess peak area values in their higher points between $8.4 \cdot 10^4$ - $9.3 \cdot 10^5$. Finally, the compound formed in the lowest concentration is 2,4,5-trichlorophenol, which followed almost the same trend, reaching the maximum at the end of the experiment, $1.1 \cdot 10^5$.

On the other hand, for the other electrolyte medium ($\text{Na}_2\text{SO}_4 + \text{NaCl}$) (Figure 3.12), the trend is a continuous increase until 60 min (highest point), and then decreased to values close to zero, with the exception of 3,4-DBO and 3,4-DCBA which reached their highest point at 30 min. Hydroquinone was the compound produced in the highest concentration, with a maximum at 60 min ($3.6 \cdot 10^6$). 1-chlorodibenzo-p-dioxin is the by-product that follows in terms of amount after HQ, with a peak area of $5.4 \cdot 10^5$ at 60 min (highest point). Cl-HQ and 3,4-DCP are formed in a less extend, both with the highest point at 60 min, and with peaks area between $9.6 \cdot 10^4$ - $4.5 \cdot 10^5$. Next, 4-nitrocatechol and 1,3-benzenediol are one of the lowest produced compounds but also in the order of 10^4 - 10^5 . Finally, 3,4-DCBA reached a maximum at 30 min ($6.4 \cdot 10^4$) being totally degraded at final time, 180 min.

3.3.4. Identification of STR intermediates: kinetic study

Lastly, in the case of sertraline, several dioxins and furans precursor compounds were detected, which are detailed in Table 3.7: 2,3,4-TCP, 2,4,5-TCP, 3,4-DCP and 2,3,4,6-TeCP. Furthermore, several STR fragments were found, some of them formed in a directly way through the breakage of the molecule by the $\cdot\text{OH}$ action, like MNA or 3,4-DCS, or fragments that have experimented some transformation, such as NAP, 3,4-DCS and 3,4-DCBA. The available literature is scarce, just like the by-products analysis during electrochemical oxidation, being the photochemical processes those who have been more widely reported.

In Table 3.7, the identified compounds during the electrochemical degradation of STR, for the two-electrolyte media mentioned, are shown in detail.

Table 3.7. Main intermediate compounds identified during the STR degradation (EOX-Intermediates. Electrolyte: NaCl and Na₂SO₄+NaCl).

NaCl		Na ₂ SO ₄ +NaCl	
RT (min) Compound	Molecule	RT (min) Compound	Molecule
5.13 Naphthalene (NAP)		5.63 3,4-dichloro styrene (3,4-DCS)	
5.67 3,4-dichloro styrene (3,4-DCS)		6.40 2,4,5-trichloro phenol (2,4,5-TCP)	
6.35 2,4,5-trichloro phenol (2,4,5-TCP)		6.49 2,3,4-trichloro phenol (2,3,4-TCP)	
6.71 3,4-dichloro phenol (3,4-DCP)		6.71 3,4-dichlorophenol (3,4-DCP)	
7.75 2,3,4,6-tetrachloro phenol (2,3,4,6-TeCP)		7.76 2,3,4,6-tetra chlorophenol (2,3,4,6-TeCP)	
8.16 N-methyl-1- naphthalenamine (MNA)		8.70 3,4-dichloro benzamide (3,4-DCBA)	

The main degradation/transformation pathways followed by STR can be summarised in five, detailed below:

- i) Ring detachment takes place through $\cdot\text{OH}$ attack (depicted in red colour in Table 3.7), generating, on the one hand, compounds like 3,4-dichlorophenol (Table 3.7), or similar chlorophenolic compounds, as 3,4-DCS and 3,4-DCBA (Table 3.7); and on the other hand, the rest of the sertraline molecule, which is MNA, or other naphthalene structures as NAP, also detected in this doctoral thesis (Table 3.7) (Calza et al., 2021; Jiménez-Holgado et al., 2021). In chloride presence, also it could be supposed the formation of other chlorophenols, detected in this thesis, from the chlorination of 3,4-DCP, such as 2,4,5-TCP, 2,3,4-TCP, or 2,3,4,6-TeCP.
- ii) Hydroxylation of the sertraline molecule (shown in blue colour in Table 3.7), in the naphthalene structure and/or in the chlorinated ring (Calza et al., 2021; Gornik et al., 2020; Jiménez-Holgado et al., 2021). None of these hydroxylated molecules have been detected in this PhD thesis.
- iii) Substitution of one of the chlorine atoms for an $\cdot\text{OH}$ radical (Calza et al., 2021; Jiménez-Holgado et al., 2021). As for pathway ii), in this study none of these molecules were detected, according to the set criteria.
- iv) Moreover, other phenomena, such as the loss of a chlorine atom (shown in pink colour, Table 3.7) (Calza et al., 2021; Jiménez-Holgado et al., 2021) can take place, producing a pseudo-STR molecule with one less Cl atom, not detected in this thesis.
- v) Oxidation of the C-N bond (depicted in yellow colour, Table 3.7) has been observed in the literature (Calza et al., 2021; Jiménez-Holgado et al., 2021). But, molecules generated through pathway iv) and v) were not detected in this doctoral thesis.

For further consultation, these pathways are summarised in Figure VI.4 of Annex VI.

To study the behaviour of the main by-products generated during the degradation of the STR (EOX-Intermediates), the kinetics of each of the intermediates shown in Table 3.6 have been represented in Figure 3.13 (NaCl medium) and 3.14 ($\text{Na}_2\text{SO}_4+\text{NaCl}$ medium).

As it can be seen in Figure 3.13 employing NaCl medium, the generated by-products (Table 3.7) increase until a maximum at different times, ending with values close to zero, except for the naphthalene (NAP), which ends with a peak area of $1.1 \cdot 10^5$. NAP is the compound generated in highest amount.

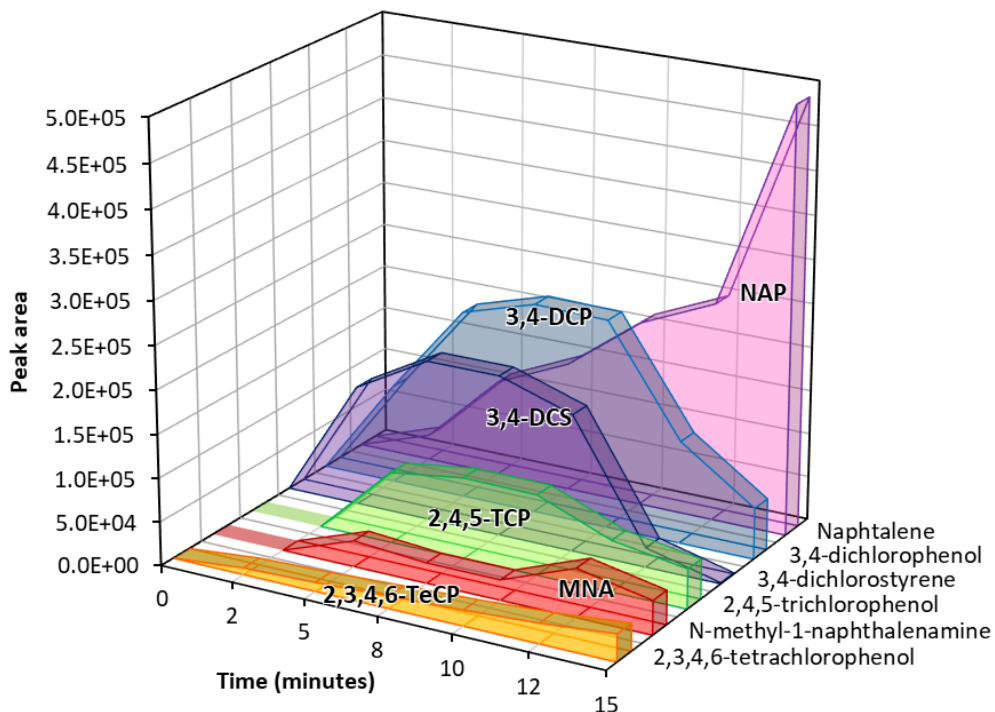


Figure 3.13. Kinetics of the by-products identified during STR degradation (Electrolyte: NaCl).

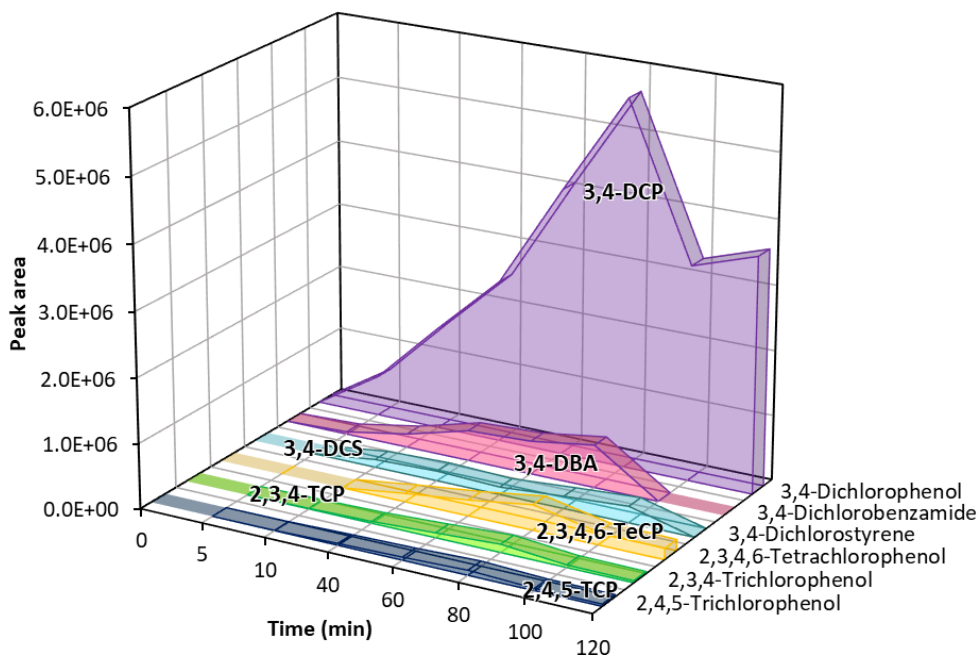


Figure 3.14. Kinetics of the by-products identified during STR degradation (Electrolyte: Na₂SO₄+NaCl).

Then 3,4-DCP and 3,4-DCS are the second and third compounds in terms of peak area, achieving their top points at 8 min (peak area of $1.8 \cdot 10^5$ and $2.4 \cdot 10^5$, respectively) (Figure 3.13). Moreover, another chlorophenol is formed, 2,4,5-trichlorophenol, probably generated due to the chlorination of 3,4-dichlorophenol, since it started to appear at 5 minutes (and 3,4-DCP appears at 2 min), with its highest point at 8 min ($9.3 \cdot 10^4$). The next compound is the remaining fragment of STR molecule when it breaks into two fragments, in the C-C middle bond, MNA (see Table 3.7), with top point value of $5.5 \cdot 10^4$ at 12 min. Finally, 2,3,4,6-tetrachlorophenol is formed in lower concentration in comparison with the other compounds, but constantly growing until the final experimental time (peak area value of $3.1 \cdot 10^4$).

Using the $\text{Na}_2\text{SO}_4 + \text{NaCl}$ case, it can be appreciated in Figure 3.14, that all the compounds increase their peak area until achieved a maximum, and end with negligible values, except for the 3,4-dichlorophenol case. 3,4-DCP is, as for NaCl case, the compound with the highest concentration, with its peak at 80 min ($5.6 \cdot 10^6$), then it decays a bit (at 100 min) and grows again at final experimental time (120 min) with a final value of $3.6 \cdot 10^6$. Following, 3,4-DCBA grows up to $6.6 \cdot 10^5$ and ends in zero value. Moreover, the behaviour for 3,4-DCS is a bit different, because its maximum point is reached at 100 min ($2.5 \cdot 10^5$). 2,3,4,6-TeCP achieved the greatest value at 80 min ($3.9 \cdot 10^5$) to end also in zero. Lastly, the two trichlorophenols, 2,4,5-TCP and 2,3,4-TCP achieved the greatest values at 80 min, $7.6 \cdot 10^4$ and $1.2 \cdot 10^5$, respectively, being completely degraded at final time.

3.4. References

- Anipsitakis, G.P., Dionysiou, D.D., Gonzalez, M.A., 2006. Cobalt-mediated activation of peroxymonosulfate and sulfate radical attack on phenolic compounds. Implications of chloride ions. *Environ. Sci. Technol.* 40, 1000–1007. <https://doi.org/10.1021/es050634b>
- Armstrong, D.A., Huie, R.E., Koppenol, W.H., Lyman, S. V., Merenyi, G., Neta, P., Ruscic, B., Stanbury, D.M., Steenken, S., Wardman, P., 2015. Standard electrode potentials involving radicals in aqueous solution: Inorganic radicals (IUPAC Technical Report). *Pure Appl. Chem.* 87, 1139–1150. <https://doi.org/10.1515/pac-2014-0502>
- Arsand, D.R., Kümmerer, K., Martins, A.F., 2013. Removal of dexamethasone from aqueous solution and hospital wastewater by electrocoagulation. *Sci. Total Environ.* 443, 351–357. <https://doi.org/10.1016/j.scitotenv.2012.10.100>
- Babu, B.R., Venkatesan, P., Kanimozhi, R., Basha, C.A., 2009. Removal of pharmaceuticals from wastewater by electrochemical oxidation using cylindrical flow reactor and optimization of treatment conditions. *J. Environ. Sci. Heal. - Part A Toxic/Hazardous Subst. Environ. Eng.* 44, 985–994. <https://doi.org/10.1080/10934520902996880>
- Barazesh, J.M., Prasse, C., Sedlak, D.L., 2016. Electrochemical Transformation of Trace Organic Contaminants in the Presence of Halide and Carbonate Ions. *Environ. Sci. Technol.* 50, 10143–10152. <https://doi.org/10.1021/acs.est.6b02232>
- Brillas, E., Sirés, I., Arias, C., Cabot, P.L., Centellas, F., Rodríguez, R.M., Garrido, J.A., 2005. Mineralization of paracetamol in aqueous medium by anodic oxidation with a boron-doped diamond electrode. *Chemosphere* 58, 399–406. <https://doi.org/10.1016/j.chemosphere.2004.09.028>
- Brito, C.D.N., De Araújo, D.M., Martínez-Huitle, C.A., Rodrigo, M.A., 2015. Understanding active chlorine species production using boron doped diamond films with lower and higher sp^3/sp^2 ratio. *Electrochem. commun.* 55, 34–38. <https://doi.org/10.1016/j.elecom.2015.03.013>
- Brocenschi, R.F., Rocha-Filho, R.C., Bocchi, N., Biaggio, S.R., 2016. Electrochemical degradation of estrone using a boron-doped diamond anode in a filter-press reactor. *Electrochim. Acta* 197, 186–193. <https://doi.org/10.1016/j.electacta.2015.09.170>
- Calza, P., Jiménez-Holgado, C., Cocha, M., Chrimatopoulos, C., Dal Bello, F., Medana, C., Sakkas, V., 2021. Study of the photoinduced transformations of sertraline in aqueous media. *Sci. Total Environ.* 756, 143805. <https://doi.org/10.1016/j.scitotenv.2020.143805>
- Calza, P., Pelizzetti, E., Brussino, M., Baiocchi, C., 2001. Ion trap tandem mass spectrometry study of dexamethasone transformation products on light activated TiO_2 surface. *J. Am. Soc. Mass Spectrom.* 12, 1286–1295. [https://doi.org/10.1016/S1044-0305\(01\)00319-1](https://doi.org/10.1016/S1044-0305(01)00319-1)

- Calzadilla, W., Espinoza, L.C., Díaz-Cruz, M.S., Sunyer, A., Aranda, M., Peña-Farfal, C., Salazar, R., 2021. Simultaneous degradation of 30 pharmaceuticals by anodic oxidation: Main intermediaries and by-products. *Chemosphere* 269. <https://doi.org/10.1016/j.chemosphere.2020.128753>
- Cañizares, P., García-Gómez, J., Fernández de Marcos, I., Rodrigo, M.A., Lobato, J., 2006. Measurement of mass-transfer coefficients by an electrochemical technique. *J. Chem. Educ.* 83, 1204–1207. <https://doi.org/10.1021/ed083p1204>
- Cañizares, P., Sáez, C., Lobato, J., Rodrigo, M.A., 2004. Electrochemical oxidation of polyhydroxybenzenes on boron-doped diamond anodes. *Ind. Eng. Chem. Res.* 43, 6629–6637. <https://doi.org/10.1021/ie049807g>
- Cantalupi, A., Maraschi, F., Pretali, L., Albin, A., Nicolis, S., Ferri, E.N., Profumo, A., Speltini, A., Sturini, M., 2020. Glucocorticoids in freshwaters: Degradation by solar light and environmental toxicity of the photoproducts. *Int. J. Environ. Res. Public Health* 17, 1–15. <https://doi.org/10.3390/ijerph17238717>
- Carvalho, C., Fernandes, A., Lopes, A., Pinheiro, H., Gonçalves, I., 2007. Electrochemical degradation applied to the metabolites of Acid Orange 7 anaerobic biotreatment. *Chemosphere* 67, 1316–1324. <https://doi.org/10.1016/j.chemosphere.2006.10.062>
- Chen, L., Lei, C., Li, Z., Yang, B., Zhang, X., Lei, L., 2018. Electrochemical activation of sulfate by BDD anode in basic medium for efficient removal of organic pollutants. *Chemosphere* 210, 516–523. <https://doi.org/10.1016/j.chemosphere.2018.07.043>
- De Luna, M.D.G., Veciana, M.L., Su, C.C., Lu, M.C., 2012. Acetaminophen degradation by electro-Fenton and photoelectro-Fenton using a double cathode electrochemical cell. *J. Hazard. Mater.* 217–218, 200–207. <https://doi.org/10.1016/j.jhazmat.2012.03.018>
- Dong, H., Duan, S., Li, L., Qiang, Z., 2021. Sulfate radical-based advanced oxidation processes for industrial wastewater treatment, Integrated and Hybrid Process Technology for Water and Wastewater Treatment. INC. <https://doi.org/10.1016/B978-0-12-823031-2.00017-3>
- Fang, G.D., Dionysiou, D.D., Wang, Y., Al-Abed, S.R., Zhou, D.M., 2012. Sulfate radical-based degradation of polychlorinated biphenyls: Effects of chloride ion and reaction kinetics. *J. Hazard. Mater.* 227–228, 394–401. <https://doi.org/10.1016/j.jhazmat.2012.05.074>
- Farhat, A., Keller, J., Tait, S., Radjenovic, J., 2015. Removal of Persistent Organic Contaminants by Electrochemically Activated Sulfate. *Environ. Sci. Technol.* 49, 14326–14333. <https://doi.org/10.1021/acs.est.5b02705>
- Fernández-Castro, P., San Román, M.F., Ortiz, I., 2016. Theoretical and experimental formation of low chlorinated dibenzo-p-dioxins and dibenzofurans in the Fenton oxidation of chlorophenol solutions. *Chemosphere* 161, 136–144. <https://doi.org/10.1016/j.chemosphere.2016.07.011>

- Fernández-Castro, P., Vallejo, M., San Román, M.F., Ortiz, I., 2015. Insight on the fundamentals of advanced oxidation processes: Role and review of the determination methods of reactive oxygen species. *J. Chem. Technol. Biotechnol.* 90, 796–820. <https://doi.org/10.1002/jctb.4634>
- Ferreira, M., Kuzniarska-Biernacka, I., Fonseca, A.M., Neves, I.C., Soares, O.S.G.P., Pereira, M.F.R., Figueiredo, J.L., Parpot, P., 2020. Electrochemical oxidation of amoxicillin on carbon nanotubes and carbon nanotube supported metal modified electrodes. *Catal. Today* 357, 322–331. <https://doi.org/10.1016/j.cattod.2019.06.039>
- Frontistis, Z., Antonopoulou, M., Venieri, D., Konstantinou, I., Mantzavinos, D., 2017. Boron-doped diamond oxidation of amoxicillin pharmaceutical formulation: Statistical evaluation of operating parameters, reaction pathways and antibacterial activity. *J. Environ. Manage.* 195, 100–109. <https://doi.org/10.1016/j.jenvman.2016.04.035>
- Ganiyu, S.O., Martínez-Huitle, C.A., Oturan, M.A., 2021. Electrochemical advanced oxidation processes for wastewater treatment: Advances in formation and detection of reactive species and mechanisms. *Curr. Opin. Electrochem.* 27, 100678. <https://doi.org/10.1016/j.coelec.2020.100678>
- Ganiyu, S.O., Oturan, N., Raffy, S., Cretin, M., Causserand, C., Oturan, M.A., 2019. Efficiency of plasma elaborated sub-stoichiometric titanium oxide (Ti₄O₇) ceramic electrode for advanced electrochemical degradation of paracetamol in different electrolyte media. *Sep. Purif. Technol.* 208, 142–152. <https://doi.org/10.1016/j.seppur.2018.03.076>
- Ganiyu, S.O., Oturan, N., Raffy, S., Cretin, M., Esmilaire, R., van Hullebusch, E., Esposito, G., Oturan, M.A., 2016. Sub-stoichiometric titanium oxide (Ti₄O₇) as a suitable ceramic anode for electrooxidation of organic pollutants: A case study of kinetics, mineralization and toxicity assessment of amoxicillin. *Water Res.* 106, 171–182. <https://doi.org/10.1016/j.watres.2016.09.056>
- Ghanbari, F., Hassani, A., Waclawek, S., Wang, Z., Matyszczyk, G., Lin, K.Y.A., Dolatabadi, M., 2021. Insights into paracetamol degradation in aqueous solutions by ultrasound-assisted heterogeneous electro-Fenton process: Key operating parameters, mineralization and toxicity assessment. *Sep. Purif. Technol.* 266. <https://doi.org/10.1016/j.seppur.2021.118533>
- Gheraout, D., Elboughdiri, N., Ghareba, S., Salih, A., 2020. Electrochemical Advanced Oxidation Processes (EAOPs) for Disinfecting Water—Fresh Perspectives. *OALib* 07, 1–12. <https://doi.org/10.4236/oalib.1106257>
- Gornik, T., Kovacic, A., Heath, E., Hollender, J., Kosjek, T., 2020. Biotransformation study of antidepressant sertraline and its removal during biological wastewater treatment. *Water Res.* 181, 115864. <https://doi.org/10.1016/j.watres.2020.115864>

- Grebel, J.E., Pignatello, J.J., Mitch, W.A., 2010. Effect of halide ions and carbonates on organic contaminant degradation by hydroxyl radical-based advanced oxidation processes in saline waters. *Environ. Sci. Technol.* 44, 6822–6828. <https://doi.org/10.1021/es1010225>
- Grilla, E., Taheri, M.E., Miserli, K., Venieri, D., Konstantinou, I., Mantzavinos, D., 2021. Degradation of dexamethasone in water using BDD anodic oxidation and persulfate: reaction kinetics and pathways. *J. Chem. Technol. Biotechnol.* 96, 2451–2460. <https://doi.org/10.1002/jctb.6833>
- Guo, Y., Rene, E.R., Han, B., Ma, W., 2021. Enhanced fluoroglucocorticoid removal from groundwater in a bio-electrochemical system with polyaniline-loaded activated carbon three-dimensional electrodes: Performance and mechanisms. *J. Hazard. Mater.* 416, 126197. <https://doi.org/10.1016/j.jhazmat.2021.126197>
- Guo, Z., Guo, A., Guo, Q., Rui, M., Zhao, Y., Zhang, H., Zhu, S., 2017. Decomposition of dexamethasone by gamma irradiation: Kinetics, degradation mechanisms and impact on algae growth. *Chem. Eng. J.* 307, 722–728. <https://doi.org/10.1016/j.cej.2016.08.138>
- Hamad, H., Bassyouni, D., El-Ashtoukhy, E.S., Amin, N., Abd El-Latif, M., 2018. Electrocatalytic degradation and minimization of specific energy consumption of synthetic azo dye from wastewater by anodic oxidation process with an emphasis on enhancing economic efficiency and reaction mechanism. *Ecotoxicol. Environ. Saf.* 148, 501–512. <https://doi.org/10.1016/j.ecoenv.2017.10.061>
- Huie, R.E., Clifton, C.L., Neta, P., 1991. Equilibria of the Carbonate and Sulfate Radical Anions. *Radiat. Phys. Chem. Int. J. Radiat. Appl. Instrum., Part C* 38, 477–481.
- Jiménez-Holgado, C., Sakkas, V., Richard, C., 2021. Phototransformation of three psychoactive drugs in presence of sedimental water extractable organic matter. *Molecules* 26, 1–17. <https://doi.org/10.3390/molecules26092466>
- Kandavelu, V., Yoshihara, S., Kumaravel, M., Muruganathan, M., 2016. Anodic oxidation of isothiazolin-3-ones in aqueous medium by using boron-doped diamond electrode. *Diam. Relat. Mater.* 69, 152–159. <https://doi.org/10.1016/j.diamond.2016.08.008>
- Lan, Y., Coetsier, C., Causserand, C., Groenen Serrano, K., 2017. On the role of salts for the treatment of wastewaters containing pharmaceuticals by electrochemical oxidation using a boron doped diamond anode. *Electrochim. Acta* 231, 309–318. <https://doi.org/10.1016/j.electacta.2017.01.160>
- Le, T.X.H., Nguyen, T. Van, Amadou Yacouba, Z., Zoungrana, L., Avril, F., Nguyen, D.L., Petit, E., Mendret, J., Bonniol, V., Bechelany, M., Lacour, S., Lesage, G., Cretin, M., 2017. Correlation between degradation pathway and toxicity of acetaminophen and its by-products by using the electro-Fenton process in aqueous media. *Chemosphere* 172, 1–9. <https://doi.org/10.1016/j.chemosphere.2016.12.060>

- Lee, J., Von Gunten, U., Kim, J.H., 2020. Persulfate-Based Advanced Oxidation: Critical Assessment of Opportunities and Roadblocks. *Environ. Sci. Technol.* 54, 3064–3081. <https://doi.org/10.1021/acs.est.9b07082>
- Lei, Y., Cheng, S., Luo, N., Yang, X., An, T., 2019. Rate constants and mechanisms of the reactions of Cl^\bullet and Cl_2^\bullet with Trace Organic Contaminants. *Environ. Sci. Technol.* <https://doi.org/10.1021/acs.est.9b02462>
- Lei, Y., Lei, X., Westerhoff, P., Zhang, X., Yang, X., 2021. Reactivity of Chlorine Radicals (Cl^\bullet and Cl_2^\bullet) with Dissolved Organic Matter and the Formation of Chlorinated Byproducts. *Environ. Sci. Technol.* 55, 689–699. <https://doi.org/10.1021/acs.est.0c05596>
- Liang, C., Wang, Z.S., Mohanty, N., 2006. Influences of carbonate and chloride ions on persulfate oxidation of trichloroethylene at 20 °C. *Sci. Total Environ.* 370, 271–277. <https://doi.org/10.1016/j.scitotenv.2006.08.028>
- Lin, M.H., Bulman, D.M., Remucal, C.K., Chaplin, B.P., 2020. Chlorinated Byproduct Formation during the Electrochemical Advanced Oxidation Process at Magnéli Phase Ti_4O_7 Electrodes. *Environ. Sci. Technol.* 54, 12673–12683. <https://doi.org/10.1021/acs.est.0c03916>
- Liu, Y.J., Hu, C.Y., Lo, S.L., 2019. Direct and indirect electrochemical oxidation of amine-containing pharmaceuticals using graphite electrodes. *J. Hazard. Mater.* 366, 592–605. <https://doi.org/10.1016/j.jhazmat.2018.12.037>
- Micó, M.M., Bacardit, J., Malfeito, J., Sans, C., 2013. Enhancement of pesticide photo-Fenton oxidation at high salinities. *Appl. Catal. B Environ.* 132–133, 162–169. <https://doi.org/10.1016/j.apcatb.2012.11.016>
- Moreira, F.C., Boaventura, R.A.R., Brillas, E., Vilar, V.J.P., 2017. Electrochemical advanced oxidation processes: A review on their application to synthetic and real wastewaters. *Appl. Catal. B Environ.* 202, 217–261. <https://doi.org/10.1016/j.apcatb.2016.08.037>
- Murugananthan, M., Latha, S.S., Bhaskar Raju, G., Yoshihara, S., 2011. Role of electrolyte on anodic mineralization of atenolol at boron doped diamond and Pt electrodes. *Sep. Purif. Technol.* 79, 56–62. <https://doi.org/10.1016/j.seppur.2011.03.011>
- Niu, T., Cai, J., Shi, P., Zhao, G., 2020. Unique electrochemical system for in situ $\text{SO}_4[\text{rad}]$ -generation and pollutants degradation. *Chem. Eng. J.* 386, 123971. <https://doi.org/10.1016/j.cej.2019.123971>
- Oh, W. Da, Dong, Z., Lim, T.T., 2016. Generation of sulfate radical through heterogeneous catalysis for organic contaminants removal: Current development, challenges and prospects. *Appl. Catal. B Environ.* 194, 169–201. <https://doi.org/10.1016/j.apcatb.2016.04.003>

- Olvera-Vargas, H., Rouch, J.C., Coetsier, C., Cretin, M., Causserand, C., 2018. Dynamic cross-flow electro-Fenton process coupled to anodic oxidation for wastewater treatment: Application to the degradation of acetaminophen. *Sep. Purif. Technol.* 203, 143–151. <https://doi.org/10.1016/j.seppur.2018.03.063>
- Orimolade, B.O., Zwane, B.N., Koiki, B.A., Rivallin, M., Bechelany, M., Mabuba, N., Lesage, G., Cretin, M., Arotiba, O.A., 2020. Coupling cathodic electro-fenton with anodic photo-electrochemical oxidation: A feasibility study on the mineralization of paracetamol. *J. Environ. Chem. Eng.* 8, 104394. <https://doi.org/10.1016/j.jece.2020.104394>
- Oturan, N., Ganiyu, S.O., Raffy, S., Oturan, M.A., 2017. Sub-stoichiometric titanium oxide as a new anode material for electro-Fenton process: Application to electrocatalytic destruction of antibiotic amoxicillin. *Appl. Catal. B Environ.* 217, 214–223. <https://doi.org/10.1016/j.apcatb.2017.05.062>
- Pan, G., Sun, X., Sun, Z., 2020. Fabrication of multi-walled carbon nanotubes and carbon black co-modified graphite felt cathode for amoxicillin removal by electrochemical advanced oxidation processes under mild pH condition. *Environ. Sci. Pollut. Res.* 27, 8231–8247. <https://doi.org/10.1007/s11356-019-07358-2>
- Pan, G., Sun, Z., 2021. Cu-doped g-C₃N₄ catalyst with stable CuO and Cu⁺ for enhanced amoxicillin degradation by heterogeneous electro-Fenton process at neutral pH. *Chemosphere* 283, 131257. <https://doi.org/10.1016/j.chemosphere.2021.131257>
- Panizza, M., Cerisola, G., 2009. Direct and mediated anodic oxidation of organic pollutants. *Chem. Rev.* 109, 6541–6569. <https://doi.org/10.1021/cr9001319>
- Park, H., Vecitis, C.D., Hoffmann, M.R., 2009. Electrochemical water splitting coupled with organic compound oxidation: The role of active chlorine species. *J. Phys. Chem. C* 113, 7935–7945. <https://doi.org/10.1021/jp810331w>
- Pastoriza Otero, C., 2011. Estudio del mecanismo de las reacciones de sustitución nucleófila sobre átomos de halógeno. University of Santiago de Compostela.
- Pazoki, M., Parsa, M., Farhadpour, R., 2016. Removal of the hormones dexamethasone (DXM) by Ag doped on TiO₂ photocatalysis. *J. Environ. Chem. Eng.* 4, 4426–4434. <https://doi.org/10.1016/j.jece.2016.09.034>
- Peralta-Hernández, J.M., de la Rosa-Juárez, C., Buzo-Muñoz, V., Paramo-Vargas, J., Cañizares-Cañizares, P., Rodrigo-Rodrigo, M.A., 2016. Synergism between anodic oxidation with diamond anodes and heterogeneous catalytic photolysis for the treatment of pharmaceutical pollutants. *Sustain. Environ. Res.* 26, 70–75. <https://doi.org/10.1016/j.serj.2015.11.003>
- Periyasamy, S., Muthuchamy, M., 2018. Electrochemical oxidation of paracetamol in water by graphite anode: Effect of pH, electrolyte concentration and current density. *J. Environ. Chem. Eng.* 6, 7358–7367. <https://doi.org/10.1016/j.jece.2018.08.036>

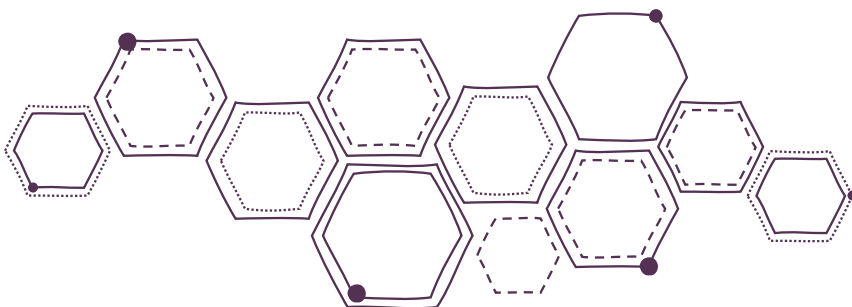
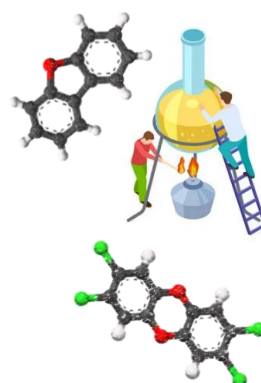
- Pretali, L., Albin, A., Cantalupi, A., Maraschi, F., Nicolis, S., Sturini, M., 2021. TiO₂-photocatalyzed water depollution, a strong, yet selective depollution method: New evidence from the solar light induced degradation of glucocorticoids in freshwaters. *Appl. Sci.* 11. <https://doi.org/10.3390/app11062486>
- Quand-Même, G.C., Auguste, A.F.T., Hélène, L.E.M., Ibrahima, S., Lassine, O., 2015. Electrochemical oxidation of amoxicillin in its pharmaceutical formulation at boron doped diamond (Bdd) electrode. *J. Electrochem. Sci. Eng.* 5, 129–143. <https://doi.org/10.5599/jese.186>
- Quaresma, A. V., Rubio, K.T.S., Taylor, J.G., Sousa, B.A., Silva, S.Q., Werle, A.A., Afonso, R.J.C.F., 2021. Removal of dexamethasone by oxidative processes: Structural characterization of degradation products and estimation of the toxicity. *J. Environ. Chem. Eng.* 9, 106884. <https://doi.org/10.1016/j.jece.2021.106884>
- Rachidi, L., Kaichouh, G., Khachani, M., Zarrouk, A., Karbane, M. El, Chakchak, H., Warad, I., Hourch, A. EL, Kacemi, K. El, Guessous, A., 2021. Optimization and modeling of the electro-Fenton process for treatment of sertraline hydrochloride: Mineralization efficiency, energy cost and biodegradability enhancement. *Chem. Data Collect.* 35, 100764. <https://doi.org/10.1016/j.cdc.2021.100764>
- Radjenovic, J., Bagastyo, A., Rozendal, R.A., Mu, Y., Keller, J., Rabaey, K., 2011. Electrochemical oxidation of trace organic contaminants in reverse osmosis concentrate using RuO₂/IrO₂-coated titanium anodes. *Water Res.* 45, 1579–1586. <https://doi.org/10.1016/j.watres.2010.11.035>
- Radjenovic, J., Petrovic, M., 2017. Removal of sulfamethoxazole by electrochemically activated sulfate: Implications of chloride addition. *J. Hazard. Mater.* 333, 242–249. <https://doi.org/10.1016/j.jhazmat.2017.03.040>
- Radjenovic, J., Sedlak, D.L., 2015. Challenges and Opportunities for Electrochemical Processes as Next-Generation Technologies for the Treatment of Contaminated Water. *Environ. Sci. Technol.* 49, 11292–11302. <https://doi.org/10.1021/acs.est.5b02414>
- Rasolevandi, T., Naseri, S., Azarpira, H., Mahvi, A.H., 2019. Photo-degradation of dexamethasone phosphate using UV/Iodide process: Kinetics, intermediates, and transformation pathways. *J. Mol. Liq.* 295, 111703. <https://doi.org/10.1016/j.molliq.2019.111703>
- Saha, P., Wang, J., Zhou, Y., Carlucci, L., Jeremiase, A.W., Rijnaarts, H.H.M., Bruning, H., 2022. Effect of electrolyte composition on electrochemical oxidation: Active sulfate formation, benzotriazole degradation, and chlorinated by-products distribution. *Environ. Res.* 211, 113057. <https://doi.org/10.1016/j.envres.2022.113057>
- Sánchez-Carretero, A., Sáez, C., Cañizares, P., Rodrigo, M.A., 2011. Electrochemical production of perchlorates using conductive diamond electrolyses. *Chem. Eng. J.* 166, 710–714. <https://doi.org/10.1016/j.cej.2010.11.037>

- Schröder, S., San-Román, M.F., Ortiz, I., 2021. Dioxins and furans toxicity during the photocatalytic remediation of emerging pollutants. Triclosan as case study. *Sci. Total Environ.* 770, 144853. <https://doi.org/10.1016/j.scitotenv.2020.144853>
- Schröder, S., San-Román, M.F., Ortiz, I., 2020. Photocatalytic transformation of triclosan. Reaction products and kinetics. *Catalysts* 10, 1–15. <https://doi.org/10.3390/catal10121468>
- Scialdone, O., Randazzo, S., Galia, A., Silvestri, G., 2009. Electrochemical oxidation of organics in water: Role of operative parameters in the absence and in the presence of NaCl. *Water Res.* 43, 2260–2272. <https://doi.org/10.1016/j.watres.2009.02.014>
- Serrano, K.G., 2018. Indirect electrochemical oxidation using hydroxyl radical, active chlorine, and peroxodisulfate, *Electrochemical Water and Wastewater Treatment*. Elsevier Inc. <https://doi.org/10.1016/B978-0-12-813160-2.00006-7>
- Sharma, V.K., 2011. Oxidation of inorganic contaminants by ferrates (VI, V, and IV)-kinetics and mechanisms: A review. *J. Environ. Manage.* 92, 1051–1073. <https://doi.org/10.1016/j.jenvman.2010.11.026>
- Siciliano, A., Guida, M., Libralato, G., Saviano, L., Luongo, G., Previtiera, L., Di Fabio, G., Zarrelli, A., 2021. Amoxicillin in water: Insights into relative reactivity, byproduct formation, and toxicological interactions during chlorination. *Appl. Sci.* 11, 1–12. <https://doi.org/10.3390/app11031076>
- Silva, F.L., Sáez, C., Lanza, M.R.V., Cañizares, P., Rodrigo, M.A., 2019. The role of mediated oxidation on the electro-irradiated treatment of amoxicillin and ampicillin polluted wastewater. *Catalysts* 9. <https://doi.org/10.3390/catal9010009>
- Sirés, I., Brillas, E., Oturan, M.A., Rodrigo, M.A., Panizza, M., 2014. Electrochemical advanced oxidation processes: Today and tomorrow. A review. *Environ. Sci. Pollut. Res.* 21, 8336–8367. <https://doi.org/10.1007/s11356-014-2783-1>
- Solá-Gutiérrez, C., 2019. Traceability of PCDD/Fs formation in the advanced oxidation of TCS. University of Cantabria.
- Solá-Gutiérrez, C., San Román, M.F., Ortiz, I., 2018. Fate and hazard of the electrochemical oxidation of triclosan. Evaluation of polychlorodibenzo-p-dioxins and polychlorodibenzofurans (PCDD/Fs) formation. *Sci. Total Environ.* 626, 126–133. <https://doi.org/10.1016/j.scitotenv.2018.01.082>
- Solá-Gutiérrez, C., Schröder, S., San Román, M.F., Ortiz, I., 2019. PCDD/Fs traceability during triclosan electrochemical oxidation. *J. Hazard. Mater.* 369, 584–592. <https://doi.org/10.1016/j.jhazmat.2019.02.066>
- Sopaj, F., Rodrigo, M.A., Oturan, N., Podvorica, F.I., Pinson, J., Oturan, M.A., 2015. Influence of the anode materials on the electrochemical oxidation efficiency. Application to oxidative degradation of the pharmaceutical amoxicillin. *Chem. Eng. J.* 262, 286–294. <https://doi.org/10.1016/j.cej.2014.09.100>

- Stanbury, D.M., 1989. Reduction potentials involving inorganic free radicals in aqueous solution. *Adv. Inorg. Chem.* 33, 11–111.
- Sulaiman, S., Khamis, M., Nir, S., Lelario, F., Scranio, L., Bufo, S.A., Karaman, R., 2014. Stability and removal of dexamethasone sodium phosphate from wastewater using modified clays. *Environ. Technol. (United Kingdom)* 35, 1945–1955. <https://doi.org/10.1080/09593330.2014.888097>
- Sun, R., Huang, W., Zhang, Q., Hong, J. ming, 2018. Facile Prepared N-Doped Graphene/Pt/TiO₂ as an Efficient Anode for Acetaminophen Degradation. *Catal. Letters* 148, 2418–2431. <https://doi.org/10.1007/s10562-018-2466-5>
- Tan, T.Y., Zeng, Z.T., Zeng, G.M., Gong, J.L., Xiao, R., Zhang, P., Song, B., Tang, W.W., Ren, X.Y., 2020. Electrochemically enhanced simultaneous degradation of sulfamethoxazole, ciprofloxacin and amoxicillin from aqueous solution by multi-walled carbon nanotube filter. *Sep. Purif. Technol.* 235, 116167. <https://doi.org/10.1016/j.seppur.2019.116167>
- Vallejo, M., San Román, M.F., Ortiz, I., 2013. Quantitative assessment of the formation of polychlorinated derivatives, PCDD/Fs, in the electrochemical oxidation of 2-chlorophenol as function of the electrolyte type. *Environ. Sci. Technol.* 47, 12400–12408. <https://doi.org/10.1021/es403246g>
- Vallejo, M., San Román, M.F., Ortiz, I., Irabien, A., 2014. The critical role of the operating conditions on the fenton oxidation of 2-chlorophenol: Assessment of PCDD/Fs formation. *J. Hazard. Mater.* 279, 579–585. <https://doi.org/10.1016/j.jhazmat.2014.07.020>
- Waterston, K., Wang, J.W., Bejan, D., Bunce, N.J., 2006. Electrochemical waste water treatment: Electrooxidation of acetaminophen. *J. Appl. Electrochem.* 36, 227–232. <https://doi.org/10.1007/s10800-005-9049-z>
- Wojnárovits, L., Takács, E., 2021. Rate constants of dichloride radical anion reactions with molecules of environmental interest in aqueous solution: a review. *Environ. Sci. Pollut. Res.* 28, 41552–41575. <https://doi.org/10.1007/s11356-021-14453-w>
- Wojnárovits, L., Takács, E., 2019. Rate constants of sulfate radical anion reactions with organic molecules: A review. *Chemosphere* 220, 1014–1032. <https://doi.org/10.1016/j.chemosphere.2018.12.156>
- Xia, X., Zhu, F., Li, J., Yang, H., Wei, L., Li, Q., Jiang, J., Zhang, G., Zhao, Q., 2020. A Review Study on Sulfate-Radical-Based Advanced Oxidation Processes for Domestic/Industrial Wastewater Treatment: Degradation, Efficiency, and Mechanism. *Front. Chem.* 8. <https://doi.org/10.3389/fchem.2020.592056>
- Zhang, Q., Huang, W., Hong, J. ming, Chen, B.Y., 2018. Deciphering acetaminophen electrical catalytic degradation using single-form S doped graphene/Pt/TiO₂. *Chem. Eng. J.* 343, 662–675. <https://doi.org/10.1016/j.cej.2018.02.089>

4

PCDD/Fs DURING EOX OF DRUGS: TOXICITY ASSESSMENT



Abstract

The electrochemical oxidation (EOX) of the drugs dexamethasone (DEX), amoxicillin (AMX), paracetamol (PAR) and sertraline (STR), using a BDD cell, has allowed 100% degradation of these drugs. However, complete mineralisation has not been reached in any of the cases, forming numerous reaction intermediates, independently of the electrolyte medium used, NaCl or Na₂SO₄+NaCl (Chapter 3). Among these by-products, stand out the precursors of precursors or, the precursors, of dioxins and furans, such as chlorinated or non-chlorinated organic compounds, which can increase the final toxicity of the sample, turning into PCDD/Fs.

Thus, in Chapter 4, the analysis of the PCDD/Fs generated during the EOX-Drugs experiments has been carried out, both for homologues and congeners, depending on the electrolytic medium used, deepening into their distribution and in the lesser or greater degree of chlorination. With this, the toxicity assessment in terms of TEQ has been performed for the degradation of each drug. Finally, an alternative methodology for TEQ calculation has been proposed from the specific case study about the photocatalytic oxidation of triclosan (TCS). For this, first, a PCDD/Fs kinetic analysis has been performed, followed by a statistical analysis in two steps: multivariable analysis and multiple linear regression, which have led to an alternative equation of the toxicity through different models, employing lower number congeners than the traditional equation, and with, this lower analytical and economic effort.

4.1. Analysis of the PCDD/Fs formed from drugs' EOX

So far, and as far as the author's knowledge, the literature does not describe works where dioxins and furans have been detected during the electrochemical oxidation of the studied compounds in this PhD thesis. Currently, the interest resides in their crescent consumption facing the fight against the virus SARS-CoV-2, and consequently their disposal to several water matrices, such as lakes or rivers, from WWTPs (Cappelli et al., 2022; Diaz-Camal et al., 2022; Khan et al., 2022; Morales-Paredes et al., 2022; Sengar and Vijayanandan, 2022), especially during the big COVID-19 waves of the years 2020 and 2021, occurring at a global level.

To recall, PCDD/Fs can be formed in an accidentally manner from several natural processes (as described in Chapter 1) and also remediation procedures of aqueous solutions, with advanced oxidation processes among them (Weber, 2007; Weber et al., 2008). In the recent literature, several works can be found where PCDD/Fs are generated when applying AOPs to solutions containing organic compounds, that can be precursors of dioxins and furans (Vallejo et al., 2015b), as the case of, on the one hand, 2-chlorophenol solutions treated with Fenton oxidation (Fernández-Castro, 2017; Fernández-Castro et al., 2016; Vallejo, 2014; Vallejo et al., 2015a, 2014) or electrochemical oxidation (Vallejo et al., 2013), or, on the other hand, triclosan (TCS) containing solutions, both when applying electrochemical oxidation (Solá-Gutiérrez, 2019; Solá-Gutiérrez et al., 2019, 2018) or photocatalysis (Schróder et al., 2021; Solá-Gutiérrez, 2019) (see Chapter 1, section 1.3). Because of the molecular structure of the drugs DEX, AMX, PAR and STR, and because they are organic compounds, by-products generated during their degradation by electrooxidation, can be potential precursors of PCDD/Fs formation in presence of a chloride medium. With the aim of validating this hypothesis, for each drug, the influence of the used electrolyte during electro-oxidation treatment in the dioxins and furans formation was analysed. The analytical method applied to identify and quantify, the possible formation of PCDD/Fs formed during the EOX process, was EPA 1613 method, which is comprehensively described in Chapter 2, section 2.4. In addition, in section 2.4.3 is detailed the quality assurance of the process, and in Annex II are detailed the recoveries for the 2,3,7,8-PCDD/Fs congeners, which are within the ranges established by US EPA (US EPA, 1994). Also, to determine the possible influence of the contamination of the electrochemical system by the potential accumulation of dioxins and furans along the experiments, blanks (ultrapure water, UP) were performed, after each chemical cleaning and before each type of EOX experiment. The UP solutions were pumped through the system working in a batch mode for eight

hours; finally, PCDD/Fs concentration were measured. The results obtained indicated negligible concentrations of PCDD/Fs or under the detection limit values. Even so, the concentrations of PCDD/Fs depicted in this chapter, were corrected by means of the subtraction of PCDD/Fs levels detected in the blank, for all experiments carried out.

4.1.1. Homologue profiles analysis

At the end of each experiment (EOX-Drugs), the homologue profiles of the DEX, AMX, PAR and STR degradation were identified and quantified. Homologue groups are classified depending on the number of chlorine atoms in the molecule from four (TCDD/Fs) to eight (OCDD/Fs) (see Chapter 1, section 1.1.2). Figure 4.1 depicts the homologue groups from TCDD to OCDD, for the experiments that employed NaCl and Na₂SO₄+NaCl as electrolyte. The concentration of the homologues is represented through non-cumulative area charts, where, in all cases, a darker colour was used to show the results of the degradation of each drug using NaCl electrolyte, and a lighter colour to show the results of the degradation of each drug when Na₂SO₄+NaCl electrolyte was used. In Figure 4.1a is presented the homologue profile for the DEX samples oxidated, and in the same direction, Figure 4.1b, 4.1c and 4.1d represent the homologue profile for AMX, PAR and STR respectively. It is worth noting that special attention in the scale of the charts should be taken, even though the generated PCDD/Fs amounts are in pg L⁻¹. The concentration values are determinant for the toxicity estimation, especially for the case of the TCDD/Fs groups, which contains the 2,3,7,8-TCDD congener, which is the most toxic one (see Table 1.4, Chapter 1) (Schröder et al., 2021). In Figure 4.1, it can be seen that the scale is 300 pg L⁻¹ for DEX and STR, double for PAR, 600 pg L⁻¹, and 10 times higher, with respect to DEX and STR scales, for the AMX (3000 pg L⁻¹). In addition, and as an aid to the understanding and analysis of the graphs, Table 4.1 presents a summary of the homologue total concentrations for both electrolytic media, and in a separated manner, PCDDs and PCDFs, with the respective percentages of its contribution to the total PCDD/Fs amount.

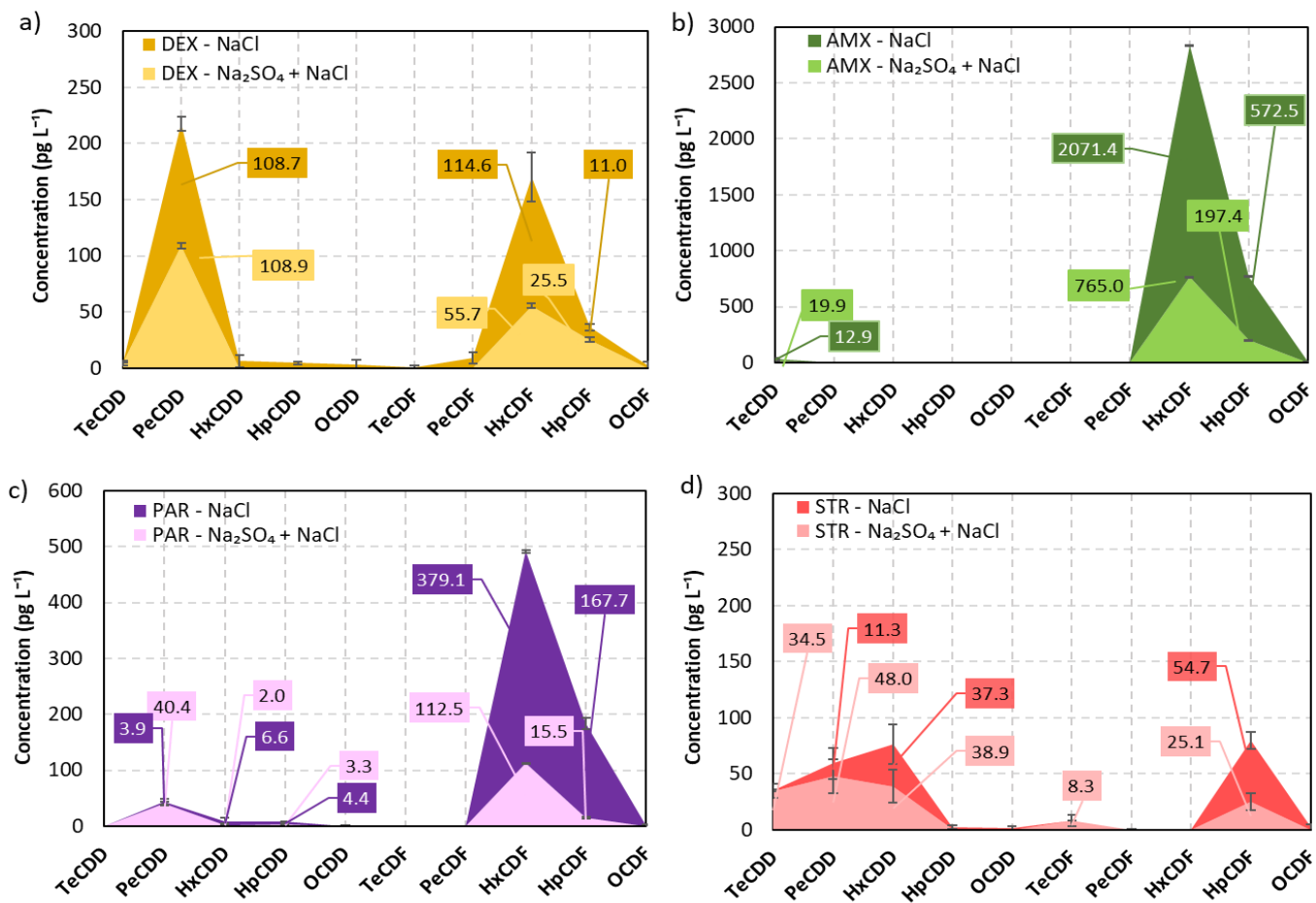


Figure 4.1. PCDD/Fs homologue profiles of the EOX-Drugs experiments of a) DEX, b) AMX, c) PAR and d) STR, for the electrolytic media, 56 mM NaCl and 21 mM Na₂SO₄ + 2.8 mM NaCl.

Table 4.1. Total amount (and percentage) of homologue groups produced (pg L^{-1}) during the DEX, AMX, PAR and STR degradation, using NaCl and Na_2SO_4 +NaCl as electrolytes.

Drugs	Electrolyte	PCDDs pg L^{-1} (%)	PCDFs pg L^{-1} (%)	TOTAL Homologues pg L^{-1} (%)
DEX	56 mM NaCl	123.2 (47.1%)	137.9 (52.9%)	261.1 (100%)
	21 mM Na_2SO_4 + 2.8 mM NaCl	113.7 (58.4%)	81.1 (41.6%)	194.8 (100%)
AMX	56 mM NaCl	12.9 (0.5%)	2648.4 (99.5%)	2661.3 (100%)
	21 mM Na_2SO_4 + 2.8 mM NaCl	20.6 (2.1%)	964.1 (97.9%)	984.7 (100%)
PAR	56 mM NaCl	15.3 (2.7%)	548.2 (97.3%)	563.5 (100%)
	21 mM Na_2SO_4 + 2.8 mM NaCl	45.7 (26.3%)	127.9 (73.7%)	173.6 (100%)
STR	56 mM NaCl	51.7 (47.5%)	57.2 (52.5%)	108.9 (100%)
	21 mM Na_2SO_4 + 2.8 mM NaCl	122.2 (78.5%)	33.5 (21.5%)	155.7 (100%)

As can be seen in Figure 4.1, in almost all cases, in a first approach, PCDD/Fs total amount was higher when using NaCl as electrolyte, except to the sertraline (STR) case, where the generated amounts of dioxins and furans were approximately of the same order, 108.9 and 155.7 pg L^{-1} for NaCl and for Na_2SO_4 +NaCl case, respectively (Figure 4.1d and Table 4.1). The highest total concentration of PCDD/Fs corresponds to the AMX for the NaCl electrolyte case, reaching 2661.3 pg L^{-1} , and on the contrary, the lowest total concentration PCDD/Fs is for the STR, with a value of 108.9 pg L^{-1} (Figure 4.1 and Table 4.1).

When analysing the electrolytic media separately, for NaCl case, furans were the predominant group in all cases, reaching high concentrations, especially for AMX and PAR, with values of 2648.4 (99.5%) and 548.2 pg L^{-1} (97.2%), respectively, (Figure 4.1b (AMX), Figure 4.1c (PAR) and Table 4.1). For DEX and STR cases, furans groups accounts from a bit more that the dioxins, achieving concentrations of 137.9 pg L^{-1} (52.9%) and 57.2 pg L^{-1} (52.5%), respectively (Figure 4.1a (DEX), Figure 4.1d (STR) and Table 4.1); and the remaining amounts are dioxins. For the Na_2SO_4 +NaCl case the trend is the same for AMX and PAR, achieving the highest PCDFs concentrations, with 964.1 (97.9%) and 127.2 pg L^{-1} (73.7%), respectively (Figure 4.1b (AMX), Figure 4.1c (PAR) and Table 4.1). DEX and

STR possess the highest dioxin values, reaching 113.7 (58.3%) and 122.2 pg L^{-1} (78.5%), respectively, (Figure 4.1a (DEX), Figure 4.1d (STR) and Table 4.1).

Dexamethasone (DEX)

Deepening into each drug, in Figure 4.1a, for dexamethasone case, the higher concentrations were found for the group of the homologue HxCDF (114.6 pg L^{-1}) in NaCl medium, and with a similar amount, PeCDD group (108.9 pg L^{-1}) for the medium $\text{Na}_2\text{SO}_4+\text{NaCl}$, accounting, respectively, for 43.8% and 55.9% of the total PCDD/Fs amount (Figure 4.1a).

Amoxicilin (AMX)

Amoxicillin (Figure 4.1b) was the compound that generated the highest concentration of PCDD/Fs, independently of the electrolytic medium employed, reaching a total value of 2661.3 pg L^{-1} for NaCl case and 984.7 pg L^{-1} for $\text{Na}_2\text{SO}_4+\text{NaCl}$ case (Table 4.1). For both electrolytes, PCDFs group is the one with the highest concentration (2648.4 and 964.1 pg L^{-1} for NaCl and $\text{Na}_2\text{SO}_4+\text{NaCl}$ case, respectively) (Table 4.1). Specifically, among furans, the more symbolic homologue group was HxCDF for both electrolytes, accounting for 77.8% and 77.7% of the total PCDD/Fs amount for NaCl case and $\text{Na}_2\text{SO}_4+\text{NaCl}$ case, correspondingly (Figure 4.1b).

Paracetamol (PAR)

As it is shown in Figure 4.1c, paracetamol follows the same behaviour that AMX, PCDFs were higher than PCDDs for both electrolyte cases, with HxCDF as the group with the highest concentration, accounting for 67.3% and 64.8% of the total amount PCDD/Fs, with 379.1 pg L^{-1} and 112.5 pg L^{-1} , for the NaCl medium and for the medium $\text{Na}_2\text{SO}_4+\text{NaCl}$, respectively. Next, the HpCDF homologue group is the second biggest group of all homologue groups for NaCl case, reaching 167.7 pg L^{-1} (29.8% of the total PCDD/Fs concentration) (Figure 4.1c). For the dioxin homologue groups, 40.4 pg L^{-1} is the highest concentration achieved for the PeCDD homologue, when using $\text{Na}_2\text{SO}_4+\text{NaCl}$ as electrolyte, accounting for 23.2% of the total PCDD/Fs amount.

Sertraline (STR)

For sertraline case (Figure 4.1d), the highest concentration belongs to HpCDF (54.7 pg L^{-1}) group with NaCl, and PeCDD group (48.0 pg L^{-1}) with $\text{Na}_2\text{SO}_4+\text{NaCl}$, accounting for 50.2% and 30.8, respectively of the total concentration of the PCDD/Fs.

4.1.2. 2,3,7,8-congeners analysis

In a second stage, regarding to the assessment of PCDD/Fs, the analysis of the 2,3,7,8-congeners was carried out. 2,3,7,8-congeners are dioxins and furans with chlorine atoms in positions 2,3,7,8 of the molecule, and 17 of them deserve special attention because of its associated toxicity (Chapter 1, section 1.1.2) (Schröder et al., 2021; Solá-Gutiérrez, 2019). These profiles, for each pharmaceutical compound, are shown in Figure 4.2 for the NaCl and Na₂SO₄+NaCl electrolyte mediums. This representation follows the same format of the homologues (Figure 4.1), a non-cumulative area chart, where the concentration of each congener is represented in area, dark coloured if the electrolyte is NaCl, and in the same colour but lighter, if the electrolyte is Na₂SO₄+NaCl. In the same direction, in Figure 4.2a it is represented the congener profile for DEX, and consecutively, Figure 4.2b, 4.2c and 4.2d represent the congener profiles for AMX, PAR and STR, respectively. As for the homologue groups, here also it is necessary to remark the scale of the congener charts (Figure 4.2), because in the congeners case, they are decisive to the further toxicity calculation, especially for the 2,3,7,8-TCDD case. This dioxin achieves the highest toxicity value (I-TEF=1, Table 1.4, Chapter 1). The scale reached 60 pg L⁻¹ for PAR and STR, the double for DEX, 120 pg L⁻¹, and 10 times higher (respecting to PAR and STR) for AMX, being 600 pg L⁻¹. Additionally, in Table 4.2 are gathered the 2,3,7,8-congeners concentrations, classified into 2,3,7,8-PCDDs and 2,3,7,8-PCDFs, with the correspondent percentages of its contribution to the total amount of congeners for each study case.

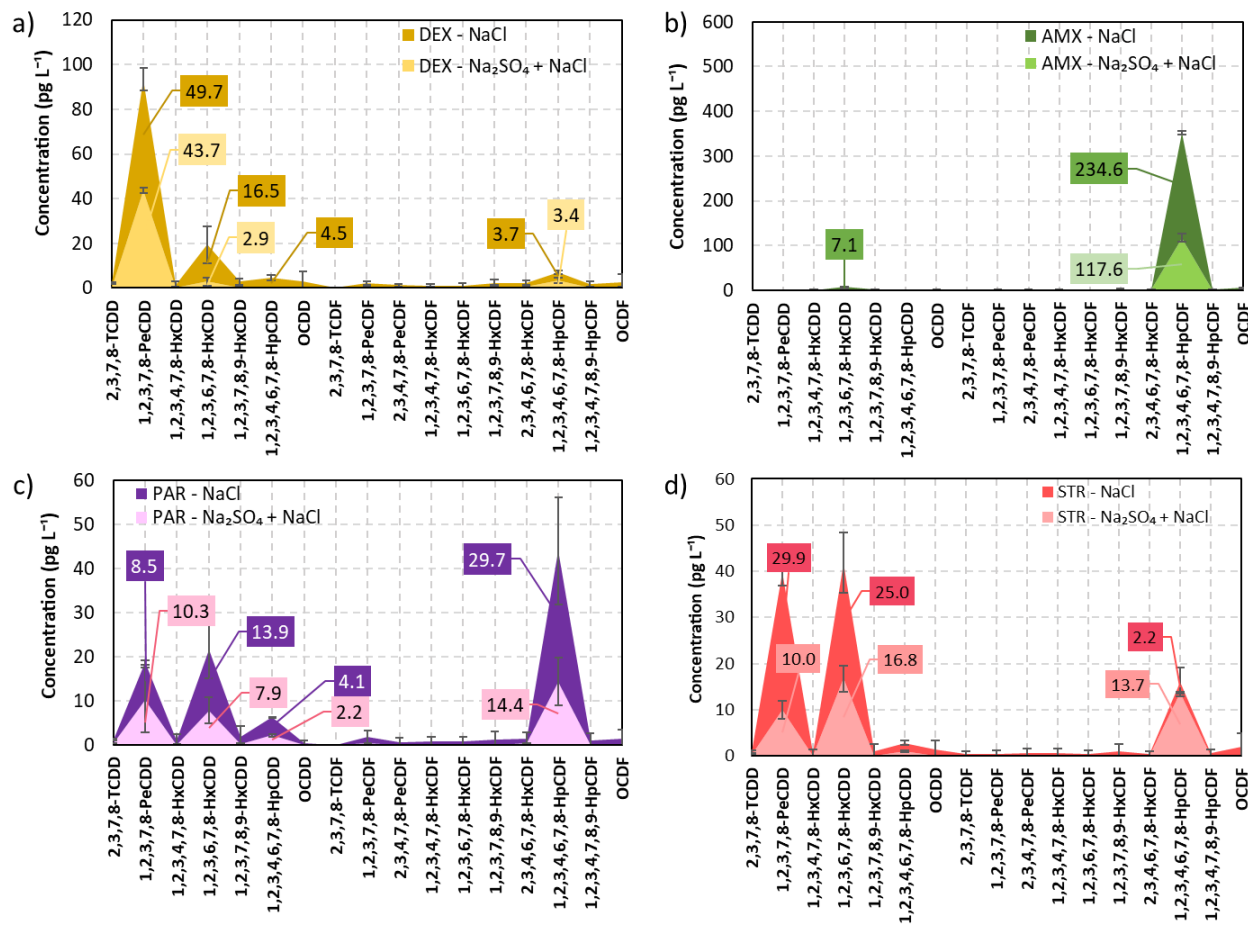


Figure 4.2. 2,3,7,8-PCDD/Fs congeners profile of the EOX-Drugs experiments of a) DEX, b) AMX, c) PAR and d) STR, for the electrolytic media, 56 mM NaCl and 21 mM Na₂SO₄ 2.8 mM NaCl.

Table 4.2. Total amount (and percentage) of 2,3,7,8-PCDD/Fs congeners produced during the DEX, AMX, PAR and STR degradation, using NaCl and Na₂SO₄+NaCl as electrolytes.

Drug	Electrolyte	2,3,7,8-PCDDs pg L ⁻¹ (%)	2,3,7,8-PCDFs pg L ⁻¹ (%)	TOTAL 2,3,7,8- congeners pg L ⁻¹ (%)
DEX	56 mM NaCl	80.2 (83.5%)	15.9 (16.5%)	96.1 (100%)
	21 mM Na ₂ SO ₄ + 2.8 mM NaCl	46.8 (89.0%)	5.8 (11.0%)	52.6 (100%)
AMX	56 mM NaCl	7.3 (2.9%)	242.0 (97.1%)	249.3 (100%)
	21 mM Na ₂ SO ₄ + 2.8 mM NaCl	4.6 (3.5%)	126.2 (96.5%)	130.8 (100%)
PAR	56 mM NaCl	30.4 (44.2%)	38.3 (55.8%)	68.7 (100%)
	21 mM Na ₂ SO ₄ + 2.8 mM NaCl	20.9 (57.9%)	15.2 (42.1%)	36.1 (100%)
STR	56 mM NaCl	60.4 (86.8%)	9.2 (13.2%)	69.6 (100%)
	21 mM Na ₂ SO ₄ + 2.8 mM NaCl	27.9 (67.1%)	13.7 (32.9%)	41.7 (100%)

As it is depicted both in Figure 4.2 and Table 4.2, the 2,3,7,8-congeners profile shows a similar trend to the corresponding homologue profile, except to the case of the dioxins congeners of AMX. The total amount of 2,3,7,8-PCDD/Fs congeners is the highest in all cases when NaCl was employed as electrolyte, being in the range between 69.6 pg L⁻¹ for the STR up to 249.3 pg L⁻¹ for the AMX. For the NaCl case, the dioxins congeners were higher for DEX and STR (Table 4.2), with values of 80.2 and 60.4 pg L⁻¹, accounting for 83.5 and 86.8% of the total 2,3,7,8-congeners, respectively. Contrarily, for AMX and PAR, the furans congeners were the predominating group, with values of 242.2 and 38.3 pg L⁻¹, accounting for 97.1 and 55.8% of the total 2,3,7,8-congeners, respectively (Table 4.2). In the Na₂SO₄+NaCl case, 2,3,7,8-PCDDs were higher in all cases except for AMX case, where the furans amount reached a value of 126.2 pg L⁻¹ accounting for 96.5% of the total congeners (Table 4.2).

The most toxic dioxin, 2,3,7,8-TCDD was found in very low concentrations, but it is important to not underestimate this concentration, because it has the highest toxicity factor (I-TEF=1). In this PhD thesis, the concentrations were, for NaCl case, 2.04, 0.78 and 0.64 pg L⁻¹ for DEX, PAR and STR, respectively; and for Na₂SO₄+NaCl case, 0.20, 0.40 and 0.40 pg L⁻¹ for DEX, PAR and STR, respectively. It was not detected in electro-oxidated AMX samples. In addition, due to the scale of the graphs in Figure 4.2 it is not possible to appreciate this 2,3,7,8-TCDD concentration.

Dexamethasone (DEX)

In the DEX degradation, the dioxins predominated the congeners profile, formed over furans for both electrolytic media, being 80.2 (83.5%) and 46.8 pg L^{-1} (89.0%), for NaCl and NaCl+Na₂SO₄ as electrolytes, respectively (Table 4.2). It can be remarked 1,2,3,7,8-PeCDD, which is the highest formed congener for both electrolytes, reaching very similar values for both electrolytes: 49.7 and 43.7 pg L^{-1} (51.7 and 93.4%) for NaCl and Na₂SO₄+NaCl, respectively (Figure 4.2a).

Amoxicilin (AMX)

As previously mentioned, AMX reached the highest congeners total concentration, for both the electrolyte NaCl and Na₂SO₄+NaCl. Specifically, 2,3,7,8-PCDFs congeners possess the highest concentration, regardless of the electrolyte employed, reaching values up to 242.0 (NaCl) and 126.2 pg L^{-1} (Na₂SO₄+NaCl), accounting for 97.1% and 96.5% of the total 2,3,7,8-PCDD/Fs (Table 4.2). The congener with higher concentration corresponds to 1,2,3,4,6,7,8-HpCDF reaching values of 234.6 pg L^{-1} (NaCl) and 117.6 pg L^{-1} (Na₂SO₄+NaCl), which accounts for 94.1% and 89.9%, respectively, of the total 2,3,7,8-PCDD/Fs for the amoxicillin case (Figure 4.2b and Table 4.2).

Paracetamol (PAR)

For the paracetamol case, the 2,3,7,8-PCDDs and PCDFs formed were approximately the same, without any influence of the electrolyte used. For the NaCl case, 30.4 pg L^{-1} of 2,3,7,8-PCDDs were obtained, accounting for 44.2% of the total congeners detected, and for the Na₂SO₄+NaCl case, 20.9 pg L^{-1} of 2,3,7,8-PCDDs were obtained, accounting for 57.9% of the total congeners detected in the electro-oxidation of PAR (Table 4.2). 1,2,3,4,6,7,8-HpCDF is the congener that reached the highest concentration, 29.7 pg L^{-1} , that accounts for 43.2% of the total 2,3,7,8-PCDD/Fs amount (Figure 4.2c and Table 4.2).

Sertraline (STR)

Finally, for the STR case, the 2,3,7,8-PCDDs were higher for both electrolytic media, being 60.4 (NaCl) and 27.9 pg L^{-1} (Na₂SO₄+NaCl), this is 86.8 and 67.1% of the total congeners, respectively (Table 4.2). Within this, two congeners are worth to highlight, both for the NaCl case, 1,2,3,7,8-PeCDD and 1,2,3,6,7,8-HxCDD, with values of 29.9 and 25.0 pg L^{-1} , which accounts for 43.0 and 35.9% of the total PCDD/Fs congeners (Figure 4.2d).

4.1.3. Toxicity assessment in terms of TEQ

As it has been defined in Chapter 1, section 1.1.2, the congeners analysis allows estimating the toxicity of a sample, in terms of TEQ, applying Eq. 1.1. In Figure 4.3 is depicted the toxicity associated with each sample, for each drug and electrolyte (EOX-Drugs), calculated through the congeners measured at final time of the experiment, which is, when the pharmaceutical compound is completely degraded.

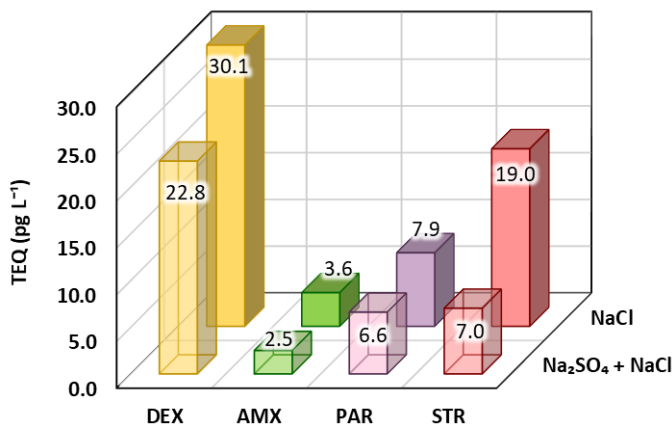


Figure 4.3. Final toxicity, expressed in terms of TEQ, for the four degraded drugs: DEX, AMX, PAR and STR (NaCl and Na₂SO₄+NaCl, EOX-Drugs).

Hereunder, the toxicity for the four pharmaceutical compounds is detailed for each one, in a separately manner, ordered according to their toxicity value (TEQ), from higher to lower quantity. It can be appreciated that the most toxic samples are those which contains the 2,3,7,8-TCDD presence, DEX, STR and PAR (in order of toxicity).

Dexamethasone (DEX)

As can be seen in Figure 4.3, the greater toxicity value belongs to dexamethasone working with both electrolytes, 30.1 for NaCl and 22.8 pg L⁻¹ for Na₂SO₄+NaCl of TEQ. These results are because of the higher amounts of the 1,2,3,7,8-PeCDD congener produced in the degraded DEX samples, 49.7 and 43.7 pg L⁻¹ of TEQ for NaCl and Na₂SO₄+NaCl (Figure 4.2a), respectively, being its value of I-TEF=0.5, the second highest I-TEF value which is one place below to the highest one, 2,3,7,8-TCDD (I-TEF=1) (Table 1.4, Chapter 1). 2,3,7,8-TCDD, the most toxic congener (I-TEF=1), was present in concentrations of 2.04 (NaCl) and 0.40 pg L⁻¹ (Na₂SO₄+NaCl).

Sertraline (STR)

Following this, STR is the next compound in toxicity terms, despite its lower 2,3,7,8-congeners concentrations, 69.6 and 41.7 pg L^{-1} for electrolytes NaCl and $\text{Na}_2\text{SO}_4+\text{NaCl}$, respectively (Table 4.2). For the NaCl case, nearly 30 pg L^{-1} of 1,2,3,7,8-PeCDD were reached, congener that provides the toxicity, as it has been mentioned above. But, for the second congener in order of concentration, 1,2,3,6,7,8-HxCDD (25 pg L^{-1}), does not contribute a lot for the TEQ, because its I-TEF value is low, 0.1. For the combined electrolytic medium ($\text{Na}_2\text{SO}_4+\text{NaCl}$), the TEQ has a lower value than for NaCl, being 7 pg L^{-1} , because the highest concentration value of the congeners belongs to 1,2,3,6,7,8-HxCDD (I-TEF=0.1) (Figure 4.2d). 2,3,7,8-TCDD, was present here in concentrations of 0.64 (NaCl) and 0.40 pg L^{-1} ($\text{Na}_2\text{SO}_4+\text{NaCl}$).

Paracetamol (PAR)

Subsequently, degraded PAR solutions appear in the third place in TEQ terms, reaching values up to 7.9 pg L^{-1} for electrolyte NaCl, and 6.6 pg L^{-1} for $\text{Na}_2\text{SO}_4+\text{NaCl}$ (Figure 4.3). In this case, the highest concentration congener formed for both electrolytic was 1,2,3,4,6,7,8-HpCDF, with 29.7 pg L^{-1} (NaCl) and 14.4 pg L^{-1} ($\text{Na}_2\text{SO}_4+\text{NaCl}$), which hardly contributes to toxicity, I-TEF=0.01, followed by 1,2,3,7,8-PeCDD, which is the second congener formed in terms of concentration for both electrolytes, 8.5 (NaCl) and 10.3 pg L^{-1} ($\text{Na}_2\text{SO}_4+\text{NaCl}$) (Figure 4.2c), contributing to the toxicity, after the TEQ conversion, with 4.2 and 5.1 pg L^{-1} (NaCl, and $\text{Na}_2\text{SO}_4+\text{NaCl}$), respectively. In these samples, 2,3,7,8-TCDD, was found with values of 0.78 (NaCl) and 0.40 pg L^{-1} ($\text{Na}_2\text{SO}_4+\text{NaCl}$).

Amoxicilin (AMX)

Opposite, and surprisingly, amoxicillin gives the lowest toxicity values, despite the fact that it possesses the highest values of the total concentration of the 2,3,7,8-congeners, 249.3 (NaCl electrolyte) and 130.8 pg L^{-1} ($\text{Na}_2\text{SO}_4+\text{NaCl}$ electrolyte) (Table 4.2). It is highlighted the value of the 1,2,3,4,6,7,8-HpCDF, 234.6 pg L^{-1} when using NaCl, which does not provide to toxicity, I-TEF=0.01, in comparison to the dioxin of higher toxicity, 2,3,7,8-TCDD (I-TEF=1.0, Table 1.4). These results contribute to total toxicity of AMX of 3.6 pg L^{-1} of TEQ (NaCl). The same conclusion can be obtained for Na_2SO_4 electrolyte (Figure 4.3). It is worth to recall that the limit established by the US EPA is 30 pg L^{-1} (US EPA, 2013), so the value determined here is above the allowed threshold for DEX in NaCl medium.

The results obtained regarding PCDD/Fs formation (Figure 4.1 and Figure 4.2) can be explained in terms of the chloride concentration present in the solution, as in the case of the degradation intermediates (EOX-Intermediates, Chapter 3, section 3.3). When NaCl is employed as electrolyte, radicals and oxidant species such as $\text{Cl}_2^{\bullet-}$, Cl^{\bullet} , $\text{ClOH}^{\bullet-}$, HClO and Cl_2 are found in the medium, which leads to the formation of chlorophenols and chlorohydroquinones, among other compounds, as a consequence of the degradation drugs DEX, AMX, PAR and STR. From the intermediates detected (several types of chlorophenols) the direct formation of low chlorination degree furans through the condensation of chlorophenols is hypothesized. Sidhu and Edwards (2002) reported the preferential formation of furans over dioxins through the combination of two 2-chlorophenoxy radicals (2-CPR) produced from 2-chlorophenol (2-CP) precursor, radical active specie that possesses enol and keto forms with the unpaired electron on the phenolic oxygen, however, due to the fact that keto forms possess higher stability than enol forms, higher formation of DCDF is expected (Fernández-Castro et al., 2016). Subsequently, the radicals and oxidant species attack low chlorinated PCDD/Fs, increasing the chlorination degree and resulting in higher chlorination degree PCDD/Fs (HxCDF and HpCDF). It is worth highlighting that all PCDD/Fs samples were taken at the final time of the experiment, being probable that at the initial time, is when lower chlorination degree furans can be produced, reaching a higher chlorination degree at the end time of the process degradation, due to successive chlorination reactions.

On the other hand, when less chloride amount is present in the medium (this is when using the combined electrolyte, $\text{Na}_2\text{SO}_4+\text{NaCl}$), the same behaviour of NaCl medium of the oxidant species and radicals of chlorine is assumed. Furans are formed in the same proportion but to a lesser extent as when using just NaCl due to the less chloride in the medium, and also, due to the fact that $\text{SO}_4^{\bullet-}$ is scavenged by the Cl^- , to produce Cl^{\bullet} , for continuing reacting with Cl^- , and generate less active radicals, as in the case of $\text{Cl}_2^{\bullet-}$ (Eqs. 3.13 and 3.22) (Lan et al., 2017; Saha et al., 2022; Wojnárovits and Takács, 2021). Moreover, it is possible that higher amounts of lower chlorinated PCDDs are formed (regarding dioxins) directly from the condensation of two 2-chlorophenoxy radicals (2-CPR), and over time they are also being chlorinated, thus, increasing the chlorination degree as has been described for furans (Fernández-Castro et al., 2016). Figure 4.4 shows a summary of the proposed hypothesis regarding to the PCDD/Fs formation from the combination of 2-CPR. First, the less chlorinated ones are formed, and then, chlorination reactions are produced, giving place to the formation of

polychlorinated PCDD/Fs. Figure 4.4 is partially adapted from Fernández-Castro et al. (2016) and Schröder et al. (2021).

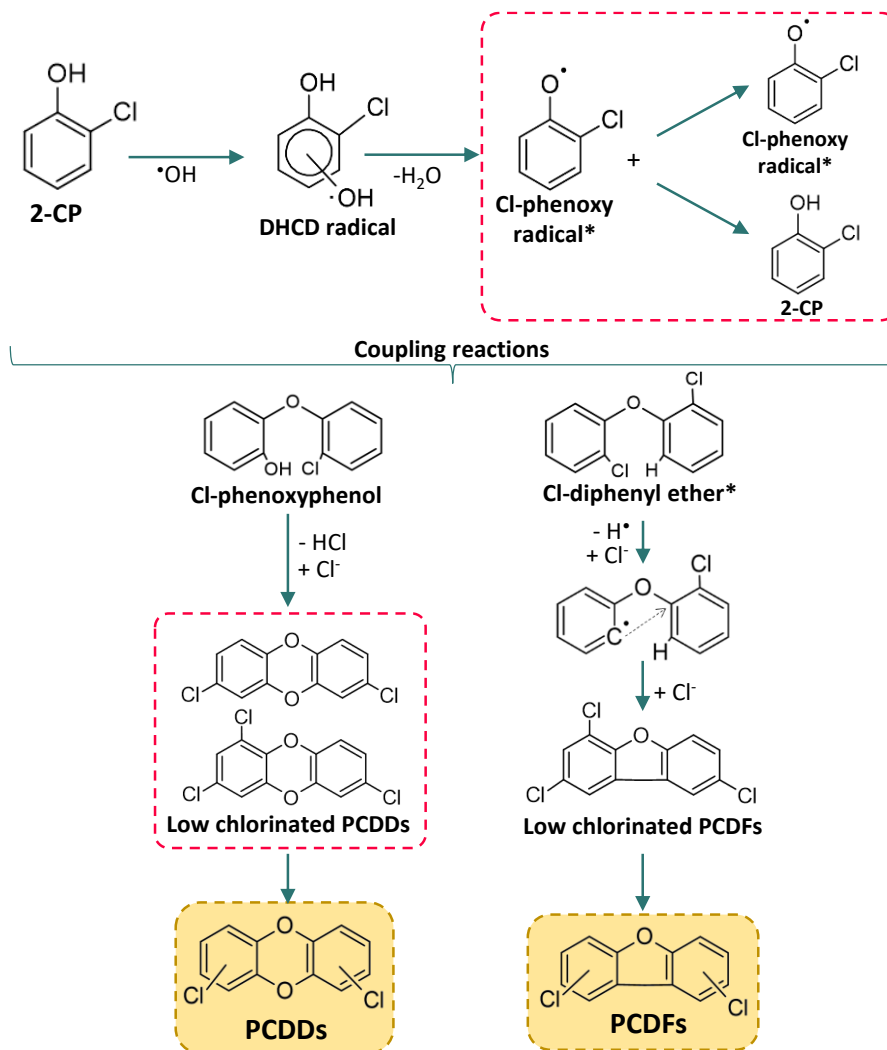


Figure 4.4. Potential PCDD/Fs formation via chlorophenols, through of the combination of two 2-chlorophenoxy radicals (Fernández-Castro et al., 2016; Schröder et al., 2021).

Despite that there are no high concentrations of 2,3,7,8-TCDD present in drugs' electro-oxidated solutions, these compounds had led to generate toxicity to a greater or lesser extent, and even though some congeners possess lower toxicity values, they are in higher concentrations, consequently providing toxicity (Schröder et al., 2021).

4.2. New methodology for TEQ calculation: TCS photocatalysis as case study.

In the framework of this doctoral thesis, other oxidation technologies for the removal of emerging pollutants have been studied with the same aim until now proposed; assess the toxicity in residual samples, containing PPCPs (Pharmaceutical and Personal Care Products), after applying advanced oxidation processes. Specifically, remediation through photocatalysis applied to polluted aqueous solutions with triclosan (TCS, 5-Chloro-2-(2,4-dichlorophenoxy)phenol), a very well-known antibacterial and antifungal compound, which belongs to PPCPs, added to many personal care products such as cosmetics, handwash soap, toothpaste, etc., has been carried out. TCS is an emergent pollutant, very persistent and resistant to degradation, being present in many parts of the environment, especially in aqueous matrices; is highly toxic, and it has been identified as an endocrine disruptor. Moreover, it has been corroborated as a precursor of the formation of dioxins and furans by several authors in the last years. In the works of Solá-Gutiérrez et al. (2019, 2018), high concentrations of PCDD/Fs were found after the application of electrochemical oxidation for the treatment of TCS-containing solutions. Afterwards, Solá-Gutiérrez, (2019) applied photocatalysis to TCS-containing solutions, also analysing the PCDD/Fs, and again obtained high concentrations.

With the aim of reducing the analytical effort, and along with this, the economic implications that the congeners analysis encompass, it can be concluded from the results until now presented (section 4.1) that not only the toxicity, but also the concentration influenced in the final toxicity assessment, and for this reason, it is necessary to obtain a TEQ expression that implies a lesser number of congeners to analyse (Schröder et al., 2021). As a case study, it was performed the analysis of the kinetics of the formation of dioxins and furans during the application of the photocatalysis to TCS aqueous solutions (Schröder et al., 2021, 2020; Solá-Gutiérrez, 2019), which results are hereafter detailed in section 4.2.1. It is of great importance to know the kinetics of any process; it can be useful to predict some behaviours for the purpose of avoiding unnecessary experimental time and its associated costs of energy and materials. Then, in section 4.2.2, a statistical analysis was applied to the congener's kinetics, in order to reduce the number of congeners that are necessary to analyse, and with it, the analytical and economic effort that implicates obtaining the toxicity in terms of TEQ from the 2,3,7,8-congeners.

The photocatalytic experiments have been carried out with the same methodology that the applied for the electrochemical oxidation drugs' experiments (see

Chapter 2, section 2.2.1), but with a small difference: each point represents the end of an experiment, due to the elevated volume necessary to analyse a PCDD/Fs sample, 0.5 L. So, to obtain the kinetic course of the PCDD/Fs formation, five experiments were necessary, carried out in duplicate (Schröder et al., 2021, 2020; Solá-Gutiérrez, 2019).

4.2.1. PCDD/Fs formation kinetics

Solutions with an initial concentration of 10 mg L^{-1} of TCS, treated under UVA-LED light using 1.5 g L^{-1} of catalyst (TiO_2), were evaluated at different operation times (0, 30, 90, 180 and 300 minutes). This amount of catalyst was employed because it provided the best results in terms of TCS degradation (Schröder et al., 2020). The obtained results are shown in Figure 4.5 and in Figure 4.6. On the one hand, Figure 4.5 shows the homologue profile corresponding to of PCDDs (Figure 4.5a) and PCDFs (Figure 4.5b) formation kinetics during TCS oxidation process. On the other hand, Figure 4.6 shows the congeners profile corresponding to of 2,3,7,8-PCDDs (Figure 4.6a) and 2,3,7,8-PCDFs (Figure 4.6b) formation kinetics during TCS oxidation process. Figure 4.5 is represented in logarithmic scale, with the aim of better comprehension and a correct visualization of the differences between the homologue concentrations. The homologue groups are depicted (Figure 4.5) in order of concentration, from higher to lower, in order to a better comprehension.

In Figure 4.5 it can be appreciated that all the dioxins and furans homologues follow almost the same trend, they increase until reaching the highest concentration, between 90 and 180 minutes, and decrease ending in almost negligible concentration values, all lower than 86.4 pg L^{-1} (corresponding to TCDD), except to the TCDF homologue group, whose final concentration is 881.4 pg L^{-1} . As can be seen, tetra-groups (both dioxins and furans) are the ones who possess the greater concentration, at all sampling times. At 90 and 180 minutes, TCDFs group represents 97.0% ($3.7 \cdot 10^4 \text{ pg L}^{-1}$) and 98.3% ($7.4 \cdot 10^4 \text{ pg L}^{-1}$) of the total PCDD/Fs amount ($3.9 \cdot 10^4 \text{ pg L}^{-1}$ and $7.5 \cdot 10^4 \text{ pg L}^{-1}$), respectively. Moreover, TCDF group is in all cases, one order of magnitude higher than TCDD group, and four orders of magnitude higher than the rest of the group of furans.

Figure 4.6 shows the congeners concentration, and as it can be seen, both 2,3,7,8-PCDDs and 2,3,7,8-PCDFs profiles increase until a maximum at 90 minutes, ending in nearly zero pg L^{-1} , i.e. they have a similar trend to the homologues (Figure 4.5). A different way of these, the most predominant congeners are OCDD and OCDF, reaching

their highest points at 90 minutes with concentrations low, around 5 pg L⁻¹. In consequence, the TEQ is minimum during all kinetic analysis.

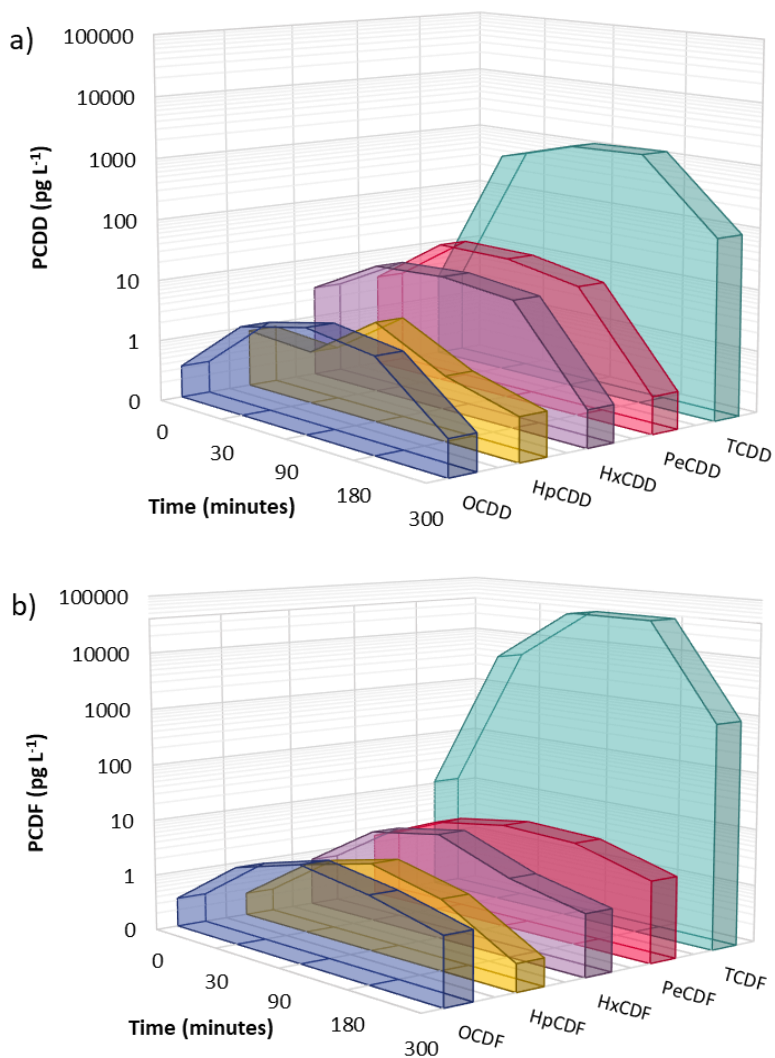


Figure 4.5. Kinetics of a) PCDDs and b) PCDFs homologue profiles generated during photocatalysis of TCS.

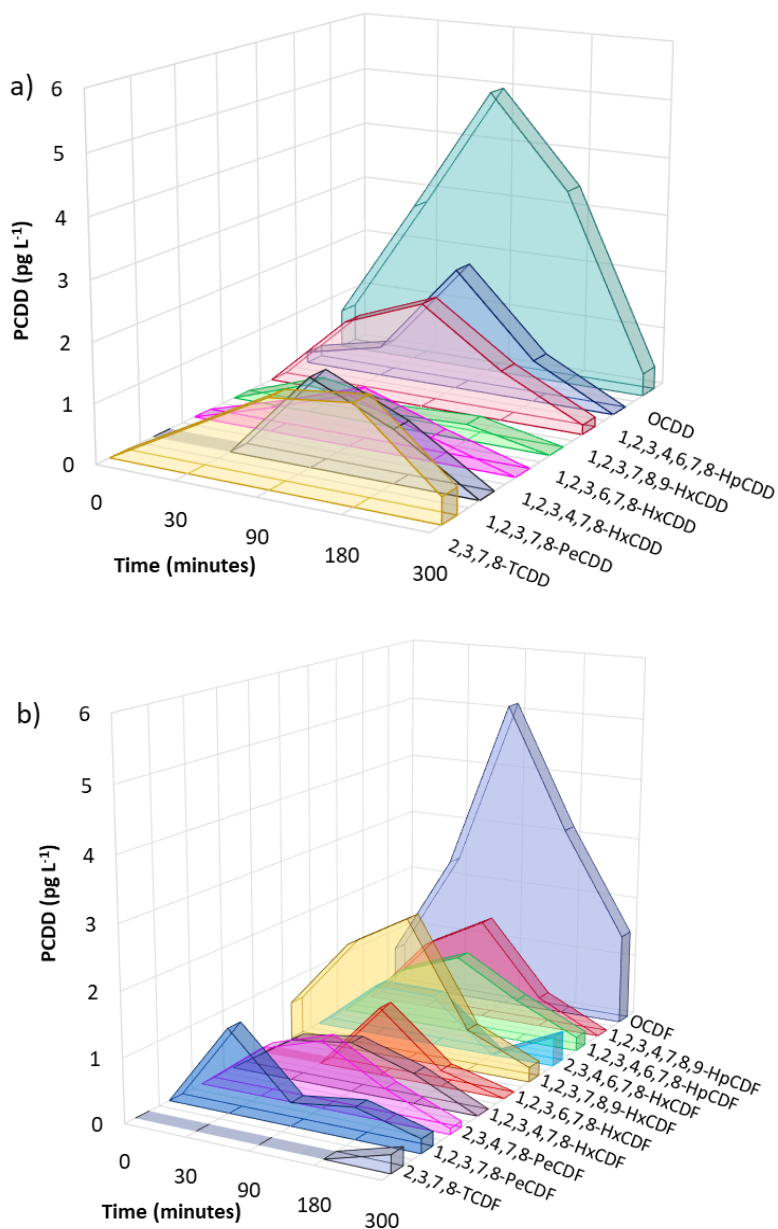


Figure 4.6. Kinetics of a) 2,3,7,8-PCDD and b) 2,3,7,8-PCDF congeners profile generated during photocatalysis of TCS.

Together with the analysis of the congeners, the toxicity in terms of TEQ has been calculated as it was described in Chapter 1, section 1.1.2. Figure 4.7 detail the toxicity in all sampling points. As it can be expected, the toxicity reaches a maximum at 90 minutes (3.6 pg L^{-1} of TEQ) and it is in continuous decrease until it reaches a minimum of 0.61 pg L^{-1} at 300 minutes. The toxicity is mainly attributed to the 2,3,7,8-TCDD congener

(depicted in light-blue colour), which reached an amount of 1.48 pg L^{-1} at 90 min (highest toxicity point of all), in spite of its low concentration, as is the congener that possesses the highest I-TEF value (I-TEF=1).

It is important to conclude that the greatest homologue groups are the TCDF and TCDD, however, the congeners 2,3,7,8-TCDD and 2,3,7,8-TCDF are present in very low concentrations, reaching a maximum of 1.64 pg L^{-1} at 180 min, and 0.28 pg L^{-1} at 300 min, but are the ones which contribute in a highest way to the toxicity, specifically, 2,3,7,8-TCDD. Hence the importance of establishing a new expression of TEQ, which is capable of reflecting this type of situation, this is, to reflect and indicate what congeners are needed to analyse, depending on the characteristics and applied treatments of the samples.

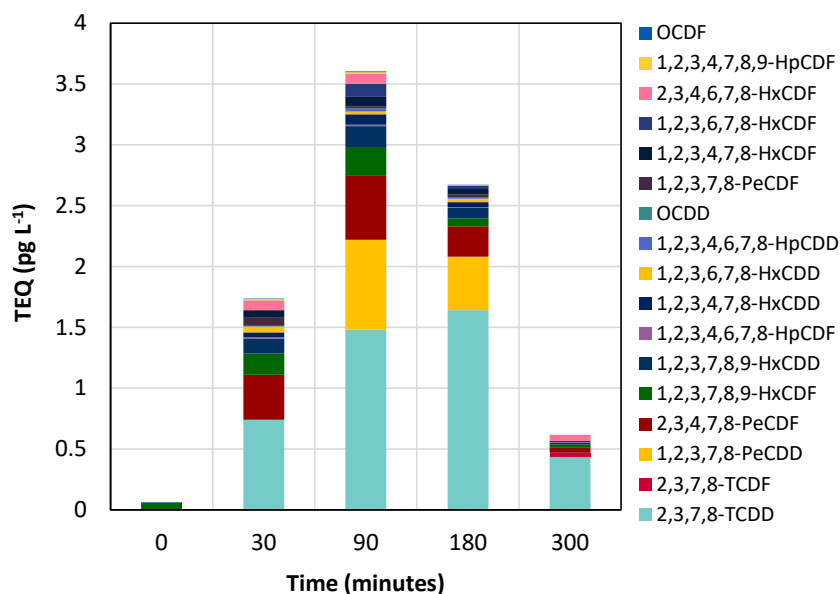


Figure 4.7. TEQ evolution during the TCS photocatalytic experiments.

4.2.2. Statistical analysis to obtain the alternative TEQ models

In this section, to obtain through statistical analysis an approach of the TEQ expression (Eq. 1.1., Chapter 1), in order to quantify the toxicity that provides the dioxins and furans generated during the oxidation processes has been proposed. The selected statistical approach consists of establishing correlations between congeners, with the aim to determine the most significant to calculate TEQ. Among the reported works, the Principal Component Analysis (PCA) is commonly employed to reduce the dimensionality

of a data set. Zhan et al. (2019) applied PCA to gas samples of 16 regenerative thermal oxidizers (RTOs) from 8 pharmaceutical industries to find the distribution of the congeners and analyse the similarities and differences, with the aim of grouping these congeners to find some pattern, and examine the possible influence of external factors, such as the chlorine concentration. After this analysis, they performed linear regression to study the correlations between TEQ and the congeners, whose results revealed that 3 congeners strongly correlated with TEQ. (Palmer et al., 2019, 2018), analysed 133 samples from municipal waste solid incinerators (MWSI) and by applying various correlations procedures, the number of congeners to determine the influence in TEQ was reduced.

All the calculations have been performed employing the statistical software, Statgraphics Centurion XVI (Statgraphics Technologies, Inc.).

Methodology applied to address the statistical analysis

The assessment started with a multivariable analysis, which is a statistical tool to define the relative contribution of different causes to a single event/outcome. The chosen data were the kinetic values of the 2,3,7,8-PCDD/Fs congener (Figure 4.6), together with the correspondent TEQ values, calculated with the Eq. (1) of Chapter 1. These data were gathered in the named \mathbb{U} matrix, composed of 17 columns (corresponding to the 17 congeners) and 5 rows (the five TEQ values which correspond to the TEQ of each sampling time) (see Table VII.1, Annex VII). Then, the following methodology was applied based on three steps:

- First, the Pearson correlation coefficient (r) was calculated and analysed to study the linear relationship between the variables. This is the most common coefficient for linear correlations. It is calculated as indicated in Eq. (4.1),

$$r = \frac{\text{covariance}}{S_x \cdot S_y} \quad (4.1)$$

being S_x and S_y the standard deviation. The covariance can be calculated as indicated in Eq. (4.2):

$$\text{Covariance} = \frac{\sum(\bar{X}-X) \cdot (\bar{Y}-Y)}{n-1} \quad (4.2)$$

- Secondly, the p -value (or probability value) was calculated to define if the correlation between the variables is significant. It describes how possible is that the analysed data would have occurred under the null hypothesis (H_0) of the statistical assessment. The null hypothesis is an affirmation over a parameter that states that there is no

relationship between the variables being studied and they should not be rejected unless the data show that is false. To calculate p -value, first is needed to find the Z-score (Eq. 4.3), which is a parameter that indicates how much a given value differs from the standard deviation, with the obtained value, the p -value is localised in statistical tables.

$$Z = \frac{X-M}{\sigma/\sqrt{n}} \quad (4.3)$$

where X is the population mean, M is the sample mean, σ the population standard deviation and n is the number of sample instances.

- Finally, the Spearman coefficient (ρ or S_ρ) was examined; it is a non-parametric measure to determine the monotonic relationship (association or interdependency) between the variables; it is used to sum up the strength and direction of the relationship between two variables.

$$S_\rho = 1 - \frac{6D}{n(n^2-1)} \quad (4.4)$$

with D , the total sum of squared differences and n , the number of pairs of data.

The settled criteria to select the correct pairs of congeners were the following: the Pearson correlation coefficient needs to be higher than 0.95 and the p -value must be lower than 0.05 to discard the null hypothesis. 0.05 is the α value, which represents the confidence level. The null hypothesis (H_0) is that there is no existing correlation between the congeners. Finally, the Spearman coefficient must be close to 1. It should be noted that the calculation of these three parameters also was performed with Statgraphics Centurion XVI. Because all congeners are produced simultaneously (see Figure 4.6), it can be expected that their formation is interrelated. As a consequence, there should be a subset of j congeners, linearly dependent on each other, which could be capable of calculating the toxicity of a sample (Palmer et al., 2019, 2018; Schröder et al., 2021).

A scatterplot matrix (or dispersion matrix) is depicted in Figure 4.8, which assembles the different scatter plots (or dispersion plots) of the correlations of the 17 pairs of the 17 congeners (17x17). A dispersion plot is a type of plot which uses Cartesian coordinates to show values for, usually, two variables for a set of data. A scatter plot matrix is a matrix of bivariate dispersions for all pairs of variables, which can suggest various kinds of correlations between variables (Utts, 2005). The data are displayed as a collection of points, each having the value of one variable determining the position on the horizontal axis (x) and the value of the other variable determining the position on

the vertical axis (y), which correspond to the different congeners' concentrations. The blue dots represent the correlation value between congeners. The selected pairs, those who meet the established criteria, are marked in yellow (Figure 4.8). For greater understanding, this scatterplot matrix is kind of a visual representation of the \mathbb{P} matrix, described hereunder.

The three coefficients selected (r , p -value, S_p) were gathered in a correlation matrix, named as \mathbb{P} matrix (17 columns x 17 rows), detailed in Table VII.2, in Annex VII, and encompasses all correlation coefficients for all the feasible combinations of the 17 congeners of PCDD/Fs. From this big \mathbb{P} matrix, 21 pairs of congeners were carefully chosen in accordance with the established criteria ($r \geq 0.95$, p -value ≤ 0.05 and $S_p \approx 1$), which are shown in different colours in Table 4.3. Each cell comprises the previously mentioned parameters: the Pearson coefficient (1st row), the p -value (2nd row) and the Spearman correlation coefficient (3rd row).

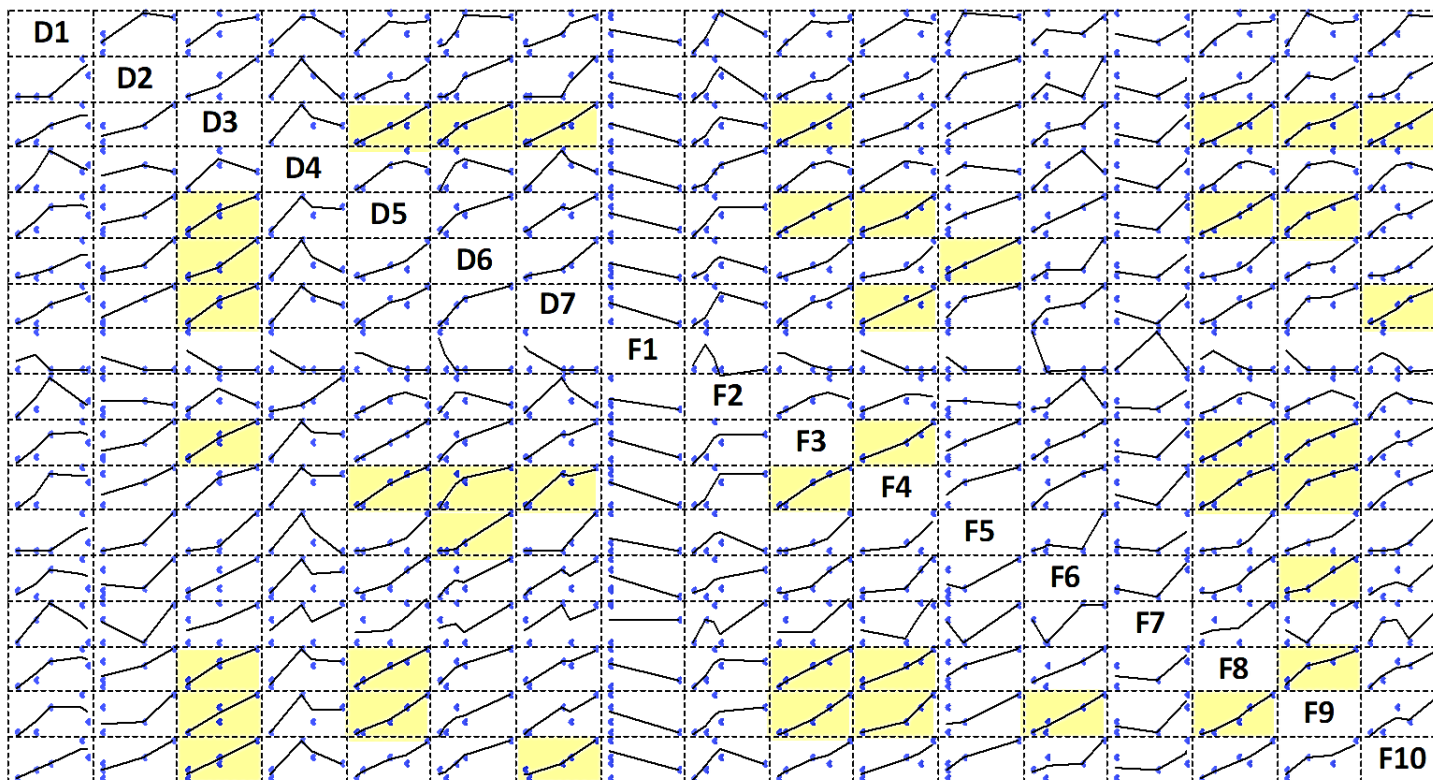


Figure 4.8. Scatterplot matrix for the concentration of the 17 congeners. The nomenclature of the 17 congeners is the following: D1, 2,3,7,8-TCDD; D2, 1,2,3,7,8-PeCDD; D3, 1,2,3,4,7,8-HxCDD; D4, 1,2,3,6,7,8-HxCDD; D5, 1,2,3,7,8,9-HxCDD; D6, 1,2,3,4,6,7,8-HpCDD; D7, OCDD; F1, 2,3,7,8-TCDF; F2, 1,2,3,7,8-PeCDF; F3, 2,3,4,7,8-PeCDF; F4, 1,2,3,4,7,8-HxCDF; F5, 1,2,3,6,7,8-HxCDF; F6, 1,2,3,7,8,9-HxCDF; F7, 2,3,4,6,7,8-HxCDF; F8, 1,2,3,4,6,7,8-HpCDF; F9, 1,2,3,4,7,8,9-HpCDF and F10, OCDF.

Table 4.3. 21 pairs of congeners proceeding from \mathbb{P} matrix that satisfy the selected criteria (r , p -value and S_p).

	1,2,3,4,7,8-HxCDD	1,2,3,7,8,9-HxCDD	1,2,3,4,6,7,8-HpCDD	OCDD	2,3,4,7,8-PeCDF	1,2,3,4,7,8-HxCDF	1,2,3,6,7,8-HxCDF	1,2,3,7,8,9-HxCDF	1,2,3,4,6,7,8-HpCDF	1,2,3,4,7,8,9-HpCDF	OCDF
1,2,3,4,7,8-HxCDD		0.970 0.006 0.949	0.954 0.012 0.949	0.982 0.003 0.949	0.970 0.006 0.949				0.969 0.007 0.949	0.952 0.012 0.973	0.970 0.006 0.949
1,2,3,7,8,9-HxCDD	0.970 0.006 0.949				1 0 1	0.983 0.003 0.975			0.995 0.001 1	0.985 0.002 0.975	
1,2,3,4,6,7,8-HpCDD	0.954 0.012 0.949						0.976 0.004 0.894				
OCDD	0.982 0.003 0.949					0.950 0.013 0.872					0.954 0.012 0.900
2,3,4,7,8-PeCDF	0.970 0.006 0.949	1 0 1				0.984 0.002 0.975			0.994 0.001 1	0.985 0.002 0.975	
1,2,3,4,7,8-HxCDF		0.983 0.003 0.975		0.950 0.013 0.872	0.984 0.002 0.975				0.9758 0.0045 0.9747	0.9540 0.0117 1	
1,2,3,6,7,8-HxCDF			0.976 0.004 0.894								
1,2,3,7,8,9-HxCDF										0.975 0.005 0.975	
1,2,3,4,6,7,8-HpCDF	0.969 0.007 0.949	0.995 0.001 1			0.994 0.001 1	0.976 0.005 0.975				0.965 0.008 0.975	
1,2,3,4,7,8,9-HpCDF	0.952 0.012 0.973	0.985 0.002 0.975			0.985 0.002 0.975	0.954 0.012 1		0.975 0.005 0.975	0.965 0.008 0.975		
OCDF	0.970 0.006 0.949			0.954 0.012 0.900							

*1st row, Pearson coefficient ($r \geq 0.95$), 2nd row, the p -value (p -value ≤ 0.05) and 3rd row, the Spearman correlation coefficient ($S_p \approx 1$).

Next, after the multicollinearity was decreased, multiple linear regression was applied to know how strong the relationship is between two or more independent variables and one dependent variable, with the objective of selecting the best-fitting model (with a line) to the data. For this, the applied methodology to the linear regression was the Ordinary Least Squares (OLS), which is commonly used to determine the relationship between one or more independent quantitative variables, and a dependent variable, by minimising the sum of the squares of the differences between the observed dependent variable and the predicted dependent variable. Eq. 4.5 represents a new model, to calculate the toxicity equivalent (TEQ) in terms of pg L^{-1} of TEQ, and the main participating 2,3,7,8-PCDD/Fs (in terms of pg L^{-1} of PCDD/Fs), β_0 , β_1 and β_2 are the determined parameters and x_1 and x_2 represent the concentration in pg L^{-1} of the corresponding congeners.

$$\text{TEQ} = \beta_0 + \beta_1 \cdot x_1 + \beta_2 \cdot x_2 \quad (4.5)$$

Accordingly, to the detailed procedure, 21 multiple linear regressions were performed, which are shown in Table 4.4. Furthermore, the 3 calculated parameters (β_0 , β_1 and β_2) are given, the two congeners involved in the equation, and other statistical parameters like the statistical R^2 , the standard error and the p -value.

From these 21 linear regressions adjustments, just 5 of them achieve the established requirements to provide results with a p -value below 0.05 (necessary value to reject the null hypothesis, H_0 , when there is no correlation between the TEQ and the congeners). The selected 5 models correspond to the first 5 models of Table 4.4, which are the numbers of the linear regressions 14, 6, 13, 7, 3, (of the total 21) newly named as A, B, C, D and E. These models are depicted separately in Table 4.5, where the three β parameters and x_1 and x_2 , which are the respective congeners needed to calculate the TEQ, as well as the main statistical parameters as R^2 , the standard error and p -value, are shown.

Table 4.4. 21 linear correlations proceeding of the multiple lineal regressions, and their correspondent statistical parameters.

No.	β_0	β_1	β_2	x_1	x_2	R^2	St. Error	p -value
14	-0.267	0.357	0.444	OCDD	OCDF	0.978	0.305	0.022
6	0.460	6.644	-1.457	1,2,3,4,7,8-HxCDD	1,2,3,4,7,8,9-HpCDF	0.961	0.408	0.040
13	-0.115	0.910	-0.996	OCDD	1,2,3,4,7,8-HxCDF	0.959	0.417	0.041
7	-0.281	0.479	0.731	1,2,3,4,7,8-HxCDD	OCDF	0.958	0.420	0.042
3	-0.099	-0.362	0.800	1,2,3,4,7,8-HxCDD	OCDD	0.953	0.445	0.047
21	-0.234	5.225	-1.775	1,2,3,4,6,7,8-HpCDF	1,2,3,4,7,8,9-HpCDF	0.927	0.554	0.073
20	1.810	-3.496	5.913	1,2,3,7,8,9-HxCDF	1,2,3,4,7,8,9-HpCDF	0.925	0.562	0.075
2	0.428	5.003	-0.502	1,2,3,4,7,8-HxCDD	1,2,3,4,6,7,8-HpCDD	0.921	0.578	0.079
11	-0.129	5.176	-3.663	1,2,3,7,8,9-HxCDD	1,2,3,4,7,8,9-HpCDF	0.920	0.580	0.080
17	-0.114	8.768	-3.640	2,3,4,7,8-PeCDF	1,2,3,4,7,8,9-HpCDF	0.920	0.580	0.080
1	0.522	5.029	-0.560	1,2,3,4,7,8-HxCDD	1,2,3,7,8,9-HxCDD	0.918	0.586	0.082
4	0.521	5.029	-0.952	1,2,3,4,7,8-HxCDD	2,3,4,7,8-PeCDF	0.918	0.586	0.082
10	-0.225	-3.720	8.388	1,2,3,7,8,9-HxCDD	1,2,3,4,6,7,8-HpCDF	0.916	0.594	0.084
5	0.374	3.251	0.477	1,2,3,4,7,8-HxCDD	1,2,3,4,6,7,8-HpCDF	0.915	0.598	0.085
16	-0.217	6.016	8.111	2,3,4,7,8-PeCDF	1,2,3,4,6,7,8-HpCDF	0.914	0.603	0.086
18	0.059	-0.825	3.344	1,2,3,4,7,8-HxCDF	1,2,3,4,6,7,8-HpCDF	0.878	0.718	0.123
9	0.315	1.230	1.133	1,2,3,7,8,9-HxCDD	1,2,3,4,7,8-HxCDF	0.829	0.847	0.171
15	0.317	2.130	1.084	2,3,4,7,8-PeCDF	1,2,3,4,7,8-HxCDF	0.829	0.848	0.171
8	0.349	-16.266	30.664	1,2,3,7,8,9-HxCDD	2,3,4,7,8-PeCDF	0.828	0.850	0.172
19	0.337	4.449	-0.414	1,2,3,4,7,8-HxCDF	1,2,3,4,7,8,9-HpCDF	0.820	0.871	0.180
12	0.395	2.757	-2.192	1,2,3,4,6,7,8-HpCDD	1,2,3,6,7,8-HxCDF	0.808	0.900	0.192

Table 4.5. Five selected models with their calculated parameters and statistical data which fulfils the required parameter (p -value<0.05).

Model	Variable	β_0	β_1	β_2	x_1	x_2
A	Value R ² =0.978 Std. Error=0.305 p -value=0.022	-0.267	0.357	0.444	OCDD	OCDF
B	Value R ² =0.960 Std. Error=0.408 p -value=0.039	0.460	6.644	-1.457	1,2,3,4,7,8-HxCDD	1,2,3,4,7,8,9-HpCDF
C	Value R ² =0.958 Std. Error=0.417 p -value=0.041	-0.115	0.909	-0.996	OCDD	1,2,3,4,7,8-HxCDF
D	Value R ² =0.958 Std. Error=0.419 p -value=0.042	-0.281	0.479	0.731	1,2,3,4,7,8-HxCDD	OCDF
E	Value R ² =0.953 Std. Error=0.446 p -value=0.047	-0.099	-0.362	0.800	1,2,3,4,7,8-HxCDD	OCDD

From this way, gathering the parameters of Table 4.5 in the five equations, the following models are proposed (Eqs. 4.6-4.10):

$$\text{Model A: TEQ} = -0.267 + 0.357 \cdot \text{OCDD} + 0.444 \cdot \text{OCDF} \quad (R^2=0.98) \quad (4.6)$$

$$\text{Model B: TEQ} = 0.460 + 6.644 \cdot 1,2,3,4,7,8\text{HxCDD} - 1.457 \cdot 1,2,3,4,7,8,9\text{HpCDF} \quad (R^2=0.96) \quad (4.7)$$

$$\text{Model C: TEQ} = -0.115 + 0.910 \cdot \text{OCDD} - 0.996 \cdot 1,2,3,4,7,8\text{HxCDF} \quad (R^2=0.96) \quad (4.8)$$

$$\text{Model D: TEQ} = -0.281 + 0.478 \cdot 1,2,3,4,7,8\text{HxCDD} + 0.731 \cdot \text{OCDF} \quad (R^2=0.96) \quad (4.9)$$

$$\text{Model E: TEQ} = -0.099 - 0.362 \cdot 1,2,3,4,7,8\text{HxCDD} + 0.800 \cdot \text{OCDD} \quad (R^2=0.95) \quad (4.10)$$

Each model is composed of two different congeners, instead of the 17 ones needed usually for the toxicity calculation in terms of TEQ. Additionally, it is needed to set up a criterion that quantifies the accuracy of these correlations. With this aim, a parity graph is presented in Figure 4.9, where the “y” axis is the TEQ values, calculated

in accordance with Eq. 1.1 (Chapter 1) and the “x” axis, is the toxicity determined via the previously adjusted models ($[\text{pg TEQ L}^{-1}]_{\text{model}}$), models A to E.

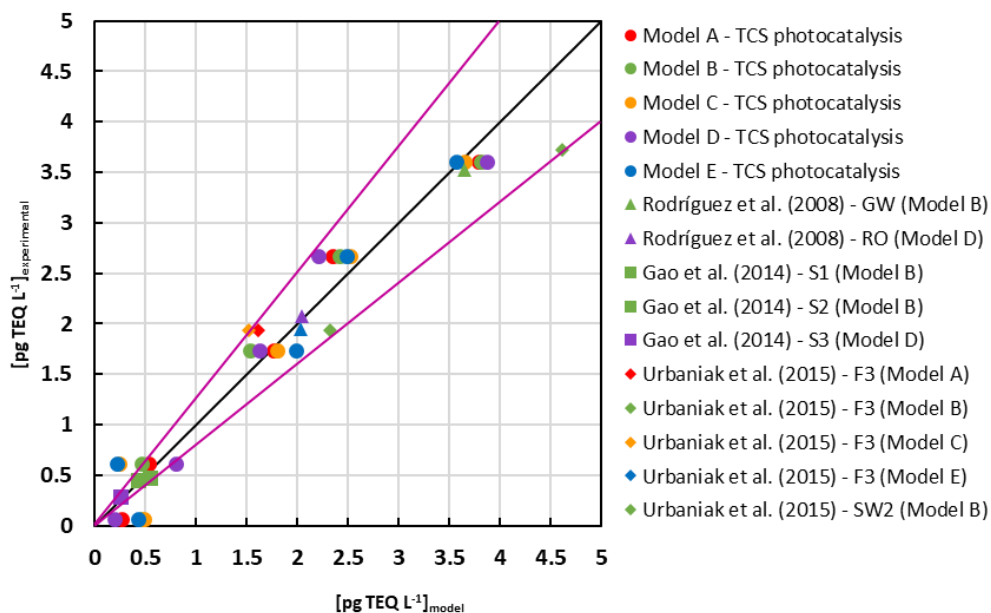


Figure 4.9. Experimental TEQ values vs. calculated TEQ values from the developed models.

These models were corroborated through a parity graph, presented in Figure 4.9, where the “y” axis is the TEQ values, calculated in accordance with Eq. 1.1 (Chapter 1) and the “x” axis, is the toxicity determined via the previously adjusted models ($[\text{pg TEQ L}^{-1}]_{\text{model}}$), models A to E. In Figure 4.9, in addition to the TEQ values obtained in this section, and in order to check the validation of the proposed models, data corresponding to PCDD/Fs data obtained from the literature were added. Among them, the congeners profile in aqueous samples was studied over different locations in Perth (Australia), where two characteristic points were evaluated (Rodríguez et al., 2008). The first point was the average concentration of several 2,3,7,8-PCDD/Fs congener profiles analysed in groundwaters samples (GW), and the second point was the average concentration of various 2,3,7,8-PCDD/Fs congeners of a set of samples after WWTPs reverse osmosis tertiary treatment. As it is depicted in Figure 4.9, it was corroborated that these profiles fitted reasonably well to the here obtained models B and D (in triangles, Figure 4.9). Three aqueous samples (S1, S2 and S3), from the work of (Gao et al., 2014) obtained from the region of Dongting Lake (China), were chosen. Between the 60s and the 90s, these areas were polluted with sodium pentachlorophenate (Na-PCP), which is a well-known PCDD/Fs precursor. Models B and D fitted adequately with the congener profile

of the three chosen samples (square shapes, Figure 4.9). Lastly, it was determined the congener profile in micropollutants-containing water samples along the Pilica River (Poland) at different seasons of the year (Urbaniak et al., 2015). These micropollutants proceed from diverse sources that discharge in the river. Toxicity in terms of TEQ has been effectively determined for two specific samples (F3 and SW2), using four of the proposed models A, B, C and E, (diamond shapes, Figure 4.9).

All studied cases confirmed that the proposed models in this section, A, B, C, D and E, can describe the behaviour and trends observed, not only in photocatalytic degradation of TCS-containing aqueous samples but also in samples of different studies as those presented here (Schröder et al., 2021). These models facilitate the toxicity estimation in terms of TEQ, just by the analysis of a reduced number of congeners: OCDD, OCDF, 1,2,3,4,7,8-HxCDD, 1,2,3,4,7,8-HxCDF and 1,2,3,4,7,8,9-HpCDF. Each equation just implies two congeners, but the analysis of the five congeners mentioned in this thesis is highly recommended for a first approach.

Finally, it is needed to highlight that, when calculating the TEQ with the common equation (Eq. 1.1), which uses the 17 congeners, those who contribute more to the total toxicity are the most toxic ones, like TCDD (I-TEF=1), 1,2,3,7,8-PCDD (I-TEF = 0.5) and 2,3,4,7,8-PCDF (I-TEF = 0.5). But, with the 5 new proposed models (Eqs. 4.6-4.10), the employed congeners are those which are present at high concentrations, like OCDD and OCDF. In the end, the total toxicity (TEQ) is similar when employing these two methodologies, although, models A-E stand out for the fact that they entail less analytical effort. This should be considered in the near future, facing the development and application of new and greener technologies, like the advanced oxidation processes (AOPs). It is needed to take into account that the proposed models involved the PCDD/Fs generated from TCS photocatalysis, thus, they are highly dependent on the kind of matrix and of the oxidation technology applied. But, even so, it has been proven that they fit well with PCDD/Fs congeners profile from the bibliography for determined conditions. In general terms, it can be established global models for each technology or compound, towards a possible standardised use (Schröder et al., 2021).

4.3. References

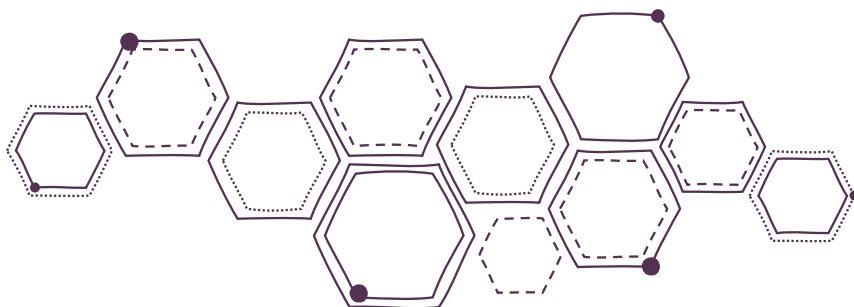
- Cappelli, F., Longoni, O., Rigato, J., Rusconi, M., Sala, A., Fochi, I., Palumbo, M.T., Polesello, S., Roscioli, C., Salerno, F., Stefani, F., Bettinetti, R., Valsecchi, S., 2022. Suspect screening of wastewaters to trace anti-COVID-19 drugs: Potential adverse effects on aquatic environment. *Sci. Total Environ.* 824, 153756. <https://doi.org/10.1016/j.scitotenv.2022.153756>
- Díaz-Camal, N., Cardoso-Vera, J.D., Islas-Flores, H., Gómez-Oliván, L.M., Mejía-García, A., 2022. Consumption and occurrence of antidepressants (SSRIs) in pre- and post-COVID-19 pandemic, their environmental impact and innovative removal methods: A review. *Sci. Total Environ.* 829. <https://doi.org/10.1016/j.scitotenv.2022.154656>
- Fernández-Castro, P., 2017. Progress in the reactivity of Advanced Oxidation media. Application to the Fenton treatment of 2-chlorophenol solutions. University of Cantabria.
- Fernández-Castro, P., San Román, M.F., Ortiz, I., 2016. Theoretical and experimental formation of low chlorinated dibenzo-p-dioxins and dibenzofurans in the Fenton oxidation of chlorophenol solutions. *Chemosphere* 161, 136–144. <https://doi.org/10.1016/j.chemosphere.2016.07.011>
- Gao, L., Zhang, Q., Zhang, B., Liu, W., Xiao, K., 2014. Polychlorinated dibenzo-p-dioxins and dibenzofurans in water and six fish species from Dongting Lake, China. *Chemosphere* 114, 150–157. <https://doi.org/10.1016/j.chemosphere.2014.04.015>
- Khan, H.K., Rehman, M.Y.A., Junaid, M., Lv, M., Yue, L., Haq, I. ul, Xu, N., Malik, R.N., 2022. Occurrence, source apportionment and potential risks of selected PPCPs in groundwater used as a source of drinking water from key urban-rural settings of Pakistan. *Sci. Total Environ.* 807, 151010. <https://doi.org/10.1016/j.scitotenv.2021.151010>
- Lan, Y., Coetsier, C., Causserand, C., Groenen Serrano, K., 2017. On the role of salts for the treatment of wastewaters containing pharmaceuticals by electrochemical oxidation using a boron doped diamond anode. *Electrochim. Acta* 231, 309–318. <https://doi.org/10.1016/j.electacta.2017.01.160>
- Morales-Paredes, C.A., Rodríguez-Díaz, J.M., Boluda-Botella, N., 2022. Pharmaceutical compounds used in the COVID-19 pandemic: A review of their presence in water and treatment techniques for their elimination. *Sci. Total Environ.* 814. <https://doi.org/10.1016/j.scitotenv.2021.152691>
- Palmer, D., Pou, J.O., Gonzalez-Sabaté, L., Díaz-Ferrero, J., 2018. Multiple linear regression based congener profile correlation to estimate the toxicity (TEQ) and dioxin concentration in atmospheric emissions. *Sci. Total Environ.* 622–623, 510–516. <https://doi.org/10.1016/j.scitotenv.2017.11.344>

- Palmer, D., Pou, J.O., Gonzalez-Sabaté, L., Díaz-Ferrero, J., Conesa, J.A., Ortuño, N., 2019. New models used to determine the dioxins total amount and toxicity (TEQ) in atmospheric emissions from thermal processes. *Energies* 12. <https://doi.org/10.3390/en12234434>
- Rodriguez, C., Cook, A., Devine, B., Van Buynder, P., Lugg, R., Linge, K., Weinstein, P., 2008. Dioxins, furans and PCBs in recycled water for indirect potable reuse. *Int. J. Environ. Res. Public Health* 5, 356–367. <https://doi.org/10.3390/ijerph5050356>
- Saha, P., Wang, J., Zhou, Y., Carlucci, L., Jeremiase, A.W., Rijnaarts, H.H.M., Bruning, H., 2022. Effect of electrolyte composition on electrochemical oxidation: Active sulfate formation, benzotriazole degradation, and chlorinated by-products distribution. *Environ. Res.* 211. <https://doi.org/10.1016/j.envres.2022.113057>
- Schröder, S., San-Román, M.F., Ortiz, I., 2021. Dioxins and furans toxicity during the photocatalytic remediation of emerging pollutants. Triclosan as case study. *Sci. Total Environ.* 770, 144853. <https://doi.org/10.1016/j.scitotenv.2020.144853>
- Schröder, S., San-Román, M.F., Ortiz, I., 2020. Photocatalytic transformation of triclosan. Reaction products and kinetics. *Catalysts* 10, 1–15. <https://doi.org/10.3390/catal10121468>
- Sengar, A., Vijayanandan, A., 2022. Human health and ecological risk assessment of 98 pharmaceuticals and personal care products (PPCPs) detected in Indian surface and wastewaters. *Sci. Total Environ.* 807, 150677. <https://doi.org/10.1016/j.scitotenv.2021.150677>
- Sidhu, S., Edwards, P., 2002. Role of phenoxy radicals in PCDD/F formation. *Int. J. Chem. Kinet.* 34, 531–541. <https://doi.org/10.1002/kin.10083>
- Solá-Gutiérrez, C., 2019. Traceability of PCDD/Fs formation in the advanced oxidation of TCS. University of Cantabria.
- Solá-Gutiérrez, C., San Román, M.F., Ortiz, I., 2018. Fate and hazard of the electrochemical oxidation of triclosan. Evaluation of polychlorodibenzo-*p*-dioxins and polychlorodibenzofurans (PCDD/Fs) formation. *Sci. Total Environ.* 626, 126–133. <https://doi.org/10.1016/j.scitotenv.2018.01.082>
- Solá-Gutiérrez, C., Schröder, S., San Román, M.F., Ortiz, I., 2019. PCDD/Fs traceability during triclosan electrochemical oxidation. *J. Hazard. Mater.* <https://doi.org/10.1016/j.jhazmat.2019.02.066>
- Urbaniak, M., Kiedrzyńska, E., Kiedrzyński, M., Zieliński, M., Grochowalski, A., 2015. The Role of Hydrology in the Polychlorinated Dibenzo-*p*-dioxin and Dibenzofuran Distributions in a Lowland River. *J. Environ. Qual.* 44, 1171–1182. <https://doi.org/10.2134/jeq2014.10.0418>
- US EPA, 2013. National Primary Drinking Water Regulations. *Drink. Water Contam.* 141–142.

- US EPA, 1994. Method 1613B Tetra- through Octa-Chlorinated Dioxins and Furans by Isotope Dilution HRGC/HRMS. Environ. Prot.
- Utts, J.M., 2005. Seeing Through Statistics, 3rd ed. Thomson Brooks/Cole.
- Vallejo, M., 2014. Assessment of polychlorinated dibenzo-p-dioxins and dibenzofurans, PCDD/Fs, in the application of advanced oxidation processes. University of Cantabria.
- Vallejo, M., Fernández-Castro, P., San Román, M.F., Ortiz, I., 2015a. Assessment of PCDD/Fs formation in the Fenton oxidation of 2-chlorophenol: influence of the iron dose applied. Chemosphere 137, 135–141. <https://doi.org/10.1016/j.chemosphere.2015.06.056>
- Vallejo, M., San Román, M.F., Ortiz, I., 2013. Quantitative assessment of the formation of polychlorinated derivatives, PCDD/Fs, in the electrochemical oxidation of 2-chlorophenol as function of the electrolyte type. Environ. Sci. Technol. 47, 12400–12408. <https://doi.org/10.1021/es403246g>
- Vallejo, M., San Román, M.F., Ortiz, I., Irabien, A., 2015b. Overview of the PCDD/Fs degradation potential and formation risk in the application of advanced oxidation processes (AOPs) to wastewater treatment. Chemosphere 118, 44–56. <https://doi.org/10.1016/j.chemosphere.2014.05.077>
- Vallejo, M., San Román, M.F., Ortiz, I., Irabien, A., 2014. The critical role of the operating conditions on the fenton oxidation of 2-chlorophenol: Assessment of PCDD/Fs formation. J. Hazard. Mater. 279, 579–585. <https://doi.org/10.1016/j.jhazmat.2014.07.020>
- Weber, R., 2007. Relevance of PCDD/PCDF formation for the evaluation of POPs destruction technologies - Review on current status and assessment gaps. Chemosphere 67, 109–117. <https://doi.org/10.1016/j.chemosphere.2006.05.094>
- Weber, R., Gaus, C., Tysklind, M., Johnston, P., Forter, M., Hollert, H., Heinisch, E., Holoubek, I., Lloyd-Smith, M., Masunaga, S., Moccarelli, P., Santillo, D., Seike, N., Symons, R., Torres, J.P.M., Verta, M., Varbelow, G., Vijgen, J., Watson, A., Costner, P., Woelz, J., Wycisk, P., Zennegg, M., 2008. Dioxin- and POP-contaminated sites - Contemporary and future relevance and challenges: Overview on background, aims and scope of the series. Environ. Sci. Pollut. Res. 15, 363–393. <https://doi.org/10.1007/s11356-008-0024-1>
- Wojnárovits, L., Takács, E., 2021. Rate constants of dichloride radical anion reactions with molecules of environmental interest in aqueous solution: a review. Environ. Sci. Pollut. Res. 28, 41552–41575. <https://doi.org/10.1007/s11356-021-14453-w>
- Zhan, M., Ma, Y., Lin, X., Chen, Z., Chen, T., Li, X., Yan, J., 2019. PCDD/F emission from pharmaceutical industries. Aerosol Air Qual. Res. 19, 2070–2082. <https://doi.org/10.4209/aaqr.2019.06.0284>

5

COMPUTATIONAL
CHEMISTRY IN THE
THEORETICAL
PCDD/Fs FORMATION
MECHANISMS



Abstract

In the last chapter of this PhD thesis, it is described in a theoretical manner the possible PCDD/Fs formation pathways from the breakage of the drugs amoxicillin (AMX), paracetamol (PAR) and sertraline (STR), and of the by-products generated, after applying electrochemical oxidation (EOX). This is a preliminary study, for which the molecules just mentioned were selected, discarding dexamethasone due to the complexity of the molecule, both for its robustness and for the various torsion angles it has, which would greatly increase the computational effort and simulation times in the framework of this thesis. On the other hand, the scarce availability of information about its degradation in the literature, is translated into a limited knowledge about the formation of the intermediates. Therefore, it will be considered for future studies, when exist more clarity and better understanding of the breakdown pathways of this molecule.

So, the study of the PCDD/Fs formation from drugs has been carried out using computational chemistry and specifically, density functional theory (DFT) has been applied. To this, a combined mechanism consisting of two steps has been proposed. The 1st step is the breakage of the drugs, and the 2nd step is the intermediate and final molecules formation. Finally, the energy profiles of the reaction mechanisms have been calculated. The computational work was mainly conducted during a three-month research stay at the Department of Chemistry and Biochemistry at Faculdade de Ciências, in the University of Porto (Portugal), under the supervision of Dr. Pedro A. Fernandes and Dr. Pedro Ferreira. This predoctoral short stay was carried out within the framework of the FPI research fellowship (PRE2018-083526).

5.1. Computational chemistry background

As it is described in Chapter 3, chlorophenols play a critical role in the formation of PCDD/Fs in highly reactive media, acting as reaction intermediates. Chlorophenols are commonly employed in the chemical industry, such as in the fabrication of herbicides or wood preservatives, or even used as intermediate compounds in the synthesis of pharmaceuticals and dyes (Olaniran and Igbinosa, 2011). They are released into the environment from diverse sources, mainly from the manufacture of the mentioned products. When analysing its presence in the environment, high concentrations have been detected, both in natural waters and wastewaters as well as in sediments and soils (Fernández-Castro et al., 2016; Vallejo et al., 2015, 2014, 2013).

During the last decade, interesting works reported information on the formation pathways from 2-chlorophenol to PCDD/Fs in aqueous medium, highlighting the role of 2-chlorophenoxy radical as the main intermediate compound (Briois et al., 2007; Fernández-Castro, 2017; Fernández-Castro et al., 2016; Vallejo, 2014; Vallejo et al., 2015, 2014, 2013). In the literature, it has been postulated that chlorophenols can follow electrophilic substitution reactions or ring opening and chain closure reactions throughout the oxidation process (Evans and Dellinger, 2005; Fernández-Castro et al., 2016; Ryu, 2008; Sidhu and Edwards, 2002; Sidhu et al., 1995; Vallejo et al., 2014; Xu et al., 2010; Zhang et al., 2010, 1990, 2014). Meanwhile, dioxins and furans can be formed through molecule-molecule reactions, molecule-radical and radical-radical combinations (Briois et al., 2007; Evans and Dellinger, 2005; Fernández-Castro et al., 2016; Li et al., 2021; Pan et al., 2013; Sidhu and Edwards, 2002; Yang et al., 2017). Nevertheless, most studies were commonly focused on gas phase reactions (Briois et al., 2007; Evans and Dellinger, 2005; Fernández-Castro et al., 2016; Hong et al., 2000; Li et al., 2021; Okamoto, 1999; Pan et al., 2013; Ryu, 2008; Sidhu and Edwards, 2002; Sidhu et al., 1995; Wiater-Protas and Louw, 2001; Xu et al., 2010; Zhang et al., 2010, 1990, 2014). In this way, as far as the author's knowledge, literature has not fully described either the degradation of drugs DEX, AMX, PAR, STR, or the PCDD/Fs formation pathways employing computational tools. Some studies apply quantum chemistry in the framework of DFT to study how paracetamol is decomposed without proposing the formation of PCDD/Fs. Recent works (Chen et al., 2021; Qutob et al., 2022) proposed a theoretical degradation pathway based on the results obtained from the analysis of the Fukui values and the highest occupied molecular orbital (HOMO) of the molecule. In this case, DFT allowed the calculation of the optimized geometry and the vibrational frequency of the different molecules involved in the reactions as well as the transition states which take part in the

chemical reactions, together with other energy parameters (like activation and reaction energies) (Pan et al., 2013).

Due to the lack of studies and information on the participating mechanisms in the formation of dioxins and furans from the organochlorinated precursors, generated during the degradation of drugs in aqueous matrices, in this Chapter, a combined mechanism that ends up in the formation of these compounds will be proposed and investigated. This mechanism has been applied to the AMX, PAR and STR molecules, given their similarities in the molecular structures, ruling out the molecule of DEX due to its complexity, which would lead, among other things, to expensive computational calculations, in terms of programming times concerned. Thus, its mechanism of degradation and subsequent formation of PCDD/Fs will be considered within a future work (Chapter 6). The mechanism starts from the three drugs, AMX, PAR and STR, and involved the common generated by-products during oxidation, to finally form the dioxins and furans. The selection of these by-products has been realised on base experimental detection, just as described in Chapter 3.

5.1.1. Computational methodology

As it has been detailed in Chapter 2, density functional theory (DFT) has been employed in order to obtain the reaction pathways, and the final energies that allow confirming the proposed pathways. Hereafter, the main steps to calculate the reaction pathways are detailed. Prior to model a chemical reaction, it is essential to find the appropriate initial state of the reaction compounds that correspond to the minimum energy of the system.

First, it has been stated what the reaction path is, or reaction pathway (RP), defined as the path that connects reactants and products through the transition state (TS). Along with this, the reaction coordinate (Figure 5.1a) is an abstract one-dimensional coordinate which represents progress along a reaction pathway (IUPAC, 2019). Moreover, the potential energy surface (PES) must be defined, a key concept in computational chemistry. The PES (depicted in Figure 5.1b) defines the potential energy of a system, principally of a compendium of atoms, in terms of specific parameters, usually the atoms' positions. This surface can describe the energy as a function of one or more coordinates (Bachrach, 2014; Cramer, 2004; Jensen, 2007; Lewars, 2016). The TS is commonly defined as a structure along the reaction coordinate (path from reactants to products, Figure 5.1a), which corresponds to the highest point of Gibbs Free energy (Figure 5.1a) and to the lowest state of the PES, known as saddle point (Figure 5.1b in

the RP from reactants to products, represented by a transversal plane). This saddle point lies at the centre of the saddle-shaped region, and it is a local minimum. A good comparison to explain the TS is like a mountain pass between two valleys. Figure 5.1b describes an example of a potential energy surface (PES), where there is an energy minimum A (reactants) and an energy minimum B (products) connected by the saddle point (transition state) (Bachrach, 2014; Lewars, 2016; Schlegel, 2003). Figure 5.1a represents a transversal section of the PES, specifically where the saddle point (TS) is located.

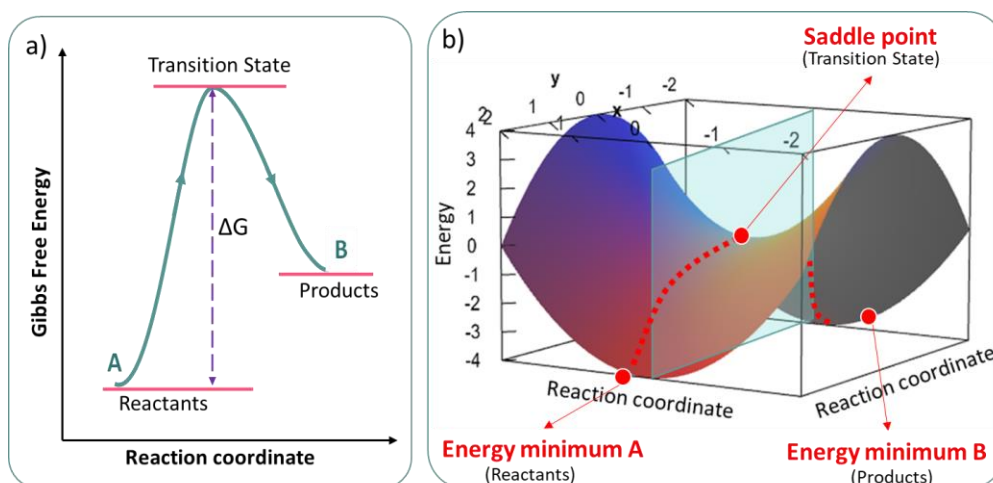


Figure 5.1. a) Schematic generic representation of pathway reaction: reactants, transition state and products b) Representation of a potential energy surface (PES): energy minimum and saddle point. Hyperbolic paraboloid partially modified from Nykamp, (2022).

Electron density

In quantum mechanics, under the probabilistic interpretation, particles cannot be considered as point-like, but they are spatially delocalised prior to determining their position. Because of the uncertainty principle, on an atomic scale, it is not possible to predict the exact location of an electron, just the probability of its being at a given position. Thus, electrons in atoms and molecules act as if they are scattered in space. By definition, electron density (ρ) is a description of the probability of finding an electron in a specific location around an atom or molecule (Cramer, 2004; Jensen, 2007; Lewars, 2016). Electron density function completely defines the charge distribution in a molecule. It is commonly denoted as $\rho(r)$. The molecular electrostatic potential (ESP) (also abbreviated as MEP) is defined as the energy of interaction of a positive point charge with a molecule. A combined plot of the electron density isosurface and ESP is a

useful visual method for defining the reactive locations of a molecule. Here, the electron density isosurface is a three-dimensional surface that illustrates the charge distributions in a molecule. Hence, the molecule electron density has a specific value, which includes a specified fraction of its electron probability density, $\rho(r)$ (Gupta, 2016). In this way, the molecular size can be approached by visualising the electron density, so and the electron density distribution can be seen around each atom of the molecule. In Figure 5.2 the ESP for a) AMX, b) PAR and c) STR are represented; and it can be appreciated the overall charge distribution. Red zones correspond to the higher electron density (lower values), and the blue colour corresponds to the region of lower electron density (higher values). The electrostatic potential grows in the following order: red < orange < yellow < green < blue. The colours have been selected with the aim to represent the attractive potential in red and the repulsive potential in blue. The more polar the molecule is, the bigger red/blue distinctions appear. Gaussian 16 with B3LYP/6-31G++ level of theory has been employed to perform the mapping of the three molecules.

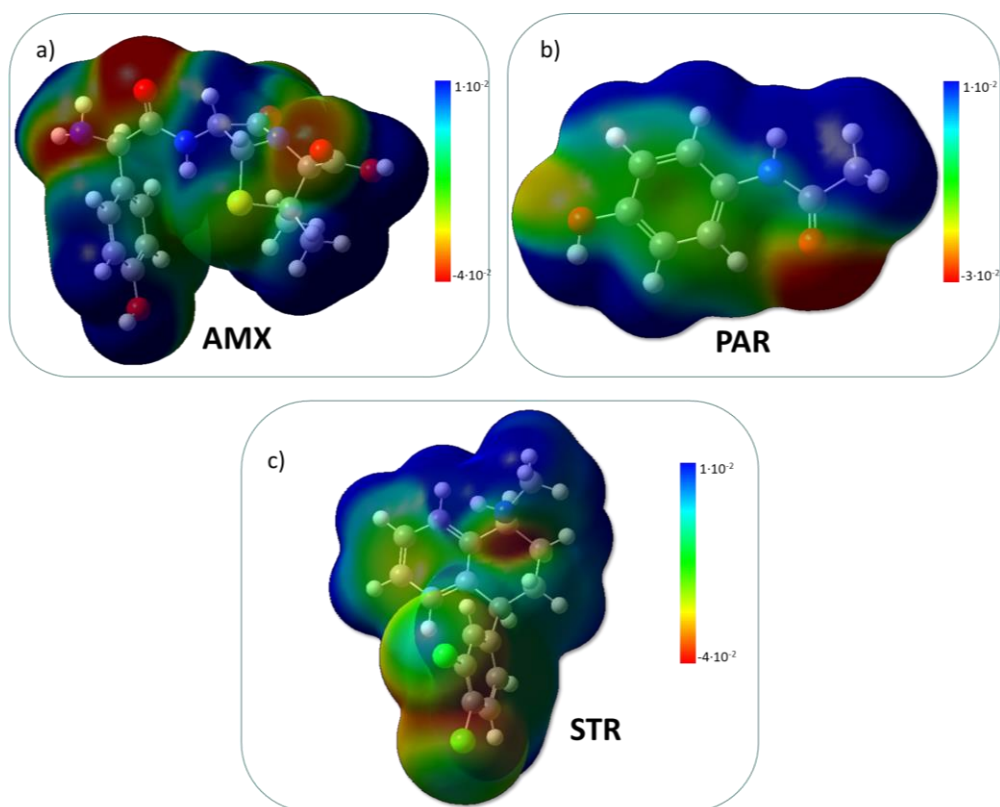


Figure 5.2. Molecular electrostatic potential mapped on the $\rho(r) = 0.0004$ au (isovalue) isodensity surface in the range from $-4 \cdot 10^{-2}$ to $1 \cdot 10^{-2}$, calculated at the B3LYP/6-31G++ level of theory. In detail: a) AMX, b) PAR and c) STR.

Computational calculation steps

Next, the methodology carried out in each stage of the reaction mechanism is described. To explain the different stages of the followed procedure, STR molecule has been selected as an example, in order to have a better understanding of the theory applied.

- **Geometry and energy optimisation.** Before starting any other calculations, it is necessary to optimise the initial geometry and energy of the starting molecule, this is, to find the geometry with the less energy. Here, the geometry will be changed and corrected in several steps, up until a stationary point (point where the derivative is equal to zero) is found on the potential surface (algorithm converges after several iterations). Furthermore, the vibrational frequencies of the system must be calculated as they confirm that the geometry has reached an energy minimum. In Figure 5.3 a schematic representation of the Gaussian algorithm employed to calculate the geometry optimisation and frequency calculation is depicted.

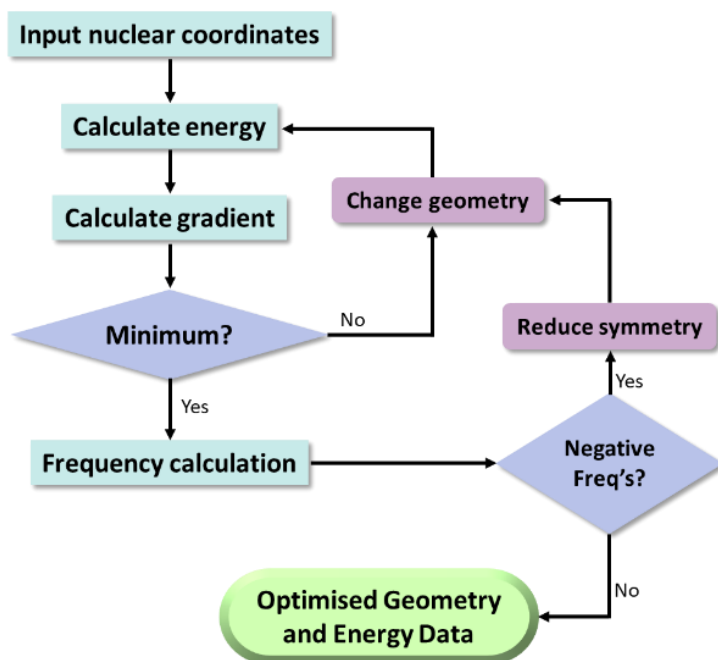


Figure 5.3. Optimisation + frequency calculation Gaussian algorithm (Williams, 2019).

As it has been explained in Chapter 2, section 2.5.1, depending on the calculation to be performed, the command line of the input program (see Figure 2.17), changes depending on the calculation to be launched. As a recall, this input program contains the atomic coordinates, the number of processors to be employed and the

mentioned command line, among other sections. So, for the optimisation stage, the following command line is added to the input program:

```
#opt ub3lyp/6-31g(d,p) scrf=(solvent=water)
geom=connectivity freq=noraman
```

Figure 5.4 shows, as an example, a representation of a molecule optimisation. Figure 5.4a and Figure 5.4b show two views from different points of sertraline molecule after the optimisation, and Figure 5.4c presents a total energy chart of the optimisation, where it can be seen that, after numerous steps (each blue point represents a step) the algorithm converges in a minimum energy point (red circle of the energy chart).

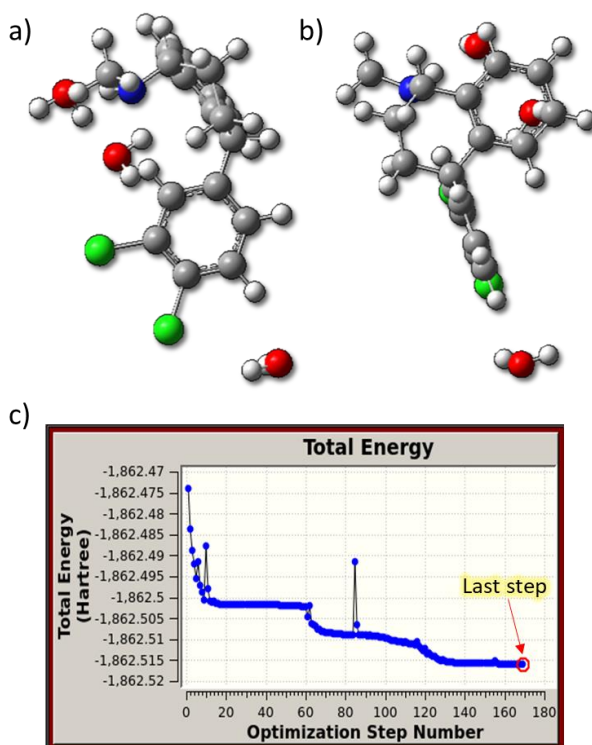


Figure 5.4. Optimised structure of the sertraline molecule including water molecules; a) view 1, b) view 2, and c) chart of the total energy.

- **Scan.** This stage can provide a rough estimation of a pathway between the reactants and products, supposing that the chosen coordinates for the scan are carefully selected, to obtain the intended structure. In this step, a PES scan is carried out, where it is possible to move the chosen atoms closer together or farther apart, to

reach the desired structure, by creating or breaking a bond. A geometry optimisation is performed at each step, while keeping the scanned variable (in this case, the selected bond) constant (relaxed PES scan). As an example, the code line necessary to perform a scan is presented, which is introduced in the “code line” block (see Figure 2.17b, in blue colour), together with a small table with the meaning of each component of the last line of the code (where the additional information is placed, see Figure 2.17b in orange colour). This last line contains the specifications of the scan, detailed in Table 5.1.

```
#opt=(modredundant,maxcycles=20) ub3lyp/6-31g(d,p)
scrf=(solvent=water) geom=connectivity
...
B 33 15 S 27 -0.05
```

Table 5.1. Specifications of the scan for the STR molecule.

B	33	15	S	58	-0.05
Bond	Atom 33 (O)	Atom 15 (C)	Scan	Steps*	Distance per step (Å) Plus sign (+) : move atoms far Minus sign (-) : move the atoms closer

*Steps: the number of steps is calculated as the difference between the distance among the atoms of interest and the bond distance.

Figure 5.5 presents the first structure of the scan, which corresponds to the first point of the energy chart, where the $\cdot\text{OH}$ is not bonded to the STR molecule. In the successive steps (in this case, 58, see Table 5.1), the $\cdot\text{OH}$ radical will gradually approach the C atom of the STR, moving 0.05 Å in each step, to finally bind in the last step of the scan (Figure 5.5b). Figure 5.5c shows the energy chart of the scan, where it is depicted the first step (Figure 5.5a), the TS (higher energy point of the graph) and the last step (Figure 5.5b).

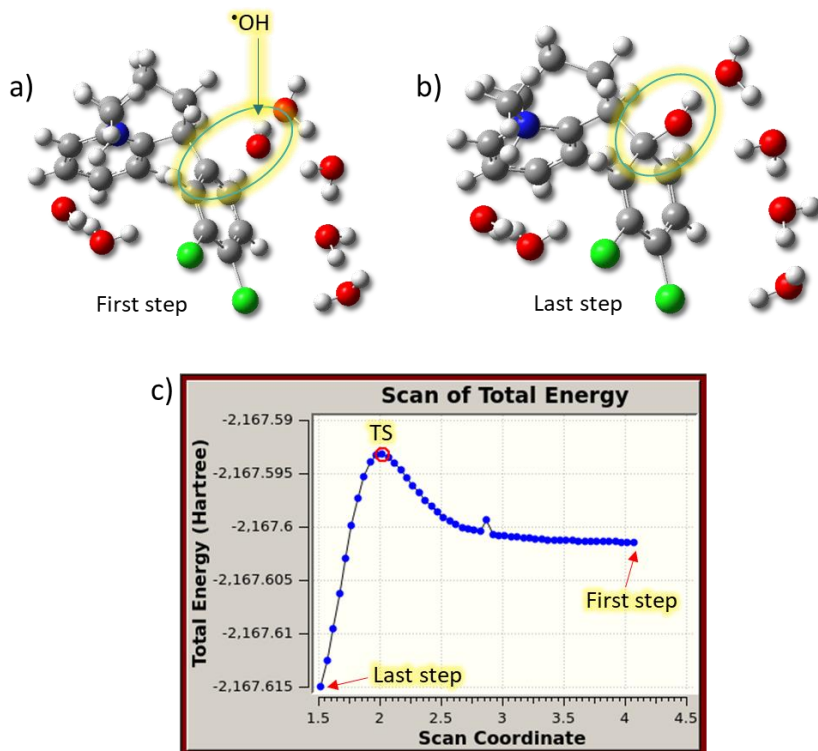


Figure 5.5. a) First step and b) last step of the scan performed to approximate the $\bullet\text{OH}$ radical; and c) total energy chart of the scan.

- Transition state and imaginary frequencies.** As it was described before, the bottleneck for structural changes is the transition state. As it is the highest point of the potential energy, the highest point of the energy graph obtained after the scan is selected for this calculation (Figure 5.5c). Furthermore, the frequency analysis describes the slight changes in geometry with respect to the energy. Vibrational frequencies are determined by calculating the second derivatives of the energy with respect to the Cartesian nuclear coordinates, and later, converting them to mass-weighted coordinates. This conversion is only applicable at a stationary point. A positive frequency value indicates that in that direction, the energy will increase; and a negative frequency (also called Imaginary Frequency) indicates the transition state, where the stationary point is reached (Bachrach, 2014; Cramer, 2004; Jensen, 2007; Lewars, 2016).

In the TS, all the geometry displacements will rise the energy except one: the direction that drives us to another energy minimum. The number of Imaginary Frequencies shows the kind of Stationary Point to which the given molecular structure corresponds. By definition, a structure that possesses n imaginary

frequencies is an n^{th} order saddle point. Rigorously, a TS of a chemical reaction is a 1^{st} order saddle point, which are stationary points with all forces zero (like the minima) and one of the second derivatives negative. TS search, thus, attempts to locate stationary points with one negative second derivative (Schlegel, 2003). Therefore, the minimum will have zero Imaginary Frequencies, and a normal transition structure will have one Imaginary Frequency because it is a 1^{st} order saddle point (Bachrach, 2014; Cramer, 2004; Lewars, 2016). The necessary code line to calculate the TS is presented below and introduced in the “code line” block (see Figure 2.17b, in blue colour).

```
#opt=(calcall, ts, noeigentest) ub31yp/6-31g(d,p)
_scrf=(solvent=water) geom=connectivity freq=noraman
```

As an example, Figure 5.6 represents the TS of the STR-OH reaction. Figure 5.6a and Figure 5.6b correspond to the two structures of the vibration that occurs in the TS, the blue arrows highlighted in yellow represent the direction of the atoms' movement with the desired vibration, getting closer (Figure 5.6a) and farther (Figure 5.6b). Figure 5.6c contains the vibrational frequencies obtained, with the first one as the imaginary frequency required, negative value of frequency, in this case, -341.63. This negative value indicates that a TS was found.

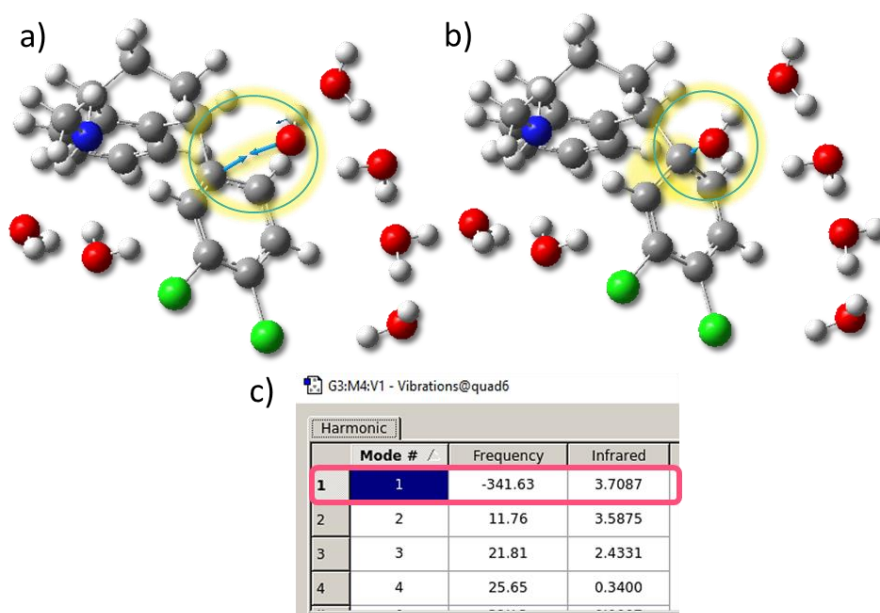


Figure 5.6. Transition state of the sertraline- \cdot OH reaction: a) atoms of interest getting closer, b) atoms of interest getting farther and c) table of vibrational frequency values.

- **IRCs (Intrinsic Reaction Coordinate).** The pathway of a chemical reaction can be followed from the transition state to the reactants, and from the transition state to the products, employing the Intrinsic Reaction Coordinate method, which assumes that the initial geometry is a fair approximation of the TS (Deng and Ziegler, 1994). This pathway is called the Intrinsic Reaction Path (IRP) and connects reactants, transition states and products. The Intrinsic Reaction Coordinate (IRC) is defined as the minimum energy route which goes through the transition state and moves substantially slowly, and its initial direction is provided by the imaginary frequency (Fukui, 1970; Ishida et al., 1976). The first IRC point starts in the TS (highest energy point), being basically a sequence of small steepest-descent paths, and it can go in one of the two possible downhill directions to a local minimum (reactants and products) (Deng and Ziegler, 1994; Jensen, 2007; Lewars, 2016). In the next code lines, it is depicted how the IRC is calculated, in the reverse direction (from the TS to reactants) and in the forward direction (from the TS to the products). This code line is introduced in the “code line” block (see Figure 2.17b, in blue colour).

```
#irc=(calcfc,recalc=-20,report=cartesian,maxpoints=200,  
maxcycle=35,stepsize=4,reverse) ub31yp/6-31g(d,p)  
scrf=(solvent=water)geom=connectivity  
  
#irc=(calcfc,recalc=-20,report=cartesian,maxpoints=200,  
maxcycle=35,stepsize=4,forward) ub31yp/6-31g(d,p)  
scrf=(solvent=water)geom=connectivity
```

Figure 5.7 represents the IRC pathway for the STR-OH reaction stated as example. Figure 5.7a and Figure 5.7b show the reverse IRC, which corresponds to the pathway from the TS to the reactants (R), being Figure 5.7a the structure representation and Figure 5.7b the energy chart corresponding to the pathway TS→R. On the other hand, Figure 5.7c and Figure 5.7d displays the forward IRC, which corresponds to the pathway from the TS to the products (P), being Figure 5.7c the structure representation where the bonds STR-OH can be appreciated, and Figure 5.7d, the energy chart corresponding to the TS→P.

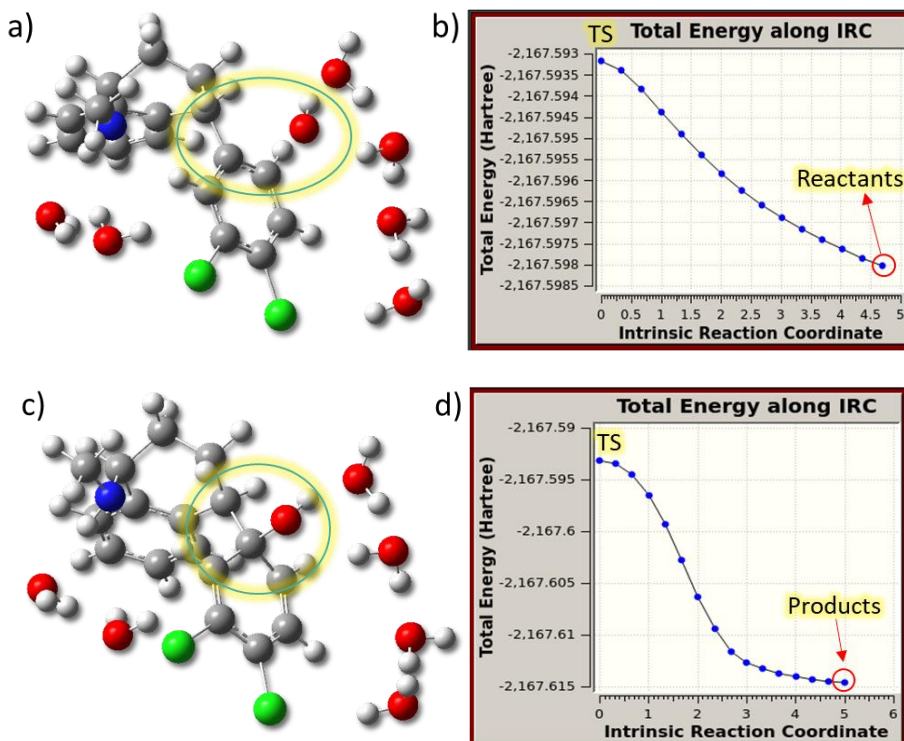


Figure 5.7. Sertraline-•OH union IRCs: a) IRC reverse structure; b) IRC forward structure, c) total energy chart of the IRC reverse and d) total energy chart of the IRC forward.

- **Optimisation.** Finally, if the final structures resulting from the IRCs reverse and forward are the desired ones, another last optimisation of these structures must be performed, together with the frequency calculation. For this, the following command line (same as for the initial optimisation of the system) is employed.

```
#opt ub3lyp/6-31g(d,p) scrf=(solvent=water)
geom=connectivity freq=noraman
```

Once all these stages have been completed for each step of each mechanism, the additional final energy calculation for each final structure must be performed, named Single Point Energy (SPE). This type of calculation does not make a geometry change, nor calculates properties, other than the energy; and it is usually applied to refine the energy obtained from a geometry optimization carried out at a lower level of theory. In this sense, a much larger basis is used facing to provide a more realistic description of the atomic orbitals, and also, an empirical dispersion term (EmpiricalDispersion=GD3BJ) is applied, which helps on the description of medium- and long-range dispersion (Van der

Waals type of interactions). The following code line to calculate the SPE is introduced in the “code line” block (see Figure 2.17b, in blue colour).

```
#ub3lyp/6-311++g(2df,2pd) scrf=(iefpcm,solvent=water)
geom=connectivity Guess=Mix EmpiricalDispersion=GD3BJ
```

After this calculation was performed, it is of great interest to know what the spin density is, to know in which atom is placed the most negative charge, which allows to confirm the mechanisms proposed, based on where the breakage or the binding takes place. The spin density is calculated through the electron density (previously described in section 5.1.1); it is the unpaired electron density at a place of interest (normally at carbon) in a radical (IUPAC, 2008), and it allows to identify where unpaired electrons should be found in a molecular system. It is well known that there are two possible values for the spin quantum number ($m_s = \pm\frac{1}{2}$), which correspond to the two possible spin states. In consequence, the spin density is defined as the total electron density of one spin (α or spin up, $m_s = +\frac{1}{2}$) minus the total electron density of the other spin (β or spin down, $m_s = -\frac{1}{2}$) for each atom. They have been calculated through the Mulliken spin population analysis. As an example, in Figure 5.8 it is shown how the spin densities appear in Gaussview. In red, the lower spin density values, and in green, the highest density values. These values are depicted in the correspondent atom, for each mechanism in figures of section 5.2.

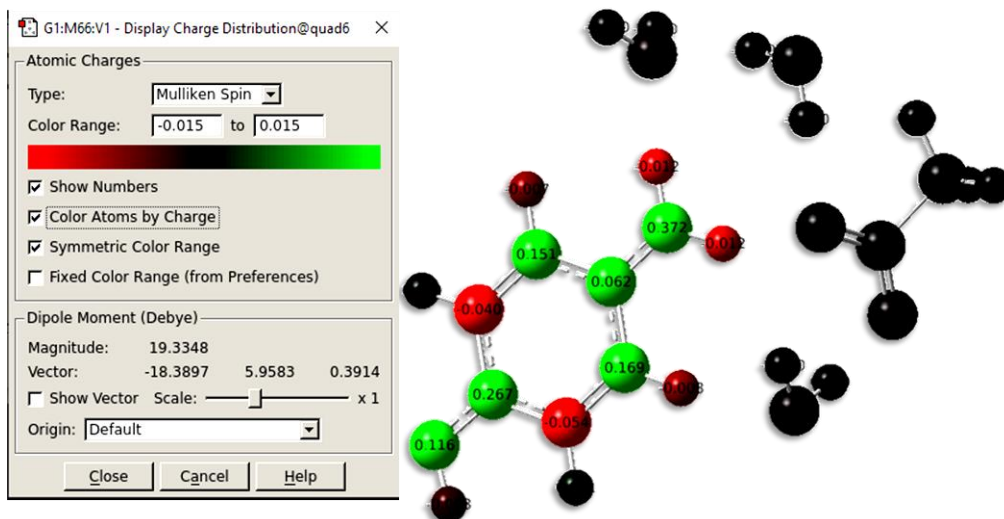


Figure 5.8. Example of the representation of spin density values representation in a PAR molecule, after its breakage through $\cdot\text{OH}$ attack.

5.1.2. Mechanism proposal from drugs to the formation of PCDD/Fs

Figure 5.9 depicts a generic scheme of the proposal of a combined mechanism to describe the PCDD/Fs formation from the degradation of the three selected drugs, AMX, PAR and STR, via the intermediates experimentally detected, mainly chlorophenols and hydroquinone molecules.

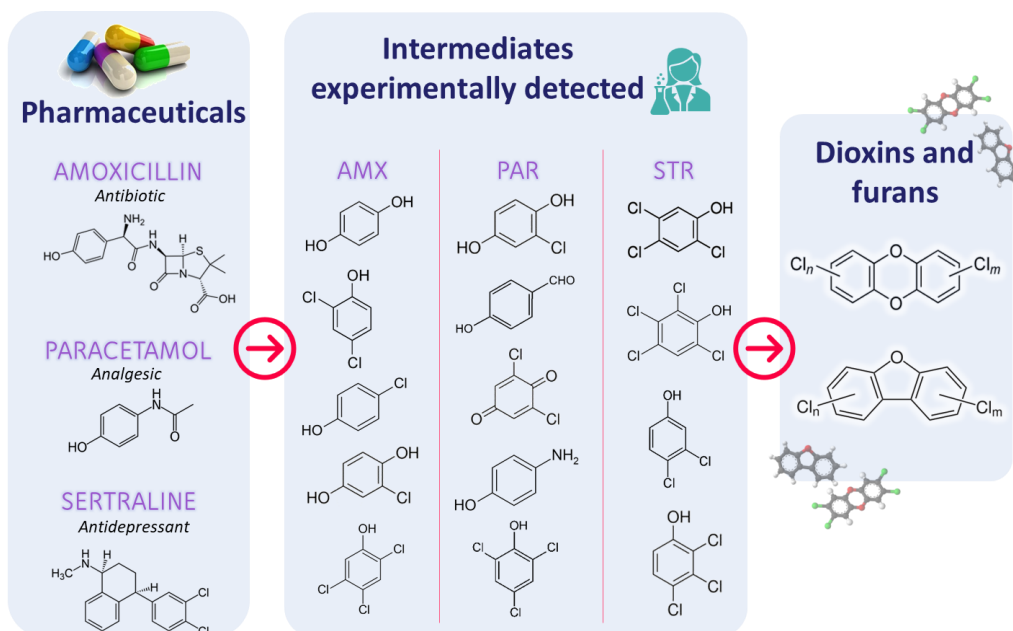


Figure 5.9. Scheme of the combined mechanism proposed for PCDD/Fs formation from AMX, PAR and STR degradation.

Entering deeply into the degradation mechanisms, an extended literature review of the selected drugs, AMX, PAR and STR, has been carried out. Taking into account the acquired knowledge and starting from the intermediate compounds identified during the high electro-oxidation concentration experiments (EOX-Intermediates experiments), the detailed mechanism of the PCDD/Fs formation from AMX, PAR and STR can be observed in Figure 5.10 and Figure 5.11.

The first stage of the combined mechanism of degradation is shown in Figure 5.10 and starts with the cleavage of PAR and AMX through $\cdot\text{OH}$ attack (depicted in blue colour), to end up in one common molecule (hydroquinone). In more detail, on the one hand, the breaking off the paracetamol molecule has been approached in two different bonds, by the attack of $\cdot\text{OH}$ radical. As a consequence, the formation of hydroquinone (HQ) can be produced from these two paths. On the other hand, amoxicillin also breaks

from the action of $\cdot\text{OH}$ radicals, forming hydroquinone. Then, and following successive chlorination steps, first, 2-chlorohydroquinone is formed, and after, the 3,4-dichlorophenol (3,4-DCP) is produced. In addition, sertraline breaks in two different parts due to the action of the $\cdot\text{OH}$, producing 3,4-dichlorophenol straightforwardly. The intermediate molecules (4-nitrophenol, hydroquinone, 2-chlorohydroquinone and 3,4-dichlorophenol) have been detected during the electro-oxidation of the drugs (see Chapter 3, and Annex IV). In Figure 5.11, it is represented the second stage of the combined mechanism, which corresponds to the PCDD/Fs formation from 3,4-dichlorophenol. 3,4-dichlorophenol is converted to 3,4-dichlorophenol radical (3,4-DCP \cdot) through the loss of an H atom. Next, two molecules of 3,4-DCP \cdot are combined to form two different dioxins: 2,3,7,8-TCDD and 1,2,7,8-TCDD. These two dioxins are formed following a series of H eliminations and cyclization of the molecule.

Before entering into a thorough description of the mechanisms, it is needed to clarify that in this thesis has been realised a preliminary computational study, where it has been developed the low chlorination dioxins mechanism formation, as they have the highest toxicity, i. e., the most representatives within the TEQ. Therefore, the high chlorination dioxins formation mechanisms and the high-low chlorination furans formation mechanisms were left aside for a future work, since their computational calculations can become extremely complex, stretching out in time (Chapter 6).

This study starts simulating the TCDD dioxins (2,3,7,8-TCDD and 1,2,7,8-TCDD). Why? On the one hand, both dioxins, corresponding to the group of TeCDD homologues, were experimentally determined, being the a group precursor of PeCDD and successive groups, and also the group which contains the most toxic congeners, although the concentrations of the TCDD groups were very low, in the range 0.56 to 34.47 $\mu\text{g L}^{-1}$ for AMX, PAR and STR using both electrolytes (NaCl and $\text{Na}_2\text{SO}_4+\text{NaCl}$) (Chapter 4, section 4.1.1). Additionally, the congener 2,3,7,8-TCDD was analysed, since is the congener that contributes the most toxicity to the TEQ, with a significant value between 0.2 to 2.1 $\mu\text{g L}^{-1}$ for AMX, PAR and STR using both electrolytes (NaCl and $\text{Na}_2\text{SO}_4+\text{NaCl}$) (Chapter 4, section 4.1.2). And on the other hand, because TCDDs are well-known precursors of more chlorinated dioxins, formed through successive chlorination reactions, as it is well described in the literature (Fernández-Castro, 2017; Fernández-Castro et al., 2016; Pan et al., 2013; Solá-Gutiérrez, 2019; Vallejo, 2014; Vallejo et al., 2015, 2014, 2013; Weber, 2007; Wiater-Protas and Louw, 2001), being in this PhD thesis the most abundant ones were PeCDD/Fs, HxCDD/Fs and HpCDD/Fs (Chapter 4, section 2.1.1), so that this simulation remains as future work, for the reasons mentioned in the previous paragraph.

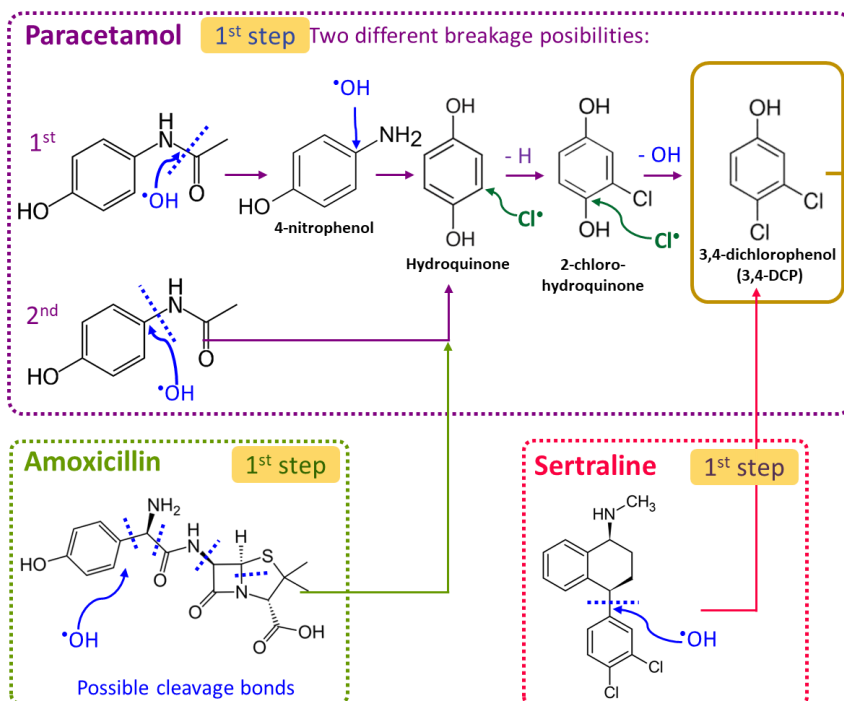


Figure 5.10. Combined mechanism proposal; degradation of AMX, PAR and STR (1st step).

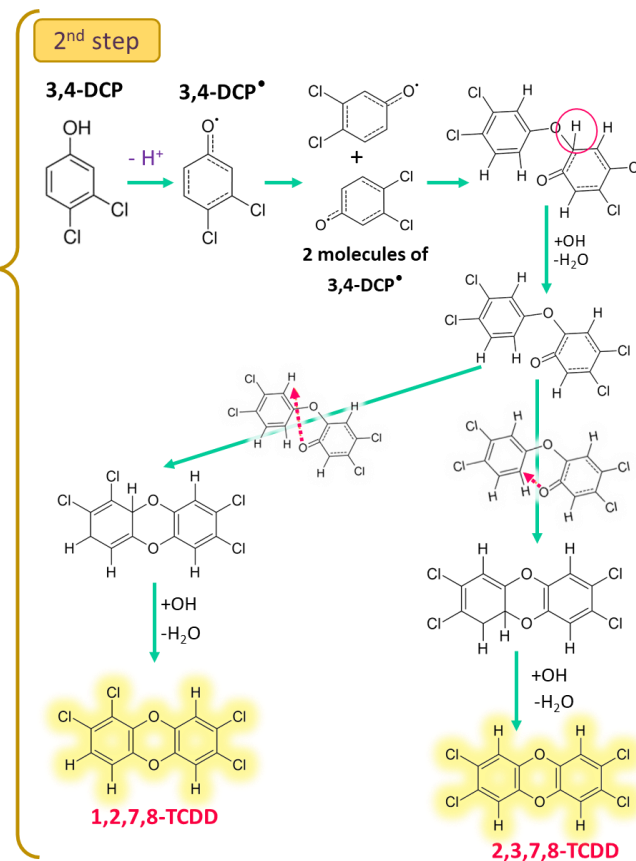


Figure 5.11. Combined mechanism proposal; PCDD/Fs formation from 3,4-dichlorophenol (2nd step).

5.2. Description of the combined mechanism through DFT

In this section, the mechanisms proposed in Figure 5.10 and 5.11 are described individually for each molecule. For all the 3D figures (DFT simulations), H atoms are depicted in white colour, C atoms in grey, O atoms in red, N atoms in blue, Cl atoms in green and S atoms in yellow, and the dashed pink lines represent the two atoms that are going to approach each other. Also, it is detailed the degradation mechanisms by a Lewis structure representation, a simplified representation of the valence shell electrons used to show how the electrons are arranged around individual atoms in a molecule. The spin values are represented in red in the corresponding atom, and the experimentally detected compounds are also depicted (yellow box). In addition, the half arrows represent the movement of the electrons.

The computational times required for each type of molecule have been very diverse, depending on the type of calculation to be performed, being from a few minutes for optimization and frequency calculations to hours-days, or even a week, for more complex calculations such as scan or IRCs. For instance, the amoxicillin scans took more than 6 days.

5.2.1. Combined mechanism: 1st step - breakage of the drugs

Amoxicillin

In the amoxicillin case, to generate the hydroquinone (HQ) molecule, it is suggested that the $\cdot\text{OH}$ attacks the C atom of the p- position of the benzene ring, in this case, placing it in the “outside” part of the molecule (Figure 5.12). It is well-known, that the amoxicillin molecule has a concave shape, and possesses several torsion angles, it is not a planar molecule as paracetamol, and consequently, the computational efforts are higher than for the planar molecules. So, in this option, the $\cdot\text{OH}$ radical is placed in the outside part of this concave molecule. As it has been stated by Frontistis et al. (2017), this C-C bond (depicted in Figure 5.12a, dotted blue line) is one of the most probable bonds to break. Figure 5.12a shows schematically the $\cdot\text{OH}$ attack to the AMX molecule and the further HQ formation, where the dashed arrows mean that more stages occur between the first molecule and the next one. Meanwhile, Figure 5.12b presents the mechanism with the 3D representation of the molecules, obtained after the computational calculations. Next, the steps depicted in the mentioned figures are detailed:

- (i) First, the approximation of the $\cdot\text{OH}$ radical takes place (Figure 5.12b, (i)).

- (ii) It is produced the hydroxylation of the AMX molecule (see Table 3.5, Chapter 3), with the formation of the AMX- $\cdot\text{OH}$ complex (Figure 5.12b, (ii)) (Ferreira et al., 2020; Frontistis et al., 2017; Pan et al., 2020; Pan and Sun, 2021).
- (iii) To finish, the breakage of the molecule occurs, on the one hand, forming HQ (Figure 5.12b, (iii)), and on the other hand, the remaining fragment of the cleavage of the AMX molecule, which has been detected in other works (Ferreira et al., 2020; Frontistis et al., 2017; Pan et al., 2020; Pan and Sun, 2021). In this doctoral thesis, just hydroquinone has been detected.

Additionally, another mechanism has been proposed, by placing the $\cdot\text{OH}$ radical in the “inner” part of the concave zone of the AMX molecule. This option can be found in Annex VIII as extra information, together with the corresponding energy profile. It has not been included in this section due to its similarity in the DFT calculations and in the final energy profile with the “outside” $\cdot\text{OH}$ attack AMX case.

In order to corroborate the proposed degradation route for the AMX, Figure 5.13 shows the mechanism employing the Lewis structure in terms of the spin values, and the other molecule possibilities (Figure 5.13, (ii)), that can lead to different bonds depending on the spin value (value shown in red colour in Figure 5.13). In the yellow colour box is represented the molecule detected in this work, HQ (Figure 5.13, (iii)), and in the blue box, the molecules detected by other authors in the literature, the AMX-OH complex, or hydroxylated amoxicillin (Figure 5.13, (ii)) and the remaining fragment (Figure 5.13, (iv)). As it is shown, three different types of hydroxylated amoxicillin can appear, depending on where the electron is placed (see spin value in red), being the one with the highest spin the one which appears in brackets, the most likely molecule to be formed. In this case, it has a value of $0.44 \text{ e}^{-1} \text{ au}^{-3}$, positioned in the C atom bonded to the OH group of the phenolic ring, hereafter called C1. The second highest value resides on the C of the m- position with respect to C1 ($0.41 \text{ e}^{-1} \text{ au}^{-3}$) (Figure 5.13, (ii)). In addition, the spin values of the fragment were also calculated, being the highest, $0.46 \text{ e}^{-1} \text{ au}^{-3}$ (Figure 5.13, (iv)).

In Annex VIII it can be found the detailed amoxicillin pathway with the corresponding spin density values, and the energy chart obtained for the other mechanism proposal (inner part).

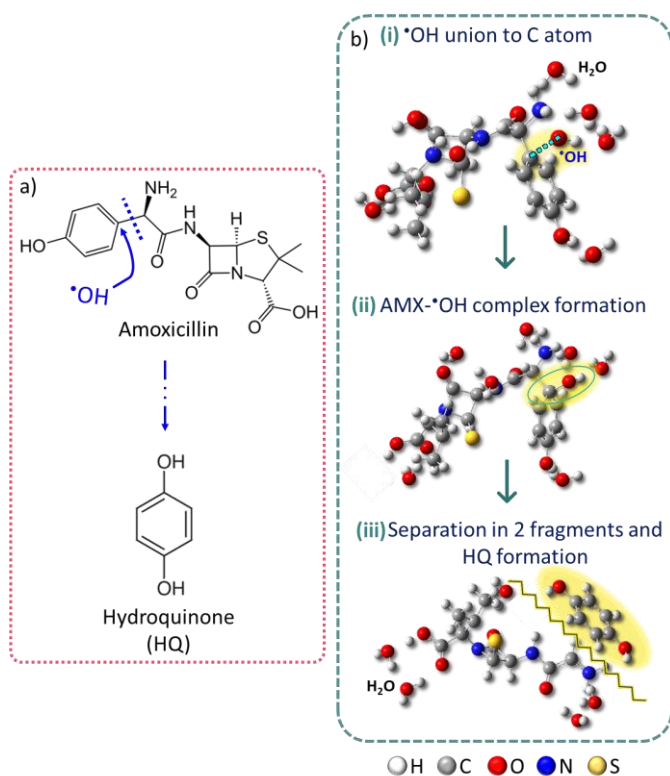


Figure 5.12. a) Scheme of the AMX breakage mechanism and b) DFT simulation of the molecule AMX rupture.

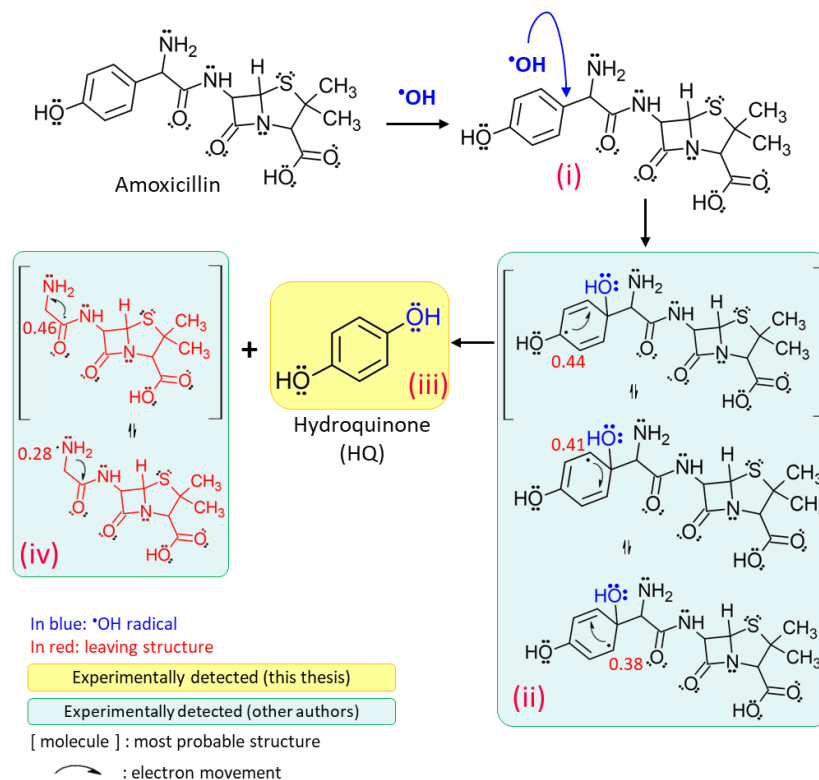


Figure 5.13. AMX degradation pathway in terms of the spin values, marked in red.

Paracetamol

For the paracetamol molecule, two different mechanisms options have been proposed in relation to the intermediate compounds detected and detailed in Chapter 3.

1st mechanism option

In Figure 5.14, it is presented the first mechanism option for the PAR breakage, proposed by Chen et al. (2021). These authors suggested this pathway based on the results obtained from the analysis of the Fukui values and the highest occupied molecular orbital (HOMO) of the PAR molecule. Figure 5.14a shows schematically the $\cdot\text{OH}$ attack to the PAR molecule and the further formation of 4-nitrophenol, to end with another $\cdot\text{OH}$ radical attack, forming the HQ. The dashed arrows mean that more stages occur between the first molecule and the next one. Figure 5.14b presents the mechanism with the 3D representations obtained after the computational calculations. Next, the steps of this mechanism are described below:

- (i) The first approach to reach hydroquinone (HQ) is by the attack of an $\cdot\text{OH}$ to the peptide bond (Figure 5.14b, (i)), marked with a dotted blue line. In the literature it is suggested that the $\cdot\text{OH}$ attacks the peptide bond, with the further formation of 4-nitrophenol (Ganiyu et al., 2019; Periyasamy and Muthuchamy, 2018; Sun et al., 2018).
- (ii) Then, the separation in two fragments is produced (Figure 5.14b, (ii)), generating a 4-nitrophenol radical molecule and the remaining fragment.
- (iii) Due to that the final product wanted is 4-nitrophenol, it is produced a H addition from the fragment, then yet producing 4-nitrophenol (Figure 5.14a and Figure 5.14b, (iii)). 4-nitrophenol has been widely detected in the literature (Ganiyu et al., 2019; Periyasamy and Muthuchamy, 2018; Sun et al., 2018) and also in this thesis (see Chapter 3, Figure 3.11).
- (iv) After this, a second $\cdot\text{OH}$ attack (Figure 5.14a, blue dotted line) occurs on the C atom bonded to the amino group (p- position with respect to the OH group) with the correspondent electrophilic addition (Figure 5.14b, (iv)) (Ganiyu et al., 2019; Olvera-Vargas et al., 2018).
- (v) Finally, the HQ is formed (Figure 5.14b, (v)) by the rupture of the C-C bond of 4-nitrophenol. In this thesis, hydroquinone was also detected in greater amounts (Chapter 3, Figures 3.11 and 3.12).

It can be appreciated that Figure 5.14a depicts fewer steps than Figure 5.14b, but when performing the computational calculations, it is common that a substantial larger number of steps are actually required to obtain the final molecule.

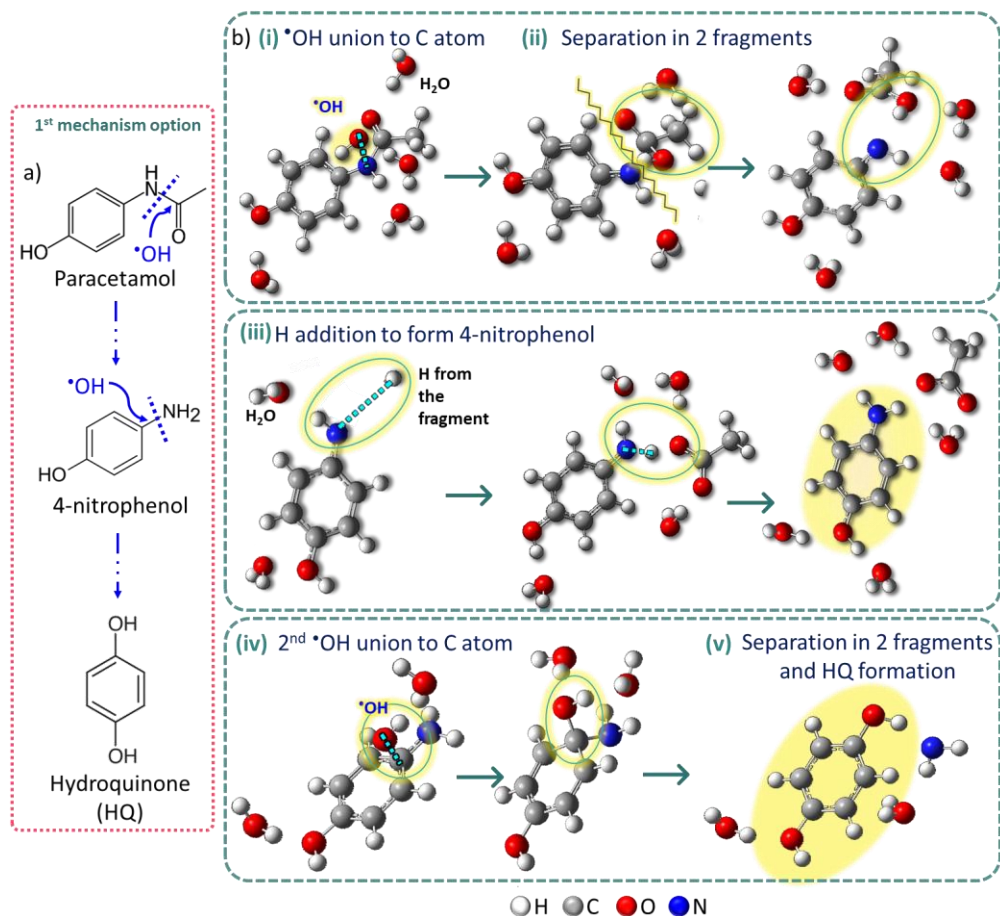


Figure 5.14. Scheme of the PAR (1st mechanism option) breakage mechanism and b) DFT simulation of the molecule PAR rupture.

2nd mechanism option

For the second mechanism option, it was proposed a direct attack of the $\cdot\text{OH}$ radical to the C atom of the p- position of the benzene ring (respecting to the OH group) to form HQ, as it is described in the literature (De Luna et al., 2012; Ganiyu et al., 2019; Le et al., 2017; Liu et al., 2019; Olvera-Vargas et al., 2018; Periyasamy and Muthuchamy, 2018). In the work of Qutob et al., (2022) is suggested this same pathway, due to the DFT results obtained when calculating the Fukui values. As for the previous cases, in Figure 5.15a is depicted the schematic way of the mechanism description and in Figure 5.15b,

is presented the mechanism with the 3D descriptions obtained after the computational calculations, again with more steps required of the computational calculations.

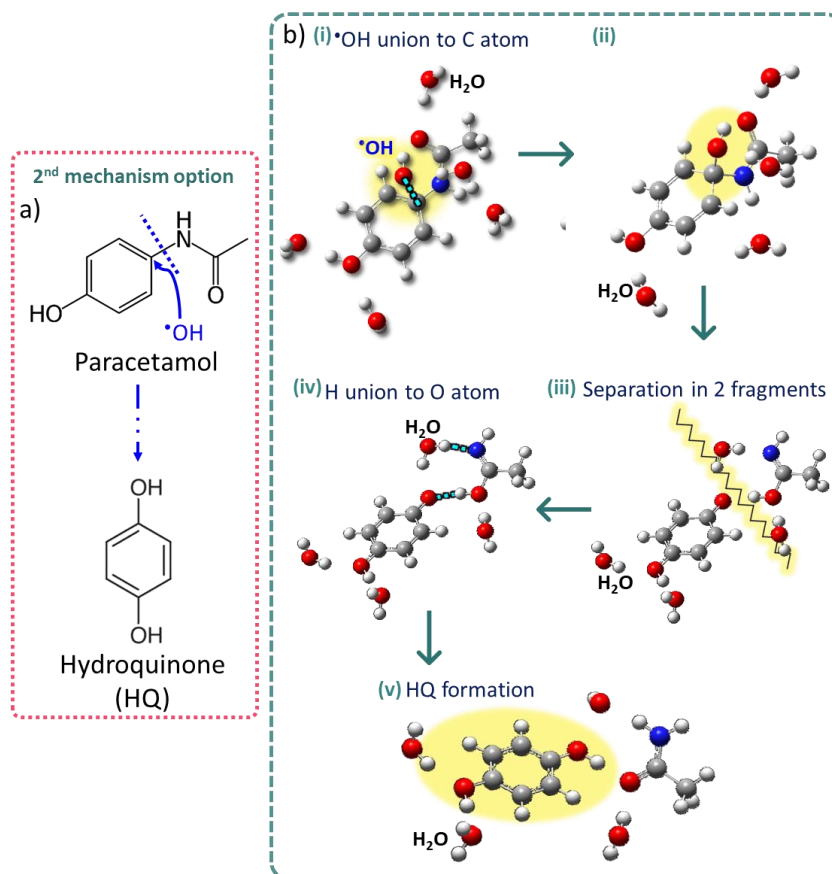


Figure 5.15. Scheme of the PAR (2nd mechanism option) breakage mechanism and b) DFT simulation of the molecule PAR rupture.

Each of the required steps for the mechanism depicted in Figure 5.15b, are described below.

- (i) The *OH radical enters directly (Figure 5.15a, marked with dotted blue line, and Figure 5.15b, (i)) by an electrophilic attack in the C atom at position 4 (p-) with respect to the OH group of the benzene ring (De Luna et al., 2012; Ganiyu et al., 2019; Le et al., 2017; Liu et al., 2019; Olvera-Vargas et al., 2018; Periyasamy and Muthuchamy, 2018).
- (ii) It is created the PAR-OH complex (Figure 5.15b, (ii)). In the literature, it has been stated that several hydroxylated PAR molecules can be formed, where the p-addition can compete with o- and m- additions (Olvera-Vargas et al., 2018).

- (iii) Then, the breakage of the C-N bond occurs, producing the separation in two fragments (Figure 5.15b, (iii)), one is the p-phenodiol radical and the other is the residual fragment. This radical is formed because during the rupture, the H of the added OH group binds with an O atom of the fragment.
- (iv) Here, to generate the final products, a H atom proceeding from the fragment is bonded to the O radical (blue dotted lines, Figure 5.15b, (iv)) because the fragment takes one H of a water molecule, and thereby transfers an H atom to the oxygen radical.
- (v) HQ is finally formed through the last step (Figure 5.15b, (iv)).

Finally, the two proposed degradation routes for PAR are corroborated in terms of the spin values, which are shown in red colour in Figure 5.16. This figure represents the two degradation pathways for paracetamol suggested in this thesis, employing the Lewis structure. In a yellow colour box are represented the molecules detected in this thesis, 4-nitrophenol (Figure 5.16, (iii)) and HQ (Figure 5.16, (iv) and (vii)), and in the blue box, the molecules detected in the literature. For the 1st option of PAR breakage (depicted as 1-Op in Figure 5.16), after the first PAR-OH is formed (Figure 5.16, (i)), two different structures appear for the first stage (Figure 5.16, (ii)), where the highest spin density value is in the N atom of the amino group ($0.57 e^{-1} au^{-3}$), and in second place, the spin with high value is located in the C atom bonded to the OH group (C1), with a value of $0.27 e^{-1} au^{-3}$. After the H addition the 4-nitrophenol is formed (Figure 5.16, (iii)). As it can be seen, also two structures can be possible, being the one with the highest value the structure with the spin value located again in the N atom ($0.37 e^{-1} au^{-3}$). After the second $\cdot OH$ attack, exist three possible PAR-OH complex structures, with the electron located in C1 ($0.45 e^{-1} au^{-3}$) with the greatest spin value ($0.45 e^{-1} au^{-3}$), the electron on m- position respecting to C1 ($0.38 e^{-1} au^{-3}$) named as C3, and the electron on the other m- position respecting to C1 ($0.41 e^{-1} au^{-3}$) named as C5. Then HQ is formed (Figure 5.16, (iv)) from the PAR-OH complex structure with the electron located in C1 ($0.45 e^{-1} au^{-3}$).

For the second mechanism option (depicted as 2-Op in Figure 5.16), the first $\cdot OH$ attack occurs, that gives place to PAR-OH complex (Figure 5.16, (v)) with the highest spin value located in C1 ($0.45 e^{-1} au^{-3}$). After this, the p-phenodiol radical (Figure 5.16, (vi)) is produced, with two possible structures with approximately the same value, $0.31 e^{-1} au^{-3}$ and $0.29 e^{-1} au^{-3}$ for the electron placed on the O radical and on the C1, respectively. In the last step, HQ is formed (Figure 5.16, (vii)) from the p-phenodiol radical.

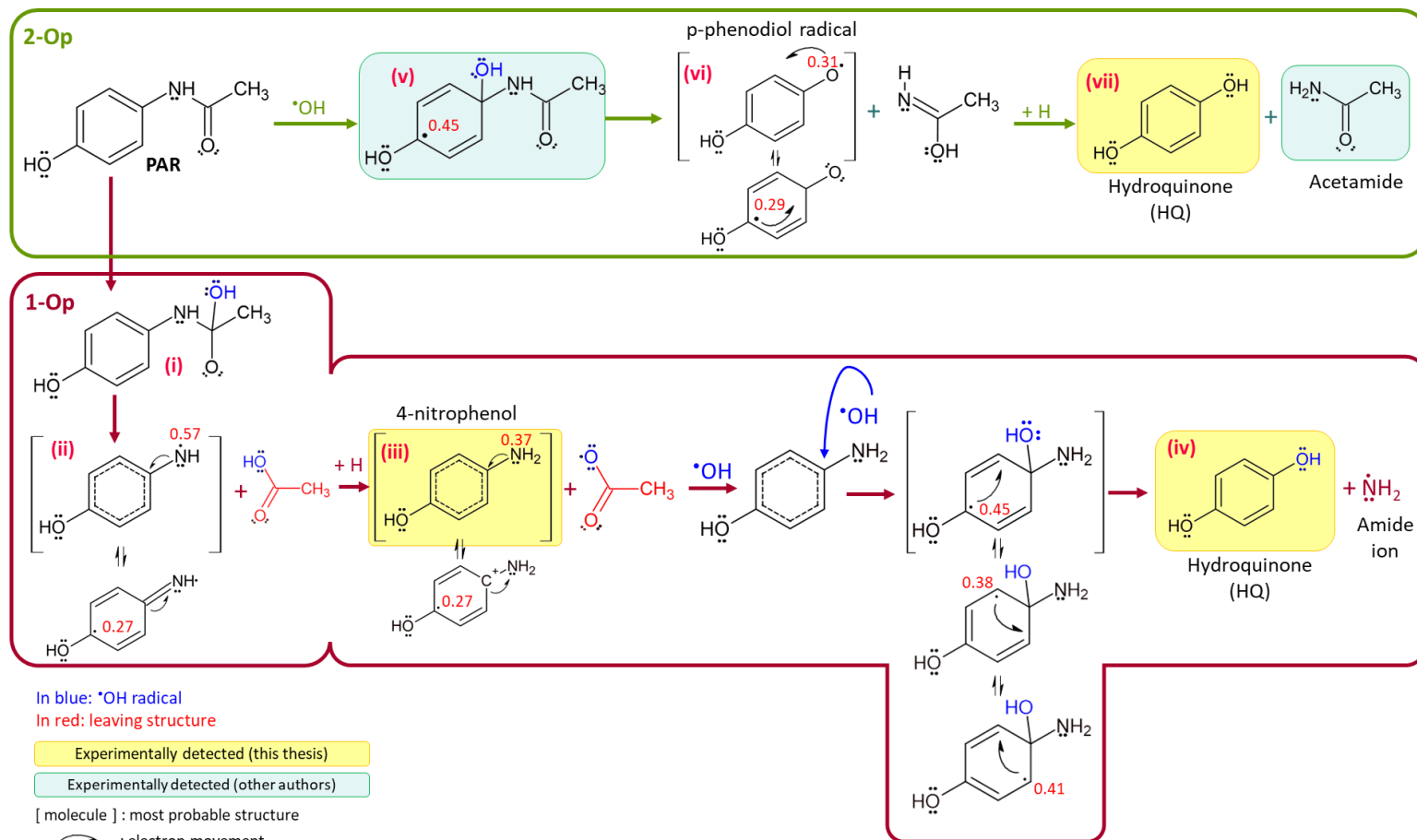


Figure 5.16. PAR degradation pathway in terms of the spin values, marked in red.

Sertraline

The STR degradation mechanism is the simplest one, because, as it can be observed in Figure 5.17 just one $\cdot\text{OH}$ attack is needed to achieve the final target molecule, 3,4-dichlorophenol (3,4-DCP), which will conduct to the PCDD/Fs formation. This way required less steps to achieve the final desired product, 3,4-dichlorophenol. The mechanism proposed in this case was based on different works of the literature, where hydroxylation of the STR molecule occurs and give rise to the 3,4-dichlorophenol (Calza et al., 2021; Gornik et al., 2020; Jiménez-Holgado et al., 2021). Figure 5.17a presents in a schematically way, the $\cdot\text{OH}$ attack to the STR molecule and the further 3,4-DCP formation, where the dashed arrows mean that more stages occur between the first molecule and the next one. Additionally, Figure 5.17b details the mechanism with the 3D molecules obtained after the computational calculations. Next, the steps depicted in the mentioned figures are detailed:

- (i) The mechanism starts with the $\cdot\text{OH}$ radical attacking the C-C bond (marked with dotted red line Figure 5.17a, and Figure 5.17b (i)). This attack is proposed recently by several authors in the literature (Calza et al., 2021; Gornik et al., 2020; Jiménez-Holgado et al., 2021).
- (ii) It is created the STR-OH complex, though a hydroxylation of the sertraline molecule (Figure 5.17b, (ii)) (Calza et al., 2021; Gornik et al., 2020; Jiménez-Holgado et al., 2021).
- (iii) Finally, the separation in two fragments due to the cleavage of the C-C bond takes place (Figure 5.17b, (iii)), one is the 3,4-dichlorophenol (Calza et al., 2021; Jiménez-Holgado et al., 2021), detected in this thesis (Chapter 3, Table 3.7) and the other one is the rest of the sertraline molecule, named as N-methyl-1-Naphthalenamine, (MNA), also detected in this thesis (Chapter 3, Table 3.7) (Calza et al., 2021; Gornik et al., 2020; Jiménez-Holgado et al., 2021).

Finally, the STR degradation mechanism has been corroborated in Figure 5.18, through the Lewis structure with the spin values pointed in red. In a yellow colour box are represented the molecules detected in this thesis, 3,4-DCP (Figure 5.18, (iii)) and MNA (Figure 5.18, (iv)), and in the blue box, the molecules detected in the literature, the STR-OH complex, better known as hydroxylated STR (Figure 5.18, (ii)). After the $\cdot\text{OH}$ radical addition forming the STR-OH complex (Figure 5.18, (ii)), three possible structures can be observed, with the highest spin value ($0.52 e^{-1} \text{ au}^{-3}$) in the C atom of the p-position respecting the C-C bond where the OH is bonded, named as C1. The second and third

spin values are positioned in the two possible m- positions respecting to C1, with the same spin value, $0.42 e^{-1} \text{ au}^{-3}$. To end, the rupture of the molecule due to the split of the C-C bond generates the 3,4-DCP (Figure 5.18, (iii)) and MNA (Figure 5.18, (iv)). MNA possess four different structures, with spin values between 0.24 and $0.74 e^{-1} \text{ au}^{-3}$, being the highest one positioned on the C atom where the C-C bond was originally placed.

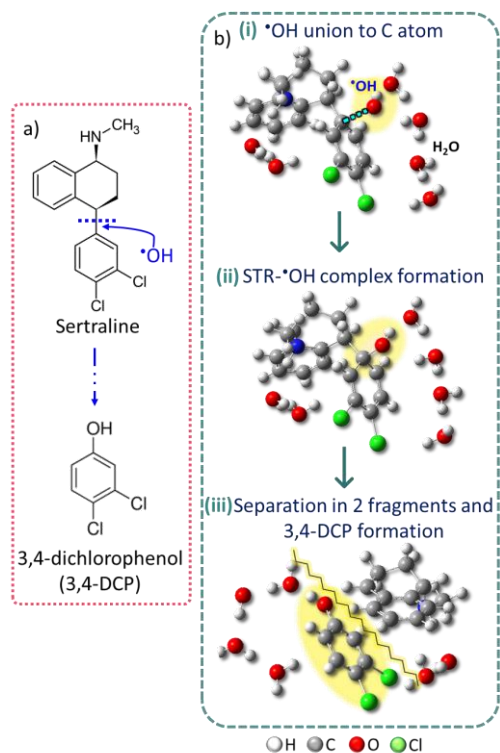


Figure 5.17. a) Scheme of the STR breakage mechanism and b) DFT simulation molecules of the STR rupture.

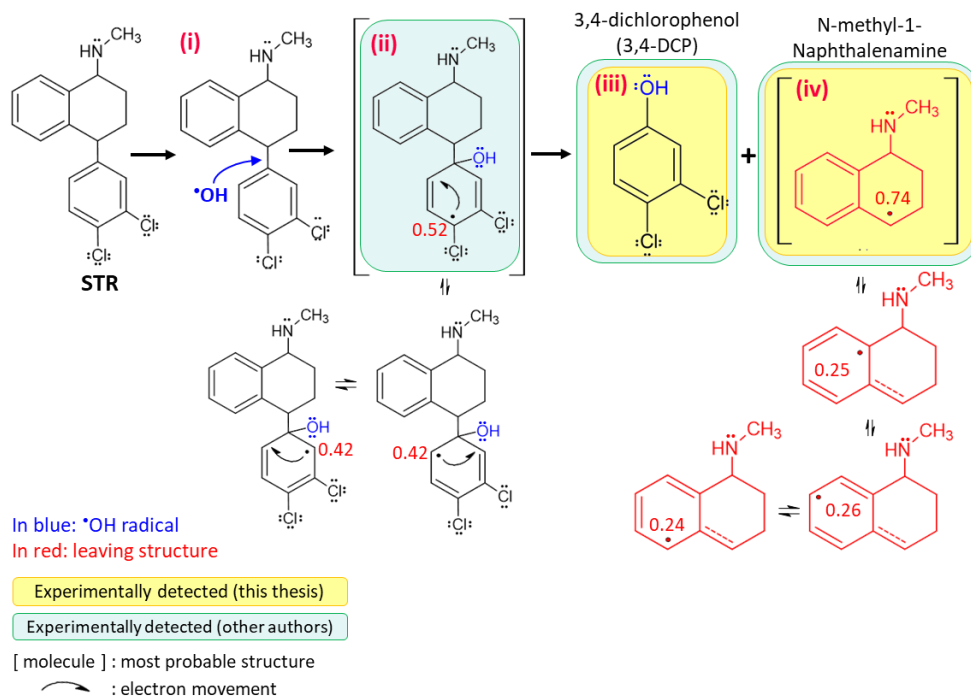


Figure 5.18. STR degradation pathway in terms of the spin values, marked in red.

5.2.2. Combined mechanism: 2nd step - intermediate and final molecules formation

In a second stage, the formation of the rest of the molecules to complete the mechanism has been studied. These are, on the one hand, the formation of 3,4-dichlorophenol from the hydroquinone molecule (obtained from the rupture of the paracetamol and amoxicillin molecules), and on the other hand, the formation of the dioxins 2,3,7,8-TCDD and 1,2,7,8-TCDD from the combination of two 3,4-dichlorophenol radicals. As it was described in section 5.1.2, both dioxins have been selected, due to i) they belong to the group of TeCDD homologues, experimentally determined, being the group or group precursor with the more toxic congeners, ii) the congener 2,3,7,8-TCDD that contributes the most to toxicity for the TEQ, was experimentally quantified, and finally, iii) because TCDDs are precursors of the more chlorinated dioxins, such as PeCDD/Fs, HxCDD/Fs and HpCDD/Fs, formed through successive chlorination reactions, and detected in this PhD Thesis (Briois et al., 2007; Evans and Dellinger, 2005; Fernández-Castro, 2017; Fernández-Castro et al., 2016; Pan et al., 2013; Ryu, 2008; Solá-Gutiérrez, 2019; Vallejo et al., 2013; Vallejo, 2014; Vallejo et al., 2015, 2014; Weber, 2007; Wiater-Protas and Louw, 2001; Xu et al., 2015; Yang et al., 2017), leaving the computational calculations of the more complexes high chlorinated dioxins formation mechanisms and the high/low chlorination furans formation mechanisms for a future work, since their computational calculations can become extremely complex (Chapter 6).

Formation of 3,4-dichlorophenol from hydroquinone

Figure 5.19a shows the summarised mechanism of the formation process, in general terms, of 3,4-dichlorophenol from hydroquinone. It starts with a Cl[•] addition to a C atom of the HQ molecule, forming 2-chlorohydroquinone (2-Cl-HQ). Through another Cl[•] radical addition, 3,4-dichlorophenol is produced. Finally, H abstraction with an [•]OH radical generates the 3,4-dichlorophenol radical (3,4-DCP[•]). In Figure 5.19b it is depicted with more detail the described mechanism, shown with the 3D representations obtained after the DFT simulations. Next, the steps depicted in the mentioned figures are detailed:

- (i) First, the H atom in position 3 of the HQ is extracted by a [•]OH radical (Figure 5.19b, (i)) (dashed blue line).
- (ii) A Cl[•] radical is added to the place occupied by the H atom, in a spontaneous manner, due to the space available in that C atom (dashed blue line), producing 2-chlorohydroquinone (Cl-HQ) (Figure 5.19b, (ii)), molecule detected in this thesis (see Chapter 3, Section 3.1.3) (Vione et al., 2005).

- (iii) After this, an H atom binds to the C atom (dashed blue line) placed in the p- position with respect to the other OH group (Figure 5.19b, (iii)) (Peller et al., 2003).
- (iv) The OH group of the C atom where the H was bonded, leaves the molecule captured by a Cl^{*} radical (Figure 5.19b, (iv)), highly present in the bulk solution.
- (v) In a combined step, a simultaneous movement takes place: another Cl^{*} radical present in the solution enters in this C atom of the p- position respecting to the OH group, pushing the H group out of the molecule, which is caught by a ^{*}OH radical (Figure 5.19b, (iv)) (Vione et al., 2005); to finally forming 3,4-dichlorophenol (Figure 5.19b, (v)).
- (vi) To end, through an H abstraction of the OH group with a ^{*}OH radical, 3,4-dichlorophenol radical (3,4-DCP^{*}) is generated (Figure 5.19b, (vi)).

To follow, in Figure 5.20 is presented the HQ transformation pathway to 3,4-dichlorophenol radical, corroborated in terms of the spin values for the different bond possibilities that can appear depending on the spin value (value shown in red colour). It was used the Lewis structure to visualise better the electron positions. In a yellow colour box is represented the molecules detected in this thesis, HQ (Figure 5.20, (i)), Cl-HQ (Figure 5.20, (ii)), and 3,4-DCP (Figure 5.20, (v)). The H abstraction generates a structure which possesses a spin value of $0.95 e^{-1} au^{-3}$ in the C of the m- position of the HQ molecule (Figure 5.20, (i)). After this, when the H atom bonds in the C of the p- position, named here as C4, it can be generated three possible structures, with similar spin values between 0.38 and $0.45 e^{-1} au^{-3}$, where the highest value is situated in the C1 (with respect to the C4) (Figure 5.20, (iii)). After the subsequent Cl^{*} addition 3-chlorophenol is formed (Figure 5.20, (iv)), and the simultaneous H abstraction (by ^{*}OH radical) and other Cl^{*} addition, 3,4-DCP is formed (Figure 5.20, (v)). Finally, 3,4-DCP^{*} is formed through H abstraction, with other three molecular possibilities, also with similar spin values, between 0.27 - $0.38 e^{-1} au^{-3}$. The molecule with the highest spin value has the electron in the C4 ($0.38 e^{-1} au^{-3}$) and the second high in the C atom of the o- position ($0.28 e^{-1} au^{-3}$).

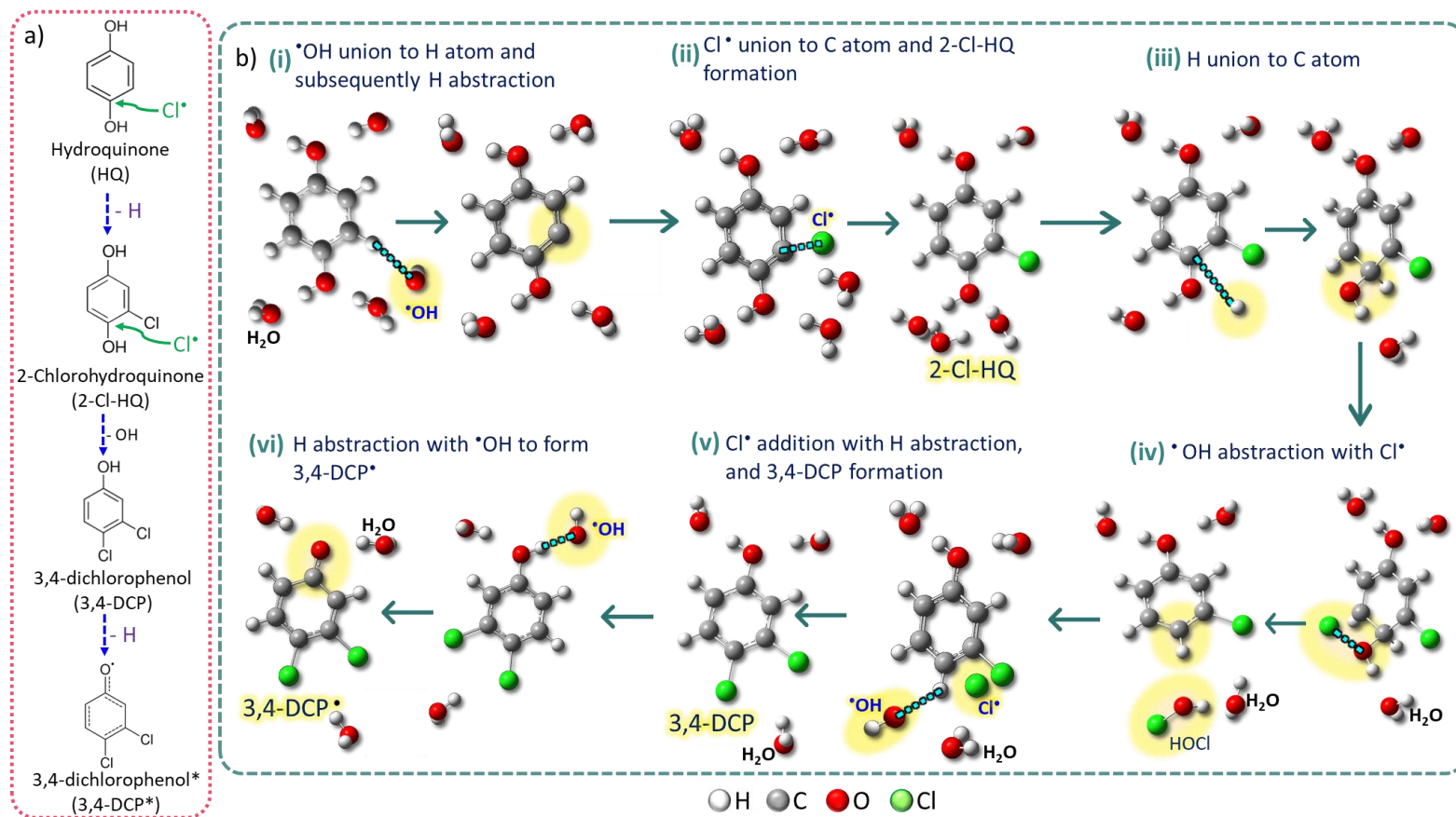


Figure 5.19. 3 a) Scheme of the 3,4-DCP* formation from HQ and b) DFT simulation molecules of the 3,4-DCP* formation.

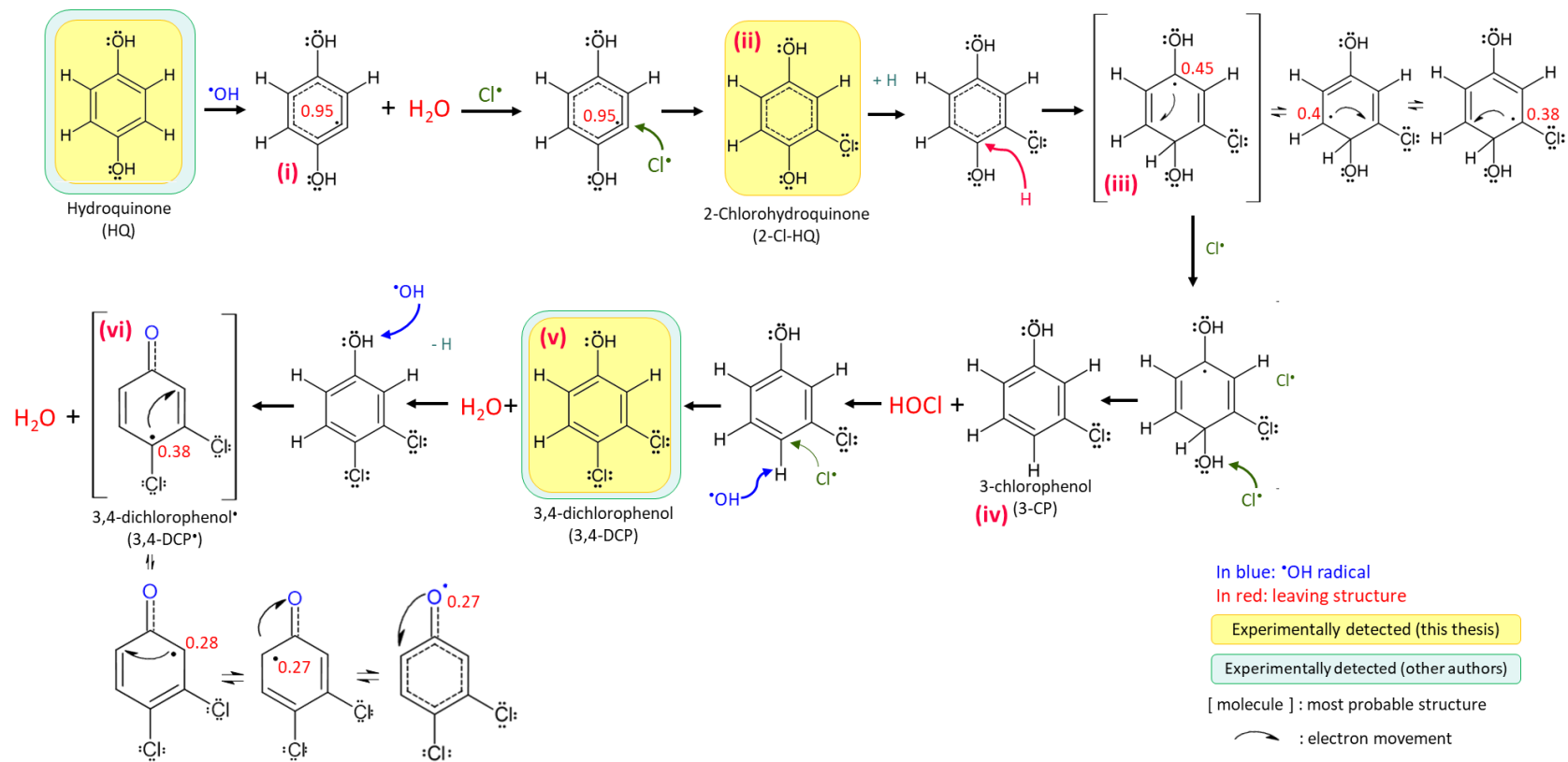


Figure 5.20. Detailed HQ to 3,4-DCP* transformation pathway in terms of the spin values, marked in red.

PCDD/Fs formation from 3,4-dichlorophenol

Part A – Combination of 3,4-DCP*

The last stage of this combined mechanism is shown in Figure 5.21. Figure 5.21a describes the common mechanism in a schematic way of the subsequent dioxins' formation, through a combination of two 3,4-dichlorophenol radicals, to form a pre dioxin (last step of Figure 5.21a). Figure 5.21b expands the information, depicting a mechanism with 3D representations of the molecules, obtained through the DFT calculations. This mechanism was broadly proposed in the literature (Briois et al., 2007; Fernández-Castro et al., 2016; Na et al., 2007; Pan et al., 2013; Ryu, 2008; Sidhu and Edwards, 2002; Sidhu et al., 1995; Vallejo, 2014; Wiater-Protas and Louw, 2001; Xu et al., 2010, 2015; Yang et al., 2017; Zhang et al., 2018, 2010, 1990, 2014) (Figure 5.11).

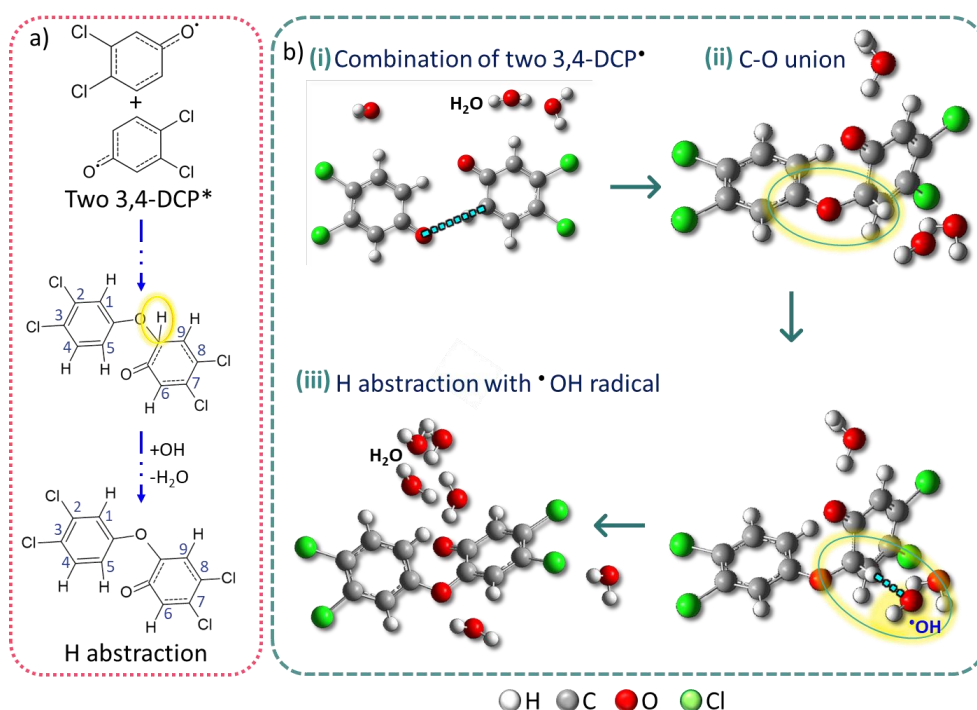


Figure 5.21. a) Scheme of the common stage of the PCDD/Fs formation and b) DFT simulation molecules of the mechanism.

Next, the steps depicted in the mentioned figures are detailed:

- (i) This mechanism starts with the combination of two 3,4-dichlorophenol radicals (Figure 5.21a and Figure 5.21b, (i)). Several authors have proposed the combination of two chlorophenol molecules to form dioxins, which can be mono-, di- or tri-chlorophenols (Briois et al., 2007; Fernández-Castro et al., 2016; Na et al., 2007; Pan

et al., 2013; Ryu, 2008; Sidhu and Edwards, 2002; Sidhu et al., 1995; Wiater-Protas and Louw, 2001; Xu et al., 2015, 2010; Yang et al., 2017; Zhang et al., 2018, 2010, 1990, 2014).

- (ii) These two molecules of 3,4-DCP* are bonded via a C-O bond (Figure 5.21a and Figure 5.21b, (ii), C1) (dashed blue line).
- (iii) Then, an H abstraction through its union to an *OH radical takes place, forming H₂O (Figure 5.21a and Figure 5.21b, (iii)).

Part B – PCDD/Fs formation

Afterwards, depending on where the C atom is going to be bonded, 2,3,7,8-TCDD or 1,2,7,8-TCDD can be formed, if the O atom bonds with C5 or C1, respectively, detailed in Figure 5.22 and Figure 5.23 with blue numbers. First, the mechanism is depicted in a schematic form (Figure 5.22a and Figure 5.23b) and second, using 3D representations, obtained after the computational calculations. Hereunder are detailed the steps carried out:

- (i) The O atom bonds with C5, Figure 5.22b, (i), or C1, twisting the molecule, Figure 5.23b, (i), respectively (see dashed blue line).
- (ii) Then, the H abstraction of the C atom where the bond has occurred takes place (C1 or C5), with a *OH radical, which leaves the molecule as H₂O (Figure 5.22b, (ii), C5; and Figure 5.23b, (ii), C1).
- (iii) Finally, 2,3,7,8-TCDD (Figure 5.22b, (iii)) and 1,2,7,8-TCDD (Figure 5.23b, (i)) are formed (see dashed blue line).

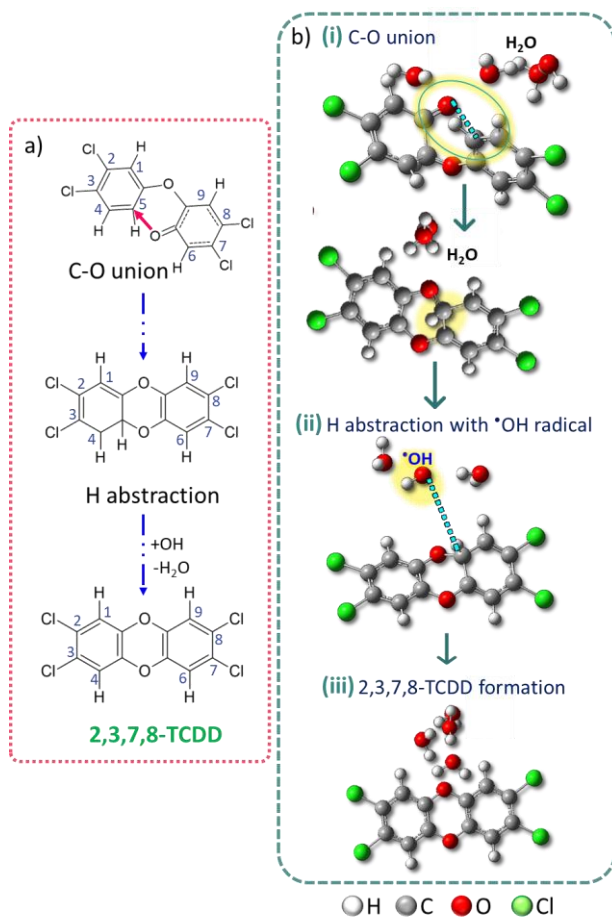


Figure 5.22. a) Scheme of the 2,3,7,8-TCDD formation and b) DFT simulation of the 2,3,7,8-TCDD.

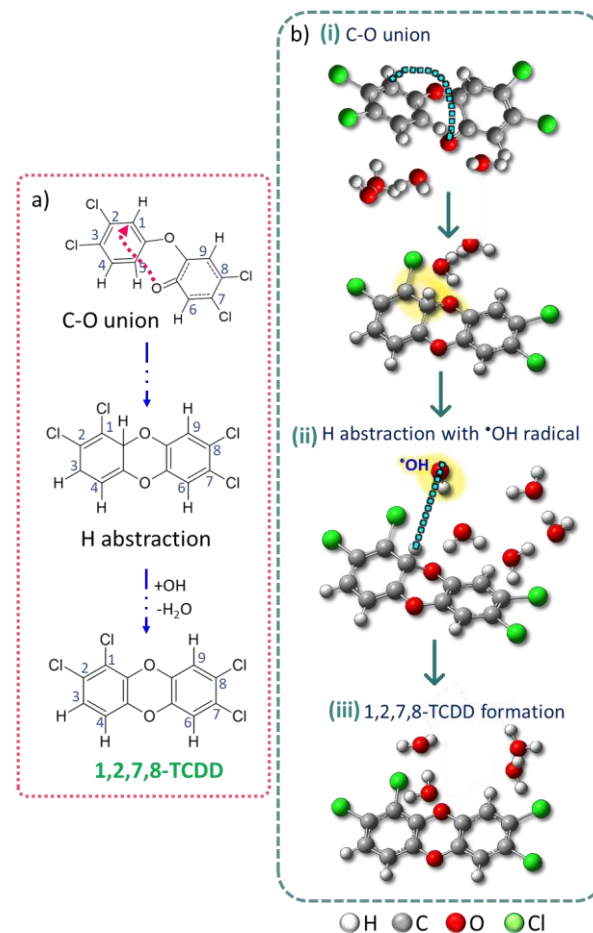


Figure 5.23. a) Scheme of the 1,2,7,8-TCDD formation and b) DFT simulation of the 1,2,7,8-TCDD.

Lastly, to corroborate the formation of these two dioxins, the 2,3,7,8-TCDD and 1,2,7,8-TCDD, in Figure 5.24 are represented the mechanisms using the Lewis structure next to the spin values (in red colour), which allow to appreciate the most probable structure, where different bond can appear. The yellow colour box represents the molecule detected in this thesis (2,3,7,8-TCDD). 2,3,7,8-TCDD is detected in the PCDD/Fs analysis through the EPA 1613 method (see Chapter 4, section 4.1.2), in low concentrations (0.2-2.1 $\mu\text{g L}^{-1}$). These values are difficult to appreciate in Figures of Chapter 4 due to the chart scale, however, the pertinent comments have been included the text. 1,2,7,8-TCDD is not detected in a direct manner, however, it is highly possible that is present in the TCDD group (see Chapter 4, section 4.1.1).

After the union of the two 3,4-DCP \cdot (Figure 5.24, (i)), four different structures are possible (Figure 5.24, (ii)), with spin values between 0.24-0.74 $\text{e}^{-1} \text{au}^{-3}$, the highest value corresponding to the C atom where the bond was created, and the second highest one, in m- position with respect to the mentioned C atom. Then, after a H abstraction (by $\cdot\text{OH}$ radical), also four different structures can be configured, with the spin values among 0.20-0.35 $\text{e}^{-1} \text{au}^{-3}$, placed in the same ring as in the previous step (Figure 5.24, (iii)). The highest spin value, 0.35 $\text{e}^{-1} \text{au}^{-3}$, is placed in the C atom of the p- position with respect to the C-O union. Following this, depending on where the next C-O union occurs, two molecules (Figure 5.24, (iv) and (v)), both with three structure possibilities, appears. Figure 5.24 (iv) possess spin values between 0.34 and 0.49 $\text{e}^{-1} \text{au}^{-3}$, with the highest value corresponding to C bonded to Cl atom in position 2; and Figure 5.24 (v), which has spin values between 0.36-0.51 $\text{e}^{-1} \text{au}^{-3}$, with the highest one on the C3 respecting the Cl atom in position 1). Starting from the molecules with high spin, identified by brackets, the target molecules, 2,3,7,8-TCDD (Figure 5.24, (vi)) and 1,2,7,8-TCDD (Figure 5.24, (vii)) are achieved.

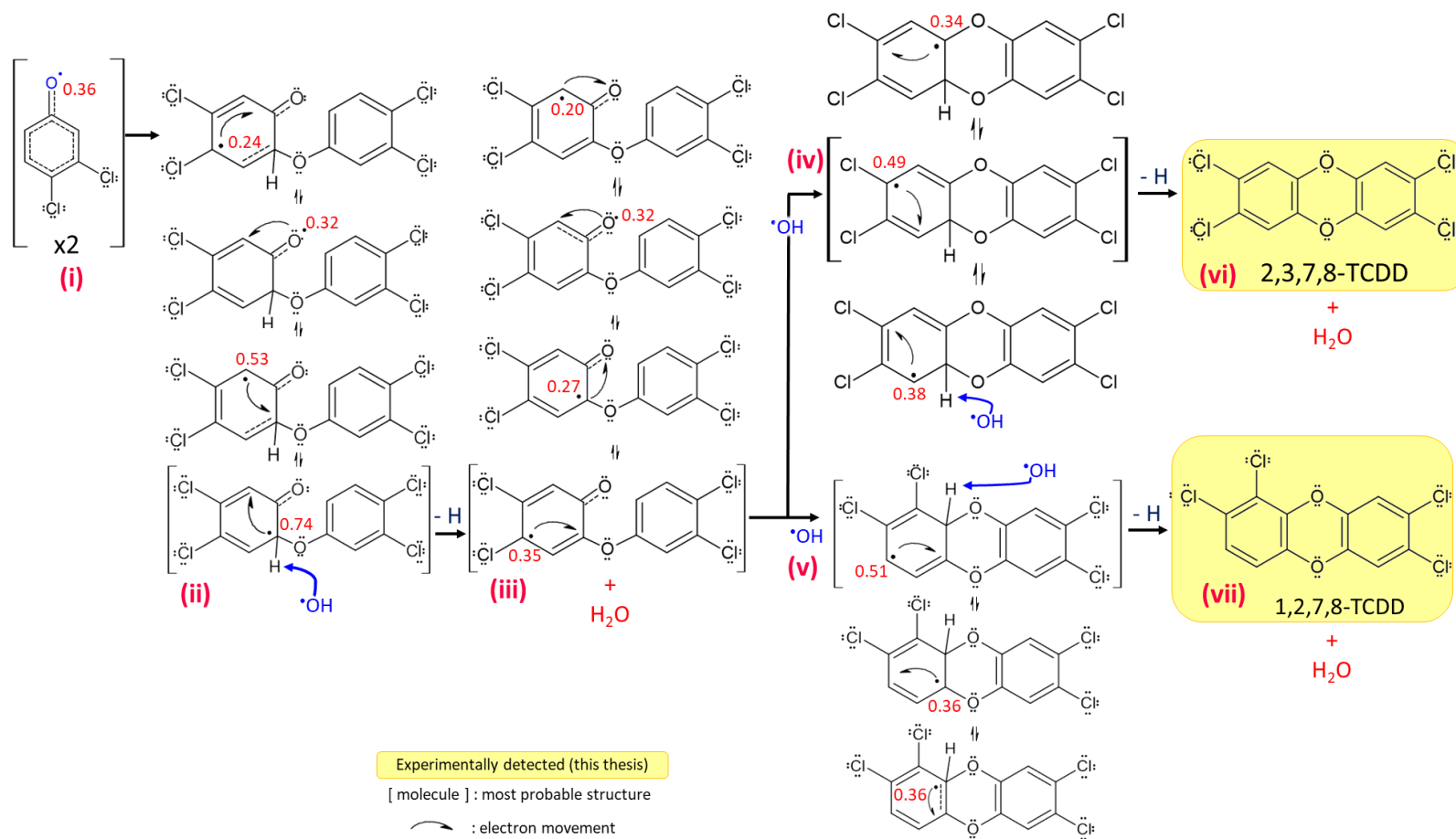


Figure 5.24. Detailed 3,4-DCP* to PCDD/Fs transformation pathway in terms of the spin values pointed out in red.

5.2.3. Energy profiles of the reaction mechanisms

Once the combined mechanisms have been developed, next, in accordance with the computational calculations carried out, in this section, energy profiles are presented for each stage. For this, the energy pathways are going to be detailed, where each point represents the energy (kcal/mol) of the reactants, products, transition states, or the different intermediates, produced along the degradation way. For all cases, in the energy charts, R corresponds to the reactants, P to the products, "Int" to the different intermediate structures, and "TS" to the transition states of each reaction. Moreover, along with the energy graphs, it is shown the vibrational frequencies obtained for each transition state, corroborating the obtention of a negative frequency (imaginary frequency) for each TS.

First, it has to be highlighted, that every time that something new was added, radicals or atoms, such as $\cdot\text{OH}$, $\text{Cl}\cdot$ or H, or eliminated from the system, it is necessary that the energy of the molecule resets to zero, due to the new geometry is different than in the previous step (there are a different number of atoms and/or atom positions). This fact applies to all the energy profiles detailed hereafter.

Drug molecules breakage

Amoxicillin

In Figure 5.25 is depicted the energy profile corresponding to the AMX degradation mechanism (Figure 5.12).

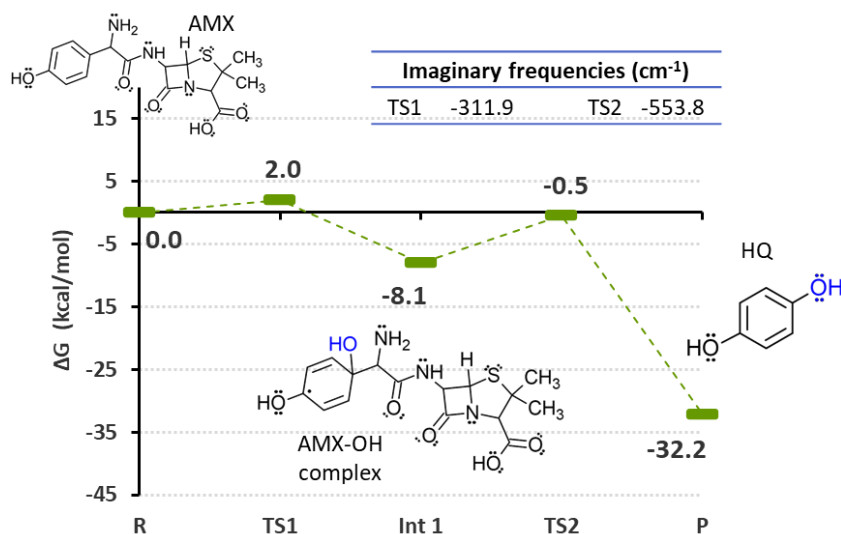


Figure 5.25. Energy profile of the AMX degradation pathway obtained by computational chemistry calculations using GAUSSIAN 16.

First, the AMX molecule is attacked by a $\cdot\text{OH}$ radical (Figure 5.25), where TS1 is the transition state correspondent to this step, with an imaginary frequency value of -311.9 cm^{-1} . Int1 is the AMX $\cdot\text{OH}$ complex formed (-8.1 kcal/mol), TS2 is the TS of the separation in two fragments of the $\cdot\text{OH}$ complex, and P is the energy of the HQ formed and the remaining fragment, -32.2 kcal/mol , corroborating that the final product is energetically stable. This mechanism, in terms of spin values, is shown in Figure 5.13. The energy profile for the other AMX mechanism can be found in Annex VIII.

Paracetamol

Figure 5.26 represents the energy profile of the PAR breakage (1st option) (detailed in Figure 5.14 and with spin values in Figure 5.16).

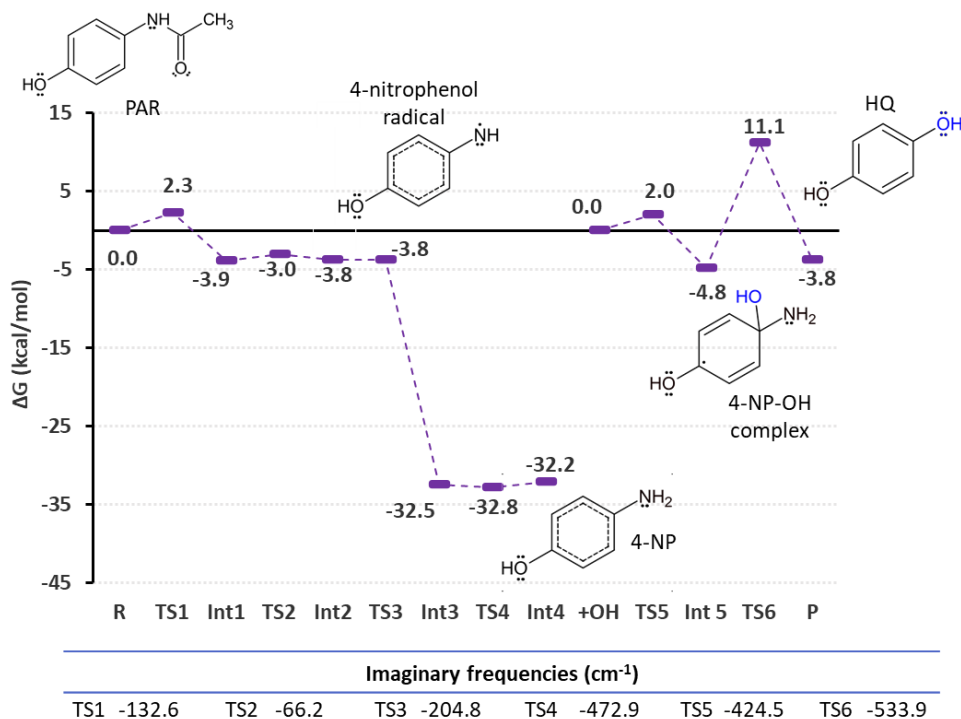


Figure 5.26. Energy profile of the PAR degradation pathway obtained by computational chemistry calculations using GAUSSIAN 16 (1st option).

As can be observed in this Figure, the first steps correspond to the $\cdot\text{OH}$ union to the peptide bond of PAR, being the TS1 the first transition state, corresponding to this stage. Next, the PAR with the OH bonded is represented by Int1, with an energy of -3.9 kcal/mol . Afterwards, the breakage of the molecule occurs, and the separation of the remaining parts takes place. This separation was carried out in two steps (T2 and TS3,

with imaginary frequencies of -66.17 and -204.84 cm^{-1}) In the first step, both fragments are close, and in the second step, the fragments are completely separated away, thus, ending in the final molecule Int3, with an energy of -32.5 kcal/mol. After the H addition, 4-nitrophenol (4-NP) is formed (Int4), being TS4 the correspondent transition state to this H addition, with an imaginary frequency of -472.86 cm^{-1} . The energy values from Int1 to Int4 vary between -3.9 and -32.2 kcal/mol. As it has explained previously, when something changes in the system, the energy is zero, here is when the last $\cdot\text{OH}$ is added to the C atom, being TS5 the TS of this $\cdot\text{OH}$ addition (-2.0 kcal/mol). Finally, the last three stages (Int5, TS6 and P), correspond with the separation of the fragments, being Int5 the 4-nitrophenol- $\cdot\text{OH}$ complex (-4.8 kcal/mol), and the final product (P), hydroquinone, which is generated after the separation of the NH_2 group of the molecule, with a final energy of -3.8 kcal/mol; which indicates that is a highly stable product. This mechanism, in terms of spin values, is shown in Figure 5.16.

In Figure 5.27 it is described the energy profile of the 2nd option of PAR breakage, with the mechanism detailed in Figure 5.15, and with the spin values in Figure 5.16. TS1 corresponds to the transition state where the Paracetamol- $\cdot\text{OH}$ complex is formed (Int1, -9.9 kcal/mol). After the separation of the fragments (TS2), the p-phenodiol radical is formed (Int2), with a energy of -17.2 kcal/mol. Then, a H addition occurs (TS3) which is further transformed into hydroquinone (P). Higher energy is obtained in the last step (1.6 kcal/mol), which means that, even though this pathway implies fewer steps than the 1st option, it is not favourable in energy terms.

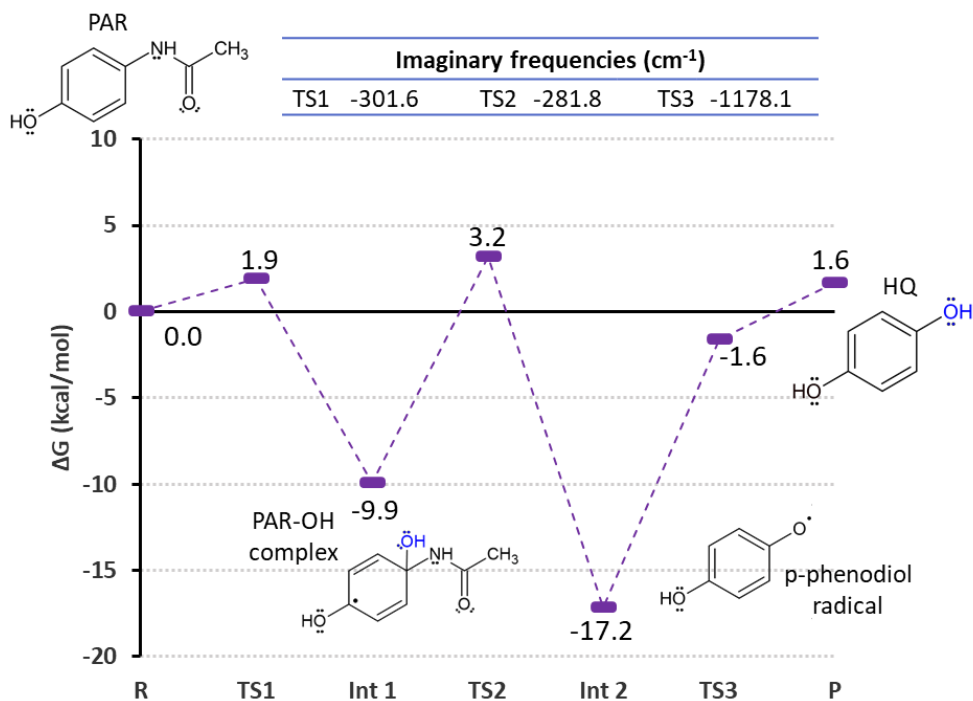


Figure 5.27. Energy profile of the PAR degradation pathway obtained by computational chemistry calculations using GAUSSIAN 16 (2nd option).

Sertraline

In Figure 5.28, the energy profile of the detailed mechanism in Figure 5.18 is represented (in terms of spin). TS1 corresponds to the [•]OH union to the PAR molecule (imaginary frequency of -341.63 cm⁻¹), with the further formation of the STR-[•]OH complex, which possesses an energy of -14.1 kcal/mol (Int1). After the separation of the fragments (TS2), the final product is formed (-33.6 kcal/mol), the 3,4-dichlorophenol and the remaining fragment (n-methyl-1-naphthalenamine). This low final energy value also demonstrates the stability of the system.

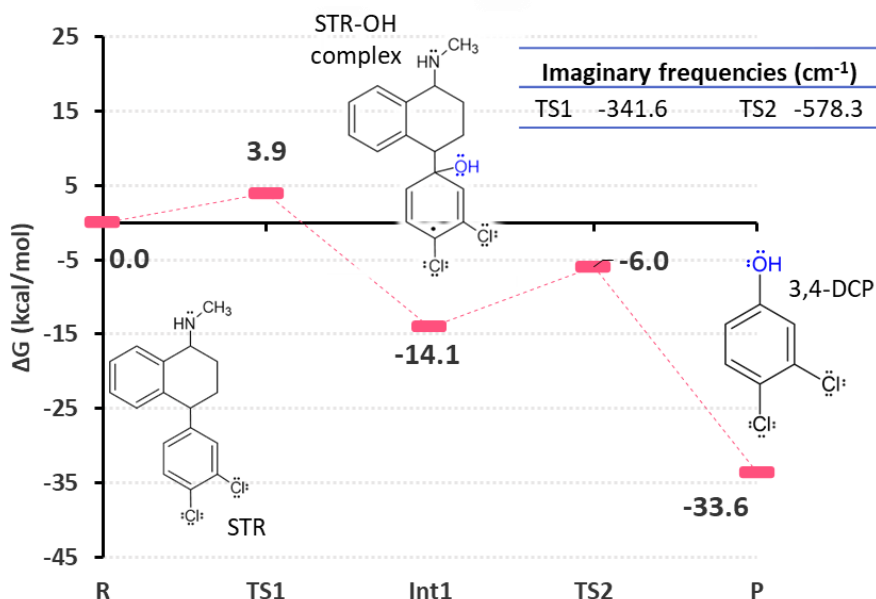


Figure 5.28. Energy profile of the STR degradation pathway obtained by computational chemistry calculations using GAUSSIAN 16.

Intermediates and PCDD/Fs formation

3,4-dichlorophenol from hydroquinone formation

The mechanism, in terms of spin values, shown in Figure 5.20, is detailed in Figure 5.29 in form of the energy profile. It starts with the HQ, which suffers a H loss (TS1) captured by a $\cdot\text{OH}$ radical (-3.8 kcal/mol). Through a $\text{Cl}\cdot$ addition, 2-chlorohydroquinone is formed (Int2), with an energy of -61.0 kcal/mol. This stage does not have an associated TS because the reaction is produced in a spontaneous way, this is by the direct addition to the molecule. Thus, it was not necessary to perform a scan and the further calculations detailed in section 5.1.1. After this, H is added to C4 of the molecule (Int3) (-20.7 kcal/mol), and subsequently, the $\cdot\text{OH}$ group leaves the molecule captured by a $\text{Cl}\cdot$ (TS3=-51.1 kcal/mol), remaining 3-chlorophenol (Int4) (-24.2 kcal/mol). Then, simultaneously, the $\text{Cl}\cdot$ addition to C atom takes place and the OH leaves the molecule (TS4), pushed away by the $\text{Cl}\cdot$ radical, generating 3,4-dichlorophenol (Int5, 72.4 kcal/mol. To summarise, Int3, Int4 and Int5 have energies in the range of -11.1 and -72.4 kcal/mol. As a final point, after a $\cdot\text{OH}$ addition (TS5), 3,4-DCP \cdot (P) is generated through a H elimination (-31.5 kcal/mol).

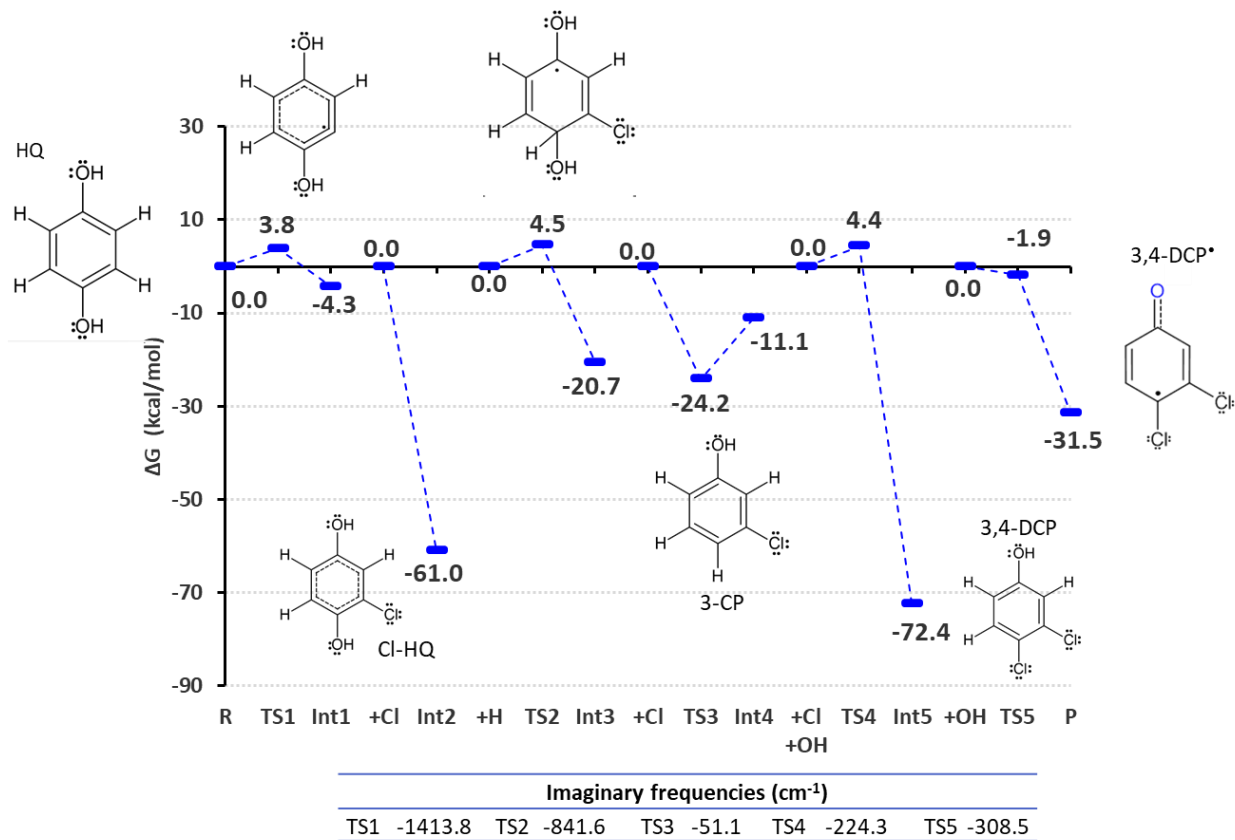


Figure 5.29. Energy profile for the HQ to 3,4DCP* transformation pathway obtained by computational chemistry calculations using GAUSSIAN 16.

2,3,7,8-TCDD and 1,2,7,8-TCDD formation from 3,4-dichlorophenol*

Finally, the energy profile for these dioxins 2,3,7,8-TCDD and 1,2,7,8-TCDD is depicted in Figure 5.30 and 5.31. These energy profiles represent the mechanism, in terms of spin values of the Figure 5.24. Starting with the combination of two 3,4-DCP*, TS1 is the corresponding transition state to the first C-O union (imaginary frequency of -579.6 cm^{-1}), and following this, TS2 is the transition state of the H atom leaving the molecule, forming Int2, with an energy of -61.9 kcal/mol . This part is common to both mechanisms, as it can be appreciated in both figures, in their energies and in the imaginary frequencies. Then, TS3 is the crucial point, when one or the other dioxin (2,3,7,8-TCDD or 1,2,7,8-TCDD) are formed, being the "2,3,7,8- option" shown in Figure 5.30 (TS3 = -232.9 cm^{-1} , -37.7 kcal/mol) and "1,2,7,8- option" in Figure 5.31 (TS3 = -209.4 cm^{-1} , -35.5 kcal/mol). Finally, after a second H abstraction with another *OH, both final products are obtained. It can be observed that 2,3,7,8-TCDD formation does not have a TS4, due to the final H abstraction occurring in a spontaneous manner (-84.0 kcal/mol). 1,2,7,8-TCDD reaches a value of the energy of -87.3 kcal/mol .

It can be understood that both pathways can occur simultaneously, because the energy profiles are pretty similar, and the difference between the final products is not relevant, because usually, the errors in energies obtained through DFT calculations can easily round 3 kcal/mol. Furthermore, the energy barriers are also equivalent, so chances are that these products are produced in similar amounts.

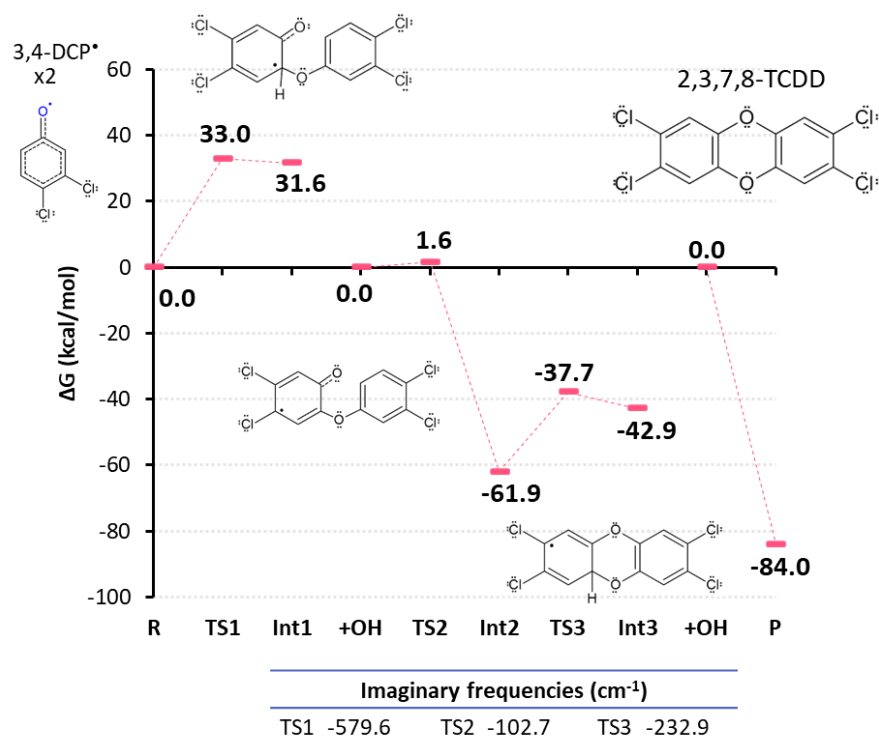


Figure 5.30. Energy profile for the 3,4DCP[•] to 2,3,7,8-TCDD transformation pathway obtained by computational chemistry calculations using GAUSSIAN 16.

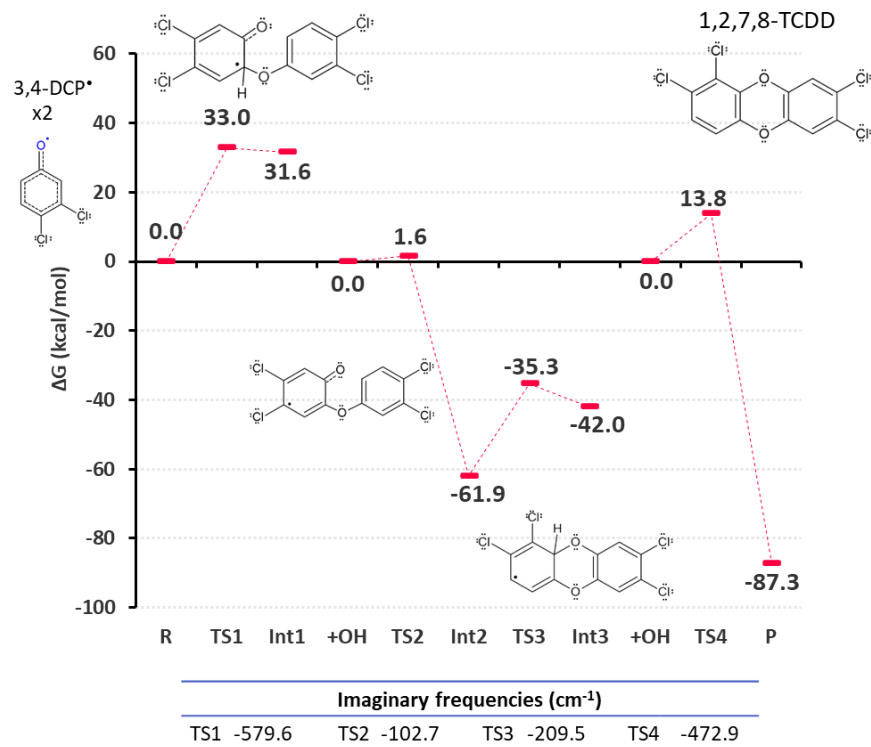


Figure 5.31. Energy profile for the 3,4DCP[•] to 1,2,7,8-TCDD transformation pathway obtained by computational chemistry calculations using GAUSSIAN 16.

5.3. References

- Bachrach, S.M., 2014. Computational organic chemistry, 2nd ed. Wiley.
- Briois, C., Ryan, S., Tabor, D., Touati, A., Gullett, B.K., 2007. Formation of polychlorinated dibenzo-p-dioxins and dibenzofurans from a mixture of chlorophenols over fly ash: Influence of water vapor. *Environ. Sci. Technol.* 41, 850–856. <https://doi.org/10.1021/es0613761>
- Calza, P., Jiménez-Holgado, C., Coha, M., Chrimatopoulos, C., Dal Bello, F., Medana, C., Sakkas, V., 2021. Study of the photoinduced transformations of sertraline in aqueous media. *Sci. Total Environ.* 756, 143805. <https://doi.org/10.1016/j.scitotenv.2020.143805>
- Chen, L., Ji, H., Qi, J., Huang, T., Wang, C.C., Liu, W., 2021. Degradation of acetaminophen by activated peroxymonosulfate using Co(OH)₂ hollow microsphere supported titanate nanotubes: Insights into sulfate radical production pathway through CoOH⁺ activation. *Chem. Eng. J.* 406, 126877. <https://doi.org/10.1016/j.cej.2020.126877>
- Cramer, C.J., 2004. Essentials of computational chemistry. Theories and models., 2nd ed. Wiley.
- De Luna, M.D.G., Veciana, M.L., Su, C.C., Lu, M.C., 2012. Acetaminophen degradation by electro-Fenton and photoelectro-Fenton using a double cathode electrochemical cell. *J. Hazard. Mater.* 217–218, 200–207. <https://doi.org/10.1016/j.jhazmat.2012.03.018>
- Deng, L., Ziegler, T., 1994. The determination of intrinsic reaction coordinates by density functional theory. *Int. J. Quantum Chem.* 52, 731–765. <https://doi.org/10.1002/qua.560520406>
- Evans, C.S., Dellinger, B., 2005. Mechanisms of dioxin formation from the high-temperature oxidation of 2-bromophenol. *Environ. Sci. Technol.* 39, 2128–2134. <https://doi.org/10.1021/es048461y>
- Fernández-Castro, P., 2017. Progress in the reactivity of Advanced Oxidation media. Application to the Fenton treatment of 2-chlorophenol solutions. University of Cantabria.
- Fernández-Castro, P., San Román, M.F., Ortiz, I., 2016. Theoretical and experimental formation of low chlorinated dibenzo-p-dioxins and dibenzofurans in the Fenton oxidation of chlorophenol solutions. *Chemosphere* 161, 136–144. <https://doi.org/10.1016/j.chemosphere.2016.07.011>
- Ferreira, M., Kuzniarska-Biernacka, I., Fonseca, A.M., Neves, I.C., Soares, O.S.G.P., Pereira, M.F.R., Figueiredo, J.L., Parpot, P., 2020. Electrochemical oxidation of amoxicillin on carbon nanotubes and carbon nanotube supported metal modified electrodes. *Catal. Today* 357, 322–331. <https://doi.org/10.1016/j.cattod.2019.06.039>

- Frontistis, Z., Antonopoulou, M., Venieri, D., Konstantinou, I., Mantzavinos, D., 2017. Boron-doped diamond oxidation of amoxicillin pharmaceutical formulation: Statistical evaluation of operating parameters, reaction pathways and antibacterial activity. *J. Environ. Manage.* 195, 100–109. <https://doi.org/10.1016/j.jenvman.2016.04.035>
- Fukui, K., 1970. A formulation of the reaction coordinate. *J. Phys. Chem.* 74, 4161. <https://doi.org/10.1021/j100717a029>
- Ganiyu, S.O., Oturan, N., Raffy, S., Cretin, M., Causserand, C., Oturan, M.A., 2019. Efficiency of plasma elaborated sub-stoichiometric titanium oxide (Ti4O7) ceramic electrode for advanced electrochemical degradation of paracetamol in different electrolyte media. *Sep. Purif. Technol.* 208, 142–152. <https://doi.org/10.1016/j.seppur.2018.03.076>
- Gornik, T., Kovacic, A., Heath, E., Hollender, J., Kosjek, T., 2020. Biotransformation study of antidepressant sertraline and its removal during biological wastewater treatment. *Water Res.* 181, 115864. <https://doi.org/10.1016/j.watres.2020.115864>
- Gupta, V.P., 2016. Electron Density Analysis and Electrostatic Potential. *Princ. Appl. Quantum Chem.* 195–214. <https://doi.org/10.1016/b978-0-12-803478-1.00006-6>
- Hong, J., Im, D., Heong, C., Ung, S., Oo, M., Im, K., 2000. "Identification of photolytical transformation products of pentachlorophenol in water." *Anal. Sci.* 16, 621–626.
- Ishida, K., Morokuma, K., Komornicki, A., 1976. The intrinsic reaction coordinate. An ab initio calculation for $\text{HNC} \rightarrow \text{HCN}$ and $\text{H} + \text{CH}_4 \rightarrow \text{CH}_3 + \text{H}$. *J. Chem. Phys.* 66, 2153–2156. <https://doi.org/10.1063/1.434152>
- IUPAC, 2019. *Compendium of Chemical Terminology*, 2nd ed. (t. ed. Blackwell Scientific Publications, Oxford (1997). <https://doi.org/https://doi.org/10.1351/goldbook.R05168>
- IUPAC, 2008. *Spin Density*, 2nd ed, *The IUPAC Compendium of Chemical Terminology*. Blackwell Scientific Publications, Oxford (1997). <https://doi.org/10.1351/goldbook.s05864>
- Jensen, F., 2007. *Introduction to Computational Chemistry, Theoretical Chemistry Accounts*.
- Jiménez-Holgado, C., Sakkas, V., Richard, C., 2021. Phototransformation of three psychoactive drugs in presence of sedimental water extractable organic matter. *Molecules* 26, 1–17. <https://doi.org/10.3390/molecules26092466>
- Le, T.X.H., Nguyen, T. Van, Amadou Yacouba, Z., Zoungrana, L., Avril, F., Nguyen, D.L., Petit, E., Mendret, J., Bonniol, V., Bechelany, M., Lacour, S., Lesage, G., Cretin, M., 2017. Correlation between degradation pathway and toxicity of acetaminophen and its by-products by using the electro-Fenton process in aqueous media. *Chemosphere* 172, 1–9. <https://doi.org/10.1016/j.chemosphere.2016.12.060>

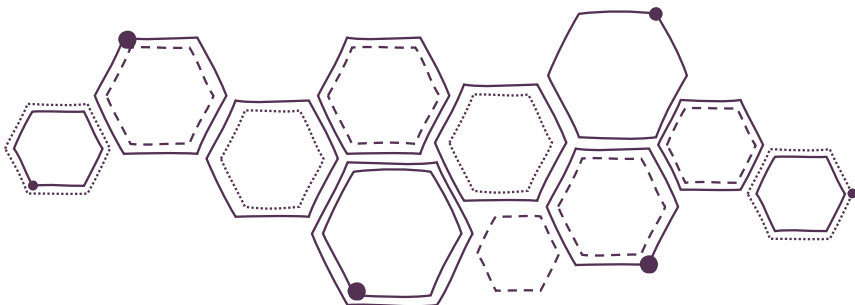
- Lewars, E.G., 2016. Computational chemistry: Introduction to the theory and applications of molecular and quantum mechanics: Third Edition 2016, Computational Chemistry: Introduction to the Theory and Applications of Molecular and Quantum Mechanics: Third Edition 2016. <https://doi.org/10.1007/978-3-319-30916-3>
- Li, Y., Han, Y., Teng, Z., Zhao, X., Sun, Y., Xu, F., Zhang, Q., Wang, W., 2021. The homogeneous gas-phase formation mechanisms of PCPTs/PCDTs/PCDFs from the radical/radical cross-condensation of 2-CPR and 2-CTPR: a theoretical, mechanistic and kinetics study. *RSC Adv.* 11, 12626–12640. <https://doi.org/10.1039/d1ra00599e>
- Liu, Y.J., Hu, C.Y., Lo, S.L., 2019. Direct and indirect electrochemical oxidation of amine-containing pharmaceuticals using graphite electrodes. *J. Hazard. Mater.* 366, 592–605. <https://doi.org/10.1016/j.jhazmat.2018.12.037>
- Na, Y.C., Kim, K.J., Park, C.S., Hong, J., 2007. Formation of tetrahalogenated dibenzo-p-dioxins (TXDDs) by pyrolysis of a mixture of 2,4,6-trichlorophenol and 2,4,6-tribromophenol. *J. Anal. Appl. Pyrolysis* 80, 254–261. <https://doi.org/10.1016/j.jaap.2007.03.002>
- Nykamp, D.Q., 2022. Graph of a hyperbolic paraboloid [WWW Document]. Math Insight. URL http://mathinsight.org/applet/graph_hyperbolic_paraboloid
- Okamoto, Y., 1999. Formation pathways from 2,4,5-trichlorophenol (TCP) to polychlorinated dibenzo-p-dioxins (PCDDs): An ab initio study. *J. Phys. Chem. A* 103, 7686–7691. <https://doi.org/10.1021/jp991383u>
- Olaniran, A.O., Igbinsosa, E.O., 2011. Chlorophenols and other related derivatives of environmental concern: Properties, distribution and microbial degradation processes. *Chemosphere* 83, 1297–1306. <https://doi.org/10.1016/j.chemosphere.2011.04.009>
- Olvera-Vargas, H., Rouch, J.C., Coetsier, C., Cretin, M., Causserand, C., 2018. Dynamic cross-flow electro-Fenton process coupled to anodic oxidation for wastewater treatment: Application to the degradation of acetaminophen. *Sep. Purif. Technol.* 203, 143–151. <https://doi.org/10.1016/j.seppur.2018.03.063>
- Pan, G., Sun, X., Sun, Z., 2020. Fabrication of multi-walled carbon nanotubes and carbon black co-modified graphite felt cathode for amoxicillin removal by electrochemical advanced oxidation processes under mild pH condition. *Environ. Sci. Pollut. Res.* 27, 8231–8247. <https://doi.org/10.1007/s11356-019-07358-2>
- Pan, G., Sun, Z., 2021. Cu-doped g-C₃N₄ catalyst with stable CuO and Cu⁺ for enhanced amoxicillin degradation by heterogeneous electro-Fenton process at neutral pH. *Chemosphere* 283, 131257. <https://doi.org/10.1016/j.chemosphere.2021.131257>
- Pan, W., Zhang, D., Han, Z., Zhan, J., Liu, C., 2013. New insight into the formation mechanism of PCDD/Fs from 2-chlorophenol precursor. *Environ. Sci. Technol.* 47, 8489–8498. <https://doi.org/10.1021/es400632j>

- Peller, J., Wiest, O., Kamat, P. V., 2003. Mechanism of Hydroxyl Radical-Induced Breakdown of the Herbicide 2,4-Dichlorophenoxyacetic Acid (2,4-D). *Chem. - A Eur. J.* 9, 5379–5387. <https://doi.org/10.1002/chem.200204469>
- Periyasamy, S., Muthuchamy, M., 2018. Electrochemical oxidation of paracetamol in water by graphite anode: Effect of pH, electrolyte concentration and current density. *J. Environ. Chem. Eng.* 6, 7358–7367. <https://doi.org/10.1016/j.jece.2018.08.036>
- Qutob, M., Hussein, M.A., Alamry, K.A., Rafatullah, M., 2022. A review on the degradation of acetaminophen by advanced oxidation process: pathway, by-products, biotoxicity, and density functional theory calculation. *RSC Adv.* 12, 18373–18396. <https://doi.org/10.1039/d2ra02469a>
- Ryu, J.Y., 2008. Formation of chlorinated phenols, dibenzo-p-dioxins, dibenzofurans, benzenes, benzoquinones and perchloroethylenes from phenols in oxidative and copper (II) chloride-catalyzed thermal process. *Chemosphere* 71, 1100–1109. <https://doi.org/10.1016/j.chemosphere.2007.10.036>
- Schlegel, H.B., 2003. Exploring potential energy surfaces for chemical reactions: An overview of some practical methods. *J. Comput. Chem.* 24, 1514–1527. <https://doi.org/10.1002/jcc.10231>
- Sidhu, S., Edwards, P., 2002. Role of phenoxy radicals in PCDD/F formation. *Int. J. Chem. Kinet.* 34, 531–541. <https://doi.org/10.1002/kin.10083>
- Sidhu, S.S., Maqsood, L., Dellinger, B., Mascolo, G., 1995. The homogeneous, gas-phase formation of chlorinated and brominated dibenzo-p-dioxin from 2,4,6-trichloro- and 2,4,6-tribromophenols. *Combust. Flame* 100, 11–20. [https://doi.org/10.1016/0010-2180\(94\)00057-Y](https://doi.org/10.1016/0010-2180(94)00057-Y)
- Solá-Gutiérrez, C., 2019. Traceability of PCDD/Fs formation in the advanced oxidation of TCS. University of Cantabria.
- Sun, R., Huang, W., Zhang, Q., Hong, J. ming, 2018. Facilely Prepared N-Doped Graphene/Pt/TiO₂ as an Efficient Anode for Acetaminophen Degradation. *Catal. Letters* 148, 2418–2431. <https://doi.org/10.1007/s10562-018-2466-5>
- Vallejo, M., 2014. Assessment of polychlorinated dibenzo-p-dioxins and dibenzofurans, PCDD/Fs, in the application of advanced oxidation processes. University of Cantabria.
- Vallejo, M., Fernández-Castro, P., San Román, M.F., Ortiz, I., 2015. Assessment of PCDD/Fs formation in the Fenton oxidation of 2-chlorophenol: influence of the iron dose applied. *Chemosphere* 137, 135–141. <https://doi.org/10.1016/j.chemosphere.2015.06.056>
- Vallejo, M., San Román, M.F., Ortiz, I., 2013. Quantitative assessment of the formation of polychlorinated derivatives, PCDD/Fs, in the electrochemical oxidation of 2-chlorophenol as function of the electrolyte type. *Environ. Sci. Technol.* 47, 12400–12408. <https://doi.org/10.1021/es403246g>

- Vallejo, M., San Román, M.F., Ortiz, I., Irabien, A., 2014. The critical role of the operating conditions on the fenton oxidation of 2-chlorophenol: Assessment of PCDD/Fs formation. *J. Hazard. Mater.* 279, 579–585. <https://doi.org/10.1016/j.jhazmat.2014.07.020>
- Vione, D., Maurino, V., Minero, C., Calza, P., Pelizzetti, E., 2005. Phenol chlorination and photochlorination in the presence of chloride ions in homogeneous aqueous solution. *Environ. Sci. Technol.* 39, 5066–5075. <https://doi.org/10.1021/es0480567>
- Weber, R., 2007. Relevance of PCDD/PCDF formation for the evaluation of POPs destruction technologies - Review on current status and assessment gaps. *Chemosphere* 67, 109–117. <https://doi.org/10.1016/j.chemosphere.2006.05.094>
- Wiater-Protas, I., Louw, R., 2001. Gas-phase chemistry of chlorinated phenols - Formation of dibenzofurans and dibenzodioxins in slow combustion. *European J. Org. Chem.* 3945–3952. [https://doi.org/10.1002/1099-0690\(200110\)2001:20<3945::AID-EJOC3945>3.0.CO;2-7](https://doi.org/10.1002/1099-0690(200110)2001:20<3945::AID-EJOC3945>3.0.CO;2-7)
- Williams, D., 2019. CHEM 4448 Physical Chemistry Lectures.
- Xu, F., Shi, X., Li, Y., Zhang, Q., 2015. Mechanistic and kinetic studies on the homogeneous gas-phase formation of PCTA/DTs from 2,4-dichlorothiophenol and 2,4,6-trichlorothiophenol. *Int. J. Mol. Sci.* 16, 20449–20467. <https://doi.org/10.3390/ijms160920449>
- Xu, F., Wang, H., Zhang, Q., Zhang, R., Qu, X., Wang, W., 2010. Kinetic properties for the complete series reactions of chlorophenols with OH radicals - Relevance for dioxin formation. *Environ. Sci. Technol.* 44, 1399–1404. <https://doi.org/10.1021/es9031776>
- Yang, L., Liu, G., Zheng, M., Zhao, Y., Jin, R., Wu, X., Xu, Y., 2017. Molecular Mechanism of Dioxin Formation from Chlorophenol based on Electron Paramagnetic Resonance Spectroscopy. *Environ. Sci. Technol.* 51, 4999–5007. <https://doi.org/10.1021/acs.est.7b00828>
- Zhang, Q., Huang, W., Hong, J. ming, Chen, B.Y., 2018. Deciphering acetaminophen electrical catalytic degradation using single-form S doped graphene/Pt/TiO₂. *Chem. Eng. J.* 343, 662–675. <https://doi.org/10.1016/j.cej.2018.02.089>
- Zhang, Q., Yu, W., Zhang, R., Zhou, Q., Gao, R., Wang, W., 2010. Quantum chemical and kinetic study on dioxin formation from the 2,4,6-TCP and 2,4-DCP precursors. *Environ. Sci. Technol.* 44, 3395–3403. <https://doi.org/10.1021/es1004285>
- Zhang, Q., Yu, W., Zhang, R., Zhou, Q., Gao, R., Wang, W., 1990. Supporting Information for Quantum Chemical and Kinetic Study on Dioxin Precursors 1–54.
- Zhang, Y., Zhang, D., Gao, J., Zhan, J., Liu, C., 2014. New understanding of the formation of PCDD/Fs from chlorophenol precursors: A mechanistic and kinetic study. *J. Phys. Chem. A* 118, 449–456. <https://doi.org/10.1021/jp410077g>



CONCLUSIONS / CONCLUSIONES



This PhD thesis has been carried out in the framework of the investigation line “Potential formation of PCDD/Fs during the treatment aqueous matrices by AOPs”, developed in the last years within the research groups Sustainable Process Engineering (SPE) and Advance Separation Process (ASP) of the University of Cantabria. This research line focuses on the evaluation of the formation of PCDD/Fs in aqueous matrices, containing precursor or not precursor compounds -in chloride medium- of these, and as consequence, after applying AOPs, the final toxicity of the aqueous sample increases respect to the initial. Therefore, the correct evaluation of the matrix, technology to be applied and operating conditions are key to the implementation of AOPs as wastewater treatment technologies. In order to corroborate this hypothesis, this doctoral thesis has assessed the formation of PCDD/Fs and the final toxicity of the samples, after applying electrochemical oxidation to matrices containing the most used drugs in the fight against COVID-19, namely, dexamethasone (DEX), amoxicillin (AMX), paracetamol (PAR) and sertraline (STR). Gathering all the results obtained in this work, together with the reviewed bibliography, this thesis has led to the following conclusions:

ELECTROCHEMICAL OXIDATION (EOX) OF COVID-19 DRUGS

In Chapter 3, the electrochemical oxidation of aqueous samples containing the COVID-19 drugs, DEX, AMX, PAR and STR, was carried out, employing a BDD anode and working in galvanostatic mode, with two different electrolyte media: NaCl (56 mM) and Na₂SO₄+NaCl (21 mM+2.8 mM). For the degradation experiments (EOX-Drugs), 10 mg L⁻¹ of each drug, as the initial concentration were employed, whereas in the experiments aimed to analyse the intermediate compounds (EOX-Intermediates), the initial concentrations were higher, 80 mg L⁻¹ for DEX and 3000 mg L⁻¹ for the rest. Consequently, the applied current density varied depending on the type of experiment.

EOX-Drugs & EOX-Intermediates

All drugs were completely oxidized, independently of the initial concentration; for EOX-Drugs, the specific electrical charge (Q) was below 0.6 A h L⁻¹ for both electrolyte media, and specifically, below 0.1 for AMX, PAR and STR in NaCl medium and 0.5 A h L⁻¹ in Na₂SO₄+NaCl medium, respectively. The fastest degradation corresponded to STR and the slowest one to DEX, in both cases when using NaCl medium. Besides, the same degradation tendency for NaCl and Na₂SO₄+NaCl electrolytes was found: STR > AMX > PAR > DEX.

Finally, the kinetics of the drugs degradation were fitted to pseudo-first-order kinetics with the following rate constants; for NaCl as electrolyte, STR $k \approx 0.101\text{-}0.999 \text{ min}^{-1}$, AMX $k \approx 0.051\text{-}0.236 \text{ min}^{-1}$, PAR $k \approx 0.036\text{-}0.145 \text{ min}^{-1}$ and DEX $k \approx 0.011 \text{ min}^{-1}$ and for Na₂SO₄+NaCl as electrolyte, STR $k \approx 0.040\text{-}0.144 \text{ min}^{-1}$, AMX $k \approx 0.033\text{-}0.044 \text{ min}^{-1}$, PAR $k \approx 0.022\text{-}0.026 \text{ min}^{-1}$ and DEX $k \approx 0.016\text{-}0.017 \text{ min}^{-1}$.

Influence of radicals in drugs' degradation

As reflected in the literature, and taking into account the formation rate of the oxidising species and radicals, the redox potential, the degradation rate of •OH radicals ($10^9\text{-}10^{11} \text{ M}^{-1}\text{s}^{-1}$) and the experimental results, the main species and radicals in NaCl medium which participate in the degradation of DEX, AMX, PAR and STR can be •OH (2.73 V), Cl• (2.43 V), Cl₂^{•-} (2.13 V), ClOH^{•-} (1.91 V), HClO (1.6 V) and Cl₂ (1.4 V).

On the other hand, analysing Na₂SO₄+NaCl medium, it can be concluded that the principal radicals and species involved in the degradation of these four mentioned drugs, are mainly •OH radical (2.73 V), followed by SO₄^{•-} radical (2.43 V) and the specie S₂O₈^{2•-} (1.44 V), and finally, given its low concentration, the rest of the radicals and chloride species, Cl• (2.43 V), Cl₂^{•-} (2.13 V), ClOH^{•-} (1.91 V), HClO (1.6 V) and Cl₂ (1.4 V), which justifies the need for a longer oxidation time compared to the experiments carried out in NaCl medium.

Intermediates: Identification and kinetic analysis

The analysis of the oxidation intermediates was carried out through the EOX-Intermediates experiments (high concentration of drugs). The main precursors or precursors compounds of precursors of PCDD/Fs identified were:

- i) For DEX, the precursor 2,4-dichlorophenol was identified in chloride medium. It can be highlighted that DEX-alike compounds, such as 1-dehydrotestosterone (DHT) and methandrostenolone (MTT) in Na₂SO₄+NaCl medium, and beclomethasone (BCM) and naphthalene (NAP) in NaCl medium, were found.
- ii) For AMX, a good number of precursor compounds of PCDD/Fs such as 2,4-dichlorophenol (2,4-DCP), 4-chlorophenol (4-CP), and 2,4,5-trichlorophenol (2,4,5-TCP), added to other precursors compounds of the precursors of PCDD/Fs as hydroquinone (HQ) or chlorohydroquinone (Cl-HQ), were found for NaCl medium. For the Na₂SO₄+NaCl medium, also HQ and Cl-HQ were detected.

- iii) For PAR, also some PCDD/Fs precursors were detected for NaCl medium, 2,4,5-TCP, and precursors of the precursors, such as HQ and Cl-HQ. For the Na₂SO₄+NaCl medium, the precursor 3,4-dichlorophenol (3,4-DCP) and some fragments of the PAR molecule, like 4-nitrophenol (4-NP) were detected.
- iv) For STR, several chlorophenols were detected in both electrolytic media, as 3,4-DCP, 2,4,5-TCP and 2,3,4,6-tetrachlorophenol (2,3,4,6-TeCP). Moreover, in Na₂SO₄+NaCl medium, another trichlorophenol was detected, 2,3,4-trichlorophenol (2,3,4-TCP). Also, for both electrolytic media, STR fragments were detected, as n-methyl-1-naphthalenamine (MNA).

PCDD/Fs DURING EOx OF DRUGS: TOXICITY ASSESSMENT

Homologues profile

In Chapter 4, the study of the formation of highly chlorinated dioxins and furans (PCDD/Fs) was conducted, for the experiments with 10 mg L⁻¹ of the primary compound, in samples where the drugs had been entirely eliminated, after applying electrochemical oxidation. PCDD/Fs were prepared and analysed by Standard Method U.S. EPA 1613 by isotope dilution and high-resolution gas chromatography coupled to high-resolution mass spectrometry (HRGC-HRMS). The main obtained conclusions were:

- i) The total amount of generated PCDD/Fs was higher in NaCl medium versus for Na₂SO₄+NaCl medium, except for the STR, where the PCDD/Fs concentration was similar for both electrolyte media. AMX presented the values higher of the total PCDD/Fs.
- ii) For NaCl medium, PCDFs were generated in greater quantities than PCDDs in all cases. For Na₂SO₄+NaCl as electrolyte, the observed trend is the opposite, except for DEX.
- iii) Deepening into the homologues, the higher chlorinated furans, such as HxCDF for samples with DEX, AMX and PAR (NaCl medium), are formed in high concentrations

Below, Table 6.1 shows a summary that includes all the results obtained.

Table 6.1. Total amount (pg L⁻¹) and percentage of homologue groups produced during the DEX, AMX, PAR and STR degradation (NaCl and Na₂SO₄+NaCl as electrolytes).

Drugs	Electrolyte	PCDDs pg L ⁻¹ (%)	PCDFs pg L ⁻¹ (%)	TOTAL Homologue pg L ⁻¹ (%)
DEX	56 mM NaCl	123.2 (47.1%)	137.9 (52.9%)	261.1 (100%)
	21 mM Na ₂ SO ₄ + 2.8 mM NaCl	113.7 (58.4%)	81.1 (41.6%)	194.8 (100%)
AMX	56 mM NaCl	12.9 (0.5%)	2648.4 (99.5%)	2661.3 (100%)
	21 mM Na ₂ SO ₄ + 2.8 mM NaCl	20.6 (2.1%)	964.1 (97.9%)	984.7 (100%)
PAR	56 mM NaCl	15.3 (2.7%)	548.2 (97.3%)	563.5 (100%)
	21 mM Na ₂ SO ₄ + 2.8 mM NaCl	45.7 (26.3%)	127.9 (73.7%)	173.6 (100%)
STR	56 mM NaCl	51.7 (47.5%)	57.2 (52.5%)	108.9 (100%)
	21 mM Na ₂ SO ₄ + 2.8 mM NaCl	122.2 (78.5%)	33.5 (21.5%)	155.7 (100%)

Congeners profile

Below, Table 6.2 shows a summary that includes all the results obtained.

Table 6.2. Total amount (pg L⁻¹) and percentage of of 2,3,7,8-PCDD/Fs congeners produced during the DEX, AMX, PAR and STR degradation (NaCl and Na₂SO₄+NaCl as electrolytes).

Drug	Electrolyte	2,3,7,8-PCDDs pg L ⁻¹ (%)	2,3,7,8-PCDFs pg L ⁻¹ (%)	TOTAL 2,3,7,8- congeners pg L ⁻¹ (%)
DEX	56 mM NaCl	80.2 (83.5%)	15.9 (16.5%)	96.1 (100%)
	21 mM Na ₂ SO ₄ + 2.8 mM NaCl	46.8 (89.0%)	5.8 (11.0%)	52.6 (100%)
AMX	56 mM NaCl	7.3 (2.9%)	242.0 (97.1%)	249.3 (100%)
	21 mM Na ₂ SO ₄ + 2.8 mM NaCl	4.6 (3.5%)	126.2 (96.5%)	130.8 (100%)
PAR	56 mM NaCl	30.4 (44.2%)	38.3 (55.8%)	68.7 (100%)
	21 mM Na ₂ SO ₄ + 2.8 mM NaCl	20.9 (57.9%)	15.2 (42.1%)	36.1 (100%)
STR	56 mM NaCl	60.4 (86.8%)	9.2 (13.2%)	69.6 (100%)
	21 mM Na ₂ SO ₄ + 2.8 mM NaCl	27.9 (67.1%)	13.7 (32.9%)	41.7 (100%)

- i) Analysing the congeners, the total amount of 2,3,7,8-PCDD/Fs congeners was, in all cases, higher when using NaCl as electrolyte than when using Na₂SO₄+NaCl electrolyte media.
- ii) For the NaCl case, the dioxins congeners were higher for DEX and STR and contrarily, for AMX and PAR, the furans congeners were the predominating group. In the Na₂SO₄+NaCl medium, 2,3,7,8-PCDDs were higher in all cases except for AMX.

- iii) The most toxic dioxin, 2,3,7,8-TCDD was found in very low concentrations, for NaCl case, 2.04, 0.78 and 0.64 pg L^{-1} for DEX, PAR and STR, respectively; and for $\text{Na}_2\text{SO}_4+\text{NaCl}$ case, 0.20, 0.40 and 0.40 pg L^{-1} for DEX, PAR and STR, respectively. The most abundant congener of the four drugs was 1,2,3,4,6,7-HpCDF (AMX with NaCl).

Toxicity in terms of TEQ

Finally, the toxicity was calculated from the analysis of the congeners:

- i) The highest toxicity value during the degradation of DEX for both electrolytes was 30.1 pg L^{-1} for NaCl and 22.7 pg L^{-1} for $\text{Na}_2\text{SO}_4+\text{NaCl}$.
- ii) The following toxicity values correspond to STR (19 pg L^{-1}) and PAR (7.8 pg L^{-1}), both when using NaCl as electrolyte medium.
- iii) The drug that showed less toxicity was AMX, with values of 3.6 and 2.5 pg L^{-1} when using NaCl and $\text{Na}_2\text{SO}_4+\text{NaCl}$ as electrolyte, respectively.

New methodology for determination TEQ

Toxicity is commonly measured in terms of toxic equivalents, or TEQ, and for its calculation, it is needed the analysis of the 17 2,3,7,8-PCDD/Fs congeners. In this thesis, a new methodology for TEQ calculation has been proposed with the aim of reducing the analytical effort and the associated costs. To extend the validity of the methodology, TCS photocatalytic oxidation was carried out, obtaining high PCDD/Fs concentrations, up to $7.5 \cdot 10^4 \text{ pg L}^{-1}$, and the highest toxicity point, $\text{TEQ}=3.6 \text{ pg L}^{-1}$, at 90 min, being the total experimental time 300 min. With these data, a statistical analysis was performed in several stages:

- i) First, by performing a multivariable analysis, with the evaluation of statistical parameters Pearson correlation coefficient (r), p -value (or probability value) and Spearman coefficient (ρ), applied to experimental results on kinetic evolution of 2,3,7,8-PCDD/Fs congeners during photocatalytic oxidation of TCS.
- ii) Second, employing the values that fulfilled statistical parameters, multiple linear regressions were performed to identify the best models. Finally, 5 models (equations) satisfied the established criteria. With these new models, only three congeners are necessary to be analysed to calculate the TEQ value. These models were applied to the data of this thesis and of the literature, obtaining a good adjustment.

Below, the following equations shows the five models of TEQ obtained.

Model A: $TEQ = -0.267 + 0.357 \cdot OCDD + 0.444 \cdot OCDF$ ($R^2=0.98$) (6.1)

Model B: $TEQ = 0.460 + 6.644 \cdot 1,2,3,4,7,8HxCDD - 1.457 \cdot 1,2,3,4,7,8,9HpCDF$ ($R^2=0.96$) (6.2)

Model C: $TEQ = -0.115 + 0.910 \cdot OCDD - 0.996 \cdot 1,2,3,4,7,8HxCDF$ ($R^2=0.96$) (6.3)

Model D: $TEQ = -0.281 + 0.478 \cdot 1,2,3,4,7,8HxCDD + 0.731 \cdot OCDF$ ($R^2=0.96$) (6.4)

Model E: $TEQ = -0.099 - 0.362 \cdot 1,2,3,4,7,8HxCDD + 0.800 \cdot OCDD$ ($R^2=0.95$) (6.5)

COMPUTATIONAL CHEMISTRY IN THE THEORETICAL PCDD/Fs FORMATION MECHANISMS

In Chapter 5, computational chemistry has employed to calculate the theoretical pathway of the oxidation of AMX, PAR and STR until the formation of PCDD/Fs. This pathway includes the intermediate compounds and PCDD/Fs detected experimentally (Chapter 3); is about a combined mechanism, starting with the three selected drugs, AMX, PAR and STR, which are degraded to intermediates, mainly chlorophenols and hydroquinone molecules, and end up with the formation of two congeners of PCDD/Fs.

Combined mechanism: 1st stage

The first stage of the combined mechanism starts with the cleavage of AMX and PAR through a $\cdot OH$ attack, to end up in one common molecule hydroquinone (HQ). Par breakage was studied from two different approaches by producing the cleavage in two different parts of the molecule. After successive chlorination steps of the HQ, first, 2-chlorohydroquinone is formed, and then 3,4-dichlorophenol (3,4-DCP) is produced. STR breaks in two fragments due to the action of the $\cdot OH$, producing directly 3,4-dichlorophenol (3,4-DCP) and the remaining fragment, n-methyl-1-naphthalenamine.

Combined mechanism: 2nd stage

This stage corresponds to the PCDD/Fs formation from 3,4-dichlorophenol. 3,4-dichlorophenol is converted to 3,4-dichlorophenol radical (3,4-DCP \cdot). Next, two molecules of 3,4-DCP \cdot are combined to form two different dioxins, through bindings between C-O atoms, successive H abstractions and cyclization of the molecule, generating the dioxins 2,3,7,8-tetrachlorodibenzo-p-dioxin and 1,2,7,8-tetrachlorodibenzo-p-dioxin.

Energy profiles

All the mechanisms are accompanied by their corresponding energy profiles, calculated from the final structures of each mechanism, by the single point energy calculation. The results showed the preference, in terms of energy, of some pathways over others:

- i) For the AMX, HQ was obtained through two transition states (TS1 and TS2), with an energy value of -32.2 kcal/mol, which corroborates the energetic stability of the final product.
- ii) For PAR, the two approaches employed showed that, option 1, with six TS, is more favourable, from a point of view energetic, than option 2 with 3 TS, even though the high number of steps required, -3.8 versus 1.6 kcal/mol.
- iii) In the STR breakage, the products generated by the cleavage appear very stable, because of the low value of energy achieved, -33.6 kcal/mol, after going through two TS.
- iv) For the transformation pathway from HQ to 3,4-DCP*, several stages were needed (five TS), with proper energy barriers and final energy of the product, -31.5 kcal/mol.
- v) The energy profile for the dioxins 2,3,7,8-TCDD and 1,2,7,8-TCDD starts with the combination of two 3,4-DCP*, employing the same transition states, TS1 and TS2. Next, TS3 is different for each dioxin; -37.7 kcal/mol for 2,3,7,8-TCDD and -35.5 kcal/mol for 1,2,7,8-TCDD. Finally, and after a second H abstraction with another $\cdot\text{OH}$, both final products are formed, reaching the energy of -84.0 kcal/mol for 2,3,7,8-TCDD and -87.3 kcal/mol for 1,2,7,8-TCDD, which is indicative of the stability of both products.

Challenges for future research

This thesis delivers new knowledge, both experimental and theoretical, to the formation of PCDD/Fs during advanced oxidation of organic molecules such as drugs dexamethasone, amoxicillin, paracetamol and sertraline, used during the COVID-19 pandemic. Nevertheless, there are still some gaps in the field that is needed to fill in. With this aim, the following suggestions are proposed for potential research:

- Usually, the drugs are not present alone in the environment, therefore, the analysis of their joint presence, both in synthetic solutions and in real samples, for instance, effluents from WWTPs, would be of great help to understand how these compounds behave and to study the synergies between them, after the application of AOPs.
- After the intensive analysis of the radicals' formation shown in this thesis, it would be interesting to perform the analysis of the radicals, by employing complex analytical techniques such as Electron Paramagnetic Resonance (EPR). Furthermore, it could be of great significance to analyse the rate constant of the radicals by laser flash photolysis experiments, to enter deeply into the understanding of the degradation mechanisms.
- Going one step further in the computational chemistry field, it would be useful to try the cleavage of the molecules not only using $\cdot\text{OH}$ radicals, but also some other radicals ($\text{Cl}\cdot$, $\text{HOCl}\cdot$, $\text{SO}_4\cdot^-$). In addition, different attacks on the molecules could be tested, trying to break other bonds in order to have a more descriptive and realistic degradation pathway. Finally, to complete the available information, the formation of the furans is another challenge to address. In addition, the study of the chlorination reactions of the low chlorinated PCDD/Fs to generate high chlorination degree PCDD/Fs would be of great interest.

CONCLUSIONES

Esta tesis doctoral se ha realizado en el marco de la línea de investigación "Formación potencial de PCDD/Fs durante el tratamiento de matrices acuosas por POAs", desarrollada en los últimos años dentro de los grupos de investigación Ingeniería de Procesos Sostenibles (IPS) y Procesos Avanzados de Separación (PAS) de la Universidad de Cantabria. Esta línea de investigación se centra en la evaluación de la formación de PCDD/Fs en matrices acuosas, conteniendo compuestos precursores o no precursores -en medio clorado- de las mismas, y como consecuencia, tras la aplicación de POAs, la toxicidad final de la muestra acuosa aumenta respecto a la inicial. Por lo tanto, la correcta evaluación de la matriz, la tecnología a aplicar y las condiciones de operación son claves para la implementación de los POAs como tecnologías de tratamiento de aguas residuales. Para corroborar esta hipótesis, en esta tesis doctoral se ha evaluado la formación de PCDD/Fs y la toxicidad final de las muestras, tras aplicar la oxidación electroquímica a matrices que contienen los fármacos más utilizados en la lucha contra el COVID-19, a saber, dexametasona (DEX), amoxicilina (AMX), paracetamol (PAR) y sertralina (STR). Recogiendo todos los resultados obtenidos en este trabajo, junto con la bibliografía revisada, esta tesis ha llevado a las siguientes conclusiones:

OXIDACIÓN ELECTROQUÍMICA (EOX) DE LOS FÁRMACOS DEL COVID-19

En el Capítulo 3 se llevó a cabo la oxidación electroquímica de muestras acuosas que contenían fármacos relacionado con el COVID-19, DEX, AMX, PAR y STR, empleando un ánodo de DDB y trabajando en modo galvanostático, con dos medios electrolíticos diferentes: NaCl (56 mM) y Na₂SO₄+NaCl (21 mM+2.8 mM). Para los experimentos de degradación (EOX-Drugs), se emplearon 10 mg L⁻¹ de cada fármaco como concentración inicial, mientras que en los experimentos destinados a analizar los compuestos intermedios (EOX-Intermediates), las concentraciones iniciales fueron mayores, 80 mg L⁻¹ para el DEX y 3000 mg L⁻¹ para el resto. En consecuencia, la densidad de corriente aplicada varió en función del tipo de experimento.

Experimentos "EOX-Drugs" y "EOX-Intermediates"

Todos los fármacos se oxidaron completamente independientemente de la concentración inicial; para los fármacos EOX, la carga eléctrica específica (Q) fue inferior a 0.6 A h L⁻¹ para ambos medios electrolíticos, y concretamente, inferior a 0.1 para AMX, PAR y STR en medio NaCl y 0.5 A h L⁻¹ en medio Na₂SO₄+NaCl, respectivamente. La degradación más rápida correspondió a STR y la más lenta a DEX, en ambos casos cuando se utilizó NaCl como electrolito. Además, se obtuvo también la misma tendencia de degradación para los electrolitos NaCl y Na₂SO₄+NaCl: STR > AMX > PAR > DEX. Finalmente, la cinética de degradación de los fármacos se ajustó a una cinética de pseudo-primer orden con las siguientes constantes de velocidad; para el NaCl como electrolito, STR $k \approx 0.101-0.999 \text{ min}^{-1}$, AMX $k \approx 0.051-0.236 \text{ min}^{-1}$, PAR $k \approx 0.036-0.145 \text{ min}^{-1}$ y DEX $k \approx 0.011 \text{ min}^{-1}$ y para Na₂SO₄+NaCl como electrolito, STR $k \approx 0.040-0.144 \text{ min}^{-1}$, AMX $k \approx 0.033-0.044 \text{ min}^{-1}$, PAR $k \approx 0.022-0.026 \text{ min}^{-1}$ y DEX $k \approx 0.016-0.017 \text{ min}^{-1}$.

Influencia de los radicales en la degradación de los fármacos

Tal y como se refleja en la literatura, y teniendo en cuenta la tasa de formación de las especies y radicales oxidantes, el potencial redox, la tasa de degradación de los radicales $\cdot\text{OH}$ ($10^9-10^{11} \text{ M}^{-1}\text{s}^{-1}$) y los resultados experimentales, las principales especies y radicales en medio de NaCl que participan en la degradación de DEX, AMX, PAR y STR pueden $\cdot\text{OH}$ (2.73 V), $\text{Cl}_2^{\cdot-}$ (2.13 V), Cl^{\cdot} (2.43 V), $\text{ClOH}^{\cdot-}$ (1.91 V), HClO (1.6 V) and Cl_2 (1.4 V).

Por otro lado, analizando el medio Na₂SO₄+NaCl, se puede concluir que los principales radicales y especies implicados en la degradación de estos cuatro fármacos mencionados, son principalmente el radical $\cdot\text{OH}$ (2.73 V), seguido del radical $\text{SO}_4^{\cdot-}$ (2.43 V) y la especie $\text{S}_2\text{O}_8^{2-\cdot}$ (1.44 V), y por último, dada su baja concentración, el resto de radicales y las especies de cloruro Cl^{\cdot} (2.43 V), $\text{Cl}_2^{\cdot-}$ (2.13 V), $\text{ClOH}^{\cdot-}$ (1.91 V), HClO (1.6 V) and Cl_2 (1.4 V), lo que justifica la necesidad de un mayor tiempo de oxidación en comparación con los experimentos realizados en medio NaCl.

Intermedios: identificación y análisis cinético

El análisis de los intermedios de oxidación se llevó a cabo mediante los experimentos EOX-Intermedios (alta concentración de fármacos). Los principales precursores o compuestos precursores de los PCDD/Fs identificados fueron:

- i) para la DEX, se identificó el precursor 2,4-diclorofenol en medio de cloruro. Cabe destacar que se encontraron compuestos similares a la DEX, como la 1-dehidrotestosterona (DHT) y la metandrostenolona (MTT) en medio $\text{Na}_2\text{SO}_4+\text{NaCl}$, y la beclometasona (BCM) y el naftaleno (NAP) en medio NaCl.
- ii) para la AMX, se encontraron una serie de compuestos precursores de PCDD/Fs como el 2,4-diclorofenol (2,4-DCP), el 4-clorofenol (4-CP) y el 2,4,5-triclorofenol (2,4,5-TCP), además de otros compuestos precursores, que pueden ser precursores de PCDD/Fs. como la hidroquinona (HQ) o la clorohidroquinona (Cl-HQ), para el medio NaCl. Para el medio $\text{Na}_2\text{SO}_4+\text{NaCl}$, también se detectaron HQ y Cl-HQ.
- iii) para el PAR, también se detectaron algunos precursores de PCDD/Fs para el medio NaCl, 2,4,5-TCP, y precursores de los precursores, como HQ y Cl-HQ. Para el medio $\text{Na}_2\text{SO}_4+\text{NaCl}$, se detectó el precursor 3,4-diclorofenol (3,4-DCP) y, sorprendentemente, una dioxina, la 1-clorodibenzo-p-dioxina (1-MCDD) en cantidad relativamente alta. Además, se detectaron algunos fragmentos de la molécula PAR, como el 4-nitrofenol (4-NP).
- iv) para la STR, se detectaron varios clorofenoles en ambos medios electrolíticos, como 3,4-DCP, 2,4,5-TCP y 2,3,4,6-tetraclorofenol (2,3,4,6-TeCP). Además, en el medio $\text{Na}_2\text{SO}_4+\text{NaCl}$, se detectó otro triclorofenol, el 2,3,4-triclorofenol (2,3,4-TCP). Asimismo, en ambos medios electrolíticos se detectaron fragmentos de STR, como n-m etil-1-naftalenamina (MNA).

PCDD/FS DURANTE LA EOX DE LOS FÁRMACOS: EVALUACIÓN DE LA TOXICIDAD

Perfil de los homólogos

En el Capítulo 4, se realizó el estudio de la formación de dioxinas y furanos altamente clorados (PCDD/Fs) para los experimentos con 10 mg L^{-1} del compuesto primario, en muestras en las que los fármacos habían sido eliminados en su totalidad. Las muestras de PCDD/Fs se prepararon y analizaron tras la aplicación del método estándar de preparación U.S. EPA 1613 mediante dilución isotópica y cromatografía de gases de alta resolución acoplada a espectrometría de masas de alta resolución (HRGC-HRMS). Las principales conclusiones obtenidas fueron:

- i) La cantidad total de PCDD/Fs generada fue mayor en el medio NaCl frente al medio $\text{Na}_2\text{SO}_4+\text{NaCl}$, excepto en el caso de la STR, donde la concentración de PCDD/Fs fue

similar para ambos medios electrolíticos. La AMX presentó los valores más altos del total de PCDD/Fs.

- ii) Para el medio NaCl, los PCDF se generaron en mayor cantidad que las PCDD en todos los casos. Para el Na₂SO₄+NaCl como electrolito, la tendencia observada es la contraria, excepto para la DEX.
- iii) Profundizando en los homólogos, los grupos de furanos altamente clorados se forman a alta concentración, como el HxCDF para las muestras con DEX, AMX y PAR (medio NaCl).

A continuación, la Tabla 6.3 muestra un resumen que incluye todos los resultados obtenidos

Table 6.3. Cantidad total (y porcentaje) de los grupos de homólogos producidos (pg L⁻¹) durante la degradación de DEX, AMX, PAR y STR (NaCl y Na₂SO₄+NaCl como electrolitos).

Fármaco	Electrolito	PCDDs pg L ⁻¹ (%)	PCDFs pg L ⁻¹ (%)	TOTAL Homólogos pg L ⁻¹ (%)
DEX	56 mM NaCl	123.2 (47.1%)	137.9 (52.9%)	261.1 (100%)
	21 mM Na ₂ SO ₄ + 2.8 mM NaCl	113.7 (58.4%)	81.1 (41.6%)	194.8 (100%)
AMX	56 mM NaCl	12.9 (0.5%)	2648.4 (99.5%)	2661.3 (100%)
	21 mM Na ₂ SO ₄ + 2.8 mM NaCl	20.6 (2.1%)	964.1 (97.9%)	984.7 (100%)
PAR	56 mM NaCl	15.3 (2.7%)	548.2 (97.3%)	563.5 (100%)
	21 mM Na ₂ SO ₄ + 2.8 mM NaCl	45.7 (26.3%)	127.9 (73.7%)	173.6 (100%)
STR	56 mM NaCl	51.7 (47.5%)	57.2 (52.5%)	108.9 (100%)
	21 mM Na ₂ SO ₄ + 2.8 mM NaCl	122.2 (78.5%)	33.5 (21.5%)	155.7 (100%)

Perfil de congéneres

A continuación, la Tabla 6.4 muestra un resumen que incluye todos los resultados obtenidos.

Table 6.4. Cantidad total (y porcentaje) de los congéneres 2,3,7,8-PCDD/Fs producidos (pg L^{-1}) durante la degradación de DEX, AMX, PAR y STR (NaCl y $\text{Na}_2\text{SO}_4+\text{NaCl}$ como electrolitos).

Fármaco	Electrolito	2,3,7,8-PCDDs pg L^{-1} (%)	2,3,7,8-PCDFs pg L^{-1} (%)	TOTAL 2,3,7,8- congéneres pg L^{-1} (%)
DEX	56 mM NaCl	80.2 (83.5%)	15.9 (16.5%)	96.1 (100%)
	21 mM Na_2SO_4 + 2.8 mM NaCl	46.8 (89.0%)	5.8 (11.0%)	52.6 (100%)
AMX	56 mM NaCl	7.3 (2.9%)	242.0 (97.1%)	249.3 (100%)
	21 mM Na_2SO_4 + 2.8 mM NaCl	4.6 (3.5%)	126.2 (96.5%)	130.8 (100%)
PAR	56 mM NaCl	30.4 (44.2%)	38.3 (55.8%)	68.7 (100%)
	21 mM Na_2SO_4 + 2.8 mM NaCl	20.9 (57.9%)	15.2 (42.1%)	36.1 (100%)
STR	56 mM NaCl	60.4 (86.8%)	9.2 (13.2%)	69.6 (100%)
	21 mM Na_2SO_4 + 2.8 mM NaCl	27.9 (67.1%)	13.7 (32.9%)	41.7 (100%)

- i) Al analizar los congéneres, la cantidad total de congéneres 2,3,7,8-PCDD/Fs fue, en todos los casos, mayor cuando se utilizó NaCl como electrolito que cuando se utilizó el medio electrolítico $\text{Na}_2\text{SO}_4+\text{NaCl}$.
- ii) En el caso del NaCl, los congéneres de dioxinas fueron mayores para DEX y STR y, por el contrario, para AMX y PAR, los congéneres de furanos fueron el grupo predominante. En el medio $\text{Na}_2\text{SO}_4+\text{NaCl}$, los 2,3,7,8-PCDD fueron más elevados en todos los casos, excepto para la AMX.
- iii) La dioxina más tóxica, la 2,3,7,8-TCDD, se encontró en concentraciones muy bajas, para el caso de NaCl, 2.04, 0.78 y 0.64 pg L^{-1} para DEX, PAR y STR, respectivamente; y para el caso de $\text{Na}_2\text{SO}_4+\text{NaCl}$, 0.20, 0.40 y 0.40 pg L^{-1} para DEX, PAR y STR, respectivamente. Además, el congéner más abundante de los cuatro fármacos fue el 1,2,3,4,6,7-HpCDF (AMX con NaCl).

Toxicidad en términos de TEQ

Por último, la toxicidad se calculó a partir del análisis de los congéneres:

- i) El valor más alto de toxicidad corresponde a las muestras de DEX para ambos electrolitos, siendo 30.1 pg L^{-1} para NaCl y 22.7 pg L^{-1} para $\text{Na}_2\text{SO}_4+\text{NaCl}$.
- ii) Los siguientes valores de toxicidad corresponden a STR (19 pg L^{-1}) y PAR (7.8 pg L^{-1}), ambos cuando se utiliza NaCl como medio electrolítico.
- iii) El fármaco que mostró menor toxicidad fue la AMX, con valores de 3.6 y 2.5 pg L^{-1} al utilizar NaCl y $\text{Na}_2\text{SO}_4+\text{NaCl}$ como electrolito, respectivamente.

Nueva metodología para el análisis del TEQ

La toxicidad se mide habitualmente en términos de equivalentes tóxicos, o TEQ, y para su cálculo es necesario el análisis de los 17 congéneres de la 2,3,7,8-PCDD/Fs. En esta tesis se ha propuesto una nueva metodología para el cálculo del TEQ con el objetivo de reducir el esfuerzo analítico y los costes asociados. Para ampliar la validez de la metodología, se llevó a cabo una oxidación fotocatalítica de TCS, obteniéndose altas concentraciones de PCDD/Fs de hasta 7.5-104 pg L⁻¹ y el punto de mayor toxicidad, TEQ=3,6 pg L⁻¹, se alcanzó a los 90 min, siendo el tiempo total del experimento de 300 min. Con estos datos, se realizó un análisis estadístico en varias etapas:

- i) Primero, realizando un análisis multivariable, a través de la evaluación de los parámetros estadísticos coeficiente de correlación de Pearson (r), valor *p* (o valor de probabilidad) y coeficiente de Spearman (ρ), aplicados a los resultados experimentales sobre la evolución cinética de los congéneres de 2,3,7,8-PCDD/Fs durante la oxidación fotocatalítica del TCS.
- ii) En segundo lugar, empleando los valores que cumplían los parámetros estadísticos, se realizaron regresiones lineales múltiples para identificar los mejores modelos. Finalmente, 5 modelos (ecuaciones) satisfacían los criterios establecidos. Con estos nuevos modelos, sólo es necesario analizar tres congéneres para calcular el valor de TEQ. Estos modelos fueron aplicados a los datos de esta tesis y de la literatura, obteniendo un buen ajuste.

Con estos datos, se realizó un análisis estadístico en varias etapas: primero, realizando un análisis multivariable, con la evaluación de algunos parámetros estadísticos (r, valor *p* y ρ) y se realizó una regresión lineal múltiple para identificar los mejores modelos; esto resultó en 5 modelos finales (ecuaciones) que satisfacían los criterios establecidos. Con estos nuevos modelos, sólo fue necesario analizar tres congéneres para calcular el valor de TEQ. Estos modelos se aplicaron a los datos de esta tesis y de la literatura, obteniendo un buen ajuste.

A continuación, las siguientes ecuaciones muestran los cinco modelos de TEQ obtenidos.

Modelo A: $TEQ = -0.267 + 0.357 \cdot OCDD + 0.444 \cdot OCDF$ (R²=0.98) (6.1)

Modelo B: $TEQ = 0.460 + 6.644 \cdot 1,2,3,4,7,8HxCDD - 1.457 \cdot 1,2,3,4,7,8,9HpCDF$ (R²=0.96) (6.2)

Modelo C: $TEQ = -0.115 + 0.910 \cdot OCDD - 0.996 \cdot 1,2,3,4,7,8HxCDF$ (R²=0.96) (6.3)

Modelo D: $TEQ = -0.281 + 0.478 \cdot 1,2,3,4,7,8HxCDD + 0.731 \cdot OCDF$ (R²=0.96) (6.4)

Modelo E: $TEQ = -0.099 - 0.362 \cdot 1,2,3,4,7,8HxCDD + 0.800 \cdot OCDD$ (R²=0.95) (6.5)

QUÍMICA COMPUTACIONAL EN LOS MECANISMOS TEÓRICOS DE FORMACIÓN DE PCDD/FS

En el Capítulo 5 se ha empleado la química computacional para calcular la vía teórica de la oxidación de AMX, PAR y STR hasta la formación de PCDD/FS. Esta vía incluye los compuestos intermedios y los PCDD/FS detectados experimentalmente (Capítulo 3); se trata de un mecanismo combinado, que comienza con los tres fármacos seleccionados, AMX, PAR y STR, que se degradan a intermedios, principalmente clorofenoles y moléculas de hidroquinona, y termina con la formación de dos congéneres de PCDD/FS.

Mecanismo combinado: 1ª etapa

La primera etapa del mecanismo combinado comienza con la ruptura de PAR y AMOX a través de un ataque $\cdot\text{OH}$, para terminar en una molécula común, la hidroquinona. La ruptura del PAR se estudió desde dos enfoques diferentes, provocándola en dos partes distintas de la molécula. Tras los sucesivos pasos de cloración de la HQ, primero se forma la 2-clorohidroquinona y luego se produce el 3,4-diclorofenol (3,4-DCP). La STR se rompe en dos fragmentos debido a la acción del $\cdot\text{OH}$, produciendo directamente 3,4-diclorofenol (3,4-DCP) y el fragmento restante, n-metil-1-naftalenamina.

Mecanismo combinado: 2ª etapa

Esta etapa corresponde a la formación de PCDD/FS a partir del 3,4-diclorofenol. El 3,4-diclorofenol se convierte en el radical 3,4-diclorofenol \cdot (3,4-DCP \cdot). A continuación, dos moléculas de 3,4-DCP \cdot se combinan para formar dos dioxinas diferentes, mediante uniones entre átomos de C-O, y sucesivas abstracciones de H y ciclación de la molécula, generando las dioxinas 2,3,7,8-tetraclorodibenzo-p-dioxina y 1,2,7,8-tetraclorodibenzo-p-dioxina

Perfiles energéticos

Todos los mecanismos van acompañados de sus correspondientes perfiles energéticos, calculados a partir de las estructuras finales de cada mecanismo, mediante el cálculo de energía "single point". Los resultados mostraron la preferencia, en términos de energía, de algunas vías sobre otras:

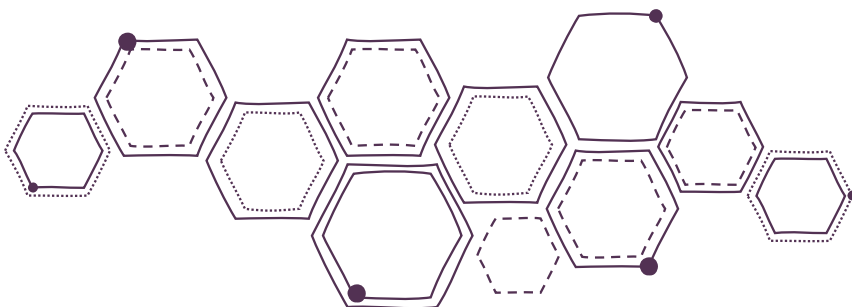
- i) Para el caso de AMX, se obtuvo HQ a través de dos estados de transición (TS), con un valor energético de -32.2 kcal/mol, lo que corrobora la estabilidad energética del producto final.
- ii) Para el PAR, los dos enfoques empleados mostraron que la opción 1, con seis TS, es más favorable, desde el punto de vista energético, que la opción 2, con tres TS, a pesar del elevado número de pasos requeridos; -3.8 frente a 1.6 kcal/mol.
- iii) En la ruptura de la STR, los productos generados de la escisión parecen muy estables, debido al bajo valor de energía alcanzado (-33,6 kcal/mol), tras pasar por dos TS.
- iv) Para la vía de transformación de HQ a 3,4-DCP*, fueron necesarias varias etapas (cinco TS), con barreras energéticas adecuadas y energía final del producto, -31.5 kcal/mol.
- v) El perfil energético para las dioxinas 2,3,7,8-TCDD y 1,2,7,8-TCDD comienza con la combinación de dos 3,4-DCP*, empleando los mismos estados de transición, TS1 y TS2. A continuación, TS3 es diferente para cada dioxina; -37.7 kcal/mol para la 2,3,7,8-TCDD y -35.5 kcal/mol para la 1,2,7,8-TCDD. Finalmente, y tras una segunda abstracción de H con otro *OH, se forman ambos productos finales, alcanzando la energía de -84.0 kcal/mol para la 2,3,7,8-TCDD y -87.3 kcal/mol para la 1,2,7,8-TCDD, lo que es indicativo de la estabilidad de ambos productos.

Propuestas de trabajo futuro

Esta tesis proporciona nuevos conocimientos, tanto experimentales como teóricos, sobre la formación de PCDD/Fs durante la oxidación avanzada de moléculas orgánicas como los fármacos dexametasona, amoxicilina, paracetamol y sertralina, utilizados durante la pandemia de COVID-19. Sin embargo, todavía existen algunas carencias en el campo que son necesarias de subsanar. Con este objetivo, se proponen las siguientes sugerencias para una posible investigación:

- Normalmente, los fármacos no se encuentran presentes de manera individual en el medio ambiente, por lo que el análisis de su presencia conjunta, tanto en soluciones sintéticas como en muestras reales, por ejemplo, efluentes de EDAR, sería de gran ayuda para entender cómo se comportan estos compuestos y estudiar las sinergias entre ellos, tras la aplicación de POAs.
- Tras el análisis intensivo de la formación de radicales mostrado en esta tesis, sería interesante realizar el análisis de los mismos, empleando técnicas analíticas complejas como la Resonancia Paramagnética de Electrones (EPR). Además, podría ser de gran importancia analizar la constante de velocidad de los radicales mediante experimentos de fotólisis flash con láser, para entrar en profundidad en la comprensión de los mecanismos de degradación.
- Dando un paso más en el campo de la química computacional, sería útil probar la ruptura de las moléculas no sólo utilizando radicales $\cdot\text{OH}$, sino también algunos otros radicales ($\text{Cl}\cdot$, $\text{HOCl}\cdot$, $\text{SO}_4^{\cdot-}$). Además, se podrían probar diferentes ataques a las moléculas, intentando romper otros enlaces para tener una vía de degradación más descriptiva y realista. Finalmente, para completar la información disponible, la formación de los furanos es otro reto a abordar. Además, el estudio de las reacciones de cloración de los PCDD/Fs poco clorados para generar PCDD/Fs de alto grado de cloración sería de gran interés.

ANNEXES



Annex I – Nomenclature

General nomenclature

•OH	Hydroxyl radical
1,3-BDO	1,3-benzenediol
1-MCDD	1-chlorodibenzo-p-dioxin
2,3,4,6-TeCP	2,3,4,6-tetrachlorophenol
2,3,4-TCP	2,3,4-trichlorophenol
2,4,5-TCP	2,4,5-trichlorophenol
2,4-DCP	2,4-dichlorophenol
2,5-DCHQ	2,5-dichloro-hydroquinone
2,5-pBQ	2,5-dichloro-p-benzoquinone
2-CP	2-chlorophenol
2-CPR	2-chlorophenoxy radical
3,4-DBA	3,4-dichloro benzenamine
3,4-DCBA	3,4-dichlorobenzamide
3,4-DCP	3,4-dichlorophenol
3,4-DCP•	3,4-dychlorophenol radical
3,4-DCS	3,4-dichlorostyrene
4-CP	4-chlorophenol
4-NC	4-nitrocatechol
ACF	Activated carbon fibre
ACN	Acetonitrile
AMX	Amoxicillin
AOPS	Advance oxidation processes
API	Active pharmaceutical ingredient
ATO	Antimony-doped tin oxide
B3LYP	Becke,three-parameter, Lee-Yang-Parr
BCM	Beclomethasone
BDD	Boron-doped diamond
BQ	p-benzoquinone
CBz	Chlorobenzenes
CCL	Contaminant candidate list
Cl-BQ	Chloro-p-benzoquinone
Cl-HQ	Chlorohydroquinone

COD	Chemical oxygen demand
CPs	Chlorophenols
DAD	Diode array detector
DCM	Dichloromethane
DEX	Dexamethasone
DFT	Density functional theory
DHT	1-dehydro-testosterone
DMD	Dimethadione
DSA	Dimensionally stable anodes
ECs	Emerging contaminants
EDCs	Endocrine-disrupting compounds
EOX	Electrochemical oxidation
F	Faraday constant
GC-MS	Gas chromatography - mass spectrometry
H₀	Null hypothesis
HBCDs	Hexabromocyclododecanes
HOMO	Highest occupied molecular orbital
HPLC	High performance liquid chromatography
HQ	Hydroquinone
HRGC-HRMS	High resolution gas chromatography - High resolution mass spectrometry
IRC	Intrinsic reaction coordinate
IRP	Intrinsic reaction path
I-TEF	International toxic equivalency factor
J	Current density
J_{lim}	Limiting current density
K_m	Mass transport coefficient
MDEO	3-methoxy-16,16-dimethyl-1,3,5(10)-estratrien-17-one
MDOD	9-(S)-methyl-delta-5(10)-octalin-1,6-dione
MEP	Molecular electrostatic potential
MMO	Mixed metal oxides
MNA	N-methyl-1-naphthaleneamine
MTBE	Methyl-t-butyl ether
MTT	Methandros-tenolone
MWSIs	Municipal waste solid incinerators
Na₂SO₄	Sodium sulphate
NAP	Napthalene
Na-PCP	Sodium pentachlorophenate

NATO/CCMS	North Atlantic Treaty Organization Committee on the Challenge of Modern Society
Nb/BDD	Niobium/Boron-doped diamond
NHE	Normal hydrogen electrode
NHPA	N-(3-Chloro-4-hydroxyphenyl) acetamide
NPDWR	National primary drinking water regulations
OLS	Ordinary least squares
P	Products
PAR	Paracetamol
PBBs	Polybrominated biphenyl
PBDD/Fs	Polybrominated dibenzo-p-dioxins and furans
PBDEs	Polybrominated diphenyl ethers
PCA	Principal component analysis
PCBs	Polychlorinated biphenyl
PCDD/Fs	Polychlorinated dibenzo-P-dioxins and furans
PCDDs	Polychlorinated dibenzo-P-dioxins
PCDEs	Polychlorinated diphenyl ethers
PCDFs	Polychlorinated dibenzo-P-furans
PES	Potential energy surface
PFAS	Perfluoroalkyl substances
PFOA	Perfluorooctanoic acid
PFOs	Perfluoro octanes sulfonates
POPs	Persistent organic pollutants
PPCPs	Pharmaceutical and personal care products
PPs	Priority pollutants
PRED	Prednisolone
PTCP	2-phenyl-2',5,5'- trichlorophenol
PTN	1-propyl-1,2,3,4-tetrahydro
p-value	Probability value
Q	Specific electrical charge
QC	Quantum chemistry
r	Pearson correlation coefficient
R	Reactans
RO	Reverse osmosis
ROC	Reverse osmosis concentrate
RP	Reaction pathway
RRFs	Relative response factors
RT	Retention time

RTOs	Regenerative thermal oxidizers
SARS-CoV-2	Severe acute respiratory syndrome coronavirus 2
SDGs	Sustainable development goals
SDWA	Save Drinking Water Act
SPE	Sustainable process engineering
SPE	Single point energy
SSRIs	Serotonine reuptake inhibitors
STR	Sertraline
TCDD	Tetrachlorodibenzo-P-dioxin
TCS	Triclosan
TEFs	Toxic equivalency factors
TEQs	Toxic equivalents
TiO₂	Titanium dioxide
TOC	Total organic carbon
TON	Theory of molecular orbitals
TS	Transition state
UF	Ultrafiltration
UP	Ultrapure water
US EPA	United States Enviromental Protection Agency
WFT	Wave function theory
WHO	World Health Organization
WHO-TEFs	World Health Organization toxic equivalency factors
WWTP	Wastewater treatment plant
ρ	Spearman coefficient
$\rho(r)$	Electron density function

PCDD/Fs nomenclature

Table I.1. Name and abbreviations used for 17 2,3,7,8-PCDD/Fs.

Name	Abbreviation
2,3,7,8-Tetrachlorodibenzo-p-furan	2,3,7,8-TCDF
2,3,7,8-Tetrachlorodibenzo-p-dioxin	2,3,7,8-TCDD
1,2,3,7,8-Pentachlorodibenzo-p-furan	1,2,3,7,8-PeCDF
2,3,4,7,8-Pentachlorodibenzo-p-furan	2,3,4,7,8-PeCDF
1,2,3,7,8-Pentachlorodibenzo-p-dioxin	1,2,3,7,8-PeCDD
1,2,3,4,7,8-Hexachlorodibenzo-p-furan	1,2,3,4,7,8-HxCDF
1,2,3,6,7,8-Hexachlorodibenzo-p-furan	1,2,3,6,7,8-HxCDF
2,3,4,6,7,8-Hexachlorodibenzo-p-furan	2,3,4,6,7,8-HxCDF
1,2,3,7,8,9-Hexachlorodibenzo-p-furan	1,2,3,7,8,9-HxCDF
1,2,3,4,7,8-Hexachlorodibenzo-p-dioxin	1,2,3,4,7,8-HxCDD
1,2,3,6,7,8-Hexachlorodibenzo-p-dioxin	1,2,3,6,7,8-HxCDD
1,2,3,7,8,9-Hexachlorodibenzo-p-dioxin	1,2,3,7,8,9-HxCDD
1,2,3,4,6,7,8-Heptachlorodibenzo-p-furan	1,2,3,4,6,7,8-HpCDF
1,2,3,4,7,8,9-Heptachlorodibenzo-p-furan	1,2,3,4,7,8,9-HpCDF
1,2,3,4,6,7,8-Heptachlorodibenzo-p-dioxin	1,2,3,4,6,7,8-HpCDD
Octachlorodibenzo-p-furan	OCDF
Octachlorodibenzo-p-dioxin	OCDD

Table I.2. Name and abbreviations used for 17 2,3,7,8-PCDD/Fs.

Name	Abbreviation
Total natives-TCDD	TCDD
Total natives-PeCDD	PeCDD
Total natives-HxCDD	HxCDD
Total natives-HpCDD	HpCDD
Total natives-TCDF	TCDF
Total natives -PeCDF	PeCDF
Total natives-HxCDF	HxCDF
Total natives-HpCDF	HpCDF

Annex II – Concentration of labelled EPA 1613 solutions

Table II.1. Concentration of PCDD/Fs in labelled EPA 1613 LCS standard solution from Wellington Laboratories Inc. It contains the PCDD/Fs isotopically labelled with $^{13}\text{C}_{12}$.

Congeners	Concentration (ng mL ⁻¹)
	LCS (Labelled compound stock solution)
2,3,7,8-Tetrachloro[$^{13}\text{C}_{12}$]dibenzo-p-dioxin	100
1,2,3,7,8-Pentachloro[$^{13}\text{C}_{12}$]dibenzo-p-dioxin	100
1,2,3,4,7,8-Hexachloro[$^{13}\text{C}_{12}$]dibenzo-p-dioxin	100
1,2,3,6,7,8-Hexachloro[$^{13}\text{C}_{12}$]dibenzo-p-dioxin	100
1,2,3,4,6,7,8-Heptachloro[$^{13}\text{C}_{12}$]dibenzo-p-dioxin	100
Octachloro[$^{13}\text{C}_{12}$]dibenzo-p-dioxin	200
2,3,7,8-Tetrachloro[$^{13}\text{C}_{12}$]dibenzofuran	100
1,2,3,7,8-Pentachloro[$^{13}\text{C}_{12}$]dibenzofuran	100
2,3,4,7,8-Pentachloro[$^{13}\text{C}_{12}$]dibenzofuran	100
1,2,3,4,7,8-Hexachloro[$^{13}\text{C}_{12}$]dibenzofuran	100
1,2,3,6,7,8-Hexachloro[$^{13}\text{C}_{12}$]dibenzofuran	100
1,2,3,7,8,9-Hexachloro[$^{13}\text{C}_{12}$]dibenzofuran	100
2,3,4,6,7,8-Hexachloro[$^{13}\text{C}_{12}$]dibenzofuran	100
1,2,3,4,6,7,8-Heptachloro[$^{13}\text{C}_{12}$]dibenzofuran	100
1,2,3,4,7,8,9-Heptachloro[$^{13}\text{C}_{12}$]dibenzofuran	100

Table II.2. Concentration of PCDD/Fs in labelled EPA 1613ISS standard solution from Wellington Laboratories Inc. It contains the PCDD/Fs isotopically labelled with $^{13}\text{C}_{12}$.

	Concentration (ng mL ⁻¹)
	ISS (Internal standard spiking solution)
2,3,7,8-Tetrachloro[$^{13}\text{C}_{12}$]dibenzo-p-dioxin	200
2,3,7,8,9-Hexachloro[$^{13}\text{C}_{12}$]dibenzo-p-dioxin	200

Table II. 3. EPA Method 1613 calibration and verification solutions CSL and CS1-CS4 from Wellington Laboratories Inc.

Congener	Concentration (ng mL ⁻¹)				
	1613CSL	1613CS1	1613CS2	1613CS3	1613CS4
2,3,7,8-Tetrachlorodibenzo-p-dioxin	0.1	0.5	2	10	40
1,2,3,7,8-Pentachlorodibenzo-p-dioxin	0.5	2.5	10	50	200
1,2,3,4,7,8-Hexachlorodibenzo-p-dioxin	0.5	2.5	10	50	200
1,2,3,6,7,8-Hexachlorodibenzo-p-dioxin	0.5	2.5	10	50	200
1,2,3,7,8,9-Hexachlorodibenzo-p-dioxin	0.5	2.5	10	50	200
1,2,3,4,6,7,8-Heptachlorodibenzo-p-dioxin	0.5	2.5	10	50	200
Octachlorodibenzo-p-dioxin	1.0	5	20	100	400
2,3,7,8-Tetrachlorodibenzofuran	0.1	0.5	2	10	40
1,2,3,7,8-Pentachlorodibenzofuran	0.5	2.5	10	50	200
2,3,4,7,8-Pentachlorodibenzofuran	0.5	2.5	10	50	200
1,2,3,4,7,8-Hexachlorodibenzofuran	0.5	2.5	10	50	200
1,2,3,6,7,8-Hexachlorodibenzofuran	0.5	2.5	10	50	200
1,2,3,7,8,9-Hexachlorodibenzofuran	0.5	2.5	10	50	200
2,3,4,6,7,8-Hexachlorodibenzofuran	0.5	2.5	10	50	200
1,2,3,4,6,7,8-Heptachlorodibenzofuran	0.5	2.5	10	50	200
1,2,3,4,7,8,9-Heptachlorodibenzofuran	0.5	2.5	10	50	200
Octachlorodibenzofuran	1.0	5	20	100	400
2,3,7,8-Tetrachloro[¹³ C ₁₂]dibenzo-p-dioxin	100	100	100	100	100
1,2,3,7,8-Pentachloro[¹³ C ₁₂]dibenzo-p-dioxin	100	100	100	100	100
1,2,3,4,7,8-Hexachloro[¹³ C ₁₂]dibenzo-p-dioxin	100	100	100	100	100
1,2,3,6,7,8-Hexachloro[¹³ C ₁₂]dibenzo-p-dioxin	100	100	100	100	100
1,2,3,4,6,7,8-Heptachloro[¹³ C ₁₂]dibenzo-p-dioxin	100	100	100	100	100
Octachloro[¹³ C ₁₂]dibenzo-p-dioxin	200	200	200	200	200
2,3,7,8-Tetrachloro[¹³ C ₁₂]dibenzofuran	100	100	100	100	100
1,2,3,7,8-Pentachloro[¹³ C ₁₂]dibenzofuran	100	100	100	100	100
2,3,4,7,8-Pentachloro[¹³ C ₁₂]dibenzofuran	100	100	100	100	100
1,2,3,4,7,8-Hexachloro[¹³ C ₁₂]dibenzofuran	100	100	100	100	100

ANNEX II

Congener	Concentration (ng mL ⁻¹)				
	1613CSL	1613CS1	1613CS2	1613CS3	1613CS4
1,2,3,6,7,8-Hexachloro[¹³ C ₁₂]dibenzofuran	100	100	100	100	100
1,2,3,7,8,9-Hexachloro[¹³ C ₁₂]dibenzofuran	100	100	100	100	100
2,3,4,6,7,8-Hexachloro[¹³ C ₁₂]dibenzofuran	100	100	100	100	100
1,2,3,4,6,7,8-Heptachloro[¹³ C ₁₂]dibenzofuran	100	100	100	100	100
1,2,3,4,7,8,9-Heptachloro[¹³ C ₁₂]dibenzofuran	100	100	100	100	100
2,3,7,8-[³⁷ Cl ₄]Tetrachlorodibenzo-p-dioxin	0.1	0.5	2	10	40
1,2,3,4-Tetrachloro[¹³ C ₁₂]dibenzo-p-dioxin	100	100	100	100	100
1,2,3,7,8,9-Hexachloro[¹³ C ₁₂]dibenzo-p-dioxin	100	100	100	100	100

Annex III – Recoveries of labelled EPA 1613 solutions

Table III.1. Labelled compound recovery in samples when all cdds/cdfs are tested.

Compound	Test conc. (ng L ⁻¹)	Labelled compound recovery (%)	
		pg L ⁻¹	%
¹³ C ₁₂ -2,3,7,8-TCDD	100	25-164	25-164
1,2,3,7,8-PeCDD ¹³ C	100	25-181	25-181
1,2,3,4,7,8-HxCDD ¹³ C	100	32-141	32-141
1,2,3,6,7,8-HxCDD ¹³ C	100	28-130	28-130
1,2,3,7,8,9-HxCDD ¹³ C	100	23-140	23-140
1,2,3,4,6,7,8-HpCDD ¹³ C	100	34-313	17-157
OCDD ¹³ C	100	24-169	24-169
2,3,7,8-TCDF ¹³ C	100	24-185	24-185
1,2,3,7,8-PeCDF ¹³ C	100	21-178	21-178
2,3,4,7,8-PeCDF ¹³ C	100	26-152	26-152
1,2,3,4,7,8-HxCDF ¹³ C	100	26-123	26-123
1,2,3,6,7,8-HxCDF ¹³ C	100	29-147	29-147
1,2,3,7,8,9-HxCDF ¹³ C	100	28-136	28-136
2,3,4,6,7,8-HxCDF ¹³ C	100	28-143	28-143
1,2,3,4,6,7,8-HpCDF ¹³ C	100	26-138	26-138
1,2,3,4,7,8,9-HpCDF ¹³ C	200	3.5-19.7	35-197
³⁷ Cl ₄ -2,3,7,8-TCDD	10	25-164	25-164

Table III.2. Recoveries of labelled PCDD/Fs in EOX-Drugs experiments ($[Drugs]_0=10 \text{ mg L}^{-1}$) for DEX, AMX, PAR and STR, using NaCl as electrolyte and performed in duplicate, I and II.

Congener	Recovery (%)							
	DEX		AMX		PAR		STR	
	I	II	I	II	I	II	I	II
2,3,7,8-TCDD ¹³ C	69	109	106	117	92	88	94	70
1,2,3,7,8-PeCDD ¹³ C	72	115	109	113	94	90	96	67
1,2,3,4,7,8-HxCDD ¹³ C	68	73	86	86	82	89	74	40
1,2,3,6,7,8-HxCDD ¹³ C	62	74	82	86	77	85	81	49
1,2,3,7,8,9-HxCDD ¹³ C	100	100	100	100	100	100	100	100
1,2,3,4,6,7,8-HpCDD ¹³ C	74	118	98	107	84	95	78	64
OCDD ¹³ C	60	106	118	114	69	71	57	52
2,3,7,8-TCDF ¹³ C	80	102	98	107	83	89	91	70
1,2,3,7,8-PeCDF ¹³ C	70	94	96	100	82	85	87	62
2,3,4,7,8-PeCDF ¹³ C	72	117	113	111	91	95	74	38
1,2,3,4,7,8-HxCDF ¹³ C	70	77	85	88	76	83	78	42
1,2,3,6,7,8-HxCDF ¹³ C	64	79	81	85	72	80	81	48
1,2,3,7,8,9-HxCDF ¹³ C	77	96	76	103	76	92	86	67
2,3,4,6,7,8-HxCDF ¹³ C	63	102	96	82	79	82	86	61
1,2,3,4,6,7,8-HpCDF ¹³ C	66	103	89	91	77	88	83	61
1,2,3,4,7,8,9-HpCDF ¹³ C	80	110	106	119	84	93	84	73

Table III.3. Recoveries of labelled PCDD/Fs in blanks of EOX-Drugs experiments ($[\text{Drugs}]_0=10 \text{ mg L}^{-1}$) for DEX, AMX, PAR and STR, using $\text{Na}_2\text{SO}_4+\text{NaCl}$ as electrolyte and performed in duplicate, I and II.

Congener	Recovery (%)							
	DEX		AMX		PAR		STR	
	I	II	I	II	I	II	I	II
2,3,7,8-TCDD ¹³ C	97	113	90	73	62	89	80	81
1,2,3,7,8-PeCDD ¹³ C	120	112	118	75	63	90	90	92
1,2,3,4,7,8-HxCDD ¹³ C	79	93	72	58	58	90	74	85
1,2,3,6,7,8-HxCDD ¹³ C	69	90	69	56	56	84	70	80
1,2,3,7,8,9-HxCDD ¹³ C	100	100	100	100	100	100	100	100
1,2,3,4,6,7,8-HpCDD ¹³ C	97	114	86	64	57	88	75	84
OCDD ¹³ C	119	126	89	72	50	66	61	63
2,3,7,8-TCDF ¹³ C	77	112	87	66	61	84	80	80
1,2,3,7,8-PeCDF ¹³ C	103	90	97	63	55	79	74	80
2,3,4,7,8-PeCDF ¹³ C	117	110	111	71	62	91	97	91
1,2,3,4,7,8-HxCDF ¹³ C	64	78	65	54	56	91	74	90
1,2,3,6,7,8-HxCDF ¹³ C	61	76	62	51	53	87	70	83
1,2,3,7,8,9-HxCDF ¹³ C	80	110	88	65	55	87	81	84
2,3,4,6,7,8-HxCDF ¹³ C	60	79	63	52	58	84	71	84
1,2,3,4,6,7,8-HpCDF ¹³ C	68	94	75	54	55	88	71	88
1,2,3,4,7,8,9-HpCDF ¹³ C	98	113	91	70	44	90	80	86

Table III.4. Recoveries of labelled PCDD/Fs in blanks of EOX-Drugs experiments.

Congener	Recovery (%)			
	DEX	AMX	PAR	STR
2,3,7,8-TCDD ¹³ C	68	99	74	78
1,2,3,7,8-PeCDD ¹³ C	68	107	95	75
1,2,3,4,7,8-HxCDD ¹³ C	54	90	75	75
1,2,3,6,7,8-HxCDD ¹³ C	50	84	71	70
1,2,3,7,8,9-HxCDD ¹³ C	100	100	100	100
1,2,3,4,6,7,8-HpCDD ¹³ C	57	97	74	74
OCDD ¹³ C	63	84	66	59
2,3,7,8-TCDF ¹³ C	72	92	96	75
1,2,3,7,8-PeCDF ¹³ C	51	88	85	73
2,3,4,7,8-PeCDF ¹³ C	73	99	94	78
1,2,3,4,7,8-HxCDF ¹³ C	52	81	78	74
1,2,3,6,7,8-HxCDF ¹³ C	51	78	73	70
1,2,3,7,8,9-HxCDF ¹³ C	53	89	90	74
2,3,4,6,7,8-HxCDF ¹³ C	51	841	73	70
1,2,3,4,6,7,8-HpCDF ¹³ C	43	88	75	70
1,2,3,4,7,8,9-HpCDF ¹³ C	81	101	90	77

Annex IV– GC-MS: by-products analysis.

Table IV.1. By-products for dexamethasone with NaCl as electrolyte.

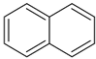
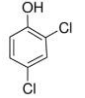
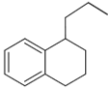
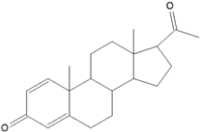
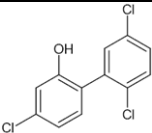
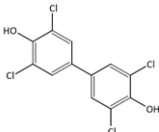
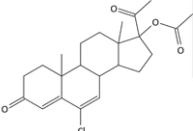
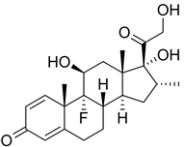
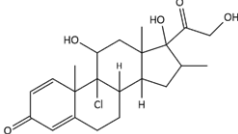
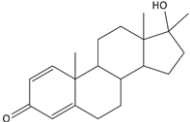
RT (min)	Compound	Molecule
4.92	Naphtalene	
6.74	2,4-dichlorophenol	
8.13	1-Propyl-1,2,3,4-tetrahydronaphthalene	
10.71	6-Pregnen-3,20-dione	
11.62	2-phenyl-2',5,5'-trichlorophenol	
14.00	3,3',5,5'-Tetrachloro[1,1'-biphenyl]-4,4'-diol	
15.15	Chlormadinone Acetate	
17.645	Dexamethasone	
18.83	Beclometasona	
19.95	Methandrostenolone	

Table IV.1. By-products for dexamethasone with NaCl as electrolyte (cont.).

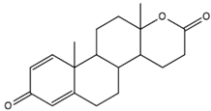
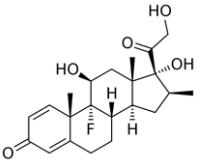
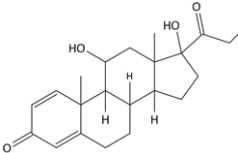
RT (min)	Compound	Molecule
20.60	Testolactone	
23.25	Betamethasone	
23.45	Prednisolone	

Table IV.2. By-products for dexamethasone with Na₂SO₄+NaCl as electrolyte.

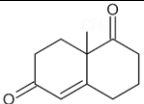
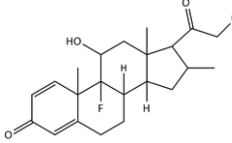
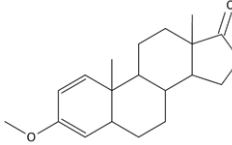
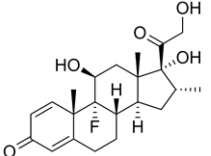
RT (min)	Compound	Molecule
8.65	9-(S)-Methyl-delta-5(10)-octalin-1,6-dione	
11.04	17-Desoxymethasone	
14.37	3-Methoxy-16,16-dimethyl-1,3,5(10)-estratrien-17-one	
17.64	Dexamethasone	

Table IV.2. By-products for dexamethasone with Na₂SO₄+NaCl as electrolyte (cont.).

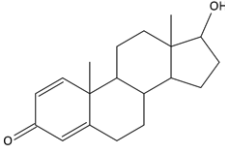
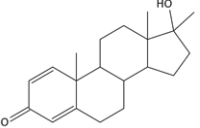
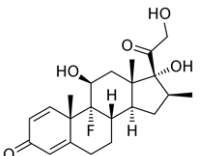
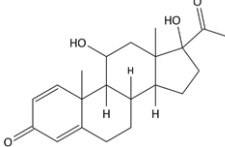
RT (min)	Compound	Molecule
19.38	1-Dehydrotestosterone	
19.95	Methandrostenolone	
23.25	Betamethasone	
23.45	Prednisolone	

Table IV.3. By-products for amoxicillin with NaCl as electrolyte.

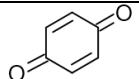
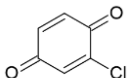
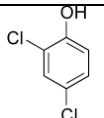
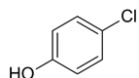
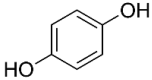
RT (min)	Compound	Molecule
3.10	p-Benzoquinone	
4.15	Chloro-p-benzoquinone	
4.88	2,4-Dichlorophenol	
4.98	4-Chlorophenol	
5.57	Hydroquinone	

Table IV.3. By-products for amoxicillin with NaCl as electrolyte (cont.).

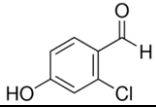
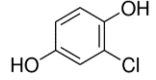
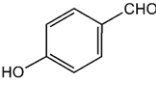
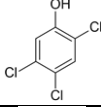
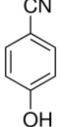
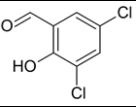
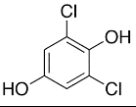
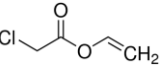
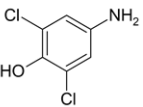
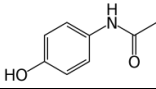
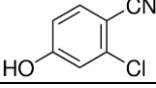
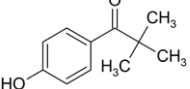
RT (min)	Compound	Molecule
5.98	2-Chloro-4-hydroxybenzaldehyde	
6.12	Chlorohydroquinone	
6.33	p-Hydroxybenzaldehyde	
6.35	2,4,5-Trichlorophenol	
6.61	p-Hydroxybenzotrile	
7.3	3,5-Dichloro-2-hydroxybenzaldehyde	
7.73	2,5-dichloro-Hydroquinone	
7.83	Vinyl chloroacetate	
7.86	2,6-Dichloro-p-aminophenol	
8.52	Acetaminophen (paracetamol)	
8.57	2-Chloro-4-hydroxybenzotrile	
8.99	4'-Hydroxy-2,2-dimethylpropiophenone	

Table IV.3. By-products for amoxicillin with NaCl as electrolyte (cont.).

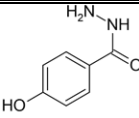
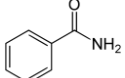
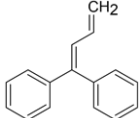
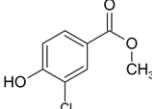
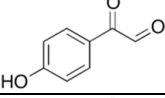
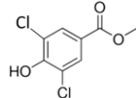
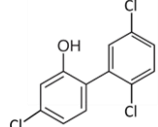
RT (min)	Compound	Molecule
9.02	4-hydroxy-hydrazide- Benzoic acid	
9.10	Benzamide	
9.26	(1-Phenyl-1,3-butadienyl) benzene	
9.38	Methyl 3-chloro-4-hydroxybenzoate	
9.61	p-Hydroxyphenyl)glyoxal	
9.96	Methyl 3,5-dichloro-4-hydroxybenzoate	
11.58	2-phenyl-2',5,5'-trichloro-Phenol	

Table IV.4. By-products for amoxicillin with Na₂SO₄+NaCl as electrolyte.

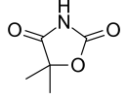
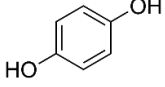
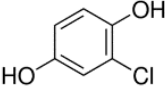
RT (min)	Compound	Molecule
4.85	Dimethadione	
5.63	Hydroquinone	
6.12	Chlorohydroquinone	

Table IV.4. By-products for amoxicillin with Na₂SO₄+NaCl as electrolyte (cont.).

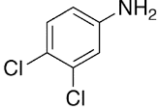
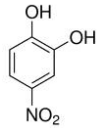
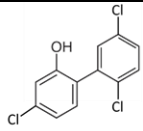
RT (min)	Compound	Molecule
6.93	3,4-dichlorobenzeneamine	
7.46	4-Nitrocatechol	
11.58	2-phenyl-2',5',5'-trichloro-Phenol	

Table IV.5. By-products for paracetamol with NaCl as electrolyte.

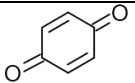
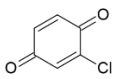
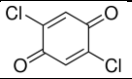
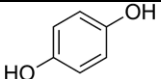
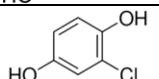
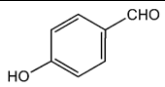
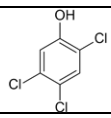
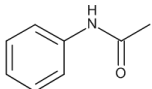
RT (min)	Compound	Molecule
3.02	p-benzoquinone	
4.14	2-chloro-p-benzoquinone	
5.36	2,5-dichloro-p-benzoquinone	
5.57	Hydroquinone	
6.10	Chlorohydroquinone	
6.29	p-hydroxy-benzaldehyde	
6.31	2,4,5-trichlorophenol	
6.46	N-phenyl-acetamide	

Table IV.5. By-products for paracetamol with NaCl as electrolyte (cont.).

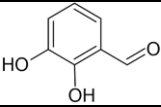
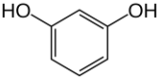
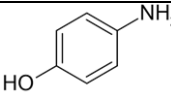
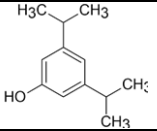
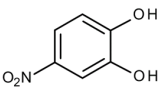
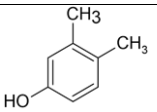
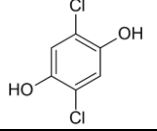
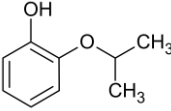
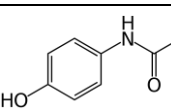
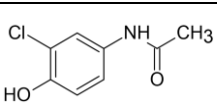
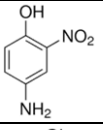
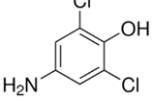
RT (min)	Compound	Molecule
6.59	2,3-dihydroxybenzaldehyde	
7.08	1,3-benzenediol	
7.11	4-nitrophenol	
7.22	3,5-diisopropylphenol	
7.42	4-nitrocatechol	
7.62	3,4-dimethylphenol	
7.75	2,5-dichloro-Hydroquinone	
7.97	2-Isopropoxyphenol	
8.83	Acetaminophen	
8.80	N-(3-Chloro-4-hydroxyphenyl) acetamide	
9.68	4-amino-2-nitro-phenol	
10.04	4-amino-2,6-dichloro-phenol	

Table IV.5. By-products for paracetamol with NaCl as electrolyte (cont.).

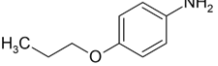
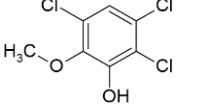
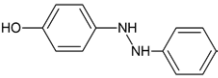
RT (min)	Compound	Molecule
10.93	4-propoxy-Benzenamine	
10.14	2,3,5-Trichloro-6-methoxyphenol	
11.90	Di-(4-hydroxy-phenyl)-diazene	

Table IV.6. By-products for paracetamol with Na₂SO₄+NaCl as electrolyte.

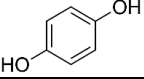
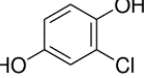
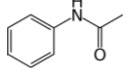
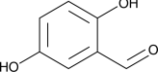
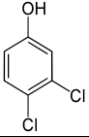
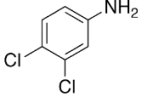
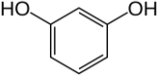
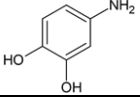
RT (min)	Compound	Molecule
5.59	Hydroquinone	
6.13	Chlorohydroquinone	
6.48	N-phenyl-Acetamide	
6.62	2,5-Dihydroxybenzaldehyde	
6.71	3,4-Dichlorophenol	
6.94	3,4-Dichlorobenzenamine	
7.10	1,3-Benzenediol	
7.44	4-Nitrocatechol	

Table IV.6. By-products for paracetamol with Na₂SO₄+NaCl as electrolyte (cont.).

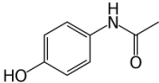
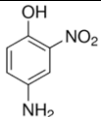
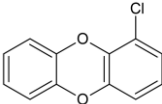
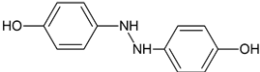
RT (min)	Compound	Molecule
8.73	Acetaminophen	
9.70	4-amino-2-nitrophenol	
10.77	1-Chlorodibenzo-p-dioxin	
11.92	Di-(4-hydroxy-phenyl)-diazene	

Table IV.7. Generated by-products for sertraline with NaCl as electrolyte.

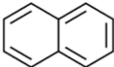
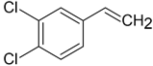
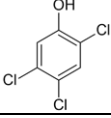
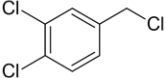
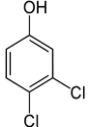
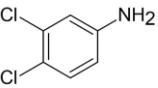
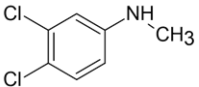
RT (min)	Compound	Molecule
5.13	Naphtalene	
5.67	3,4-Dichlorostyrene	
6.35	2,4,5-Trichlorophenol	
6.65	1,2-dichloro-4-(chloromethyl)- Benzene	
6.71	3,4-Dichlorophenol	
6.93	3,4-dichloro-Benzenamine	
7.48	3,4-Dichloro-N-methylaniline	

Table IV.7. Generated by-products for sertraline with NaCl as electrolyte (cont.).

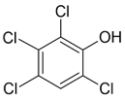
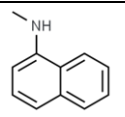
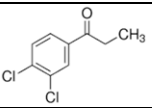
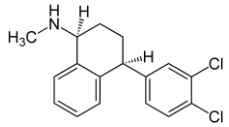
RT (min)	Compound	Molecule
7.75	2,3,4,6-Tetrachlorophenol	
8.16	N-methyl-1-Naphthalenamine	
8.91	3,4-Dichloropropiophenone	
12.20	Sertralina	

Table IV.8. By-products for sertraline with Na₂SO₄+NaCl as electrolyte.

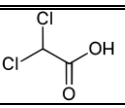
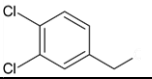
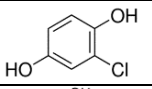
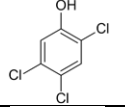
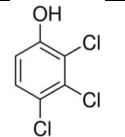
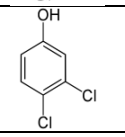
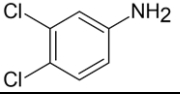
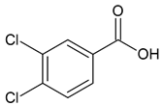
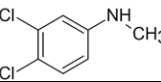
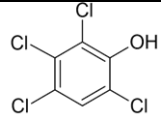
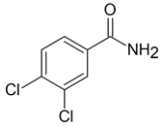
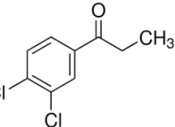
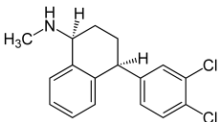
RT (min)	Compound	Molecule
3.72	Dicloroacetic acid	
5.63	3,4-Dichlorostyrene	
6.11	Chlorohydroquinone	
6.40	2,4,5-Trichlorophenol	
6.49	2,3,4-Trichlorophenol	
6.71	3,4-Dichlorophenol	
6.94	3,4-Dichlorobenzenamine	

Table IV.8. By-products for sertraline with Na₂SO₄+NaCl as electrolyte (cont.).

RT (min)	Compound	Molecule
7.40	3,4-Dichlorobenzoic acid	
7.48	3,4-Dichloro-N-methylaniline	
7.76	2,3,4,6-Tetrachlorophenol	
8.70	3,4-Dichlorobenzamide	
8.91	3,4-Dichloropropiophenone	
12.21	Sertraline	

Annex V – GC-MS chromatograms

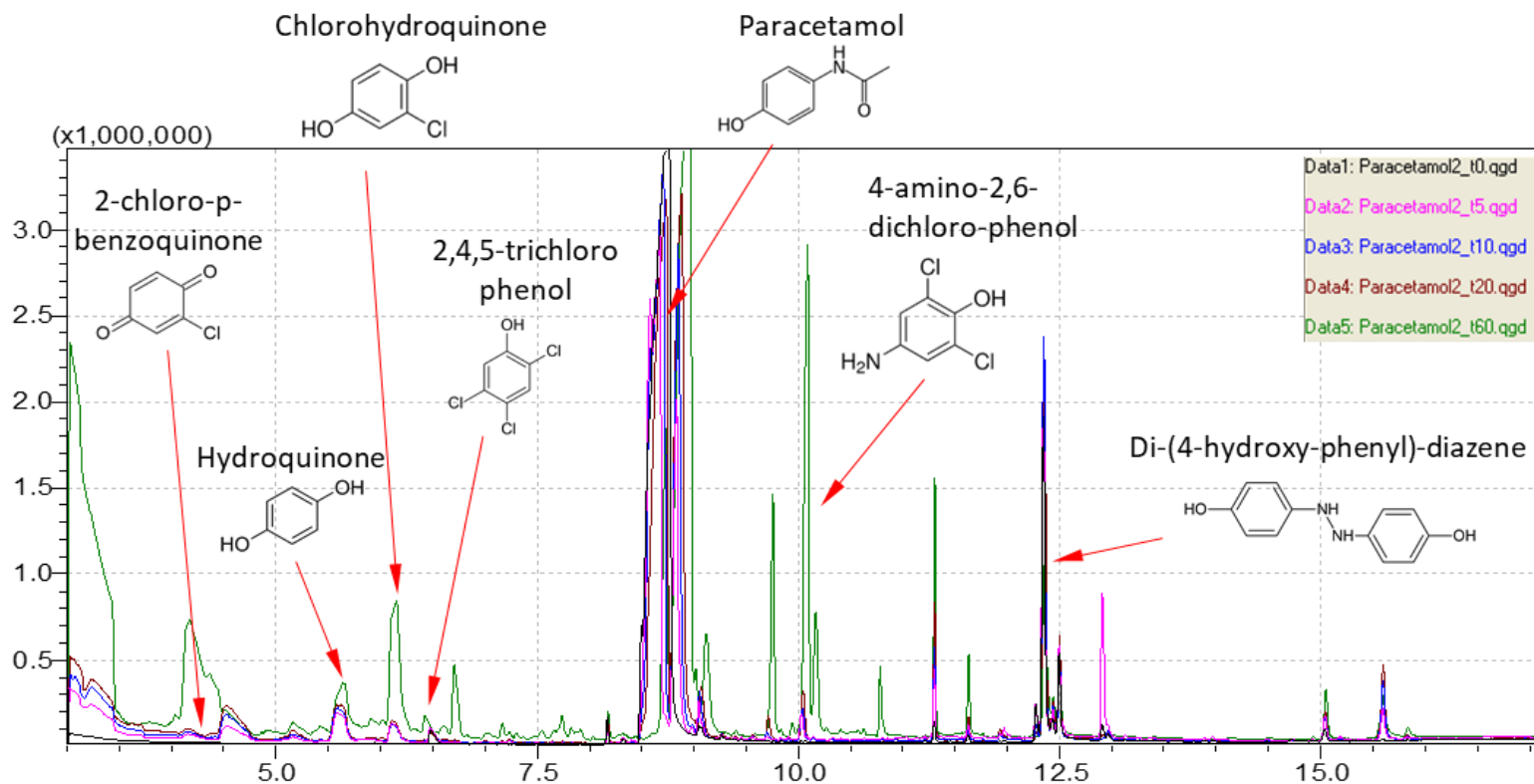


Table V.1. Example of a chromatogram (paracetamol with NaCl as electrolyte) with its most important peaks marked.

Annex VI – Degradation mechanisms

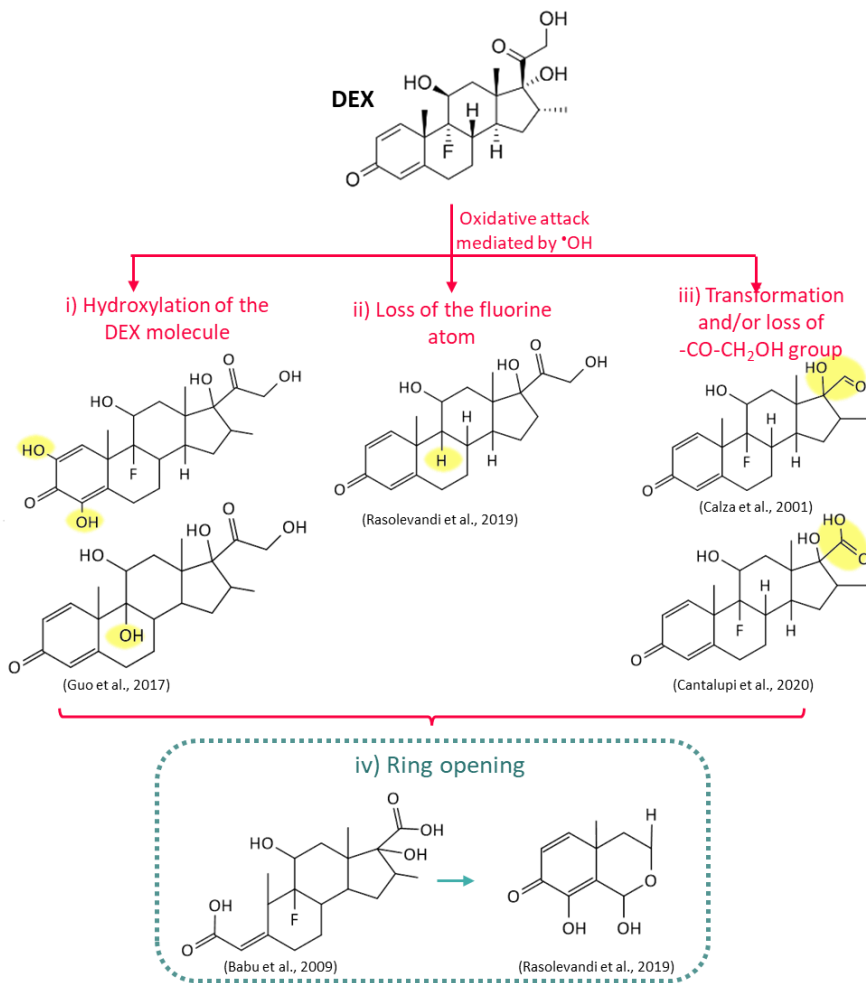


Figure VI.1. Resume of the DEX degradation pathways, with some molecules as example.

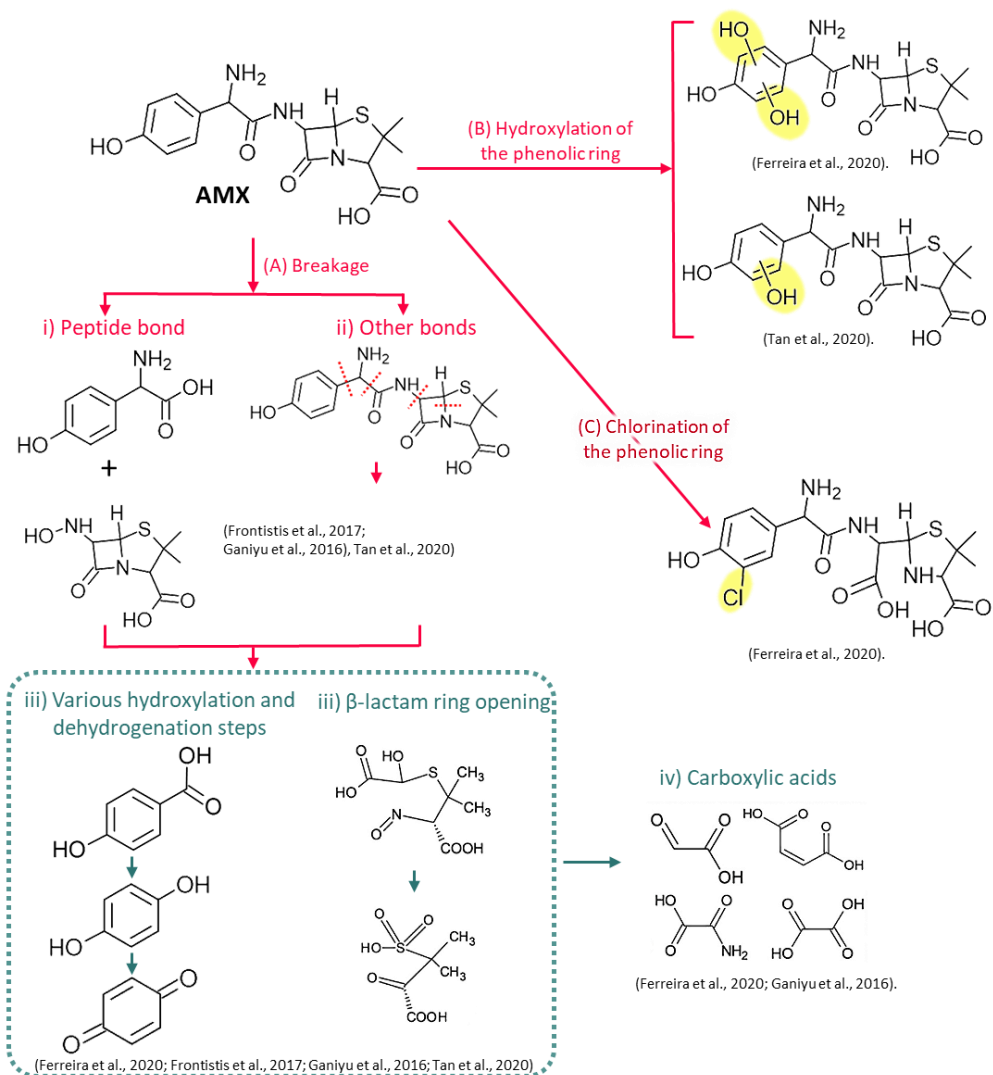


Figure VI.2. Resume of the AMX degradation pathways, with some molecules as example.

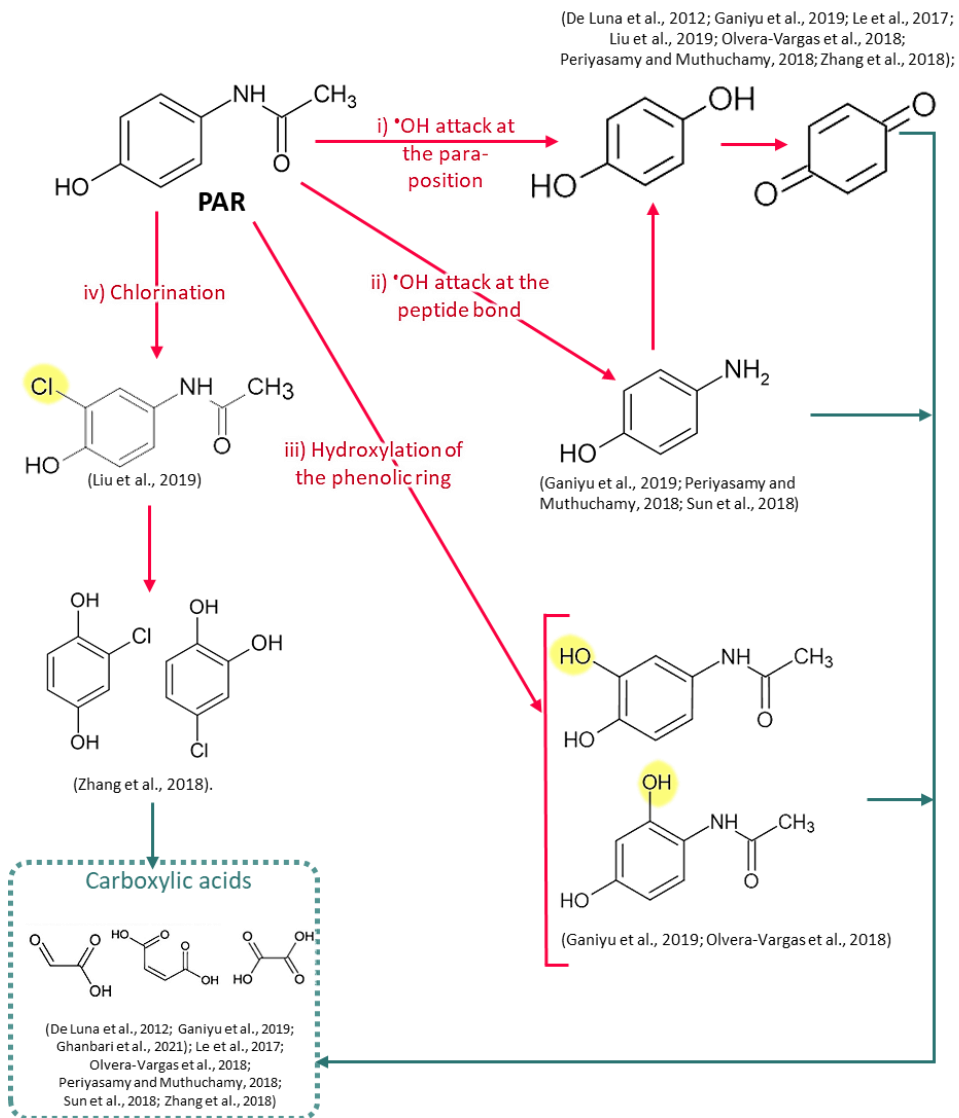


Figure VI.3. Resume of the PAR degradation pathways, with some molecules as example.

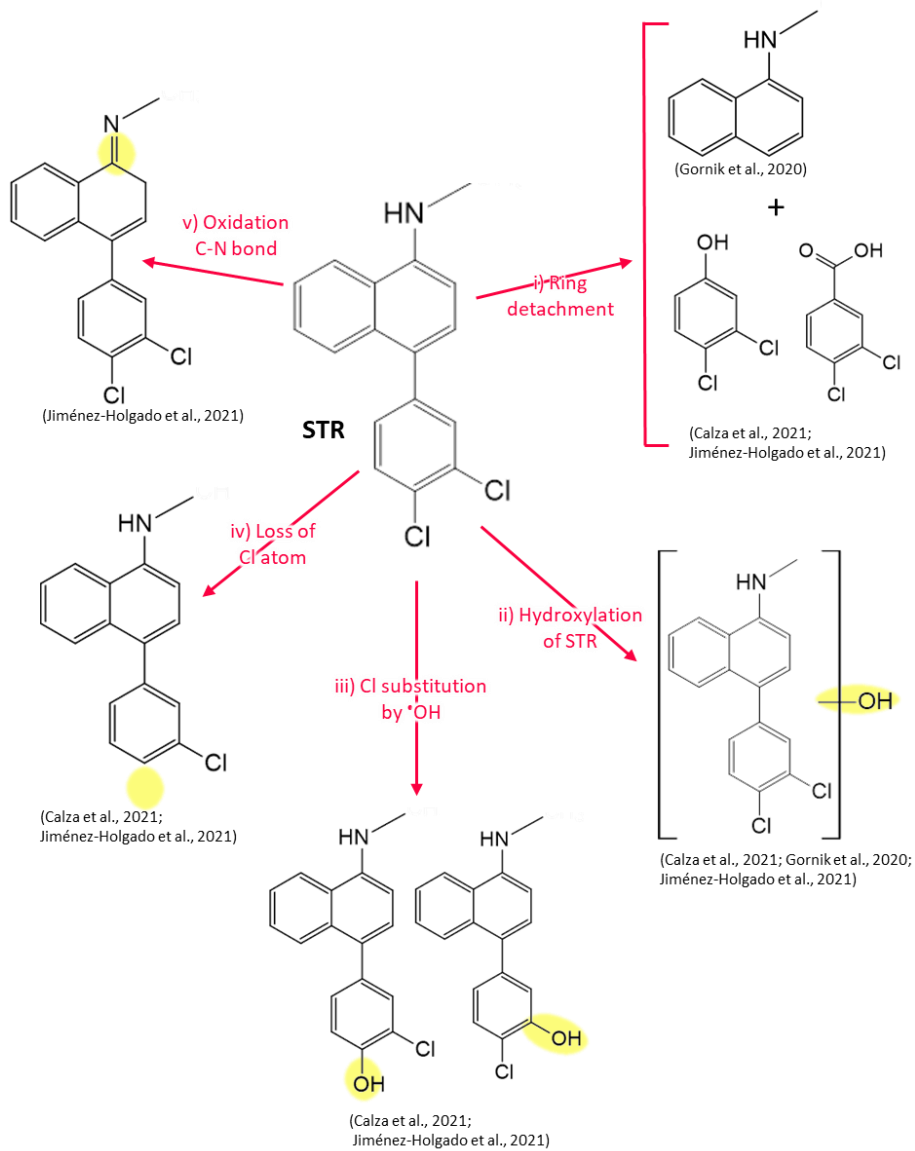


Figure VI.4. Resume of the STR degradation pathways, with some molecules as example.

Annex VII – Additional tables

Table VII.1. \mathbb{U} matrix, composed of 17 columns (corresponding to the 17 congeners) and 5 rows (the five TEQ values which correspond to the TEQ of each sampling time).

0.00	0.00	0.00	0.00	0.00	0.19	0.66	0.00	0.00	0.00	0.00	0.00	0.59	0.00	0.00	0.00	0.65
0.74	0.00	0.40	0.47	1.26	0.50	2.79	0.00	1.31	0.74	0.63	0.00	1.73	0.81	0.85	1.09	2.34
1.48	1.48	0.86	0.21	1.79	2.10	4.98	0.00	0.36	1.05	0.77	1.08	2.29	0.80	1.23	1.62	5.12
1.64	0.88	0.40	0.27	0.85	0.71	3.41	0.00	0.49	0.50	0.47	0.26	0.66	0.00	0.67	0.48	3.14
0.44	0.00	0.00	0.00	0.16	0.00	0.39	0.28	0.22	0.09	0.00	0.00	0.23	0.47	0.22	0.00	1.47

For a better comprehension, each column possesses the TEQ value of each congener, following this order: 2,3,7,8-TCDD; 1,2,3,7,8-PeCDD; 1,2,3,4,7,8-HxCDD; 1,2,3,6,7,8-HxCDD; 1,2,3,7,8,9-HxCDD; 1,2,3,4,6,7,8-HpCDD; OCDD; 2,3,7,8-TCDF; 1,2,3,7,8-PeCDF; 2,3,4,7,8-PeCDF; 1,2,3,4,7,8-HxCDF; 1,2,3,6,7,8-HxCDF; 1,2,3,7,8,9-HxCDF; 2,3,4,6,7,8-HxCDF; 1,2,3,4,6,7,8-HpCDF; 1,2,3,4,7,8,9-HpCDF and OCDF.

Table VII.2. \mathbb{P} matrix of the correlation coefficients for all the possible combinations of the 17 congeners of PCDD/Fs.

	2,3,7,8-TCDD	1,2,3,7,8-PeCDD	1,2,3,4,7,8-HxCDD	1,2,3,6,7,8-HxCDD	1,2,3,7,8,9-HxCDD	1,2,3,4,6,7,8-HpCDD	OCDD	2,3,7,8-TCDF	1,2,3,7,8-PeCDF	2,3,4,7,8-PeCDF	1,2,3,4,7,8-HxCDF	1,2,3,6,7,8-HxCDF	1,2,3,7,8,9-HxCDF	2,3,4,6,7,8-HxCDF	1,2,3,4,6,7,8-HpCDF	1,2,3,4,7,8,9-HpCDF	OCDF
2,3,7,8-TCDD	0.8502	0.8062	0.8062	0.1569	0.7484	0.7098	0.8749	-0.3386	0.2564	0.7488	0.6726	0.4657	0.1799	0.7992	0.6351	0.8756	
	0.0680	0.0994	0.3725	0.1457	0.1793	0.0521	0.5773	0.6772	0.1453	0.1238	0.2135	0.4292	0.7722	0.1047	0.2496	0.0517	
	0.7826	0.7906	0.6669	0.7000	0.8000	0.8000	-0.3536	0.7000	0.6669	0.7000	0.6669	0.7826	0.6000	0.1026	0.6669	0.9000	
1,2,3,7,8-PeCDD	0.8502	0.8672	0.1853	0.7268	0.9223	0.8761	-0.3879	-0.1171	0.7268	0.6893	0.9389	0.5808	0.1841	0.7530	0.6818	0.9291	
	0.0680	0.0569	0.7655	0.1642	0.0257	0.0514	0.5188	0.8513	0.1642	0.1979	0.0180	0.3045	0.7669	0.1418	0.2049	0.0224	
	0.7826	0.8250	0.2294	0.6708	0.8944	0.8944	-0.3953	0.2236	0.6708	0.6882	1.0000	0.6708	0.0000	0.6708	0.6882	0.8944	
1,2,3,4,7,8-HxCDD	0.8062	0.8672	0.5698	0.9696	0.9539	0.9823	-0.5205	0.3356	0.9697	0.9440	0.8815	0.8867	0.5584	0.9686	0.9522	0.9695	
	0.0994	0.0569	0.3159	0.0063	0.0118	0.0028	0.3685	0.5809	0.0063	0.0158	0.0481	0.0450	0.3279	0.0066	0.0124	0.0064	
	0.7906	0.8250	0.6489	0.9487	0.9487	0.9487	-0.5590	0.6325	0.9487	0.9733	0.8250	0.9487	0.4867	0.9487	0.9733	0.9487	
1,2,3,6,7,8-HxCDD	0.5169	0.1853	0.5698	0.7173	0.3081	0.6233	-0.5354	0.9355	0.7188	0.8086	0.1143	0.6193	0.4793	0.7028	0.6689	0.4452	
	0.3725	0.7655	0.3159	0.1726	0.6140	0.2613	0.3524	0.0195	0.1713	0.0976	0.8548	0.2653	0.4140	0.1856	0.2170	0.4525	
	0.6669	0.2294	0.6489	0.6669	0.5643	0.5643	-0.5441	0.9747	0.6669	0.6842	0.2294	0.6669	0.5000	0.6669	0.6842	0.5643	
1,2,3,7,8,9-HxCDD	0.7484	0.7268	0.9696	0.7173	0.8658	0.9449	-0.4867	0.5432	1.0000	0.9834	0.7610	0.9257	0.6938	0.9945	0.9853	0.9124	
	0.1457	0.1642	0.0063	0.1726	0.0578	0.0154	0.4057	0.3440	0.0000	0.0026	0.1351	0.0241	0.1938	0.0005	0.0021	0.0307	
	0.7000	0.6708	0.9487	0.6669	0.8000	0.8000	-0.3536	0.7000	1.0000	0.9747	0.6708	0.9000	0.7182	1.0000	0.9747	0.9000	
1,2,3,4,6,7,8-HpCDD	0.7098	0.9223	0.9539	0.3081	0.8658	0.9125	-0.4719	0.0560	0.8656	0.8068	0.9764	0.8339	0.4698	0.8607	0.8745	0.9439	
	0.1793	0.0257	0.0118	0.6140	0.0578	0.0307	0.4222	0.9288	0.0579	0.0990	0.0043	0.0792	0.4246	0.0611	0.0524	0.0158	
	0.8000	0.8944	0.9487	0.5643	0.8000	1.0000	-0.7071	0.5000	0.8000	0.8721	0.8944	0.9000	0.2052	0.8000	0.8721	0.9000	
OCDD	0.8749	0.8761	0.9823	0.6233	0.9449	0.9125	-0.5958	0.3582	0.9455	0.9500	0.8278	0.8209	0.4301	0.9489	0.9041	0.9535	
	0.0521	0.0514	0.0028	0.2613	0.0154	0.0307	0.2891	0.5539	0.0151	0.0133	0.0835	0.0885	0.4698	0.0138	0.0351	0.0120	
	0.8000	0.8944	0.9487	0.5643	0.8000	1.0000	-0.7071	0.5000	0.8000	0.8721	0.8944	0.9000	0.2052	0.8000	0.8721	0.9000	
2,3,7,8-TCDF	-0.3386	-0.3879	-0.5205	-0.5354	-0.4867	-0.4719	-0.5958	-0.2860	-0.4901	-0.5848	-0.3203	-0.5594	0.0748	-0.4249	-0.5034	-0.3500	
	0.5773	0.5188	0.3524	0.4057	0.4222	0.2891	0.6408	0.4019	0.3004	0.5992	0.3269	0.9049	0.4758	0.3872	0.5637		
	-0.3536	-0.3953	-0.5590	-0.5441	-0.3536	-0.7071	-0.7071	-0.3536	-0.3536	-0.5441	-0.3953	-0.7071	0.0000	-0.3536	-0.5441	-0.3536	
1,2,3,7,8-PeCDF	0.2564	-0.1171	0.3356	0.5432	0.0560	0.3582	-0.2860	0.5440	0.6187	-0.1300	0.4866	0.5724	0.5134	0.2085	0.5134	0.2085	
	0.6772	0.8513	0.5809	0.0195	0.3440	0.9288	0.5539	0.6408	0.3432	0.2659	0.8350	0.4058	0.3132	0.3612	0.3763	0.7365	
	0.7000	0.2236	0.6325	0.9747	0.7000	0.5000	0.5000	-0.3536	0.7000	0.6669	0.2236	0.6000	0.5643	0.7000	0.6669	0.6000	
2,3,4,7,8-PeCDF	0.7488	0.7268	0.9697	0.7188	1.0000	0.8656	0.9455	-0.4901	0.5440	0.9840	0.7603	0.9257	0.6916	0.9943	0.9852	0.9119	
	0.1453	0.1642	0.0063	0.1713	0.0000	0.0579	0.0151	0.4019	0.3432	0.0024	0.1357	0.0240	0.1958	0.0005	0.0022	0.0310	
	0.7000	0.6708	0.9487	0.6669	1.0000	0.8000	0.8000	-0.3536	0.7000	0.9747	0.6708	0.9000	0.7182	1.0000	0.9747	0.9000	
1,2,3,4,7,8-HxCDF	0.7749	0.6893	0.9440	0.8086	0.9834	0.8068	0.9500	-0.5848	0.6187	0.9840	0.6768	0.8898	0.6035	0.9758	0.9540	0.8702	
	0.1238	0.1979	0.0158	0.0976	0.0026	0.0990	0.0133	0.3004	0.2659	0.0024	0.2096	0.0432	0.2812	0.0045	0.0117	0.0550	
	0.6669	0.6882	0.9733	0.6842	0.9747	0.8721	0.8721	-0.5441	0.6669	0.9747	0.6882	0.9747	0.6579	0.9747	1.0000	0.8721	
1,2,3,6,7,8-HxCDF	0.6726	0.9389	0.8815	0.1143	0.7610	0.8278	-0.3203	-0.1300	0.7603	0.6768	0.7199	0.4060	0.7677	0.7677	0.7692	0.9151	
	0.2135	0.0180	0.0481	0.8548	0.1351	0.0043	0.8350	0.1357	0.2096	0.6882	0.1703	0.4977	0.1284	0.0293	0.1284	0.0293	
	0.7826	1.0000	0.8250	0.2294	0.6708	0.8944	0.8944	-0.3953	0.2236	0.6708	0.6882	0.6708	0.0000	0.6708	0.6882	0.8944	
1,2,3,7,8,9-HxCDF	0.4657	0.5808	0.8867	0.6193	0.9257	0.8339	0.8209	-0.5594	0.4866	0.9257	0.8898	0.7199	0.7504	0.8841	0.9754	0.7668	
	0.4292	0.3045	0.0450	0.2653	0.0241	0.0792	0.0885	0.3269	0.4058	0.0240	0.0432	0.1703	0.1439	0.0465	0.0046	0.1304	
	0.6000	0.6708	0.9487	0.6669	0.9000	0.9000	0.9000	-0.7071	0.6000	0.9000	0.9747	0.6708	0.5643	0.9000	0.9747	0.8000	
2,3,4,6,7,8-HpCDF	0.1799	0.1841	0.5584	0.4793	0.6938	0.4698	0.4301	0.0748	0.5724	0.6916	0.6035	0.4060	0.7504	0.6802	0.7447	0.5021	
	0.7722	0.7669	0.3279	0.4140	0.1938	0.4246	0.4698	0.9049	0.3132	0.1958	0.2812	0.4977	0.1439	0.2064	0.1488	0.3887	
	0.1026	0.0000	0.4867	0.5000	0.7182	0.2052	0.2052	0.0000	0.5643	0.7182	0.6579	0.0000	0.5643	0.7182	0.6579	0.3591	
1,2,3,4,6,7,8-HpCDF	0.7992	0.7530	0.9686	0.7028	0.9945	0.8607	0.9489	-0.4249	0.5273	0.9943	0.9758	0.7677	0.8841	0.6802	0.9651	0.9352	
	0.1047	0.1418	0.0066	0.1856	0.0005	0.0611	0.0138	0.4758	0.3612	0.0005	0.0045	0.1296	0.0465	0.2064	0.0078	0.0196	
	0.7000	0.6708	0.9487	0.6669	1.0000	0.8000	0.8000	-0.3536	0.7000	1.0000	0.9747	0.6708	0.9000	0.7182	0.9747	0.9000	
1,2,3,4,7,8,9-HpCDF	0.6351	0.6818	0.9522	0.6689	0.9853	0.8745	0.9041	-0.5034	0.5134	0.9852	0.9540	0.7692	0.9754	0.7447	0.9651	0.8715	
	0.2496	0.2049	0.0124	0.2170	0.0021	0.0524	0.0351	0.3872	0.3763	0.0022	0.0117	0.1284	0.0046	0.1488	0.0078	0.0542	
	0.6669	0.6882	0.9733	0.6842	0.9747	0.8721	0.8721	-0.5441	0.6669	0.9747	1.0000	0.6882	0.9747	0.6579	0.9747	0.8721	
OCDF	0.8756	0.9291	0.9695	0.4452	0.9124	0.9439	0.9535	-0.3500	0.2085	0.9119	0.8702	0.9151	0.7668	0.5021	0.9352	0.8715	
	0.0517	0.0224	0.0064	0.4525	0.0307	0.0158	0.0120	0.5637	0.7365	0.0310	0.0550	0.0293	0.1304	0.3887	0.0196	0.0542	
	0.9000	0.8944	0.9487	0.5643	0.9000	0.9000	0.9000	-0.3536	0.6000	0.9000	0.8721	0.8944	0.8000	0.3591	0.9000	0.8721	

Annex VIII – Additional AMX pathway

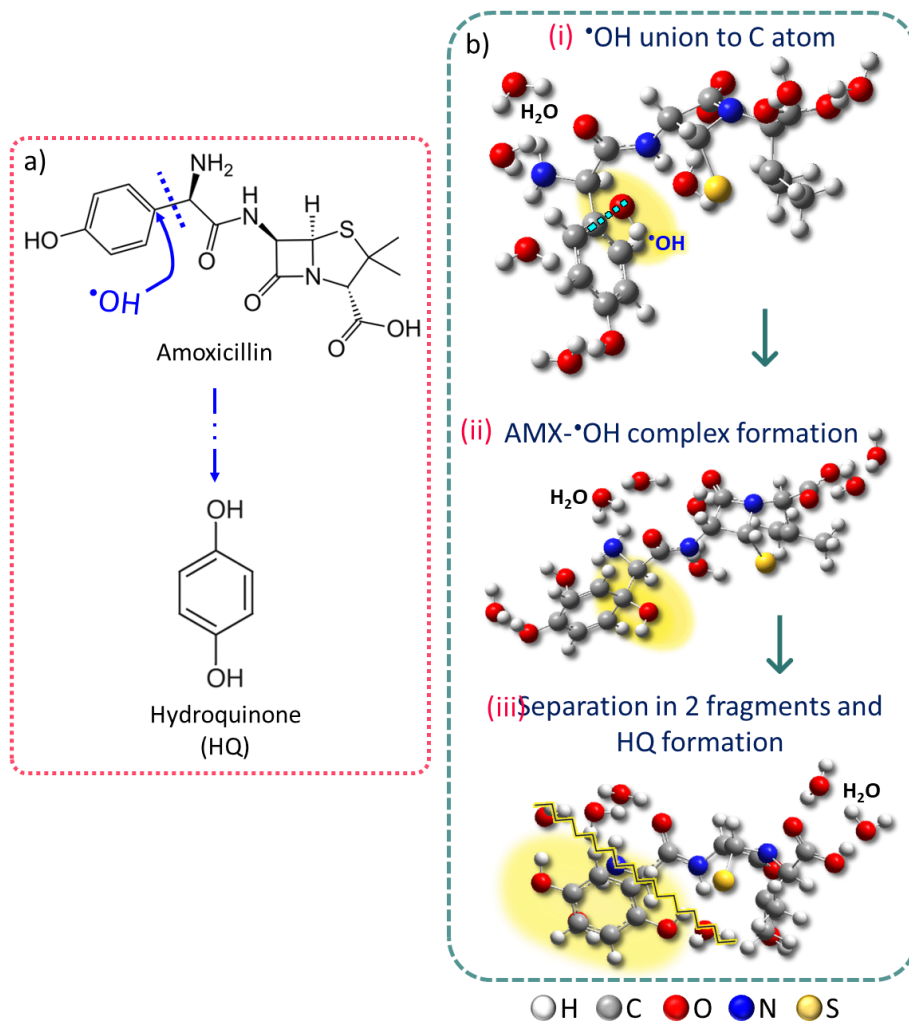


Figure VIII.1. a) Scheme of the AMX formation and b) DFT simulation of the AMX formation (Version 1, "inside").

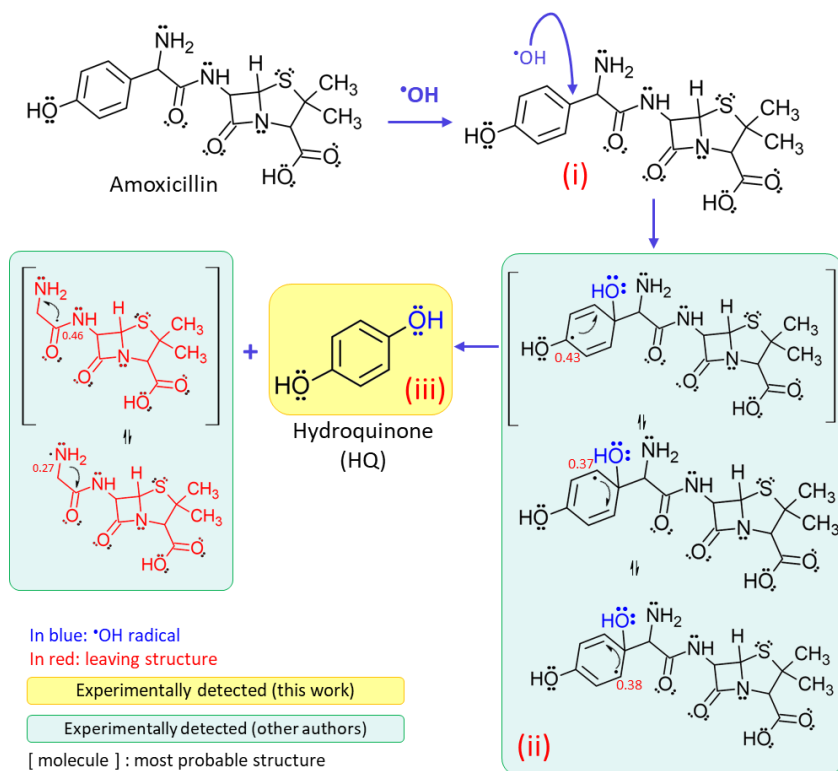


Figure VIII.2. AMX degradation pathway in terms of the spin values, marked in red.

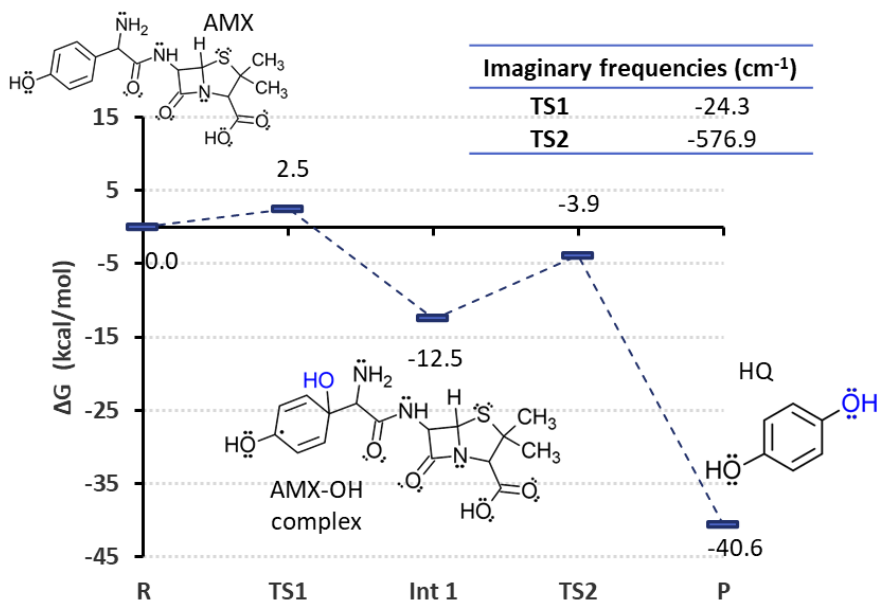


Figure VIII.3. Energy profile of the AMX degradation pathway, obtained by computational chemistry calculations GAUSSIAN 16.

Annex IX – Scientific contributions

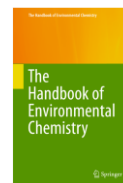
IX.1. List of papers published in indexed journals

1. PCDD/Fs traceability during triclosan electrochemical oxidation. Solá-Gutiérrez, C., Schröder, S., San Román, M.F., Ortiz, I., 2019. J. Hazard. Mater. 369, 584–592. (JCR IF (2019): 9.04, Q1)
2. Critical review on the mechanistic photolytic and photocatalytic degradation of triclosan. Solá-Gutiérrez, C., Schröder, S., San-Román, M.F., Ortiz, I., 2020. J. Environ. Manage. (JCR IF (2020): 6.79, Q1)
3. Potential formation of PCDD/Fs in triclosan wastewater treatment: An overall toxicity assessment under a life cycle approach. San-Román, M.F., Solá-Gutiérrez, C., Schröder, S., Laso, J., Margallo, M., Vázquez-Rowe, I., Ortiz, I., Irabien, A., Aldaco, R., 2020. Sci. Total Environ. 707, 135981. (JCR IF (2020): 7.96, Q1)
4. Schröder, S., San-Román, M.F., Ortiz, I., 2020. Photocatalytic transformation of triclosan. Reaction products and kinetics. Catalysts 10, 1–15. (JCR IF (2020): 4.15, Q2)
5. Schröder, S., San-Román, M.F., Ortiz, I., 2021. Dioxins and furans toxicity during the photocatalytic remediation of emerging pollutants. Triclosan as case study. Sci. Total Environ. 770, 144853. (JCR IF (2021): 10.75, Q1)
6. Schröder, S., San-Román, M.F., Ortiz, I., 2022. Dioxins and furans (PCDD/Fs) detection in the course of the electrochemical oxidation of polluted waters with pharmaceuticals used in the fight against COVID-19. J. Environ. Chem. Eng. *Accepted*. (JCR IF (2021): 7.97, Q1)



IX.2. Book chapter

1. Schröder, S., San Román, M.F., Ortiz, I., 2022. "Emerging Pollutants That Can Be Transformed into PCDD/Fs". In: The Handbook of Environmental Chemistry, vol 114. Springer, Berlin, Heidelberg. https://doi.org/10.1007/978-3-662-62851-1_14



IX.3. Congress contributions

1. Solá-Gutiérrez, C., **Schröder, S.**, San Román, M.F., Ortiz, I. "Aqueous oxidation of Triclosan: The potential formation of PCDD/Fs". 38th International Symposium on Halogenated Persistent Organic Pollutants (POPs) & 10th International PCB Workshop: Dioxin 2018. Krakow, Poland, August 26-31, 2018. *Poster presentation.*
2. Solá-Gutiérrez, C., **Schröder, S.**, San Román, M.F., Ortiz, I. "Formation of chlorinated organic compounds during triclosan electrochemical oxidation: Determination of PCDD/Fs". ANQUE-ICCE-CBIQ 2019. Santander, Spain, June 19-21, 2019. *Oral communication.*
3. Solá-Gutiérrez, C., **Schröder, S.**, San Román, M.F., Ortiz, I. "Aqueous electrochemical oxidation of Triclosan: the potential formation of PCDD/Fs". ECCE12-ECAB5, the 12th European Congress of Chemical Engineering. Florence, Italy, September 15-19, 2019. *Oral communication.*
4. Solá-Gutiérrez, C., **Schröder, S.**, San Román, M.F., Ortiz, I. "Photolytic degradation of Triclosan". SDEWES, 14th conference on sustainable development of energy, water and environmental systems. Dubrovnik, Croatia, October 1-6, 2019. *Poster presentation.*
5. Solá-Gutiérrez, C., **Schröder, S.**, San Román, M.F., Ortiz, I. "Determination of chlorinated organic compounds and PCDD/Fs during Triclosan electrochemical oxidation". SDEWES, 14th conference on sustainable development of energy, water and environmental systems. Dubrovnik, Croatia, October 1-6, 2019. *Oral communication.*



6. San Román, M.F., **Schröder, S.**, Laso J., Margallo, M., Vázquez-Rowe I., Aldaco, R. "Evaluation of the potential formation of dioxins in wastewater treatment using LCA". ISIE Americas 2020 (International Society for Industrial Ecology Conference). Online. July 6-8, 2020. *Poster presentation*.
7. **Schröder, S.**, San Román, M.F., Ortiz, I. "Potencial formación de PCDD/Fs durante la oxidación electroquímica de Triclosan". V Workshop de la Red E3TECH / I Workshop Iberoamericano a Distancia 'Aplicaciones Medioambientales y Energéticas de la Tecnología Electroquímica' (V E3TECH). Online, October 28-31, 2020. *Poster presentation*.
8. **Schröder, S.**, San Román, M.F., Ortiz, I. "Photocatalytic degradation of triclosan: study of the operating conditions and assessment of potential formation of organo-chlorinated by-products". CHISA 2021 Virtually. Online, March 15-19, 2021. *Keynote lecture*.
9. **Schröder, S.**, San Román, M.F., Ortiz, I. "Triclosan degradation employing Advanced Oxidation Processes (AOPs)- Assessment of dioxins and furans (PCDD/Fs) formation". Dioxin 2021 Tianjin - 41st International Symposium on Halogenated Persistent Organic Pollutants. Online, November 8-11, 2021. *Oral communication*.
10. **Schröder, S.**, San Román, M.F., Ortiz, I. "PCDD/Fs formation during Triclosan oxidation: Electrochemical oxidation vs. photocatalysis". 6th International Symposium on "Green and Smart Technologies for a Sustainable Society". Online, December 9-10, 2021. *Video oral communication*.
11. **Schröder, S.**, San Román, M.F., Ortiz, I. "Electrochemical oxidation of pharmaceutical compounds used in the COVID-19 pandemic: analysis of the formed by-products and of the final toxicity". XXXVIII Reunión Bial de la Sociedad Española De Química. Granada, Spain, June 27-30, 2022. *Poster presentation*.



IX.4. Dissemination activities

1. **Schröder, S.** European Researchers' Night. Diffusion activities of the Research Group IPS. Santander, September 2018, 2019, 2020, 2021.



2. **Schröder, S.** Diffusion activities in the Scientific Week at University of Cantabria. Santander, November 2020.



3. **Schröder, S.** Mini-lectures and videos in the International Day of Woman and Girls in Science. ETSIIT and several high schools. February 2019, 2020, 2021.



IX.5. Final degree project co-direction

Title: ESTUDIO DE LA POTENCIAL FORMACIÓN DE PCDD/Fs DURANTE LA OXIDACIÓN ELECTROQUÍMICA DE SERTRALINA (STR)/(Study of potential formation of PCDD/Fs in electrochemical oxidation of sertraline (STR))

Student: David Navarro Tumar

Director: María Fresnedo San Román San Emeterio/

Co-director: Sophie Mary Schröder Barraza

Group: Ingeniería de Procesos Sostenibles (IPS) / Sustainable Process Engineering (SPE)

Department and University: Department of Chemical and Biomolecular Engineering, University of Cantabria

ABOUT THE AUTHOR



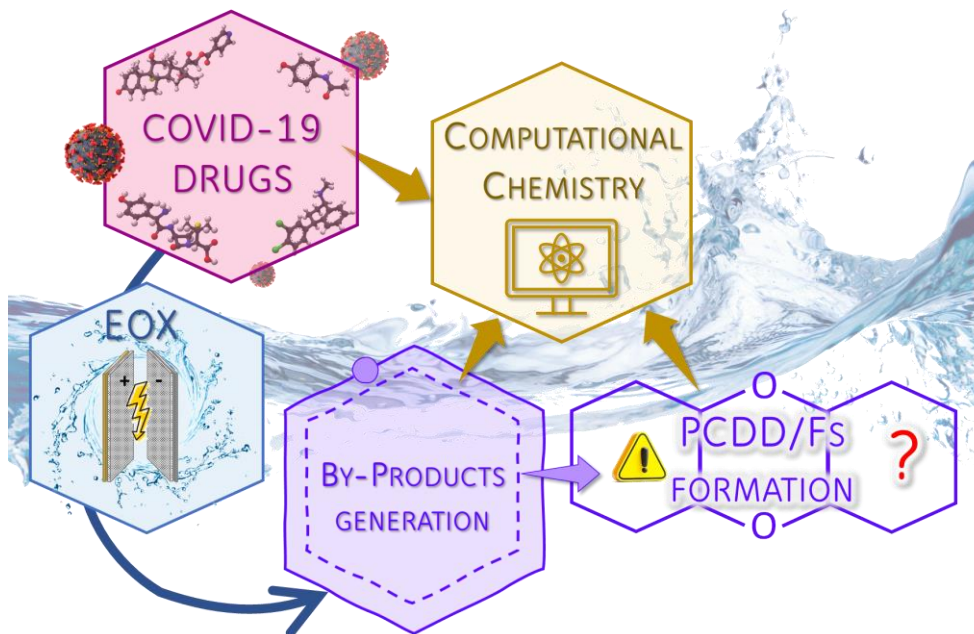
Sophie M. Schröder Barraza was born in Burgos (Spain) on August 9th, 1991. She obtained a BSc in 2015 and MSc in 2017 in Chemical Engineering at the University of Cantabria. After finishing her studies, she joined the Chemical and Biomolecular Engineering Department to start her research career.

In November 2017, she started working under the supervision of Dr. María Fresnedo San Román in different research projects. In December 2018 she started her

doctoral studies in the PhD program of Chemical Engineering, Energy and Processes under the supervision of Prof. Inmaculada Ortiz Uribe and Dr. María Fresnedo San Román. To this end, she was granted with a predoctoral contract FPI of the Spanish Ministry of Science and Innovation. The work has been carried out in the Department of Chemical and Biomolecular Engineering of the University of Cantabria in the research group of Sustainable Process Engineering (SPE) and in the Advanced Separation Processes group (ASP).

During her PhD, she performed a research stay of three months in the Faculdade de Ciências da Universidade do Porto, in Porto (Portugal), under the supervision of Dr. Pedro A. Fernandes and Dr. Pedro Ferreira.

At the time of writing, she is the author of five scientific articles in indexed journals, a book chapter, and eleven contributions to international and national conferences. Besides, she participated in some diffusion activities aimed at public awareness of science and chemical engineering.



La situación actual de los recursos hídricos, en el marco de la pandemia mundial COVID-19, es el punto de partida de esta tesis doctoral. El tratamiento aplicado en la lucha contra el virus SARS-CoV-2, ha llevado al consumo intensivo de los fármacos dexametasona (DEX), amoxicilina (AMX), paracetamol (PAR) y sertralina (STR), que finalmente acaban en el medio acuático como Contaminantes Emergentes (CEs). En este contexto, los procesos de oxidación avanzada (POAs) se presentan como una opción atractiva, destacándose la oxidación electroquímica (EOX). Sin embargo, estudios previos han demostrado, que, bajo la aplicación de algunos POAs, es posible que se generen compuestos intermedios, quizás más tóxicos que los iniciales, como las dibenzo-p-dioxinas policloradas y los furanos (PCDD/Fs). Para corroborar esta hipótesis, esta tesis doctoral ha evaluado, experimental y teóricamente (química computacional) la formación de PCDD/Fs y la toxicidad final de las muestras, tras aplicar EOX a matrices que contienen los fármacos COVID-19, dexametasona (DEX), amoxicilina (AMX), paracetamol (PAR) y sertralina (STR).

The current situation of water resources, within the framework of the global pandemic COVID-19, centers the starting point of this doctoral thesis. The treatments applied in the fight against the SARS-CoV-2 virus, has led to intensive consumption of the drugs dexamethasone (DEX), amoxicillin (AMX), paracetamol (PAR) and sertraline (STR), which finally end in the aquatic medium as Emerging Contaminants (EC). In this context, the advanced oxidation processes (AOPs) are presented as an attractive option, standing out electrochemical oxidation (EOX). Nevertheless, previous studies have demonstrated that under the application of some AOPs, it may be possible that intermediate compounds can be generated, possibly more toxic than the initial ones, like polychlorinated dibenzo-p-dioxin and furans (PCDD/Fs). In order to corroborate this hypothesis, this doctoral thesis has assessed, in an experimental and theoretical way (computational chemistry) the formation of PCDD/Fs and the final toxicity of the samples, after applying EOX to matrices containing the COVID-19 drugs, dexamethasone (DEX), amoxicillin (AMX), paracetamol (PAR) and sertraline (STR).